DEVELOPMENT OF P-OP LIGANDS WITH NEW STRUCTURAL MOTIFS FOR RHODIUM- AND IRIDIUM- MEDIATED ASYMMETRIC HYDROGENATIONS

Balakrishna Bugga

Development of P–OP Ligands with New Structural Motifs for Rhodium- and Iridium-Mediated Asymmetric Hydrogenations

Ph.D. Thesis presented by:

Balakrishna Bugga

Developed under the supervision of:

Prof. Anton Vidal Ferran

Department of Analytical and Organic Chemistry (URV)
and Institute of Chemical Research of Catalonia (ICIQ)

UNIVERSITAT ROVIRA i VIRGILI

TARRAGONA, 2016

ICIQ
Institut Català d'Investigació Química

UNIVERSITAT ROVIRA I VIRGILI
DEPARTAMENT DE QUIMICA ANALITICA I QUIMICA ORGANICA
C/ Marcel.lí Domingo s/n
Campus Sescelades
43007 Tarragona
Tel. 34 977 55 97 69
Fax 34 977 55 84 46
e-mail: secqaqo@urv.net

Prof. Anton Vidal Ferran, Group Leader of the Institute of Chemical Research of Catalonia (ICIQ) and Research Professor of the Catalan Institution for Research and Advanced Studies (ICREA),

CERTIFY that the present Doctoral Thesis entitled: "*Development of P–OP Ligands with New Structural Motifs for Rhodium- and Iridium-Mediated Asymmetric Hydrogenations*", that Balakrishna Bugga presents to obtain the PhD degree in chemistry, has been carried out under his supervision, in the corresponding research group at the Institute of Chemical Research of Catalonia (ICIQ).

Tarragona, 9th September, 2016

Ph.D. Thesis supervisor

Prof. Anton Vidal Ferran

Acknowledgements

Honestly, it is very hard to describe how many wonderful moments I had with many people since I began my Ph.D. at the ICIQ. Nevertheless, I will try to summarize some of the important points.

First of all, I would like to express my gratitude to my supervisor Prof. Anton Vidal for the opportunity to become a member of his group; for his constant support and direction during the entire time of my studies and for the opportunities that he kindly offered me.

I am also grateful to the thesis committee for their time and consideration of my thesis evaluation.

I would also like to express special thanks to the past and present members of the group: Dr. Héctor Fernández (Group Scientific Coordinator), Dr. José Luis Núñez, Dr. Mónica Vaquero, Dr. Rajesh Pudi, Dr. Pablo Etayo, Ignacio Mon, Laura Rovira, Joan Ramon Lao, Lucas Carreras, Alicia Martínez, Nuria Llorente, Dominik Lichte and, Ester Iniesta, who helped me growing both on professional and personal side, inside and outside of the lab. You have ALWAYS taken the time to support me with valuable discussions during the period of my stay in ICIQ. You people spent your valuable time in proof reading my thesis and other documents. Particularly, Héctor, José Luis, Joan and Lucas, I will never forget your assistance. I strongly believe that without your suggestions and help I could not be in this situation. Your support was highly appreciated!!! I had a great time in your company and I enjoyed a lot by using my Spandian words (…de la India,...etc.) in lab.

I would like to thank the people that collaborated in the one way or other with the chemistry work that I am presenting. In particular, Prof.

Antonio Frontera and his student Antonio Bauzá for their valuable DFT studies to our chemistry. In addition, I would like to thank all technical support area and administrative staff in ICIQ. Special thanks to Paula Segovia for all the help with the paperwork. It would have been so difficult without your help.

I would like to take this opportunity to gratefully thank all those friends who shared thousands of happy moments during the sports time. Particularly, Aurélien Viterisi, Samuel Drouet, Lucas Carreras, Carles Rodríguez, Laura, Mónica and Christina, your friendship added many values to my life here. Additionally, other beach-volley players and badminton players, you all were big competitors for me. That made me to have more fun and excitement in playing with you. Thanks a lot to all of you!!! I would also like to thank all the present and past Tarragona Indian friends particularly Sandeep Reddy, Prasad Ganji, Vijay Ch., Suva, Rajesh, Muralidhar, Sayantan, Asmaul, Tharun, Purushotham (Muni), Rositha, Noufal, Venkat N. Karri, Raju Sharma, Venkat P., Veera Reddy and Raju Reddy (our Tarragona cricket team and poker team), your coordination, care and support was precious, important and unforgettable for me.

I would like to extend my sincere thanks to all my DC-friends and seniors in India, particularly, Srinu D., Raju P., Ravi G., Cnu Reddy, Naresh J., Chakri K., N. N. Swamy, Venkat Rao P., Omkar R. and Sandeep KM., who treated me like a part of their family and supported me always for my goals. I also would like to thank my contemporary foreign Ph.D. friends Sai Kumar I. and Lingaraju G. for keeping in touch during all the period and sharing the experiences and giving the valuable suggestion during the time I have stayed in Spain. Your suggestions were always motivated me to go forward.

Above all, I would like to thank my family members Bugga Rajaiah (Father) Bugga Andamma (Mother) Bugga Beeraiah and Bugga Balaraju (Brothers), Parijatha (Sister-in-law), Sheshi Varun (Nephew), Risitha (Niece) and other family relatives for their endless love and constant support during all my life. They ALWAYS trusted me and supported me with every decision I made and also every time they tried to help me as much as they could.

Probably, it is impossible to count how many times I am grateful to everybody for this period time that I spent here in Tarragona. Thank you very much to all of you.

The work developed in the present doctoral thesis has been possible thanks to the funding received from AGAUR for a pre-doctoral fellowship (2013FI-B 00545, 2013-2016). We would also like to thank ICIQ Foundation, MINECO (CTQ2014-60256-P, CTQ2014-57393-C2-1-P and Severo Ochoa Excellence Accreditation 2014-2018 SEV-2013-0319) for financial support.

List of Acronyms and Abbreviations

In this document the abbreviations and acronyms most commonly used in organic chemistry have been used, according to the recommendations of the ACS "Guidelines for authors":

http://pubs.acs.org/paragonplus/submission/joceah/joceah_abbreviations.pdf

Ac	Acetyl
API	Active Pharmaceutical Ingredient
BArF	Tetrakis[(3,5-trifluoromethyl)phenyl]borate
Bn	Benzyl
BNP	4-Hydroxydinaphtho[2,1-*d*:1',2'-*f*][1,3,2]dioxaphosphepine4-oxide
Boc	*tert*-Butoxycarbonyl
Bz	Benzoyl
calcd	Calculated
Cbz	Benzyloxycarbonyl
Cod	1,5-Cyclooctadiene
Conv.	Conversion
Cy	Cyclohexyl
CSA	Camphorsulfonic Acid
DABCO	1,4-Diazabicyclo[2.2.2]octane
DCE	Dichloroethane
DCM	Dichloromethane
DFT	Density Functional Theory
DIPE	Diisopropyl ether
DMAP	4-(Dimethylamino)pyridine

DMC	Dimethyl Carbonate
DMI	Dimethyl Itaconate
DME	1,2-Dimethoxyethane
DMF	*N*,*N*-Dimethylformamide
DMS	Dimethylsulfide
DPP	Diphenylphosphoric Acid
dr	Diastereomeric Ratio
ESI	Electrospray Ionization
ee	Enantiomeric Excess
FID	Flame Ionization Detector
Fmoc	9-Fluorenylmethoxycarbonyl
GABA	γ-Aminobutyric Acid
GC	Gas Chromatotraphy
HPLC	High Performance Liquid Chromatography
HRMS	High-Resolution Mass Spectrometry
IR	Infrared
L-DOPA	(*S*)-3',4'-Dihydroxyphenylalanine
m-CPBA	*meta*-Chloroperoxybenzoic Acid
MAA	Methyl (*N*)-(acetylamino)acrylate
MeTHF	2-Methyltetrahydrofuran
MOM	Methoxymethyl
MsOH	Methanesulfonic Acid
mp	Melting Point
m/z	Mass-to-Charge Ratio (not *m/e*)
min	Minute(s)
Nbd	1,5-Norbornadiene
n-BuLi	*n*-Butyllithium

NMR	Nuclear Magnetic Resonance
ORTEP	Oak Ridge Thermal Ellipsoid Plot Program
RT	Room Temperature
SPS	Solvent Purification System
Tfb	Tetrafluorobarrelene
TFA	Trifluoroacetic Acid
TFE	Trifluoroethanol
THF	Tetrahydrofuran
TOF	Turnover Frequency
TON	Turnover Number
Tr	Trityl
TS	Transition State
R_f	Retention Factor (in chromatography)
UV	Ultraviolet
TsOH	*p*-Toluenesulfonic Acid
Z-MAC	Methyl (*Z*)-(*N*)-acetylaminocinnamate
°C	Degrees Celsius

List of Publications

Some of the results presented in this thesis have been published in:

- "*Ring-opening of Enantiomerically Pure Oxa-containing Heterocycles with Phosphorus Nucleophiles*"
  Fernández-Pérez, H.; Etayo, P.; Núñez-Rico, J. L.; **Balakrishna, B.**; Vidal-Ferran, A. *RSC Adv.* **2014**, *4*, 58440–58447.

- "*Substrate Activation in the Catalytic Asymmetric Hydrogenation of N-Heteroarenes*"
  Balakrishna, B.; Núñez-Rico, J. L.; Vidal-Ferran, A. *Eur. J. Org. Chem.* **2015**, *2015*, 5293–5303.

- "*A Practical Synthesis of Rhodium Precatalysts for Enantioselective Hydrogenative Transformations*"
  Balakrishna, B.; Vidal-Ferran, A. *Synthesis* **2016**, *48*, 997–1001.

- "*Asymmetric Hydrogenation of Seven-membered C=N-containing Heterocycles and Rationalization of the Enantioselectivity*"
  Balakrishna, B.; Bauzá, A.; Frontera, A.; Vidal-Ferran, A. *Chem. – Eur. J.* **2016**, *22*, 10607–10613.

Furthermore, one manuscript is under preparation. The discussion on the screening of TADDOL- and (H8)-BINOL-based P–OP ligands in rhodium-mediated asymmetric hydrogenation presented in Chapter-3, which will be submitted as a research article in an appropriate journal in due time.

To My Family and Beloved Friends

Table of Contents

Introduction

Any living system is a pool of chirality, as most of the chemical building blocks of biological systems are present in an enantiopure form.[1] For example, all amino acids that constitute the proteins (except the achiral amino acid glycine) have an L- or (*S*)-configured carbon bearing the amino and carboxyl substituents. Carbohydrates, which are one of the components of nucleic acids, as well as energy storage materials in living organisms, belong exclusively to the D-series.[2]

Enantiomers (or stereoisomers that are non-superimposable mirror images of one another) can generally result in four types of relative biological effects: 1) The enantiomers have the same biological activity; 2) the enantiomers have qualitatively identical biological effects but their intensities are different; 3) only one enantiomer is biologically active; 4) the two enantiomers have very different biological properties. For instance, Iclaprim (Figure 1), which is a drug marketed as a racemate and used in the treatment of bacterial infections, is an example where both enantiomers exhibit similar activity against the dihydrofolate reductase enzyme (DHFR) and a similar antimicrobial activity against a broad range of bacteria.[3] On the other hand, enantiopure (*S*)-ibuprofen (Figure 1) reaches therapeutic concentrations in blood in 12 minutes while racemic mixtures require 30 minutes.[4] (*S*,*S*)-ethambutol (Figure 1) is used for the treatment of tuberculosis while (*R*,*R*)-ethambutol has been found to cause blindness.[5] Even inactive enantiomers, that cause no side effects, have to be metabolized by the human organism, which results in an unnecessary physiological burden.[6] Therefore, in pharmacology, enantiopurity is of paramount importance, and efficient methods to obtain enantiopure substances are required.

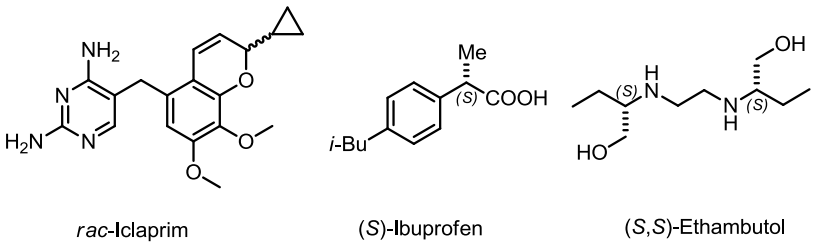

rac-Iclaprim (*S*)-Ibuprofen (*S*,*S*)-Ethambutol

Figure 1. Selected examples of pharmaceutical active compounds.

Asymmetric catalysis,[7] in which each molecule of a chiral catalyst produces many molecules of enantioenriched products by being continuously regenerated, has significant potential advantages over non-catalytic methods. The transfer of chirality from the catalyst to the product normally occurs in the transition state (TS) of the stereo-determining step (Figure 2). When a substrate containing prochiral elements interacts with the catalyst, two transition states, namely TS_R and TS_S, are generated, leading to the (*R*)-configured and (*S*)-configured product, respectively. The activation energy difference (E_R *vs.* E_S) between the two TS's determines the enantioselectivity of the reaction, and the pathway with the lower activation energy (*e.g.* E_R in Figure 2) will be kinetically dominant. This will result in the production of a higher fraction of the enantiomer arising from that pathway.

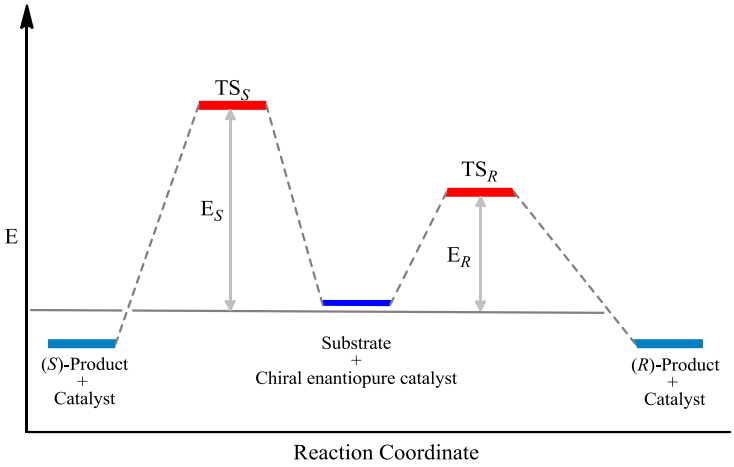

Figure 2. Simplified energy diagram for an enantioselective catalytic process.

Asymmetric biocatalysis, metal-based catalysis, and organocatalysis are the three principal areas in the field of asymmetric catalysis. Many achievements have been made in these three domains. Although biocatalysis and organocatalysis are very important classes of enantioselective catalysts, they are beyond the scope of this thesis and, hence, will not be discussed herein.

Among the different approaches to achieve enantiocontrol, the use of enantiopure transition metal-based complexes as homogeneous catalysts is one of the most powerful strategies.[8] Significant progress has been achieved in transition metal-based asymmetric catalysis, as made evident by the 2001 Nobel Prize in Chemistry awarded to William S. Knowles, K. Barry Sharpless and Ryoji Noyori for their contribution to asymmetric transition metal-based catalysis.[9]

Furthermore, the use of enantiopure transition metal catalysts may contribute with several advantages to the chemical transformation, such as atom economy in the chemical transformation, simplicity in large scale reactions, energy-saving, minimal by-product formation, and due to the generally low catalyst loadings, lower cost.[9b]

The critical step in most asymmetric transition metal-based catalytic processes is the formation of a supramolecular system around a metal center involving the substrate(s), the metal precursor and an enantiopure molecule (*the chiral ligand*). The ligand is generally bound to the metal center through several functional groups. In this supramolecular system, the metal center provides a low-energy reaction pathway that enables catalysis, whereas the enantiomerically pure ligand enables preferential recognition of one of the enantiotopic elements of the substrate. Figure 3 illustrates a general example of an asymmetric transition metal-based transformation.

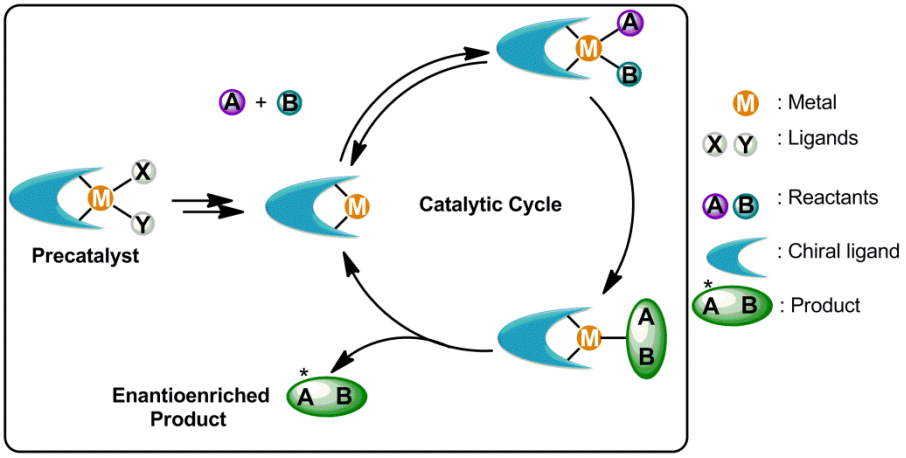

Figure 3. Schematic representation of a catalytic enantioselective process.

Ligand tuning has been successfully employed to develop efficient catalytic systems for diverse substrates/reagents in a given transformation.[10] The principle in this strategy for developing efficient enantioselective catalysts is to design enantiopure ligands that incorporate several independent modules or molecular fragments arranged around a carbon backbone. Stereogenic elements of different nature are incorporated into the molecular fragments and/or modules. Such modules are designed to influence the catalytic center: the steric and electronics of the different

molecular fragments are considered the *input parameters* for catalyst optimization. Selective modification of these parameters based on mechanistic insight, molecular recognition principles, or the intuition of chemists themselves has yielded higher-performing catalytic systems in terms of conversion, enantioselectivity and/or substrate scope.

During the last few decades, significant attention has been dedicated to the asymmetric hydrogenation of substrates containing prochiral elements (*e.g.* C=C, C=N or C=O double bonds), mostly catalyzed by enantiopure Rh-, Ir-, and Ru-coordination compounds (mostly phosphorus-containing derivatives). Efficient Rh-, Ir- or Ru-based catalysts have been developed for the asymmetric hydrogenation of a structurally diverse array of C=C-, C=O- or C=N-containing substrates (Figure 4). Thus, asymmetric hydrogenation can certainly be considered as one of the most reliable methodologies in asymmetric catalysis.[11]

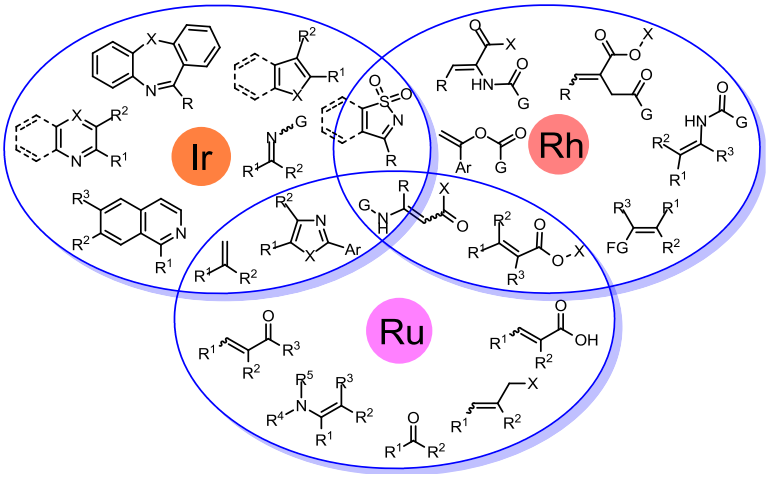

Figure 4. Rh-, Ir- and Ru-mediated asymmetric hydrogenations.

Phosphine-phosphite (P–OP) ligands are one of the examples of non-symmetric bidendate ligands that differ in the electronic and steric properties of their P-binding groups. Since the reports of the seminal

phosphine-phosphite ligands developed by Takaya[12] and Pringle,[13] several other related ligands have been described. These P–OP ligands encompass diverse carbon backbones and stereogenic elements as well as different distances between the two phosphorus functionalities.[14]

Our research group has developed a highly modular synthesis for 1,2-P–OP ligands containing two stereogenic carbons between the two phosphorus functionalities. The combination of the modular nature of the developed 1,2-P–OP ligands with a ligand-tuning methodology guided by computational analysis has led to highly efficient catalytic systems derived from 1,2-P–OP ligands for asymmetric hydrogenation. A series of 1,2-P–OP ligands based on the use of enantiomerically pure epoxides as starting materials (Sharpless epoxy ethers) has been prepared (see Scheme 1). The ligand synthesis starts with the ring-opening of the epoxide with a nucleophilic trivalent phosphorus derivative (Step A, Scheme 1) and continued with the *O*-phosphorylation of the phosphino alcohol intermediate with trivalent phosphorus electrophiles (*i.e.* a chlorophosphite derived from an enantiomerically pure diol; Step B). As regards to Step A (Scheme 1), the ring-opening proceeded smoothly at –30 ºC to room temperature. The ring-opened product, which proved to be rather prone to oxidation, was protected *in situ* as the corresponding borane adduct in order to make handling and storage easier. The corresponding borane complexes were isolated in high yield after column chromatography as air-stable solids.[15] In Step B, the free phosphino alcohol was obtained by cleavage of the borane adduct, using 1,4-diazabicyclo[2.2.2]octane (DABCO, 2.2 equiv.) at 60 ºC in toluene for two hours. After removing excess of DABCO by a short chromatographic filtration through SiO_2 under inert atmosphere, the free phosphino alcohol was transformed into a set of P–OP ligands by derivatization with the required chlorophosphite (1.1 equiv.) in the presence of a base (2.0 equiv. of NEt_3). The final P–OP

ligands were obtained in good yields after a careful chromatographic purification over neutral Al_2O_3 under an inert atmosphere.[16]

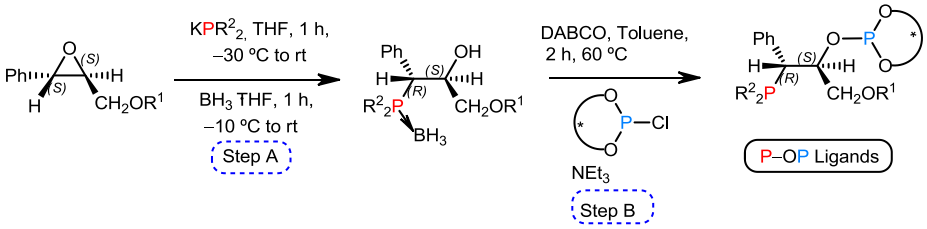

Scheme 1. Synthesis of P–OP ligands from Sharpless epoxy ethers.

By the commencement of the research work presented in this Thesis, efficient P–OP ligands (see Figure 5) had been developed for Rh-mediated asymmetric hydrogenation of functionalized alkenes (Ligands **L1**, **L3** and **L4**)[16a,b,d,e,f] and Ir-mediated asymmetric hydrogenation of C=N-containing compounds (Ligand **L2**).[17]

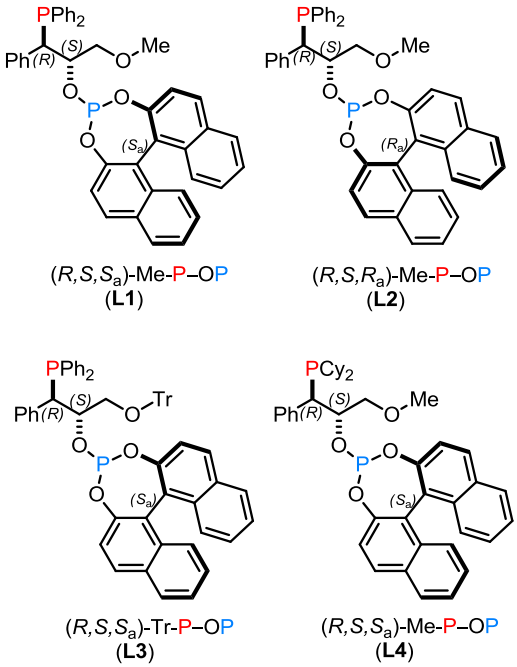

Figure 5. Highest performing P–OP ligands for asymmetric hydrogenations.

These bidentate P–OP ligands were able to form stable, well-defined cationic rhodium(I) complexes. These complexes were prepared in good yields by reacting stoichiometric amounts of the chiral phosphine–phosphite ligands and $[Rh(nbd)_2]BF_4$ in dichloromethane. The desired complexes were completely characterized by standard analytical techniques (NMR and HRMS). Furthermore, single crystals of the complexes suitable for X-ray diffraction were obtained, thereby unambiguously confirming a six-membered chelating coordination mode of the P–OP ligands to the Rh center.[16b]

In the evaluation of the activity and selectivity in rhodium-mediated asymmetric hydrogenations, the reactions were performed using rhodium-P–OP complexes generated *in situ* from 1.0 mol % of $[Rh(nbd)_2]BF_4$ and a 10 mol % excess of the P–OP ligand with respect to Rh precursor, under 20 bar H_2. Ligand **L1**, which contained a phosphite group derived from (S_a)-BINOL (BINOL = [1,1'-binaphthalene]-2,2'-diol), afforded excellent results with complete conversions and up to 99% ee. The ligand **L2**, whose only difference with respect to **L1** is the opposite configuration of the phosphite group, provides the opposite absolute configuration of the hydrogenated product, though with lower enantioselectivities. This is an indication that the direction of stereo-discrimination in rhodium-mediated hydrogenations is predominantly controlled by the binaphthyl group and that **L1** contains the matched combination of stereogenic elements in the structure of the ligand. The ligand **L1** proved to be highly efficient in the Rh-catalyzed asymmetric reduction of a wide variety of functionalized alkenes (see Scheme 2), including α-(acylamino)acrylates, itaconic acid derivatives and analogues, α-substituted enol ester derivatives and α-arylenamides.[16a,b,f] Furthermore, the "lead" ligand (**L1**) tolerates a broad range of carbamate-type amino-protecting groups (Boc, Cbz, and Fmoc).[16b] A substrate-to-catalyst ratio (S/C) up to 10000:1 provided fully

hydrogenated dimethyl itaconate, with no loss in conversion or enantioselectivity with respect to higher catalyst loadings.[16f]

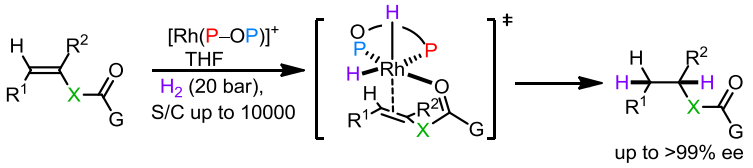

α-(acylamino)acrylates: (XC(O)G = NHAc, NHBoc, NHCbz, NHFmoc, 2-oxopyrrolidin-1-yl; R^1 = H, alkyl, alkoxy, aryl; R^2 = CO_2H, CO_2Me), 31 examples.
itaconic acid derivatives and analogues: (XC(O)G = CH_2CO_2H, CH_2CO_2Me, CH_2CONH_2, CH_2OH; R^1 = H; R^2 = CO_2H, CO_2Me, CO_2Et), 7 examples.
α-substituted enamides: (XC(O)G = NHAc; R^1 = H; R^2 = alkyl, aryl), 10 examples.
α-arylenol acetates: (XC(O)G = OAc, OBz; R^1 = H; R^2 = aryl, $PO(OMe)_2$), 11 examples.

Scheme 2. Rh-mediated asymmetric hydrogenation of functionalized alkenes.

In addition to ligand **L1**, ligand **L3** (see Figure 5) incorporating a triphenylmethoxy group at the R^1-oxy position (see Scheme 1) of the carbon backbone was also very efficient in the Rh-mediated asymmetric hydrogenation of functionalized alkenes, offering slightly higher enantioselectivities for particular substrates.[16d,f]

The highly modular design of the P–OP ligands enabled the optimization of the catalytic systems by modifying the steric and electronic properties of the phosphino functionality. Our research group developed a convenient synthetic route for the preparation of cationic rhodium complexes, in which the PPh_2 moiety had been replaced by the electron-richer PCy_2 group. The preformed Rh-precatalyst derived from **L4** gave excellent enantioselectivities (up to 99% ee) and catalytic activities (>2500 TON) for a wide array of substrates. Our synthetic methodology was successfully applied for the first time to the enantioselective hydrogenation of β-alkoxy-substituted α-(acylamino)acrylate derivatives, which allowed the efficient preparation, with total selectivity and perfect enantioselectivity (*i.e.* 99% ee), of an advanced synthetic intermediate of the antiepileptic drug (*R*)-lacosamide (*i.e.* Vimpat®).[16e]

In short, P–OP ligands **L1**, **L3** and **L4** containing (S_a)-configured BINOL-derived phosphite groups (Figure 5) proved to be the highest performing ligands for the Rh-mediated asymmetric hydrogenation of functionalized alkenes with high enantioselectivities (up to >99%) for a wide variety of functionalized alkenes. The catalytic systems derived from these P–OP ligands provided straightforward access to enantiomerically pure (or highly enantioenriched) α-amino acid, carboxylic acid, amine and alcohol derivatives that are highly valuable building blocks for the preparation of more complex molecules. It is also noteworthy to mention that our methodology has been successfully applied to the enantioselective synthesis of a number of intermediates of active pharmaceutical ingredients (or APIs) by asymmetric hydrogenation.[16d]

Besides the efficient application of P–OP ligands in the Rh-mediated asymmetric hydrogenation of functionalized alkenes, the group's attention was also shifted to use the P–OP ligands in Ir-catalyzed asymmetric hydrogenations of C=N-containing derivatives.

The P–OP ligands were also able to form well-defined neutral iridium(I) complexes [Ir(Cl)(cod)(P–OP)] by mixing stoichiometric amounts of the iridium precursor ([{Ir(μ-Cl)(cod)}$_2$]) and the P–OP ligand (see Scheme 3). Although attempts to isolate these complexes have repeatedly been unsuccessful, the *in situ* generated iridium(I) complexes [Ir(Cl)(cod)(P–OP)] have been successfully used in asymmetric hydrogenation of *N*-containing heterocyclic compounds.

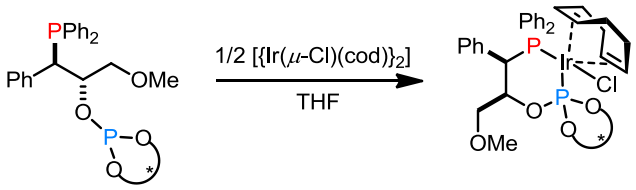

Scheme 3. Preparation of [Ir(Cl)(cod)(P–OP)] complexes derived from phosphine-phosphite ligands.

The catalytic activity and selectivity of such complexes in the hydrogenation of *N*-containing heterocyclic compounds was evaluated. Interestingly, the ligand **L2** was the best performing ligand in the reduction of 2-methylquinoline as model substrate. Several additives were tested for the reduction of 2-methylquinoline catalyzed by [Ir(Cl)(cod)(**L2**)] and, remarkably, the addition of 10 mol % of anhydrous HCl facilitated the reaction by increasing the conversion.[17a]

The Ir-precatalyst derived from ligand **L2**, in combination with catalytic amounts of anhydrous HCl, gave excellent enantioselectivities (up to 92% ee) in the hydrogenation of a set of structurally diverse quinolines (9 examples). 2-Methyl-substituded quinoxaline was also enantioselectively hydrogenated under the same conditions with ligand **L1** to afford the hydrogenated compound in 70% ee.[17a]

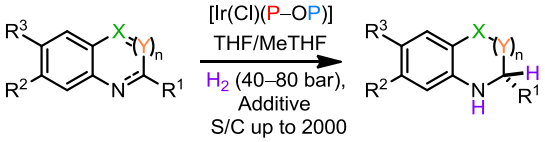

quinolines (X = CH; Y = CH; n = 1; R^1 = alkyl, aryl; R^2 = H; R^3 = H, halogen, alkyl, alkoxy), 9 examples.
quinoxalines (X = N; Y = CH; n = 1; R^1 = alkyl; R^2 = H; R^3 = H), 1 example.
benzoxazines (X = O; Y = CH_2; n = 1; R^1 = aryl; R^2 = H, halogen; R^3 = H), 8 examples.
benzoxazinones (X = O; Y = CO; n = 1; R^1 = aryl; R^2 = H, halogen, alkyl; R^3 = H), 5 examples.
benzothiazinones (X = S; Y = CO; n = 1; R^1 = aryl; R^2 = H; R^3 = H), 3 examples.
quinoxalinones (X = NH, N(alkyl), N(alkoxy); Y = CO; n = 1; R^1 = alkyl, aryl; R^2 = H, halogen, alkyl; R^3 = H, halogen, alkyl), 9 examples.
indoles (X = CH; n = 0; R^1 = alkyl; R^2 = H; R^3 = H, halogen, alkyl; X-R^1 = -$(CH_2)_4$-), 6 examples.

Scheme 4. Ir-(P–OP**)** catalyzed asymmetric hydrogenation of *N*-containing heterocyclic compounds.

Furthermore, the "lead" precatalyst [Ir(Cl)(cod)(**L2**)] was also successfully employed for the asymmetric hydrogenation of other types of C=N-containing heterocyclic compounds.[17b] Benzoxazines (see Scheme 4 for the structures) were efficiently hydrogenated with full conversion and up to 95% ee in THF at room temperature under 40 bar of H_2 using 0.5 mol % of [Ir(Cl)(cod)(**L2**)] as the precatalyst (8 examples). In contrast, their carbonyl-containing analogs (*i.e.* benzoxazinones) required higher pressure (80 instead of 40 bar H_2) and catalyst loadings (2 mol % instead of 0.5 mol %). Under such conditions the corresponding hydrogenated products were obtained with excellent enantioselectivities (up to 99% ee; 5 examples). By using the same reaction conditions, benzothiazinone derivatives (see Scheme 4 for the structures) were efficiently hydrogenated with full conversion and in up to 96% ee (3 examples). Quinoxalinones were also efficiently hydrogenated (conversions ranging from 89 to 99%, ee values ranging from 90 to 99%, 9 examples) at lower pressure and lower catalyst loading than their sulfur containing analogs. Remarkably, the catalytic system tolerates diverse substitution patterns at the trivalent nitrogen with excellent enantioselectivities (up to 99% ee): either no protecting group or a wide variety of protecting groups, including Me, MOM, and Bn substituents. Furthermore, the *N*-methyl substituted derivative was hydrogenated with a catalyst loading as low as 0.05 mol % with almost complete conversion (96%) and perfect enantioselectivity (99% ee).[17b]

An additional application of the already mentioned iridium-derived catalytic system has also been developed for the asymmetric hydrogenation of an array of diversely substituted indoles (see Scheme 4 for the structures).[17c] The synthetic strategy required the use of stoichiometric amounts of a Brønsted acid to break indole's aromaticity and facilitate the hydrogenation of the indole's five-membered ring. The optimized conditions implied the use of the environmentally friendly solvent 2-

methyltetrahydrofuran (MeTHF). Unprotected indoles have been efficiently converted to enantiomerically enriched indolines (up to 91% ee; 6 examples) by a stepwise process: Brønsted acid-mediated C=C isomerization followed by the enantioselective hydrogenation of the resulting C=N bond using the above mentioned iridium catalyst. The research group also developed a "greener" hydrogenation alternative that involved the use of reusable heterogeneous additives (solid-supported sulfonic acids). Results were comparable to those obtained with the homogeneous catalyts derived from ligand **L2**.[17c]

As summarized in this introduction, efficient P–OP ligands containing BINOL-derived phosphite fragments had been developed and successfully applied by our research group in rhodium- and iridium-mediated asymmetric hydrogenations. However, the synthesis of the highest performing P–OP ligands for rhodium- and iridium-mediated asymmetric hydrogenations had only been developed for multi-milligram amounts of the ligand. Moreover, the developed synthetic protocols involved chromatographic purifications that had to be performed in a very careful way under inert conditions. We considered that it would be highly interesting to develop a practical method for the preparation of rhodium complexes of the highest performing P–OP ligands in gram amounts, as the "asymmetric catalytic community" could in this way gain easy access to our precatalysts for enantioselective hydrogenations and benefit by applying them to their own transformations of interest.

Iridium-mediated asymmetric hydrogenation studies of C=N-containing heterocycles had been restricted by our group to five- and six-membered heterocyclic derivatives. Although nitrogenated seven-membered heterocyclic motifs with stereogenic centers constitute an important pharmacophore, examples of asymmetric reduction of seven-membered

heterocyclic derivatives were scarce in the literature by the commencement of the research work presented in this Thesis.

Furthermore, no reports on the effects of TADDOL-derived phosphite groups [TADDOL = (2,2-dimethyl-1,3-dioxolane-4,5-diyl)bis(diphenyl-methanol)] and biaryl-containing phosphite groups with substituents at the 3 and 3' positions of the [1,1'-biaryl]-2,2'-diol motif on the enantioselectivity of the rhodium- and iridium-mediated hydrogenations had been published at the beginning of the research work presented in this Thesis.

Therefore, the general aims of this thesis are:

1. To optimize and develop a chromatography-free and practical preparation method for the best performing $[Rh(P–OP)]^+$ catalysts applied in various enantioselective hydrogenative transformations.
2. To expand the scope of iridium-(P–OP)-mediated asymmetric hydrogenations to new C=N-containing heterocyclic systems (*i.e.* seven-membered C=N-containing heterocyclic systems).
3. To prepare new P–OP ligands with TADDOL- and 3,3'-disubstituted-BINOL-derived phosphite groups and study their catalytic performance in iridium- and rhodium-mediated asymmetric hydrogenations.

References:

(1) Flügel, R. M.; *Chirality and Life: A Short Introduction to the Early Phases of Chemical Evolution*; Springer-Verlag: Berlin, Heidelberg, 2011.
(2) Almost all carbohydrates contain stereogenic carbons. Monomeric sugars (*i.e.* monosaccharides) of natural origin belong to the D-series: the stereogenic carbon furthest from the carbonyl group has the same absolute configuration as the one in D-(+)-glyceraldehyde ((*R*)-(+)-2,3-dihydroxypropanal).
(3) Schneider, P.; Hawser, S.; Islam, K. *Bioorg. Med. Chem. Lett.* **2003**, *13*, 4217.
(4) Evans, A. M. *Clin. Rheumatol.* **2014**, *20*, 9.
(5) Lim, S.-A. *Ann. Acad. Med. Singapore* **2006**, *35*, 274.
(6) Donald, T. H.; Bingyun, L. *Chiral Drug Separation*. In *Encyclopedia of Chemical Processing*, Lee, S., Ed.; Taylor & Francis: New York, 2007.
(7) (a) *Catalytic Asymmetric Synthesis*, Ojima, I., Ed.; VCH Publishers, Cambridge, 1993. (b) Noyori, R. *Asymmetric Catalysis in Organic Synthesis*, Noyori, R., Ed.; John Wiley and Sons, New York, 1999. (c) *Comprehensive Asymmetric Catalysis*, Jacobsen, E. N., Pfaltz, A., Yamamoto, H., Eds.; Springer, New York, 1999. (d) Walsh, P. J. Kozlowski, M. C. In: *Fundamentals of Asymmetric Catalysis*, University Science Books, 2009. (e) *Comprehensive Chirality*, Vol 1–9, Carreira, E M and Yamamoto, H. Eds.; Elsevier B.V, Oxford, UK, 2012.
(8) Sandoval, C. A.; Noyori, R. In *An Overview of Recent Developments in Metal-Catalyzed Asymmetric Transformations*; Wiley-VCH Verlag GmbH & Co. KGaA: Weinheim, Germany, 2012, pp 335.
(9) (a) Knowles, W. S. *Angew. Chem., Int. Ed.* **2002**, *41*, 1998. (b) Noyori, R. *Angew. Chem., Int. Ed.* **2002**, *41*, 2008. (c) Sharpless, K. B. *Angew. Chem., Int. Ed.* **2002**, *41*, 2024.
(10) (a) Rajanbabu, T. V.; Casalnuovo, A. L.; Ayers, T. A. *Adv. Catal. Processes* **1997**, *2*, 1. (b) RajanBabu, T. V.; Casalnuovo, A. L.; Ayers, T. A.; Nomura, N.; Jin, J.; Park, H.; Nandi, M. *Curr. Org. Chem.* **2003**, *7*, 301.
(11) See for example: (a) Shang, G.; Li, W.; Zhang, X. In *Transition Metal-Catalyzed Homogeneous Asymmetric Hydrogenation*, John Wiley & Sons, Inc.: Hoboken, NJ, USA, 2010, pp 343. (b) Fleury-Bregeot, N.; de la Fuente, V.; Castillón, S.; Claver, C. *ChemCatChem* **2010**, *2*, 1346. (c) Xie, J.-H.; Zhu, S.-F.; Zhou, Q.-L. *Chem. Rev.* **2011**, *111*, 1713. (d) Imamoto, T. In *Asymmetric Hydrogenation*, InTech, 2012, pp 3.
(12) Sakai, N.; Mano, S.; Nozaki, K.; Takaya, H. *J. Am. Chem. Soc.* **1993**, *115*, 7033.
(13) Baker, M. J.; Pringle, P. G. *J. Chem. Soc., Chem. Commun.* **1993**, 314.
(14) Fernández-Pérez, H.; Etayo, P.; Panossian, A.; Vidal-Ferran, A. *Chem. Rev.* **2011**, *111*, 2119.
(15) Fernández-Pérez, H.; Etayo, P.; Núñez-Rico, J. L.; Balakrishna, B.; Vidal-Ferran, A. *RSC Adv.* **2014**, *4*, 58440.
(16) (a) Fernández-Pérez, H.; Pericàs, M. A.; Vidal-Ferran, A. *Adv. Synth. Catal.* **2008**, *350*, 1984. (b) Fernández-Pérez, H.; Donald, S. M. A.; Munslow, I. J.; Benet-Buchholz, J.; Maseras, F.; Vidal-Ferran, A. *Chem. –Eur. J.* **2010**, *16*,

6495. (c) Panossian, A.; Fernández-Pérez, H.; Popa, D.; Vidal-Ferran, A. *Tetrahedron: Asymmetry* **2010**, *21*, 2281. (d) Etayo, P.; Núñez-Rico, J. L.; Fernández-Pérez, H.; Vidal-Ferran, A. *Chem. –Eur. J.* **2011**, *17*, 13978. (e) Etayo, P.; Núñez-Rico, J. L.; Vidal-Ferran, A. *Organometallics* **2011**, *30*, 6718. (f) Núñez-Rico, J. L.; Etayo, P.; Fernández-Pérez, H.; Vidal-Ferran, A. *Adv. Synth. Catal.* **2012**, *354*, 3025.

(17) (a) Núñez-Rico, J. L.; Fernández-Pérez, H.; Benet-Buchholz, J.; Vidal-Ferran, A. *Organometallics* **2010**, *29*, 6627. (b) Núñez-Rico, J. L.; Vidal-Ferran, A. *Org. Lett.* **2013**, *15*, 2066. (c) Núñez-Rico, J. L.; Fernández-Pérez, H.; Vidal-Ferran, A. *Green Chem.* **2014**, *16*, 1153.

CHAPTER-1

A Practical Synthesis of Rhodium Precatalysts for Enantioselective Hydrogenative Transformations

Table of Contents:

A Practical Synthesis of Rhodium Precatalysts for Enantioselective Hydrogenative Transformations

Bugga Balakrishna,[†] Anton Vidal-Ferran*[,†,‡]

[†] Institute of Chemical Research of Catalonia (ICIQ), Avinguda Països Catalans 16, E-43007, Tarragona, Spain.

[‡] Catalan Institution for Research and Advanced Studies (ICREA), Passeig Lluís Companys 23, E-08010, Barcelona, Spain.

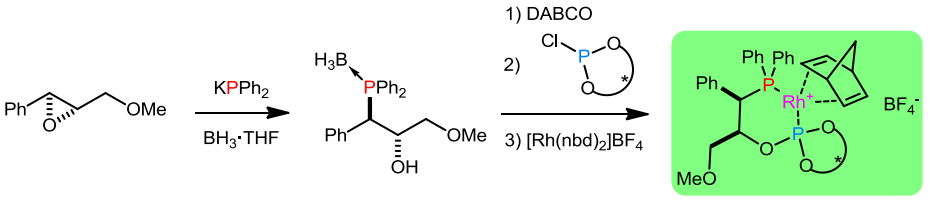

Practical two-step synthesis of *rhodium hydrogenation precatalysts*
(52–95% overall yield) in gram amounts

1.1 Abstract

Herein is described a practical method of preparing enantiopure rhodium(I) complexes that can be used as efficient catalysts for the asymmetric hydrogenation of functionalized alkenes, the hydrogenative kinetic resolution of vinyl sulfoxides and the desymmetrization of achiral dienes. All these rhodium precatalysts incorporate enantiopure phosphine-phosphite (P–OP) ligands as stereochemical directors of the hydrogenative transformations. The synthetic route starts with the ring-opening of an enantiopure Sharpless epoxy ether with a phosphorus nucleophile followed by isolation of the borane-protected phosphino alcohol derivative by

crystallization. The subsequent cleavage of this borane complex, the *O*-phosphorylation of the resulting phosphino alcohol with the corresponding phosphorus electrophiles (chlorophosphite derivatives), and finally the complexation of the *in situ* generated P–OP ligands with $[Rh(nbd)_2]BF_4$, followed by crystallization, rendered the target precatalysts.

1.2 Introduction

The regulatory demands and environmental requests faced by the chemical and pharmaceutical industries have fueled the application of catalytic enantioselective methods for the preparation of biologically relevant compounds at the industrial level. Asymmetric hydrogenation can be considered a well-established synthetic methodology that has already been incorporated into the standard "tool-box" of industrial chemists.[1] This transformation is considered a convenient method for the preparation of enantioenriched compounds, as catalytic amounts of a coordination compound (mainly Rh, Ru and Ir complexes) incorporating an enantiopure ligand (mostly phosphorus-containing derivatives[2]) mediate the addition of dihydrogen to prochiral C=C, C=N or C=O bonds with high yields and enantioselectivities.[3] Furthermore, hydrogenation reactions can easily be scaled up at an industrial level as chemical companies have developed safe hydrogenation protocols.[1a] Despite the remarkably advanced state of the field, research efforts are still directed towards catalytic systems with higher activity and stereoselectivity. In other cases, researchers seek to improve the industrial profile of hydrogenation catalysts by developing easier preparation methods and by making sure they do not fall within the claims of any patent currently in force.

1.3 Results and Discussion

Our group has previously developed an array of structurally diverse P–OP ligands based on the use of enantiomerically pure Sharpless epoxy ether **1** as a starting material, which is transformed into the final ligands in two steps: ring-opening of the epoxide with a nucleophilic trivalent phosphorus derivative (Step A, Scheme 1) followed by *O*-phosphorylation of the phosphino alcohol intermediate with trivalent phosphorus electrophiles (*i.e.* a chlorophosphite derived from an enantiomerically pure diol; Step B, Scheme 1). As regards Step A (Scheme 1), the ring-opening proceeded smoothly at –30 ºC to room temperature. The ring-opened product, which proved to be rather prone to oxidation, was protected *in situ* as the corresponding borane adduct **2** in order to make handling and storage easier. Borane complex **2** was isolated in high yield after column chromatography as a crystalline[4] and air-stable solid. In Step B (Scheme 1), the free phosphino alcohol was obtained by cleavage of the borane adduct **2**, using 1,4-diazabicyclo[2.2.2]octane (DABCO, 2.2 equiv.) at 60 ºC in toluene for two hours.[5] After removing excess DABCO by a short chromatographic filtration through SiO_2 under an inert atmosphere, the free phosphino alcohol was transformed into P–OP ligands by derivatization with the required chlorophosphite (1.1 equiv.) in the presence of a base (2.0 equiv. of NEt_3).[5] The final P–OP ligands were obtained in good yields after a careful chromatographic purification over neutral Al_2O_3 under an inert atmosphere.[6]

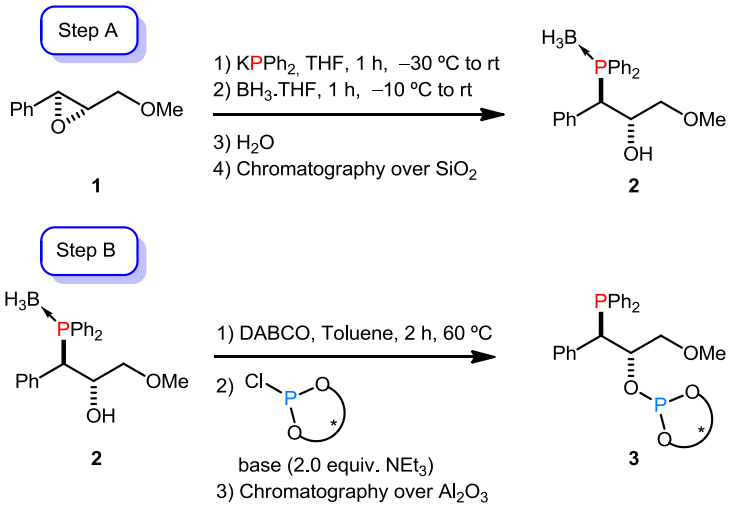

Scheme 1. Conventional synthetic strategy for the preparation of P–OP ligands.

We have also demonstrated the general ability of P–OP ligands to form suitable rhodium(I) precatalysts for hydrogenative reactions by reacting ligands **3** and $[Rh(nbd)_2]BF_4$ (nbd = norbornadiene).[6c,d,g,h] The $[Rh(nbd)(P–OP)]BF_4$ complexes were quantitatively formed in solution and could be isolated, if desired, by crystallization. For the sake of convenience, we have almost exclusively performed the asymmetric hydrogenations using $[Rh(nbd)(P–OP)]BF_4$ complexes, which had been generated *in situ* from $[Rh(nbd)_2]BF_4$ and a 10 mol % excess of the the P–OP ligand **3**, with respect to rhodium precursor.

Interestingly, P–OP-based rhodium precatalysts **4a–c** efficiently mediated three different types of hydrogenative transformations providing high catalytic activities and enantioselectivities (up to 99% ee, Scheme 2). These transformations encompass the hydrogenation of functionalized alkenes[6] (see structure **5** in Scheme 2), the hydrogenative kinetic resolution of racemic vinyl sulfoxides[7] (substrates **7** in Scheme 2) and the hydrogenative desymmetrization of achiral dienes[8] (substrates **9** in Scheme

2). Taking these results into account, we considered that by developing a practical method for the preparation of complexes **4a–c** in gram amounts, the "asymmetric catalytic community" could gain easy access to our precatalysts for enantioselective hydrogenations and benefit by applying them to their own transformations of interest. Thus, we describe herein our efforts to develop and optimize a practical preparation method for rhodium precatalysts **4a–c**.

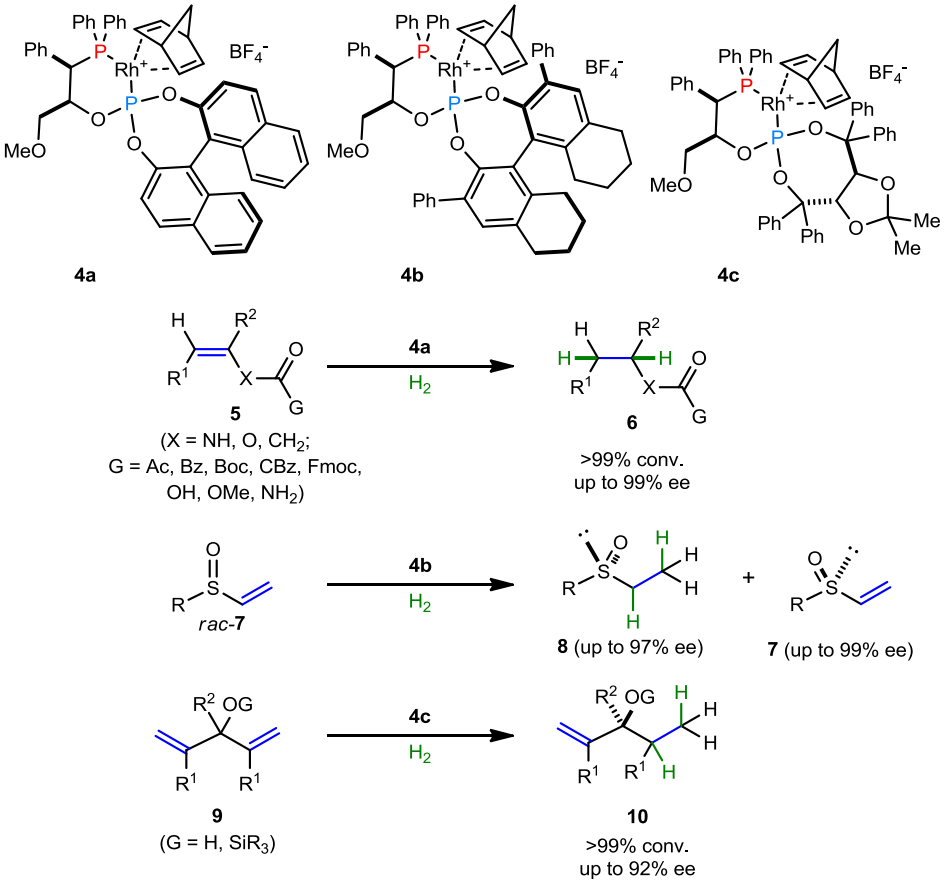

Scheme 2. Lead P–OP-based rhodium precatalysts for enantioselective hydrogenative transformations.

For the optimization of the ring-opening step (Step A in Scheme 1), we took advantage of the crystallinity of compound **2** and developed crystallization conditions for isolating the target compound.

Research activities in this field within this PhD thesis have allowed for the growth of single crystals of phosphine-borane alcohol **2** and analysis of its structure by X-ray diffraction. These studies have confirmed previously published results[9] on the regio- and absolute stereo-chemistry of the products derived from the ring-opening of *trans*-epoxides: *anti*-arrangement of the hydroxyl and phosphino functionalities, arising from a stereospecific S_N2 epoxide ring-opening (inversion of the absolute configuration at the attacked carbon, and retention at the other one). This recently obtained crystallographic information is included herein and can be found in the Experimental Section. Thus, ring-opening was basically performed under the same conditions as those previously used in the group (molar ratio of $KPPh_2$:**1**:BH_3 = 1:1.02:3).[4,6a] After an aqueous work-up of the reaction mixture, product **2** was extracted, dried and recrystallized from a *n*-hexane:EtOAc mixture (see Experimental Section for details). The solution containing product **2** was filtered while hot and the product was isolated as a crystalline material after leaving it standing at 5 ºC for a few hours (86% yield). Both the yield and the spectroscopic data were in agreement with those previously reported[4,6a,6b] using the usual synthetic protocol[6a–g] that involves a chromatographic purification over SiO_2 (80% average yield for 6 experiments).

Next, we envisaged that the preparation of the target rhodium precatalysts **4a–c** could be accomplished in three consecutive synthetic steps starting from the borane-protected phosphino alcohol **2** (Scheme 3): first, borane cleavage; second, *O*-phosphorylation; and last, complexation with $[Rh(nbd)_2]BF_4$ as the metal precursor, where we planned to use this rhodium derivative as the limiting reagent of the synthetic sequence. We

also decided to perform these three steps with no chromatographic separation as we expected to be able to isolate complexes **4a–c** by crystallization.

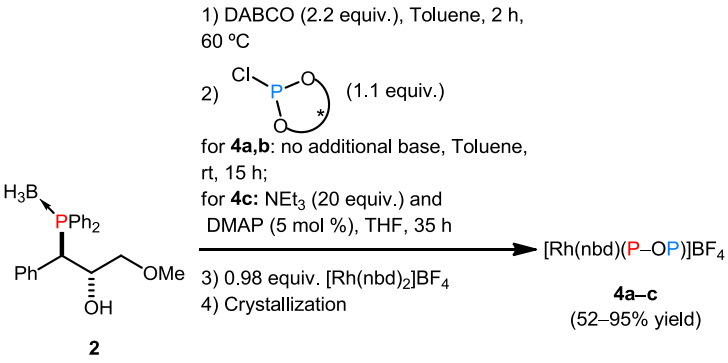

Scheme 3. Preparation of [Rh(nbd)(P–OP)]BF_4 complexes **4a–c**.

Regarding borane cleavage, the free phosphino alcohol was quantitatively obtained by deprotection of **2** using DABCO (2.0 equiv.) in toluene at 60 ºC for 2 hours. The *in situ* generated phosphino alcohol was subsequently derivatized by treatment with the corresponding chlorophosphites (1.1 equiv.). In particular, for the chlorophosphites leading to rhodium complexes **4a** and **4b**, no additional base was required for achieving complete *O*-phosphorylation. DABCO, which was present in excess in the reaction media from the borane-cleavage step, sufficed for quantitatively mediating the reaction between the free phosphino alcohol and the chlorophosphite. However, the reaction of the free diphenylphosphino alcohol with the chlorophosphite leading to **4c** proceeded in THF at a slower rate and required the addition of a base (NEt_3, 20 equiv. with respect to the chlorophosphite) and catalytic amounts of *N*,*N*-dimethylpyridin-4-amine (DMAP, 5 mol %).[10] In all cases, the *O*-phosphorylation reactions were monitored by ^{31}P NMR spectroscopy in

order to optimize the reaction times (see experimental procedures for details).

The *O*-phosphorylation reaction mixtures toward complexes **4a** and **4b** were filtered through a short SiO_2 pad. The resulting material was allowed to react with $[Rh(nbd)_2]BF_4$ (*ca*. 0.98 equiv. with respect to the amount of P–OP ligand, which was roughly estimated by integration of the ^{31}P NMR spectra). The Rh-(P–OP) complexes **4a** and **4b** were isolated by crystallization in 77% and 95% overall yield respectively (referring to the amount of Rh-precursor). For the preparation of complex **4c**, a slightly modified procedure was followed. In this case the ligand was purified by crystallizing most of the *P*-containing impurities out of the solution after removing the solvents from the *O*-phosphorylation step. A complexation process analogous to that previously described was then followed (52% yield, see experimental procedures for details).

The $^{31}P\{^1H\}$ NMR spectra of **4a–c** showed two sharp doublets of doublets at around 29 ppm (phosphino group) and 135 ppm (phosphite group) for each rhodium complex. The multiplicity of phosphorus signals is due to a direct $^{31}P–^{103}Rh$ coupling (average $^1J_{P\text{-}Rh} \approx 266$ Hz for phosphite and $^1J_{P\text{-}Rh} \approx 146$ Hz for phosphine groups) along with a geminal $^{31}P–^{31}P$ coupling (average $^2J_{P\text{-}P} \approx 68$ Hz). The rest of the NMR data and HRMS measurements unequivocally confirmed the structure of rhodium complexes **4a–c**.

1.4 Experimental Section

All manipulations and reactions were run under inert atmosphere using anhydrous solvents in either a glove box or with standard Schlenck-type techniques. All solvents were dried by using a Solvent Purification System (SPS). ^1H NMR and $^{13}C\{^1H\}$ NMR chemical shifts are quoted in ppm

relative to residual solvent peaks, whereas $^{31}P\{^{1}H\}$ or ^{31}P NMR chemical shifts are quoted in ppm relative to 85% phosphoric acid in water. $^{11}B\{^{1}H\}$ NMR and $^{19}F\{^{1}H\}$ NMR chemical shifts are quoted in ppm relative to $BF_3{\cdot}OEt_2$ in $CDCl_3$. High resolution mass spectra (HRMS) were recorded by using the ESI ionization method in positive mode. Melting points were measured in open capillaries and are uncorrected.

Preparation of 2. A solution of $KPPh_2$ in THF (15.7 mmol, 31.4 mL of a 0.5 M solution) was added dropwise under Ar to a cooled solution (–30 ºC) of **1** (16.0 mmol, 2.623 g) in dry THF (50 mL). The mixture was stirred for 1 h at this temperature and then slowly allowed to reach rt and stirred for one additional hour. The mixture was then cooled at –10 ºC and BH_3•THF (47.0 mmol, 47 mL of a 1 M solution) was added dropwise. The mixture was stirred for 1h at this temperature and then allowed to reach rt and stirred for one further hour. The reaction mixture was quenched with water (50 mL) and the two phases were separated. The aqueous phase was extracted with EtOAc (3 × 50 mL). The combined organic phases were washed with brine (2 × 50 mL), dried over $MgSO_4$ and concentrated under reduced pressure. The resulting residue was re-dissolved in *n*-hexane:EtOAc (70:30, 75 mL, 10.9 mL per gram of crude mixture) while heating at 50 ºC. The solution was filtered while hot and allowed to stand overnight at 5 ºC. A white solid was formed, which was filtered, washed with hot *n*-hexane and dried *in vacuo* (3.826 g, 10.50 mmol, 66.9% yield). The mother liquors were concentrated *in vacuo* and the crystallization process was repeated in *n*-hexane:EtOAc (70:30, 25 mL, 12.4 mL per gram of crude mixture). The second fraction of compound **2** was obtained (1.106 g, 3.04 mmol, 19.3% yield). mp 108–110 °C (reported value:[6a] 117.1–117.6 ºC); $[\alpha]_D^{25}$ = –147.3 (*c* 0.1, $CHCl_3$) (reported value:[6a]

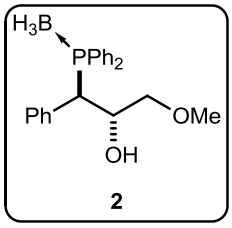

2

$[\alpha]_D^{25}$ = –154.2; *c* 1.0, $CHCl_3$). Spectroscopic data were in agreement with the reported ones.[6a]

Single crystal X-ray analysis of compound 2

X-ray Data: Single crystals of enantiopure compound **2** suitable for X-ray diffraction analysis were grown by slow diffusion of *n*-hexane into an EtOAc solution of the compound at room temperature.

Data collection: Crystal structure determination for **2** was carried out using a Apex DUO Kappa 4-axis goniometer equipped with an APPEX 2 4K CCD area detector, a Microfocus Source E025 IuS using $Mo_{K\alpha}$ radiation, Quazar MX multilayer Optics as monochromator and a Oxford Cryosystems low temperature device Cryostream 700 plus (T = –173 °C). Full-sphere data collection was used with ω and φ scans. Programs used: Data collection APEX-2,[11] data reduction Bruker Saint,[12] and absorption correction SADABS.[13]

Structure Solution and Refinement: Crystal structure solution was achieved using direct methods as implemented in SHELXTL [14] and visualized using the program XP. Absolute configuration was determined based on the Flack parameter.[15] Missing atoms were subsequently located from difference Fourier synthesis and added to the atom list. Least-squares refinement on F2 using all measured intensities was carried out using the program SHELXTL. All non-hydrogen atoms were refined including anisotropic displacement parameters.

Crystal data for 2: $C_{22}H_{26}BO_2P$, Mw = 364.21; monoclinic; space group $P2_1$, a = 9.3550(7) Å, b = 33.043(3) Å, c = 13.5151(11) Å, β = 107.899(2)°, V = 3975.6(5) Å³, Z = 8, ρcal = 1.217 Mg/m³, μ = 0.151 mm^{-1}, 52980 reflections were collected of which 20660 are unique (Rint = 0.0572), 18650 Fo > 4 σ(Fo), 1003 refined parameters, R1 [I > 2σ(I)] =

0.0554, wR2 [I > 2σ(I)] = 0.1304, Flack parameter: 0.06(6), Goodness of fit on F2 = 1.077, maximum residual electron density 0.553 (–0.326) e Å^3.

CCDC 931317 contains the supplementary crystallographic data for **2**. This data can be obtained free of charge from The Cambridge Crystallographic Data Centre via www.ccdc.cam.ac.uk/data_request/cif.

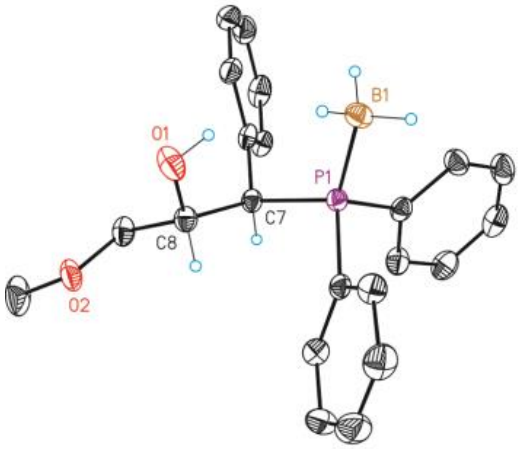

Figure 1. X-ray structure of **2** (ORTEP drawing showing thermal ellipsoids at 50% probability). Non-relevant hydrogen atoms have been omitted for clarity.

Synthesis of 4a. The phosphino-borane adduct **2** (1.046 g, 2.87 mmol) was azeotropically dried with 16 mL of toluene. DABCO (0.724 g, 6.45 mmol) was added to the residue and after three freeze-and-thaw cycles under Ar, 18 mL of toluene were syringed into the Schlenk tube containing compound **2** and DABCO. The solution was stirred for 2 h at 60 ºC. The residue was left to cool down to rt and a freshly prepared solution of the chlorophosphite[16] (1.108 g, 3.16 mmol, 36 mL of toluene) was added dropwise to the previous solution. The reaction mixture was left to stir for 15 h at rt. The reaction mixture was filtered through a short, dry, deoxygenated SiO_2 pad (5 mL) and the SiO_2 subsequently washed with dry toluene (2 × 6.0 mL). The filtrate was collected in a Schlenk flask under inert atmosphere and concentrated *in vacuo* to obtain a spongy white solid that corresponded to the raw phosphine-phosphite ligand (1.554 g, *ca*. 2.10 mmol, *ca*. 90% purity by integration of the signals of the ligand with respect to the rest of the signals in the ^{31}P NMR spectrum). A freshly prepared solution of the raw phosphine-phosphite ligand (1.554 g, *ca*. 2.10 mmol, 16 mL of dichloromethane) was slowly added to a solution of $[Rh(nbd)_2]BF_4$ (0.762 g, 2.04 mmol, 12 mL of dichloromethane) and stirred at rt for 4 h. After this period of time, 75% of the solvent amount was evaporated off *in vacuo*. Anhydrous Et_2O (24 mL) was carefully layered onto the remaining solution of the complex. With gradual stirring of the solution, an orange solid was formed. The mother liquors were filtered off and the residue was washed with anhydrous Et_2O (2 x 10 mL) and dried *in vacuo* to afford 1.49 g (1.57 mmol, 77% overall yield with respect to $[Rh(nbd)_2]BF_4$) of complex **4a** as an orange powder. mp 207–209 °C; $[\alpha]_D^{25}$ = +13.0 (*c* 0.1, THF). Spectroscopic data were in agreement with the reported ones.[6b]

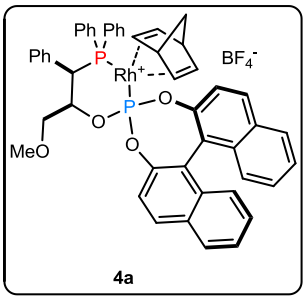

4a

Synthesis of 4b. The same protocol as for **4a** was used, with the following amounts of reagents (solvent amounts were adapted so that concentrations were the same): compound **2** (1.578 g, 4.33 mmol), DABCO (1.042 g, 9.29 mmol), chlorophosphite [17] (2.54 g, 4.97 mmol) and $[Rh(nbd)_2]BF_4$ (1.084 g, 2.90 mmol). A spongy white solid that corresponded to the raw phosphine-phosphite ligand (2.74 g, *ca*. 2.96 mmol, *ca*. 89% purity by integration of the signals of the ligand with respect to the rest of the signals in the ^{31}P NMR spectrum) was obtained. After following a crystallization process identical to that described above, 3.06 g (2.76 mmol, 95% overall yield with respect to $[Rh(nbd)_2]BF_4$) of complex **4b** as an orange powder were obtained. mp 224.3–226.3 °C; $[\alpha]_D^{25}$ = +52.7 (*c* 0.12, THF). ^1H NMR (400 MHz, CD_2Cl_2): δ = 8.02–8.00 (m, 2H, H_{arom}), 7.85–7.82 (m, 2H, H_{arom}), 7.72–7.30 (m, 14H, H_{arom}), 7.19–7.03 (m, 5H, H_{arom}), 6.71–6.61 (m, 4H, H_{arom}), 5.95 (bs, 1H, =C*H* vinylic, nbd), 5.41 (bs, 1H, =C*H* vinylic, nbd), 4.77 (bs, 1H, =C*H* vinylic, nbd), 4.42 (bs, 1H, =C*H* vinylic, nbd), 4.18 (bs, 1H, C*H* allylic, nbd), 3.88 (bs, 1H, C*H* allylic, nbd), 3.83–3.70 (m, 2H, C*H*-PPh_2 and C*H*-OPO), 3.07–2.92 (m, 7H, OCH_3 and 2 x CH_2 *o*-Ph-H8-BINOL), 2.80–2.61 (m, 3H, C*H*H-OMe and 1 x CH_2 *o*-Ph-H8-BINOL), 2.49–2.36 (m, 3H, CH*H*-OMe and 1 x CH_2 *o*-Ph-H8-BINOL), 1.97–1.67 (m, 10H, CH_2 nbd and 4 x CH_2 *o*-Ph-H8-BINOL). $^{13}C\{^1H\}$ NMR (125 MHz, CD_2Cl_2) δ = 142.20 ($C_{q\ arom}$), 142.16 ($C_{q\ arom}$), 141.9 ($C_{q\ arom}$), 141.8 ($C_{q\ arom}$), 139.35 ($C_{q\ arom}$), 139.34 ($C_{q\ arom}$), 138.38 ($C_{q\ arom}$), 138.37 ($C_{q\ arom}$), 137.2 ($C_{q\ arom}$), 137.10 ($C_{q\ arom}$), 137.09 ($C_{q\ arom}$), 136.5 ($C_{q\ arom}$), 136.2 ($C_{q\ arom}$), 135.4 (CH_{arom}), 135.3 (CH_{arom}), 132.6 ($C_{q\ arom}$), 132.2 ($C_{q\ arom}$), 131.85 ($C_{q\ arom}$), 131.82 ($C_{q\ arom}$), 131.6 (CH_{arom}), 131.54 (CH_{arom}), 131.48 (CH_{arom}), 131.44 (CH_{arom}), 131.40 (CH_{arom}), 131.35 (CH_{arom}), 131.27 (CH_{arom}), 130.3 (CH_{arom}), 129.8 (CH_{arom}), 129.65 (CH_{arom}), 129.57 (CH_{arom}), 129.3 (CH_{arom}), 128.8 (CH_{arom}), 128.7 (CH_{arom}), 128.6 (CH_{arom}), 128.4 (CH_{arom}), 128.0 (CH_{arom}),

127.94 (*C*H $_{arom}$), 127.92 (*C*H $_{arom}$), 127.4 (*C*H $_{arom}$), 126.2 ($C_{q\ arom}$), 125.8 ($C_{q\ arom}$), 103.7 (=*C*H vinylic, nbd), 100.6 (d, *J* = 12.3 Hz, =*C*H vinylic, nbd), 93.1 (=*C*H vinylic, nbd), 79.8 (=*C*H vinylic, nbd), 75.4 (dd, *J* = 6.1 Hz, *C*H-OPO), 72.4 (*C*H_2 nbd), 69.8 (dd, *J* = 8.8 Hz, *C*H_2-OMe), 58.2 (O*C*H_3), 55.6 (*C*H allylic, nbd), 55.3 (*C*H allylic, nbd), 42.0 (d, *J* = 28.7 Hz, *C*H-PPh_2), 29.3 (*C*H_2), 29.2 (*C*H_2), 27.8 (*C*H_2), 27.7 (*C*H_2), 22.6 (*C*H_2), 22.53 (*C*H_2), 22.46 (*C*H_2), 22.4 (*C*H_2). $^{31}P\{^1H\}$ NMR (202 MHz, CD_2Cl_2): δ = 130.3 (dd, *J* = 263.8, 69.7 Hz, *P*–O), 23.7 (dd, *J* = 146.0, 69.7 Hz, *P*–C). $^{11}B\{^1H\}$ NMR (128 MHz, CD_2Cl_2): δ = –1.1 (s, *B*F_4). $^{19}F\{^1H\}$ NMR (376 MHz, CD_2Cl_2): δ = –153.2 (s, B*F*$_4$). HRMS (ESI$^+$): *m*/*z* $[M-BF_4]^+$ calcd for $C_{61}H_{58}O_4P_2Rh$: 1019.2860; found: 1019.2865.

Synthesis of 4c. The same experimental protocol as for **4a** was used, with the following amounts of reagents (solvent amounts were adapted so that concentrations were the same): compound **2** (2.475 g, 6.80 mmol), DABCO (1.675 g, 14.95 mmol), chlorophosphite [18] (3.98 g, 7.50 mmol) and $[Rh(nbd)_2]BF_4$ (0.690 g, 1.85 mmol). Additionally, the following changes to the original recipe were made. After the borane cleavage, the solvent was removed and substituted by THF (135 mL). NEt_3 (19 mL, 136 mmol) and DMAP (0.415 g, 0.34 mmol) were added to the reaction mixture under N_2. A spongy white solid that corresponded to the raw phosphine-phosphite ligand (2.715 g, *ca*. 1.83 mmol, *ca*. 58% purity by integration of the signals of the ligand with respect to the rest of the signals in the ^{31}P NMR spectrum) was obtained after precipitating (40 mL, *n*-hexane:Et_2O 75:25) and filtering out *P*-containing impurities (this precipitation/filtration process was repeated twice). The rhodium complex obtained as indicated for **4a** was recrystallized by layering *n*-hexane (15 mL) onto a solution of the complex in DCM (5 mL). Compound **4c** was isolated as an orange powder (1.07 g, 0.95 mmol, 52% overall yield with respect to $[Rh(nbd)_2]BF_4$) after filtering, washing with anhydrous Et_2O (2 x 10 mL) and drying *in vacuo*. mp 182–185 °C; $[\alpha]_D^{27}$ = +324.0 (*c* 0.10, THF). ^1H NMR (500 MHz, CD_2Cl_2): δ = 7.94–7.90 (m, 2H, H_{arom}), 7.82–7.78 (m, 1H, H_{arom}), 7.72–7.69 (m, 2H, H_{arom}), 7.59–7.40 (m, 14H, H_{arom}), 7.33–7.13 (m, 10H, H_{arom}), 7.05–6.99 (m, 4H, H_{arom}), 6.64–6.60 (m, 2H, H_{arom}), 6.16 (bs, 1H, =C*H* vinylic, nbd), 5.46 (d, *J* = 8.0 Hz, 1H, OC*H*-CHO, TADDOL), 5.33 (bs, 1H, =C*H* vinylic, nbd), 5.26 (bs, 1H, =C*H* vinylic, nbd), 5.14 (d, *J* = 8.0 Hz, 1H, OCH-C*H*O, TADDOL), 4.85 (bs, 1H, =C*H* vinylic, nbd), 4.33 (bs, 1H, C*H* allylic, nbd), 4.04 (bs, 1H, C*H* allylic, nbd), 3.94 (d, *J* = 8.0

Hz, 1H, C*H*-PPh_2), 3.36–3.31 (m, 1H, C*H*-OPO), 2.92 (s, 3H, OCH_3), 2.31 (dd, *J* = 9.4 Hz, 1H, C*H*H-OMe), 1.95–1.92 (m, 1H, C*H*H, nbd), 1.79–1.74 (m, 2H, CH*H*-OMe and CH*H*, nbd), 1.10 (s, 3H, CH_3, TADDOL), 0.34 (s, 3H, CH_3, TADDOL). $^{13}C\{^1H\}$ NMR (125 MHz, CD_2Cl_2): δ = 144.3 ($C_{q\ arom}$), 144.2 ($C_{q\ arom}$), 143.8 ($C_{q\ arom}$), 139.72 ($C_{q\ arom}$), 139.66 ($C_{q\ arom}$), 138.6 ($C_{q\ arom}$), 134.9 (*C*H $_{arom}$), 134.8 (*C*H $_{arom}$), 132.8 (*C*H $_{arom}$), 132.43 (*C*H $_{arom}$), 132.35 (*C*H $_{arom}$), 131.6 ($C_{q\ arom}$), 130.91 (*C*H $_{arom}$), 130.89 (*C*H $_{arom}$), 130.4 ($C_{q\ arom}$), 130.1 (*C*H $_{arom}$), 130.0 (*C*H $_{arom}$), 129.0 (*C*H $_{arom}$), 128.93 (*C*H $_{arom}$), 128.90 (*C*H $_{arom}$), 128.7 (*C*H $_{arom}$), 128.64 (*C*H $_{arom}$), 128.61 (*C*H $_{arom}$), 128.5 ($C_{q\ arom}$), 128.3 (*C*H $_{arom}$), 128.2 ($C_{q\ arom}$), 127.9 (*C*H $_{arom}$), 127.7 (*C*H $_{arom}$), 127.2 (*C*H $_{arom}$), 126.9 (*C*H $_{arom}$), 114.0 (*C*-Me_2, TADDOL), 95.8 (=*C*H vinylic, nbd), 95.7 (=*C*H vinylic, nbd), 90.8 (d, *J* = 19.1 Hz, O*C*-Ph_2, TADDOL), 90.2 (d, *J* = 17.6 Hz, O*C*-Ph_2, TADDOL), 88.3 (=*C*H vinylic, nbd), 87.4 (=*C*H vinylic, nbd), 80.6 (d, *J* = 3.2 Hz, O*C*H-CHO, TADDOL), 78.5 (d, *J* = 4.6 Hz, OCH-*C*HO, TADDOL), 74.5 (d, *J* = 7.9 Hz, *C*H-OPO), 71.5 (CH_2, nbd), 68.7 (dd, *J* = 8.7 Hz, CH_2-OMe), 58.3 (OCH_3), 55.6 (*C*H allylic, nbd), 54.8 (*C*H allylic, nbd), 40.6 (d, *J* = 29.7 Hz, *C*H-PPh_2), 27.0 (CH_3, TADDOL), 25.5 (CH_3, TADDOL). $^{31}P\{^1H\}$ NMR (202 MHz, CD_2Cl_2): δ = 108.0 (dd, *J* = 267.0, 68.1 Hz, *P*–O), 26.4 (dd, *J* = 148.1, 68.1 Hz, *P*–C). $^{11}B\{^1H\}$ NMR (128 MHz, CD_2Cl_2): δ = –1.1 (s, *B*F_4). $^{19}F\{^1H\}$ NMR (376 MHz, CD_2Cl_2): δ = –153.2 (s, B*F*$_4$). HRMS (ESI$^+$): *m/z* $[M–BF_4]^+$ calcd for $C_{60}H_{58}O_6P_2Rh$: 1039.2758; found: 1039.2772.

1.5 Additional Experiments

1.5.1 Neutral Rh-complexes containing the acetylacetonate ligand

Besides the cationic [Rh(nbd)(P–OP)]BF_4 complexes, whose practical preparation has already been described, we have also prepared neutral Rh

complexes incorporating the P–OP and the acetylacetonate (acac) ligands following the same strategy. We considered that the [Rh(κ^2O,O'-acac)(P–OP)] complexes could find application both in asymmetric hydrogenation and hydroformylation reactions as precatalysts.[19] An analogous protocol to that described for **4a–c** was used in this case, but employing [Rh(κ^2O,O'-acac)(cod)] as the rhodium precursor (see Scheme 4 for the synthetic strategy and structures **5a** and **5b** for the complexes prepared). The one-pot synthesis starting from **2** by deprotection and *O*-phosphorylation with the chlorophosphites derived from (S_a)-BINOL and (R_a)-BINOL[16] (BINOL = [1,1'-binaphthalene]-2,2'-diol) provided crude mixtures of the corresponding P–OP ligands (purity by ^{31}P NMR *ca.* 94%). Subsequent complexation with substoichiometric amounts of [Rh(κ^2O,O'-acac)(cod)] (*i.e.* 0.98 equiv.) and then isolation of the target complexes by crystallization afforded a yellow fine powder corresponding to the [Rh(κ^2O,O'-acac)(P–OP)] complexes **5a** and **5b** in high yield (74% and 89% respectively, see Scheme 4). Their structure was determined by standard spectroscopic techniques (NMR spectroscopy and HRMS-MALDI spectrometry) and unambiguously confirmed by X-ray single crystal analysis.

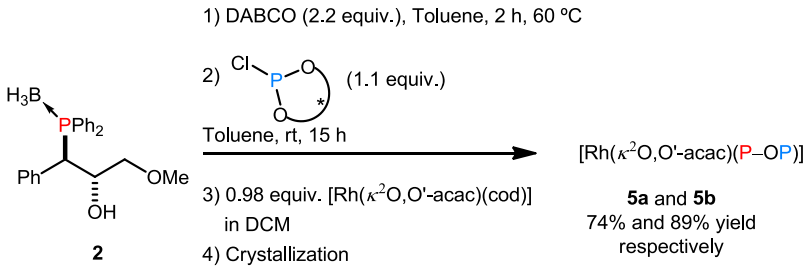

Scheme 4. Preparation of [Rh(κ^2O,O'-acac)(P–OP)] complexes **5a** and **5b**.

Synthesis of 5a. The same protocol as for **4a** was used, with the following amounts of reagents (solvent amounts were adapted so that concentrations were the same): compound **2** (1.408 g, 3.86 mmol), DABCO (0.974 g, 8.5 mmol), chlorophosphite[16] (1.492 g, 4.26 mmol) and [Rh(κ^2O,O'-acac)(cod)] (0.866 g, 2.74 mmol). A spongy white solid that corresponded to the raw phosphine-phosphite ligand (1.974 g, *ca*. 2.8 mmol, *ca*. 94% purity by integration of the signals of the ligand with respect to the rest of the signals in the ^{31}P NMR spectrum) was obtained. After following a crystallization process identical to that described above, 1.758 g (2.028 mmol, 74% overall yield with respect to [Rh(κ^2O,O'-acac)(cod)]) of complex **5a** as a yellow powder were obtained. $[\alpha]_D^{24}$ = −16.3 (*c* 0.17, THF). ^{1}H NMR (500 MHz, CD_2Cl_2) δ 8.19–8.14 (m, 2H, *H* $_{arom}$), 8.01–7.99 (m, 1H, *H* $_{arom}$), 7.98–7.94 (m, 1H, *H* $_{arom}$), 7.90–7.86 (m, 3H, *H* $_{arom}$), 7.69 (bs, 2H, *H* $_{arom}$), 7.55–6.99 (m, 18H, *H* $_{arom}$), 5.26 (s, 1H, =C*H*, acac), 4.90–4.78 (m, 1H, C*H*-OPO), 4.04 (dd, *J* = 14.8, 3.1 Hz, 1H, C*H*-PPh$_2$), 3.26 (s, 3H, O-C*H*$_3$), 3.09 (dd, *J* = 9.4, 5.4 Hz, 1H, C*H*H-OMe), 3.00 (t, *J* = 9.0 Hz, 1H, CH*H*-OMe), 1.61 (s, 3H, C-C*H*$_3$, acac), 1.23 (s, 3H, C-C*H*$_3$, acac); ^{13}C{^{1}H} NMR (125 MHz, CD_2Cl_2) δ 186.5 (*C*=O, acac), 185.0 (*C*=O, acac), 149.1 (*C*$_{q\ arom}$), 149.0 (*C*$_{q\ arom}$), 148.5 (*C*$_{q\ arom}$), 148.4 (*C*$_{q\ arom}$), 136.7 (*C*H $_{arom}$), 136.3 (*C*H $_{arom}$), 135.64 (*C*H $_{arom}$), 135.55 (*C*H $_{arom}$), 134.4 (*C*H $_{arom}$), 134.3 (*C*H $_{arom}$), 133.9 (*C*$_{q\ arom}$), 133.2 (*C*$_{q\ arom}$), 132.5 (*C*H $_{arom}$), 132.4 (*C*H $_{arom}$), 132.3 (*C*$_{q\ arom}$), 132.1 (*C*$_{q\ arom}$), 131.9 (*C*$_{q\ arom}$), 131.8 (*C*$_{q\ arom}$), 130.4 (*C*H $_{arom}$), 130.3 (*C*H $_{arom}$), 130.0 (*C*H $_{arom}$), 129.9 (*C*H $_{arom}$), 128.9 (*C*H $_{arom}$), 128.83 (*C*H $_{arom}$), 128.77 (*C*H $_{arom}$), 128.7 (*C*H $_{arom}$), 128.2 (*C*H $_{arom}$), 127.50 (*C*H $_{arom}$), 127.48 (*C*H $_{arom}$), 127.43 (*C*H $_{arom}$), 127.35 (*C*H $_{arom}$), 126.7 (*C*H $_{arom}$), 126.4 (*C*H $_{arom}$), 125.5 (*C*H $_{arom}$), 125.43 (*C*H $_{arom}$), 124.4 (*C*H $_{arom}$), 123.3 (*C*$_{q\ arom}$), 122.8 (*C*$_{q\ arom}$), 122.2 (*C*H $_{arom}$), 100.1 (=*C*H, acac), 74.3-74.1 (m, *CH*-

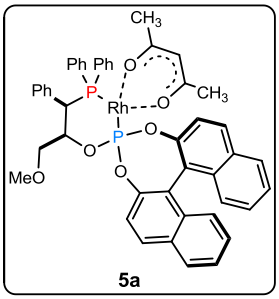

5a

OPO), 72.5 (dd, J = 8.7 Hz, CH_2-O-CH_3), 59.4 (O-CH_3), 41.1 (d, J = 34.3 Hz, CH-PPh_2), 27.4 (CH_3, acac), 27.1 (CH_3, acac); $^{31}P\{^1H\}$ NMR (202 MHz, CD_2Cl_2) δ 144.3 (dd, J = 302.3, 96.7 Hz, P-O), 45.3 (dd, J = 174.5, 96.8 Hz, P-O); HRMS (MALDI$^+$): m/z calcd for $C_{47}H_{41}O_6P_2Rh$ 866.1428, found 866.1540.

Single crystal X-ray analysis of compound 5a

X-ray Data: Single crystals of enantiopure Rh complex **5a** suitable for X-ray diffraction analysis were grown by slow diffusion of diethyl ether into an EtOAc (3:1 of Et_2O:EtOAc) and left in the freezer (–22 ºC) of the glove box.

Data collection and structure solution and refinement of **5a** were carried out as compound **2**.

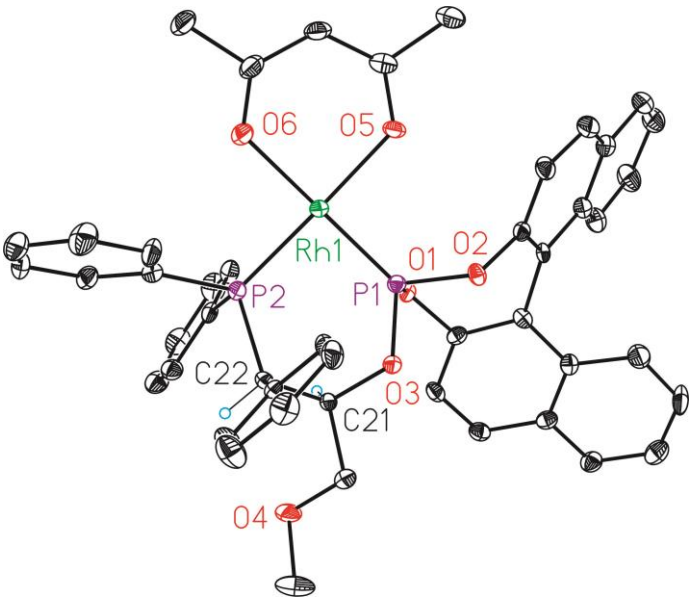

Figure 2. X-ray structure of **5a** (ORTEP drawing showing thermal ellipsoids at 50% probability). Non-relevant hydrogen atoms have been omitted for clarity. Selected bond lengths [Å] and angles [º]: Rh1-O5 = 2.064(3), Rh1-O6 = 2.062(3), Rh1-P1 = 2.1340(10), Rh1-P2 = 2.2056(10), P1-Rh1-P2 = 90.61(4).

Table 1. Crystal data and structure refinement of **5a**.

Empirical formula	$C_{51}H_{51}O_7P_2Rh$
Formula weight	940.77
Temperature	100(2) K
Wavelength	0.71073 Å
Crystal system	Monoclinic
Space group	P2(1)
Unit cell dimensions	a = 9.8775(4) Å, α = 90°
	b = 18.4163(7) Å, β = 99.8204(15)°
	c = 12.3470(5) Å, γ = 90°.
Volume	2213.10(15) $Å^3$
Z	2
Density (calculated)	1.412 Mg/m^3
Absorption coefficient	0.511 mm^{-1}
F(000)	976
Crystal size	0.20 x 0.20 x 0.03 mm^3
Theta range for data collection	2.006 to 30.527°.
Index ranges	$-14\leq h\leq 13$, $-25\leq k\leq 20$,
	$-17\leq l\leq 14$
Reflections collected	21153
Independent reflections	11697 [R(int) = 0.0360]
Completeness to theta = 30.527°	97.2%
Absorption correction	Empirical
Max. and min. transmission	0.985 and 0.921
Refinement method	Full-matrix least-squares on F^2
Data / restraints / parameters	11697/ 1/ 555
Goodness-of-fit on F^2	1.023
Final R indices [I>2 σ(I)]	R1 = 0.0396, wR2 = 0.0662
R indices (all data)	R1 = 0.0507, wR2 = 0.0708
Flack parameter	x = –0.004(13)
Largest diff. peak and hole	0.737 and –0.441 $e.Å^{-3}$

Synthesis of 5b. The same protocol as for **4a** was used, with the following amounts of reagents (solvent amounts were adapted so that concentrations were the same): compound **2** (0.850 g, 2.34 mmol), DABCO (0.588 g, 5.14 mmol), chlorophosphite[16] (0.958 g, 2.56 mmol) and [Rh(κ^2O,O'-acac)(cod)] (0.572 g, 1.81 mmol). A spongy white solid that corresponded to the raw phosphine-phosphite ligand (1.306 g, *ca*. 1.846 mmol, *ca*. 94% purity by integration of the signals of the ligand with respect to the rest of the signals in the ^{31}P NMR spectrum) was obtained. After following a crystallization process identical to that described above, 1.404 g (1.619 mmol, 89% overall yield with respect to [Rh(κ^2O,O'-acac)(cod)]) of complex **5b** as a yellow powder were obtained. $[\alpha]_D^{24}$ = –85.6 (*c* 0.090, THF). ^{1}H NMR (500 MHz, CD_2Cl_2) δ 8.29–8.18 (m, 2H, *H* $_{arom}$), 7.99–7.86 (m, 4H, *H* $_{arom}$), 7.86–7.82 (m, 1H, *H* $_{arom}$), 7.62–7.50 (m, 4H, *H* $_{arom}$), 7.47–7.37 (m, 5H, *H* $_{arom}$), 7.36–7.19 (m, 8H, *H* $_{arom}$), 7.14–7.10 (m, 1H, *H* $_{arom}$), 7.03–6.98 (m, 2H, *H* $_{arom}$), 5.19 (s, 1H, =C*H*, acac), 4.74–4.52 (m, 1H, C*H*-OPO), 4.07–3.93 (m, 1H, C*H*-PPh_2), 3.12 (s, 3H, O-CH_3), 3.09–2.98 (m, 2H, CH_2-OMe), 1.62 (s, 3H, C-CH_3, acac), 0.87 (s, 3H, C-CH_3, acac); ^{13}C{^{1}H} NMR (125 MHz, CD_2Cl_2) δ 186.4 (*C*=O, acac), 184.9 (*C*=O, acac), 149.1 ($C_{q\ arom}$), 149.0 ($C_{q\ arom}$), 148.5 ($C_{q\ arom}$), 148.5 ($C_{q\ arom}$), 136.4 ($C_{q\ arom}$), 136.1 ($C_{q\ arom}$), 135.3 (*C*H $_{arom}$), 135.2 (*C*H $_{arom}$), 134.4 (*C*H $_{arom}$), 134.3 (*C*H $_{arom}$), 134.0 ($C_{q\ arom}$), 132.7 (*C*H $_{arom}$), 132.6 (*C*H $_{arom}$), 132.2 ($C_{q\ arom}$), 131.9 ($C_{q\ arom}$), 131.7 ($C_{q\ arom}$), 130.6 (*C*H $_{arom}$), 130.1 (*C*H $_{arom}$), 129.9 (*C*H $_{arom}$), 129.8 (*C*H $_{arom}$), 129.83 (*C*H $_{arom}$), 129.1 (*C*H $_{arom}$), 129.0 (*C*H $_{arom}$), 128.82 (*C*H $_{arom}$), 128.76 (*C*H $_{arom}$), 128.3 (*C*H $_{arom}$), 127.6 (*C*H $_{arom}$), 127.5 (*C*H $_{arom}$), 127.4 (*C*H $_{arom}$), 127.36 (*C*H $_{arom}$), 127.3 (*C*H $_{arom}$), 126.6 (*C*H $_{arom}$), 126.4 (*C*H $_{arom}$), 125.4 (*C*H $_{arom}$), 125.36 (*C*H $_{arom}$), 123.8 (*C*H $_{arom}$), 123.6 ($C_{q\ arom}$), 123.0 ($C_{q\ arom}$), 122.6 (*C*H $_{arom}$), 99.8 (=*C*H, acac), 74.8–74.6 (m, *CH*-OPO), 72.8 (dd, *J* = 8.2 Hz, *C*H_2-

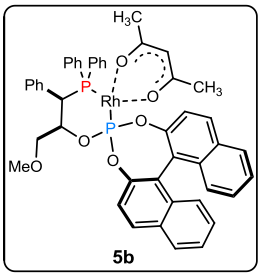

5b

OCH_3), 59.4 (O-*C*H_3), 40.6 (d, *J* = 34.7 Hz, *C*H-PPh_2), 27.6 (*C*H_3, acac 26.7 (*C*H_3, acac); $^{31}P\{^1H\}$ NMR (202 MHz, CD_2Cl_2) δ 144.7 (dd, *J* = 299.4, 98.4 Hz, *P*-O), 46.9 (dd, *J* = 175.5, 98.4 Hz, *P*-C); HRMS (MALDI$^+$): *m/z* [M^+] calcd for $C_{47}H_{41}O_6P_2Rh$ 866.1428, found 866.1774.

Single crystal X-ray analysis of compound 5b

X-ray Data: Single crystals of enantiopure Rh complex **5b** suitable for X-ray diffraction analysis were grown by slow diffusion of diethyl ether into an EtOAc (3:1 of Et_2O:EtOAc) and left in the freezer (–22 ºC) of the glove box.

Data collection and structure solution and refinement of **5b** were carried out as compound **2**.

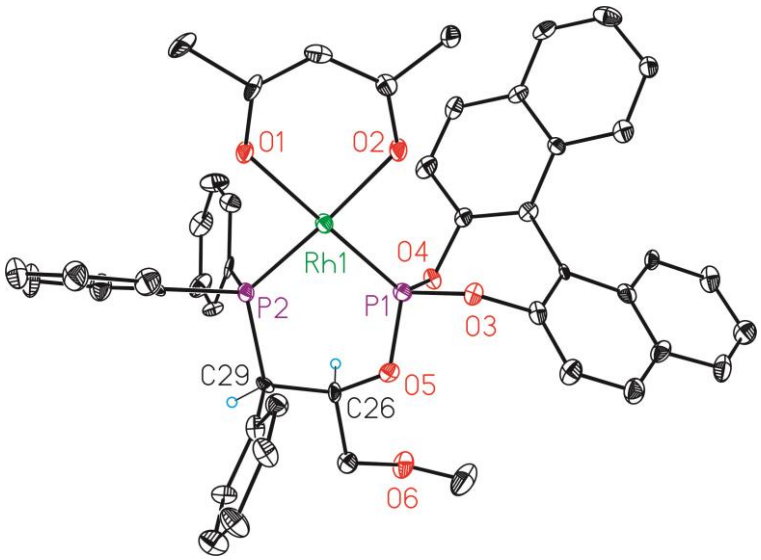

Figure 3. X-ray structure of **5b** (ORTEP drawing showing thermal ellipsoids at 50% probability). Non-relevant hydrogen atoms have been omitted for clarity. Selected bond lengths [Å] and angles [º]: Rh1-O1 = 2.071(8), Rh1-O2 = 2.065(6), Rh1-P1 = 2.123(3), Rh1-P2 = 2.204(3), P1-Rh1-P2 = 90.75(12).

Table 2. Crystal data and structure refinement of **5b**.

Empirical formula	$C_{47}H_{41}O_6P_2Rh$
Formula weight	866.65
Temperature	100(2) K
Wavelength	0.71073 Å
Crystal system	Orthorhombic
Space group	P2(1)2(1)2(1)
Unit cell dimensions	a = 9.786(6) Å, α = 90°
	b = 10.684(9) Å, β = 90°
	c = 37.861(19) Å, γ = 90°
Volume	3958(4) $Å^3$
Z	4
Density (calculated)	1.454 Mg/m^3
Absorption coefficient	0.563 mm^{-1}
F(000)	1784
Crystal size	0.08 x 0.02 x 0.01 mm^3
Theta range for data collection	1.980 to 25.730°
Index ranges	$-10\leq h\leq 11, -12\leq k\leq 13,$
	$-43\leq l\leq 46$
Reflections collected	36493
Independent reflections	7116[R(int) = 0.2059]
Completeness to theta = 25.730°	95.3%
Absorption correction	Empirical
Max. and min. transmission	0.994 and 0.592
Refinement method	Full-matrix least-squares on F^2
Data/ restraints/ parameters	7116/ 336/ 508
Goodness-of-fit on F^2	1.004
Final R indices [$I>2\sigma(I)$]	R1 = 0.0674, wR2 = 0.1259
R indices (all data)	R1 = 0.1330, wR2 = 0.1531
Flack parameter	x = –0.02(5)
Largest diff. peak and hole	0.963 and –1.482 e $Å^{-3}$

1.6 Conclusion and Outlook

In conclusion, we have developed and optimized a practical synthesis for "lead" enantiopure rhodium complexes derived from P–OP ligands. We have previously reported that these rhodium complexes have been efficiently applied as precatalysts in a number of enantioselective hydrogenative transformations. The herein described synthetic protocols may enable these efficient hydrogenation catalysts to be easily accessed by the "asymmetric catalytic community". This protocol was also applied for the practical synthesis of neutral Rh(I)-complexes containing the P–OP and the acetylacetonate (acac) ligands. Finally, this methodology may be further extended to other metal complexes to be used as catalysts in other asymmetric transformations of interest.

1.7 Supporting Information

1.7.1 NMR spectra of 4a

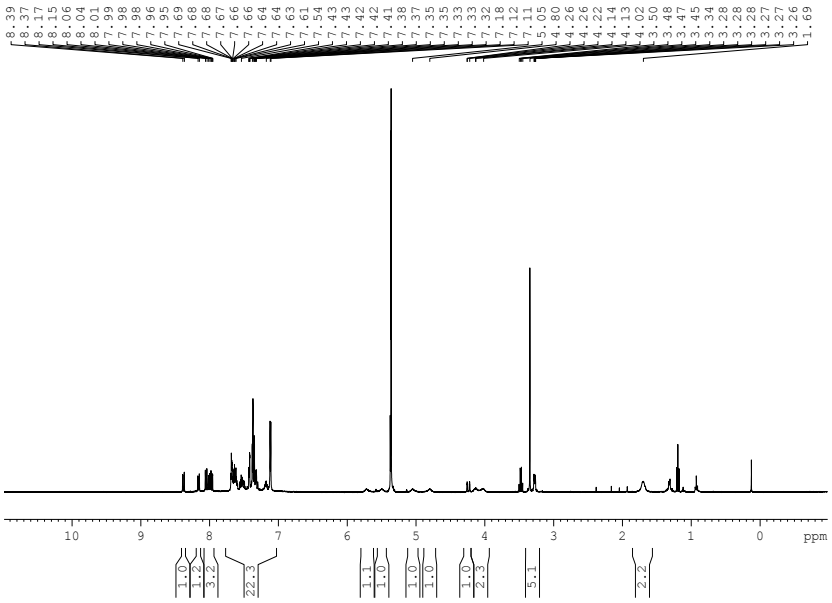

^{1}H NMR spectrum of **4a**

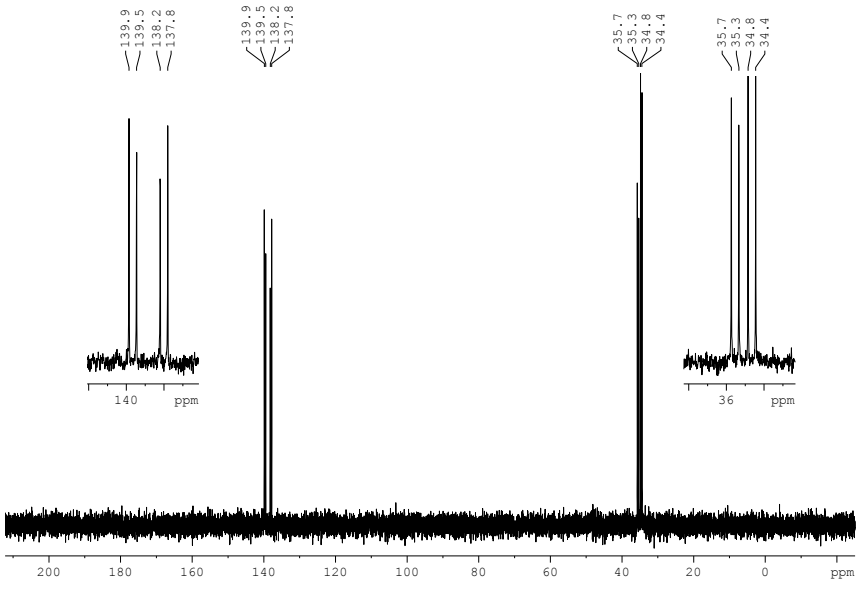

^{31}P{^{1}H} NMR spectrum of **4a**

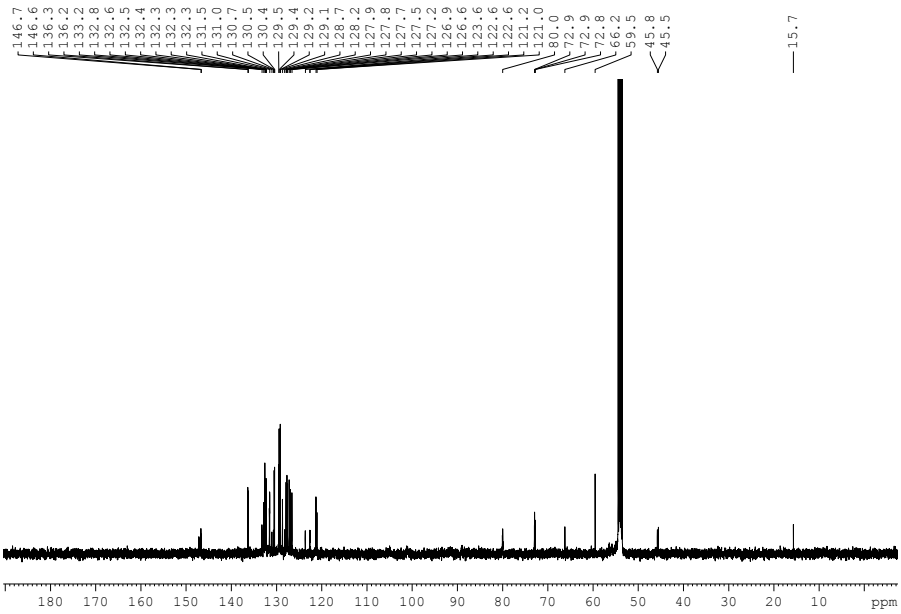

$^{13}C\{^{1}H\}$ NMR spectrum of **4a**

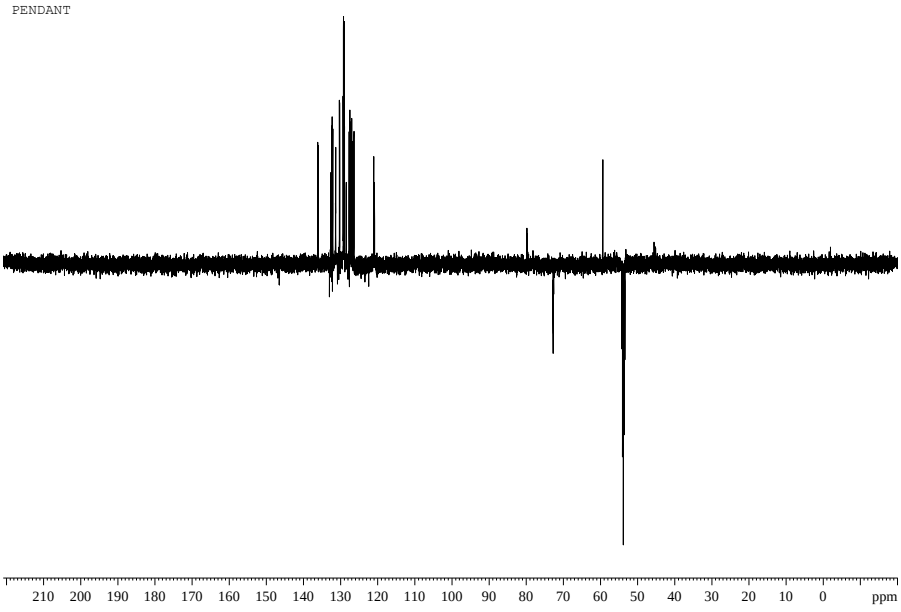

Pendant NMR spectrum of **4a**

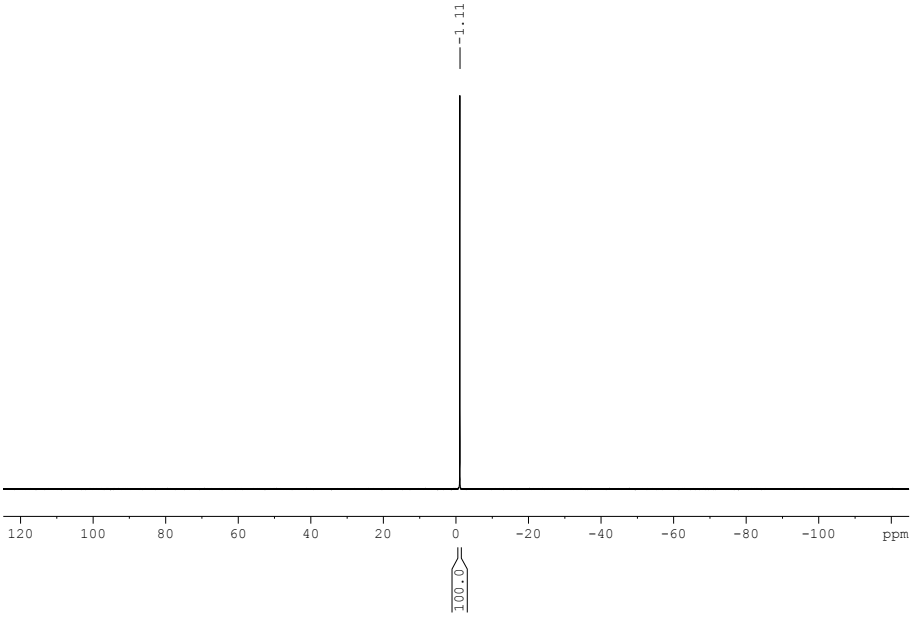

$^{11}B\{^{1}H\}$ NMR spectrum of **4a**

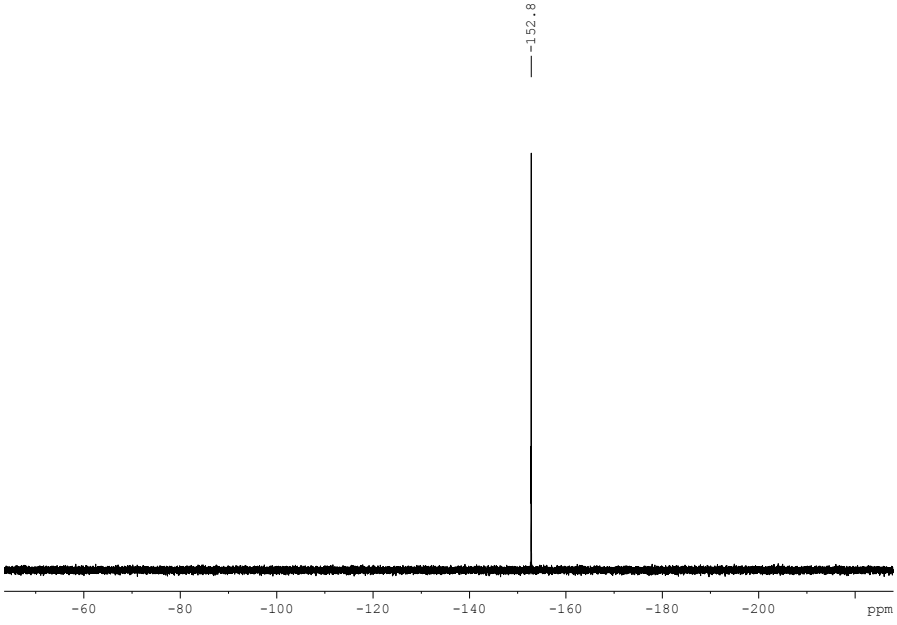

$^{19}F\{^{1}H\}$ NMR spectrum of **4a**

1.7.2 NMR spectra of 4b

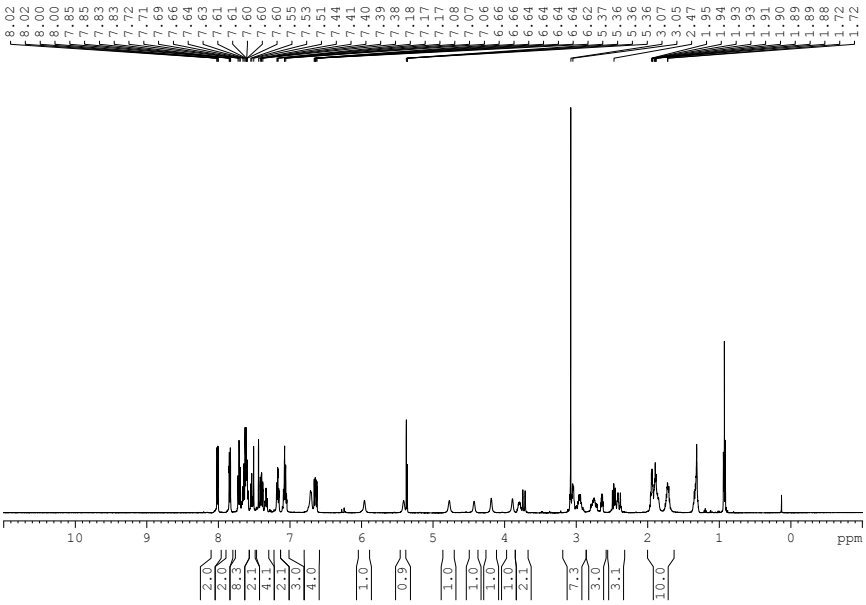

^{1}H NMR spectrum of **4b**

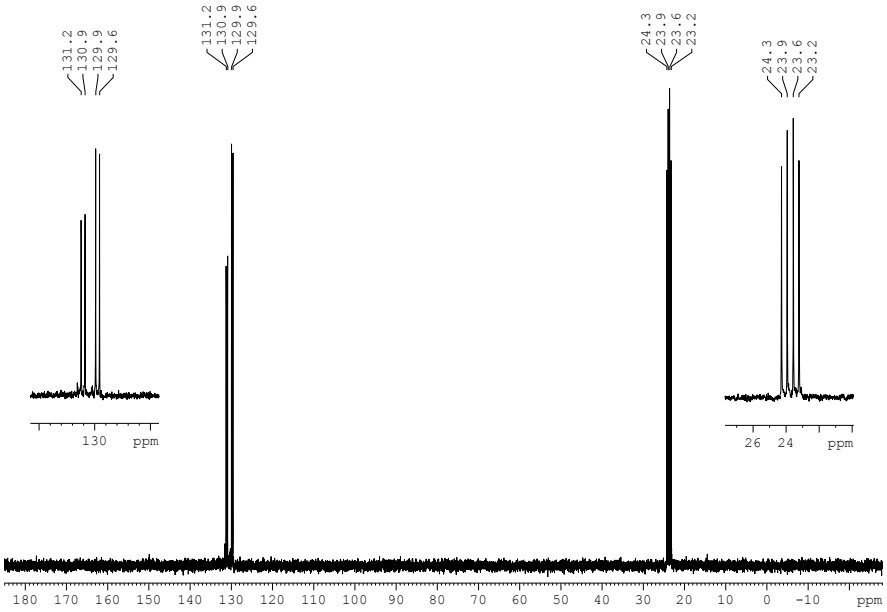

^{31}P{^{1}H} NMR spectrum of **4b**

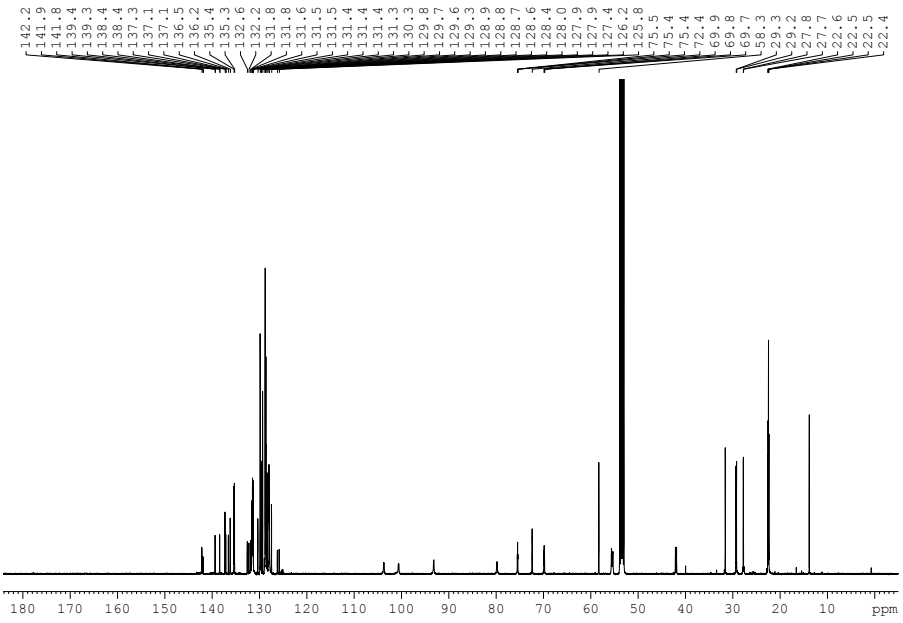

$^{13}C\{^{1}H\}$ NMR spectrum of **4b**

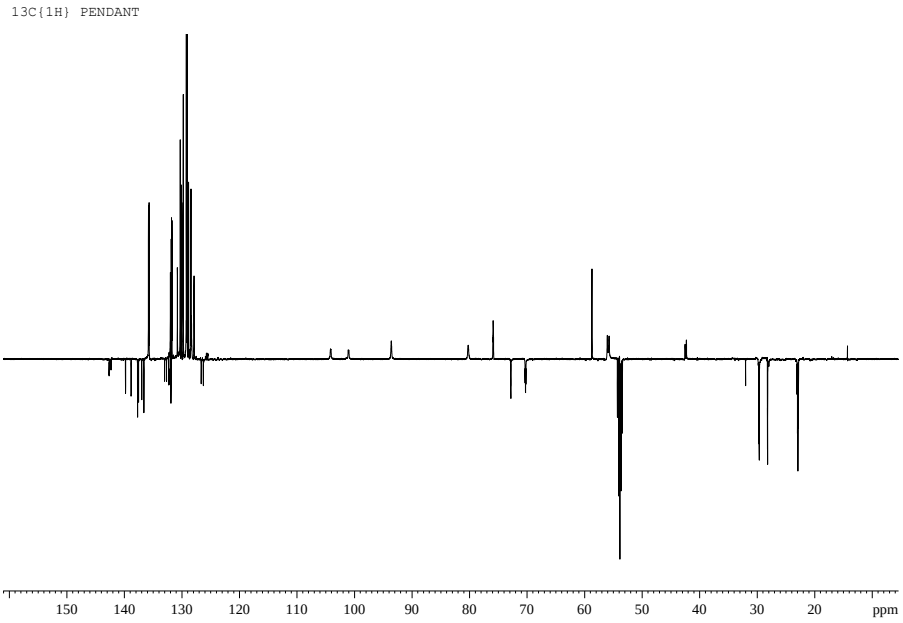

Pendant NMR spectrum of **4b**

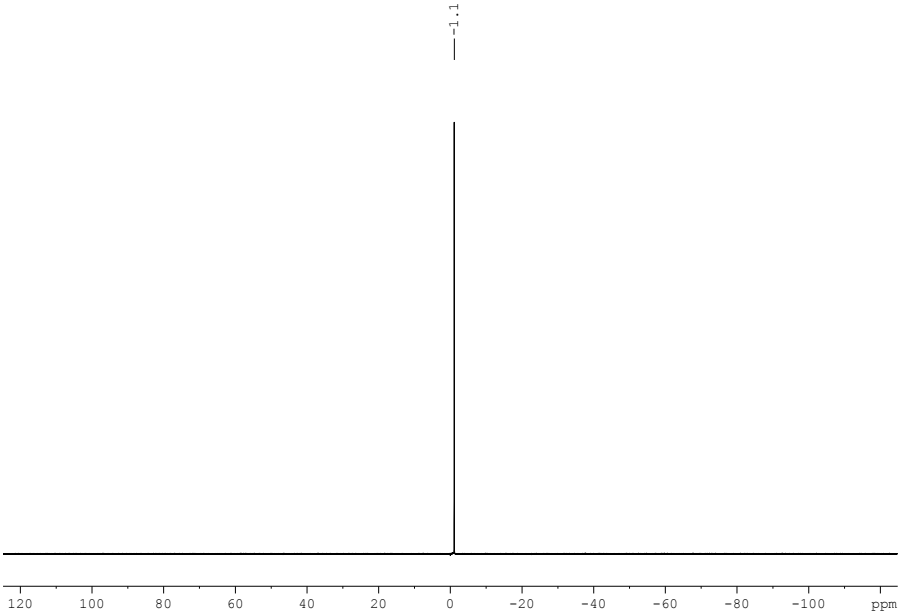

$^{11}B\{^{1}H\}$ NMR spectrum of **4b**

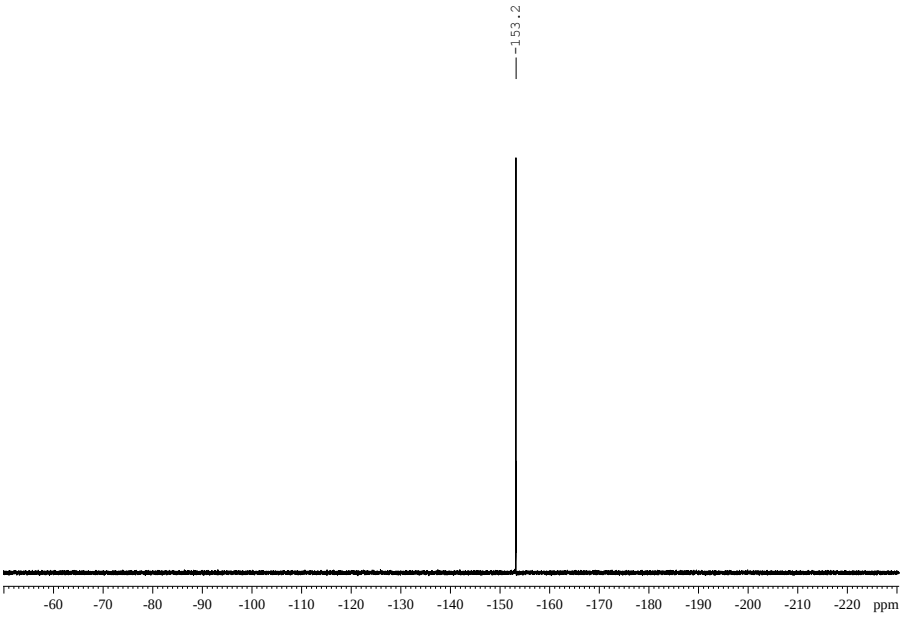

$^{19}F\{^{1}H\}$ NMR spectrum of **4b**

1.7.3 NMR spectra of 4c

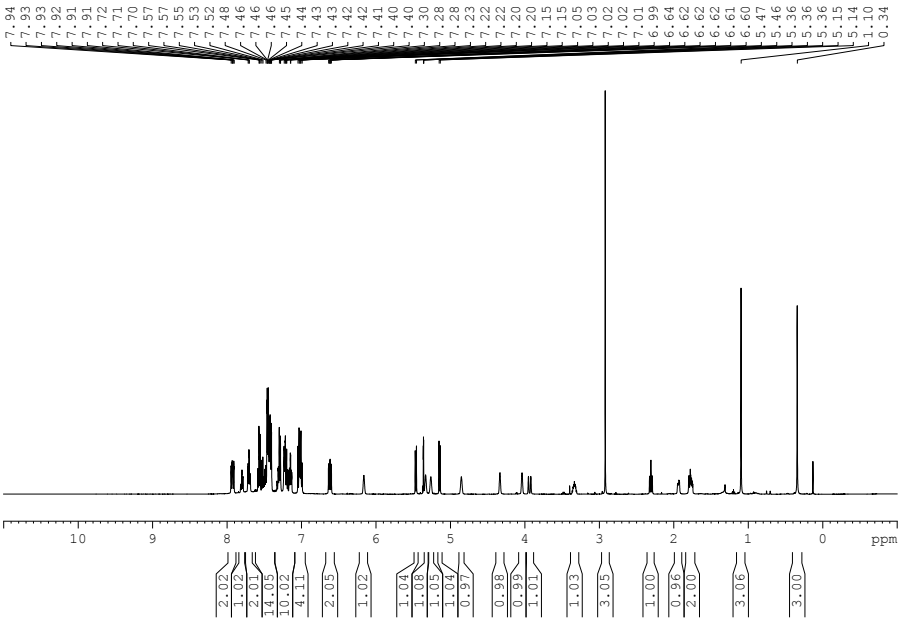

^{1}H NMR spectrum of **4c**

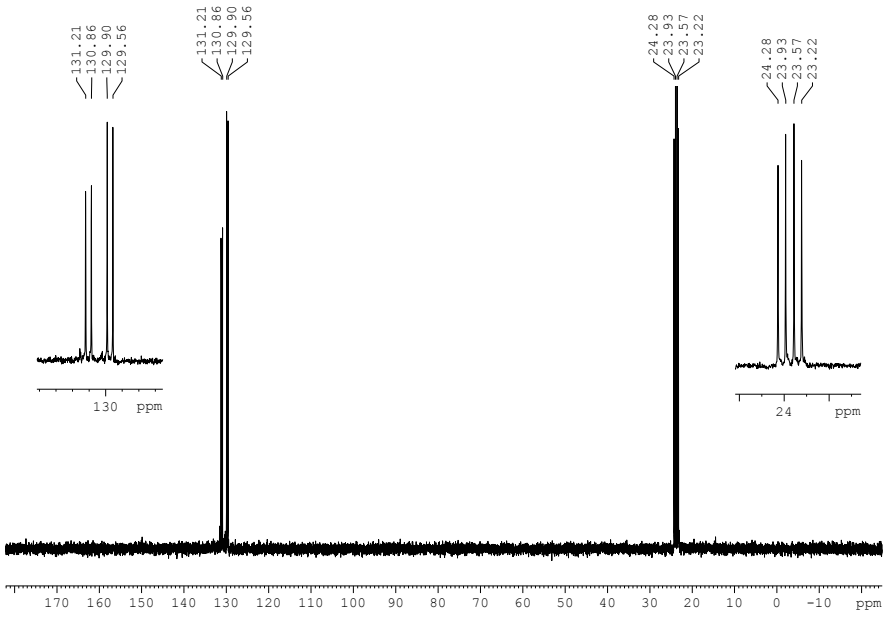

^{31}P{^{1}H} NMR spectrum of **4c**

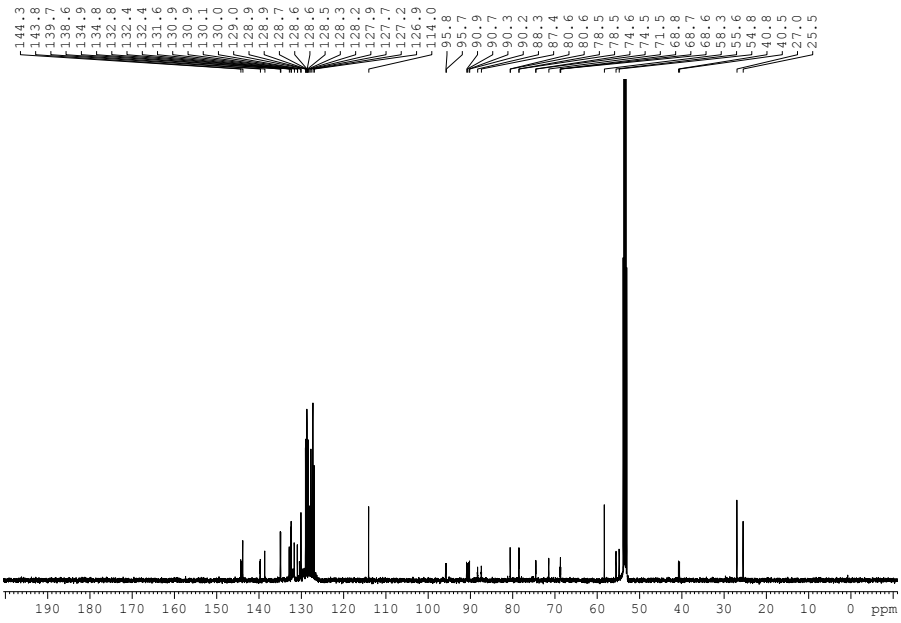

$^{13}C\{^{1}H\}$ NMR spectrum of **4c**

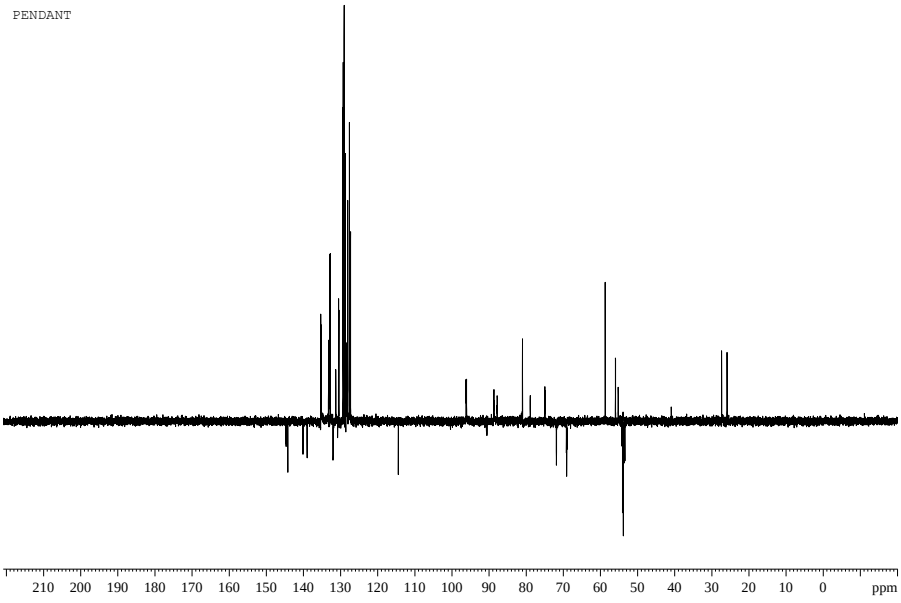

Pendant NMR spectrum of **4c**

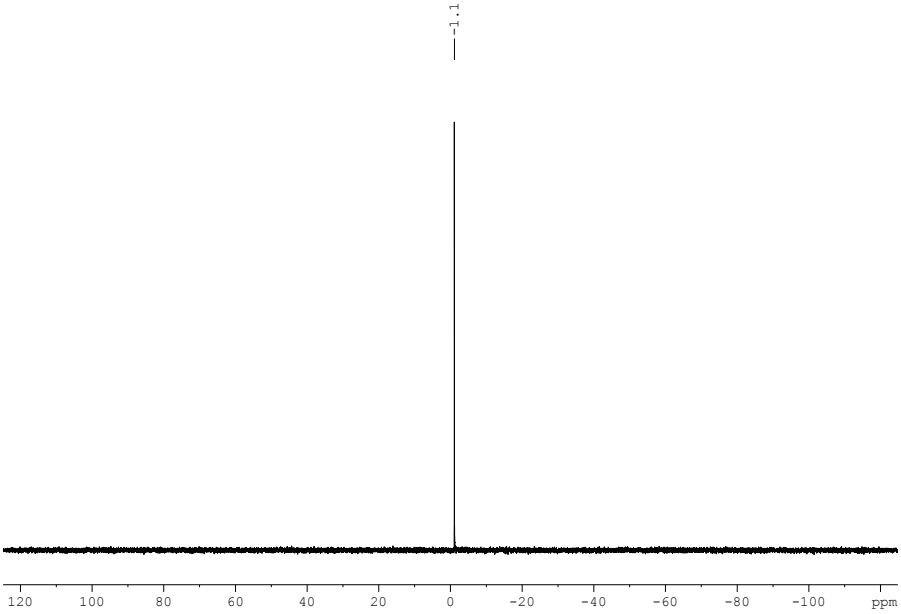

$^{11}B\{^{1}H\}$ NMR spectrum of **4c**

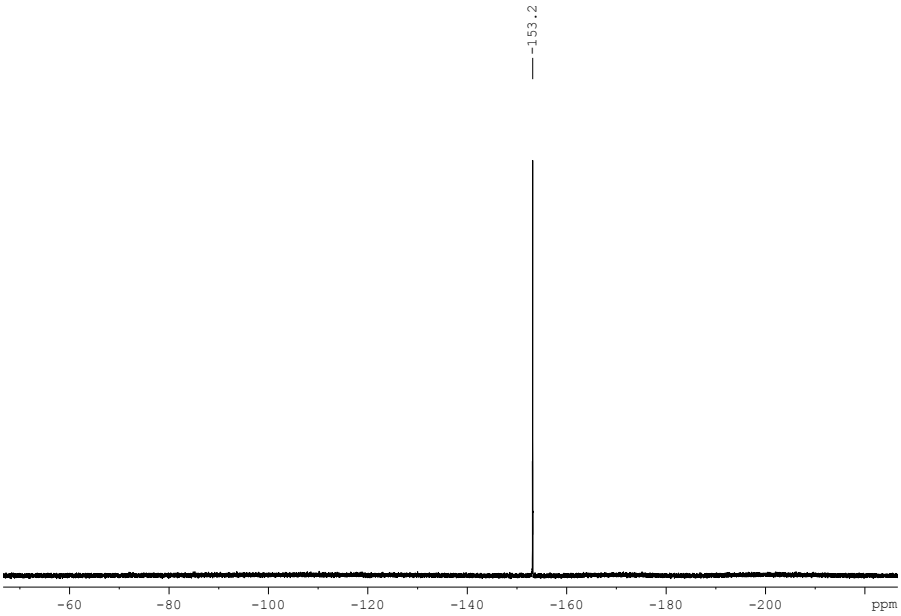

$^{19}F\{^{1}H\}$ NMR spectrum of **4c**

1.7.4 NMR spectra of 5a

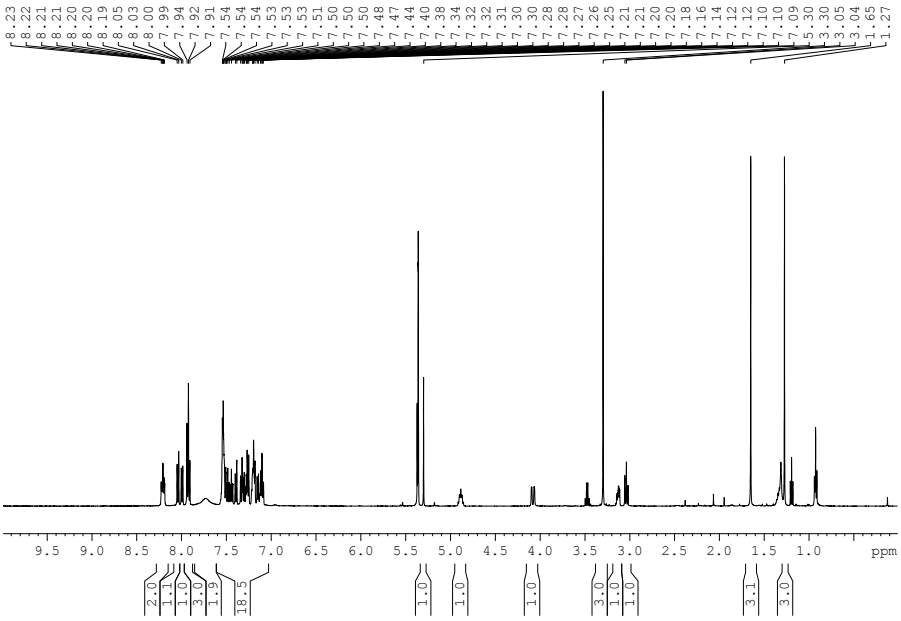

^{1}H NMR spectrum of **5a**

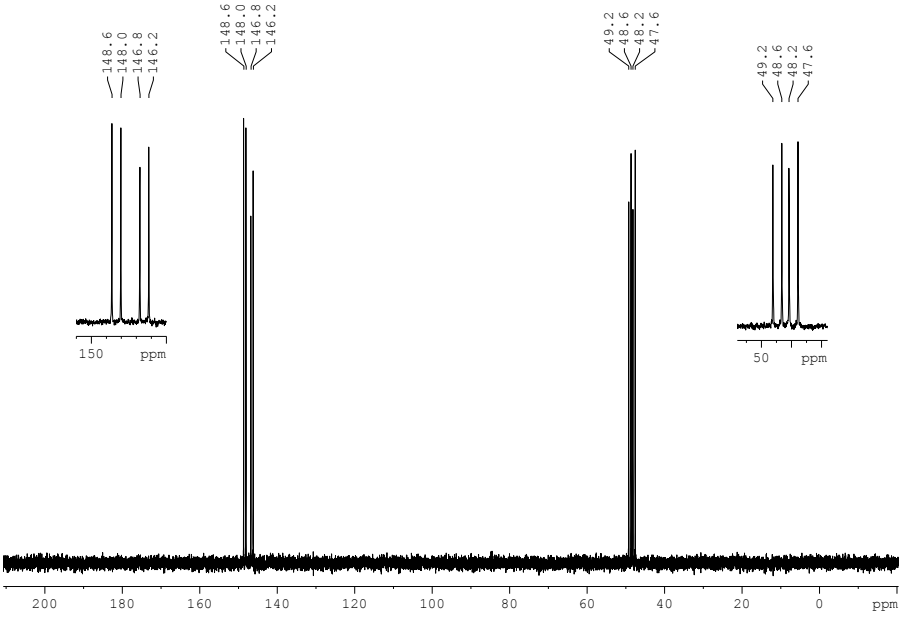

^{31}P{^{1}H} NMR spectrum of **5a**

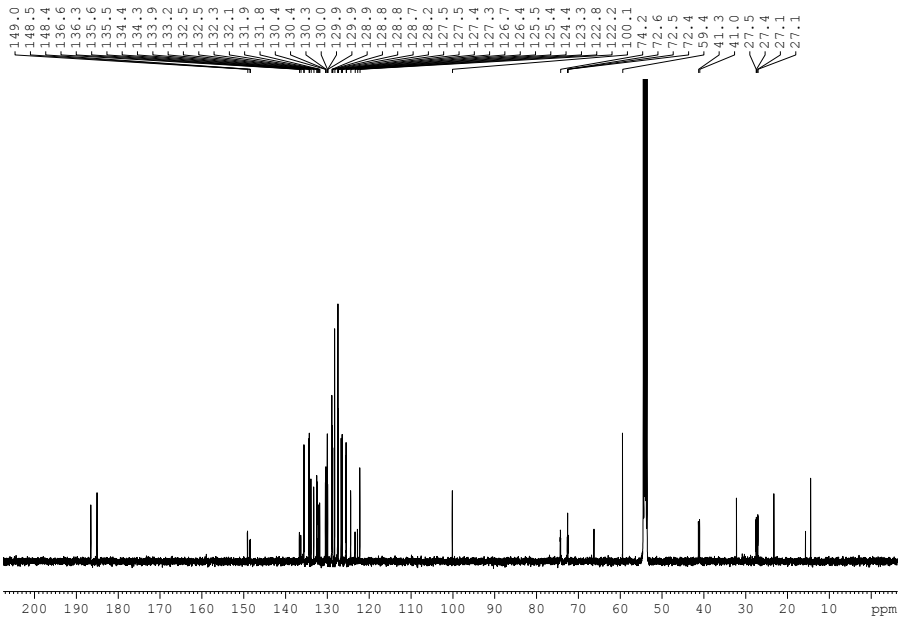

$^{13}C\{^{1}H\}$ NMR spectrum of **5a**

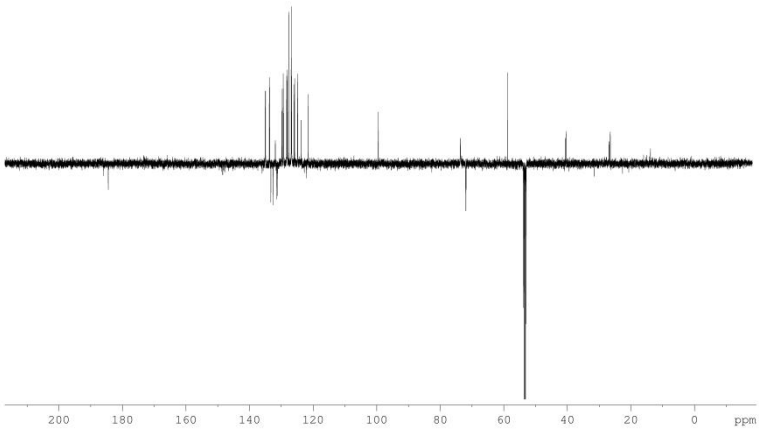

DEPTQ-135 NMR spectrum of **5a**

1.7.2 NMR spectra of 5b

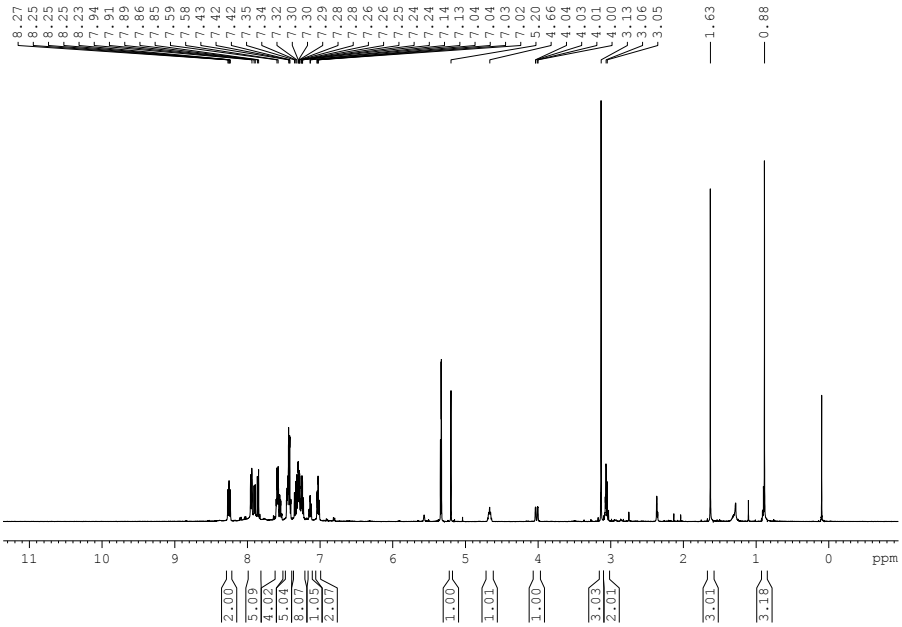

^{1}H NMR Spectra of **5b**

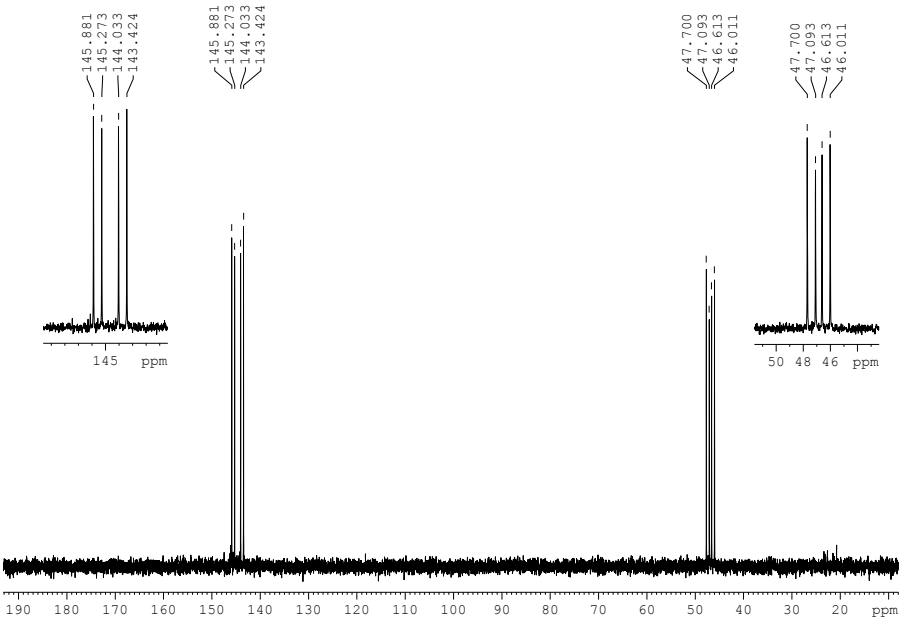

^{31}P{^{1}H} NMR spectrum of **5b**

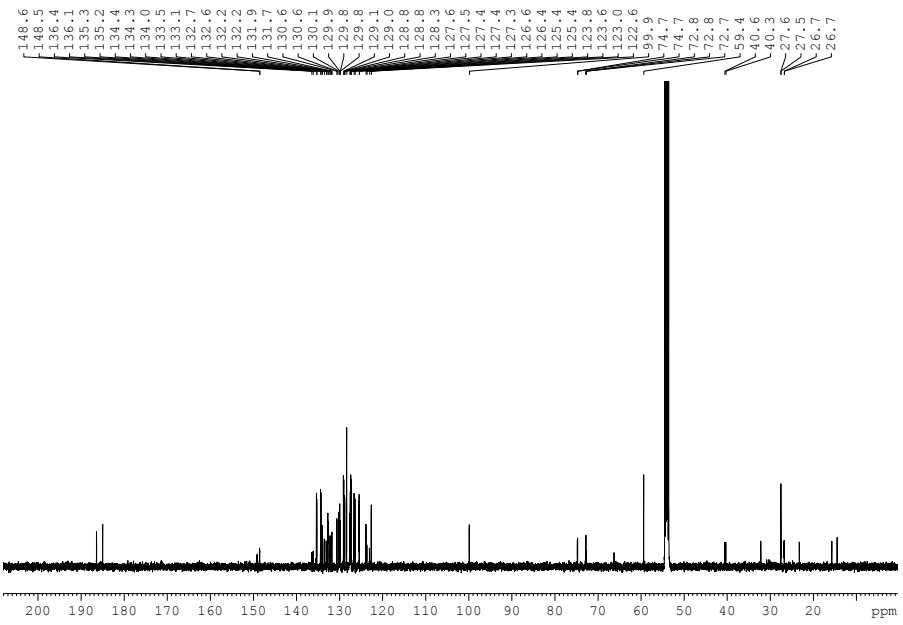

$^{13}C\{^{1}H\}$ NMR spectrum of **5b**

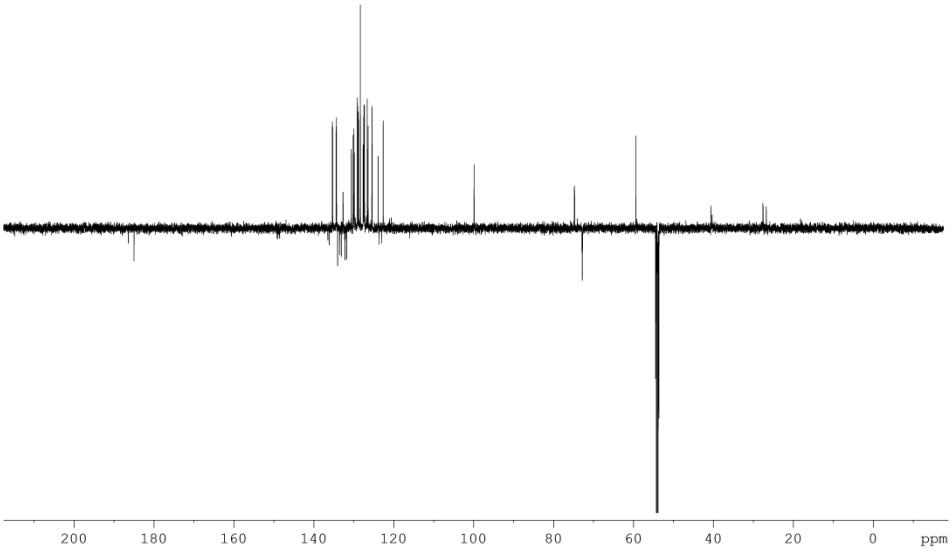

Pendant NMR spectrum of **5b**

1.8 References

(1) See for example: (a) Blaser, H. U.; Schmidt, E. *Asymmetric Catalysis on Industrial Scale: Challenges, Approaches and Solutions*. 1st ed.; Wiley-VCH: Weinheim, Germany, 2004. (b) Blaser, H.-U.; Pugin, B.; Spindler, F.; Thommen, M. *Acc. Chem. Res.* **2007**, *40*, 1240. (c) Nugent, T. C.; El-Shazly, M. *Adv. Synth. Catal.* **2010**, *352*, 753. (d) Busacca, C. A.; Fandrick, D. R.; Song, J. J.; Senanayake, C. H. *Adv. Synth. Catal.* **2011**, *353*, 1825. (e) Ager, D. J.; de Vries, A. H. M.; de Vries, J. G. *Chem. Soc. Rev.* **2012**, *41*, 3340. (f) Etayo, P.; Vidal-Ferran, A. *Chem. Soc. Rev.* **2013**, *42*, 728.

(2) See for example: (a) Börner, A. *Phosphorus Ligands in Asymmetric Catalysis*. 1st ed.; Wiley-VCH: Weinheim, Germany, 2008; Vols. I-III. (b) Fernández-Pérez, H.; Etayo, P.; Panossian, A.; Vidal-Ferran, A. *Chem. Rev.* **2011**, *111*, 2119.

(3) See for example: (a) *Handbook of Homogeneous Hydrogenation*, 1st ed.; de Vries, J. G.; Elsevier, C. J., Eds.; Wiley-VCH Verlag GmbH & Co. KGaA, Weinheim, Germany, 2007, Vols. I-III. (b) Wang, D.-S.; Chen, Q.-A.; Lu, S.-M.; Zhou, Y.-G. *Chem. Rev.* **2012**, *112*, 2557. (c) Xie, J.-H.; Zhu, S.-F.; Zhou, Q.-L. *Chem. Soc. Rev.* **2012**, *41*, 4126. (d) Hopmann, K. H.; Bayer, A. *Coord. Chem. Rev.* **2014**, *268*, 59.

(4) Fernández-Pérez, H.; Etayo, P.; Núñez-Rico, J. L.; Balakrishna, B.; Vidal-Ferran, A. *RSC Adv.* **2014**, *4*, 58440.

(5) We have simplified the discussion by indicating only the reagents required for synthesizing the rhodium complexes, whose synthesis has been published (*i.e.* the antecedents of complexes **4a** and **4b**). The reader is referred to the original publications for the exact reaction conditions employed for a particular P–OP ligand.

(6) (a) Fernández-Pérez, H.; Donald, S. M. A.; Munslow, I. J.; Benet-Buchholz, J.; Maseras, F.; Vidal-Ferran, A. *Chem. –Eur. J.* **2010**, *16*, 6495. (b) Panossian, A.; Fernández-Pérez, H.; Popa, D.; Vidal-Ferran, A. *Tetrahedron: Asymmetry* **2010**, *21*, 2281. (c) Etayo, P.; Núñez-Rico, J. L.; Fernández-Pérez, H.; Vidal-Ferran, A. *Chem. –Eur. J.* **2011**, *17*, 13978. (d) Etayo, P.; Núñez-Rico, J. L.; Vidal-Ferran, A. *Organometallics* **2011**, *30*, 6718. (e) Núñez-Rico, J. L.; Etayo, P.; Fernández-Pérez, H.; Vidal-Ferran, A. *Adv. Synth. Catal.* **2012**, *354*, 3025. (f) Fernández-Pérez, H.; Benet-Buchholz, J.; Vidal-Ferran, A. *Org. Lett.* **2013**, *15*, 3634. (g) Fernández-Pérez, H.; Benet-Buchholz, J.; Vidal-Ferran, A. *Chem. –Eur. J.* **2014**, *20*, 15375. (h) Lao, J. R.; Benet-Buchholz, J.; Vidal-Ferran, A. *Organometallics* **2014**, *33*, 2960.

(7) Lao, J. R.; Fernández-Pérez, H.; Vidal-Ferran, A. *Org. Lett.* **2015**, *17*, 4114.

(8) Fernández-Pérez, H.; Lao, J. R.; Vidal-Ferran, A. *Org. Lett.* **2016**, *18*, 2836.

(9) See, Fernández-Pérez, H.; Pericàs, M. A.; Vidal-Ferran, A. *Adv. Synth. Catal.* **2008**, *350*, 1984.

(10) It has been reported that *O*-phosphorylations employing the chlorophosphite derived from ((4*S*,5*S*)-2,2-dimethyl-1,3-dioxolane-4,5-diyl)bis(diphenyl-methanol) are not so favored as those involving chlorophosphites from [1,1'-

biaryl]-2,2'-diols and require a large excess of base (see for example: Kranich, R.; Eis, K.; Geis, O.; Mühle, S.; Bats, J. W.; Schmalz, H.-G. *Chem. –Eur. J.* **2000**, *6*, 2874.).

(11) Data collection with: *APEX II* version v2009.1-02, Bruker AXS Inc., Madison, Wisconsin, USA, 2007.

(12) Data reduction with: *SAINT* version V7.60A, Bruker AXS Inc., Madison, Wisconsin, USA, 2003/2007.

(13) *SADABS*, V2008/1, Bruker AXS Inc., Madison, Wisconsin, USA, 2003/2001, see: Blessing, R. H. *Acta Crystallogr., Sect. A: Found. Crystallogr.* **1995**, *A51*, 33..

(14) *SHELXTL*, versions 6.14, see: Sheldrick, G. M. *Acta Crystallogr., Sect. A: Found. Crystallogr.* **2008**, *64*, 112.

(15) (a) Flack, H. D. *Acta Crystallogr., Sect. A: Found. Crystallogr.* **1983**, *A39*, 876. (b) Flack, H. D.; Bernardinelli, G. *J. Appl. Crystallogr.* **2000**, *33*, 1143.

(16) The required chlorophosphite was prepared following the recipe indicated in Scherer, J.; Huttner, G.; Büchner, M.; Bakos, J. *J. Organomet. Chem.* **1996**, *520*, 45.

(17) The required chlorophosphite was prepared following the recipe indicated in Chikkali, S. H.; Bellini, R.; de Bruin, B.; van der Vlugt, J. I.; Reek, J. N. H. *J. Am. Chem. Soc.* **2012**, *134*, 6607.

(18) The required chlorophosphite was prepared following the recipe indicated in Wassenaar, J.; de Bruin, B.; Reek, J. N. H. *Organometallics* **2010**, *29*, 2767.

(19) For references on the use of neutral rhodium complexes in hydrogenations, see: (a) Blaser, H.-U.; Pugin, B.; Spindler, F. *Top. Organomet. Chem.* **2012**, *42*, 65. For references on the use of neutral rhodium complexes in asymmetric hydroformylations, see: (b) Klosin, J.; Landis, C. R. *Acc. Chem. Res.* **2007**, *40*, 1251. (c) Claver, C.; Godard, C.; Ruiz, A.; Pàmies, O.; Diéguez, M. In *Enantioselective Carbonylation Reactions*, 2008; Wiley-VCH Verlag GmbH & Co. KGaA: 2008; pp 65. (d) Gual, A.; Godard, C.; Castillón, S.; Claver, C. *Tetrahedron: Asymmetry* **2010**, *21*, 1135. (e) Perandones Bernabe, F.; Godard, C.; Claver, C. Asymmetric Hydroformylation. In *Top. Curr. Chem.*, 2013; Vol. 342, pp 79. (f) Chikkali, S. H.; van der Vlugt, J. I.; Reek, J. N. H. *Coord. Chem. Rev.* **2014**, *262*, 1.

CHAPTER-2

Catalytic Asymmetric Hydrogenation of C=N-Containing Heterocyclic Compounds

Table of Contents:

Subchapter A- Background on the Activation of Heteroaromatic Compounds towards Hydrogenation

Substrate Activation in the Catalytic Asymmetric Hydrogenation of *N*-Heteroarenes

Bugga Balakrishna,[†] José Luis Núñez-Rico,[†]
Anton Vidal-Ferran*[,†,‡]

† Institute of Chemical Research of Catalonia (ICIQ), Avinguda Països Catalans 16, E-43007, Tarragona, Spain.
‡ Catalan Institution for Research and Advanced Studies (ICREA), Passeig Lluís Companys 23, E-08010 Barcelona, Spain

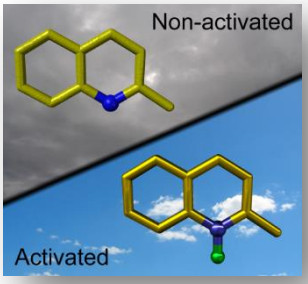

2A.1 Abstract

Different methods for transforming *N*-heteroarenes into more reactive derivatives for catalytic asymmetric hydrogenation are highlighted. The first strategy consists of facilitating hydrogenation by the formation of positively charged derivatives of the heteroarene. Catalyst deactivation

processes arising upon binding of the substrate to the metal center can thus be prevented and, additionally, hydrogenation of positively charged heteroarenes may also be more favored than that of their neutral analogues. The second strategy is based on introducing a ligating group onto the substrate to assist its coordination to the metal center and facilitate hydrogenation by chelation assistance. The last strategy involves breaking the aromaticity of the heteroarene by inducing a double bond migration process. This microreview summarizes advances made in the above mentioned strategies, which have allowed the development of highly enantioselective catalytic hydrogenation of *N*-heteroarenes for the production of fully or partially saturated chiral heterocycles.

2A.2 Introduction

Enantiopure organic compounds are important constituents of commercially produced chemicals including plastics, active pharmaceutical ingredients, agrochemicals, food additives, etc.[1] The ever-increasing demand for compounds of this kind has fueled the development of efficient synthetic methods for their preparation.[2] Asymmetric catalysis, in which a small amount of a chiral catalyst, by virtue of being regenerated many times, yields a much larger amount of enantiomerically pure product, is *a priori* the most elegant, productive, and resource-efficient approach for synthesizing enantiomerically pure (or enantioenriched) compounds. Thanks to intensive research efforts in academia[2] and industry,[2, 3] asymmetric catalysis has evolved significantly since its onset and now encompasses nearly all transformations subject to three-dimensional bias.

Asymmetric hydrogenation is considered to be a straightforward entry to the preparation of enantiopure compounds,[4] because many transition-metal coordination compounds (mostly phosphorus-containing complexes[5]) mediate the addition of dihydrogen to prochiral C=O, C=C and C=N

double bonds with high enantioselectivities. Thus, many highly efficient catalysts have been developed for the asymmetric hydrogenation of prochiral ketones, alkenes and imines.[6]

Many valuable biologically active compounds contain a chiral heterocyclic structural motif.[7] Asymmetric hydrogenation of the corresponding heteroaromatic precursors can be considered one of the most practical and atom-efficient methods for synthesizing fully or partly reduced heteroaromatic derivatives in enantiomerically pure form (Scheme 1).[8] This synthetic strategy also benefits from a great diversity of starting materials. In terms of synthetic simplicity, asymmetric hydrogenation is also an attractive route, as it minimizes the manipulation of functional groups during the preparation of the target heterocyclic compounds in enantiomerically pure form.

Despite the attractiveness of the asymmetric hydrogenation of heteroaromatic compounds, this area of chemistry is much less explored, with many fewer successful examples than in the cases of the asymmetric hydrogenation of prochiral ketones, alkenes, and imines. Several factors are behind the difficulties in asymmetrically hydrogenating heteroaromatic compounds:

- Firstly, heteroaromatic compounds are highly stable, which translates into a requirement for harsh hydrogenation conditions in order to break the aromaticity of the starting materials (*i.e.* high hydrogen pressures and temperatures). Although high pressures are normally not a problem and result only in a more demanding reaction setup, high temperatures may unfortunately be associated with low enantioselectivities in the final hydrogenated products. In this respect, there are many examples of partial hydrogenation of bicyclic heteroaromatic compounds with good enantioselectivities and with one aromatic ring being preserved, but literature examples of highly

selective hydrogenation of monocyclic heteroaromatic compounds are scarce.

- Secondly, many of the heteroaromatic derivatives to be hydrogenated lack an auxiliary coordination group to the metal center. Many successful applications of enantiomerically pure transition-metal complexes in asymmetric hydrogenation rely on the ability of the substrate to form a metal chelate involving the double bond to be hydrogenated and a donor atom from the substrate (for instance, the chelation-assistance of an acyl group is the classical paradigm for achieving high reactivity and enantioselectivity in rhodium-mediated asymmetric hydrogenations). [9] A lack of auxiliary coordination between the heteroaromatic substrate and the catalyst may result in more than one low-energy direction of approach for the substrate to the metal center with overall low enantioselectivity in the transformation.
- Lastly, the activity of the catalyst may be reduced, or even suppressed altogether, by the substrates or hydrogenation products, because both compounds may contain ligating groups, such as nitrogen or sulfur, capable of coordinating to the metal center with subsequent loss of catalytic activity.

  Chemists have developed various strategies for overcoming these difficulties:

  - ***"Ligand tuning"*** has enabled the development of efficient catalytic systems for certain types of heteroaromatic compounds. Catalyst activation involving the addition of additives to form more reactive catalytic systems complements ligand design and tuning and has also been successfully exploited in this chemistry. Ligand tuning and

catalyst activation have recently been reviewed and are both outside the scope of this text.[8]

- Hydrogenation or reduction of a heteroaromatic compound involves the sequential reduction of several C=C and/or C=N bonds. An elegant strategy has been devised that first involves the partial reduction of the initial heteroaromatic compound to a new prochiral heterocyclic compound by the use of an achiral catalytic system. The subsequent reduction of this intermediate heterocyclic compound to the final enantiopure derivative is mediated by a second catalytic system present in the reaction mixture, which is responsible for enantioselection. This strategy is known as "***relay catalysis***" and has also recently been reviewed.[10]

2A.3 Substrate Activation

The heteroarene to be hydrogenated has been synthetically manipulated and transformed into a related heterocyclic system that is more reactive in asymmetric hydrogenation ("***Substrate Activation***"). A first strategy consists in facilitating hydrogenation by the formation of positively charged derivatives of the heteroarene. Catalyst deactivation processes arising upon binding of the substrate to the metal center can thus be prevented and it is worth noting that, with this strategy, the coordinating ability of the ligating groups of the substrate and/or product toward the catalyst are neutralized (see Strategy I in Scheme 1). The hydrogenation of positively charged heteroarenes may also be more favored than that of their neutral analogues. In a second approach, the heteroarene is synthetically modified to introduce a ligating auxiliary group to assist its coordination to the metal center and facilitate hydrogenation by chelation-assistance. In addition to the activation effects produced by the ligating

auxiliary group, it should be noted that Strategy II also benefits from the advantages of quaternizing the sp^2-nitrogen group previously mentioned for Strategy I. Overall, the hydrogenation of the modified substrate may proceed more rapidly than that of the original derivative (see Strategy II in Scheme 1). The last strategy involves breaking the aromaticity of the heteroaromatic compound by inducing an acid- or base-mediated double-bond migration process (see Strategy III in Scheme 1). It is worth mentioning that, whilst the products arising from Strategies I and II may not correspond exactly to the hydrogenated substrate, the hydrogenated products obtained by Strategy III are formal hydrogenation products of the starting heteroarenes.

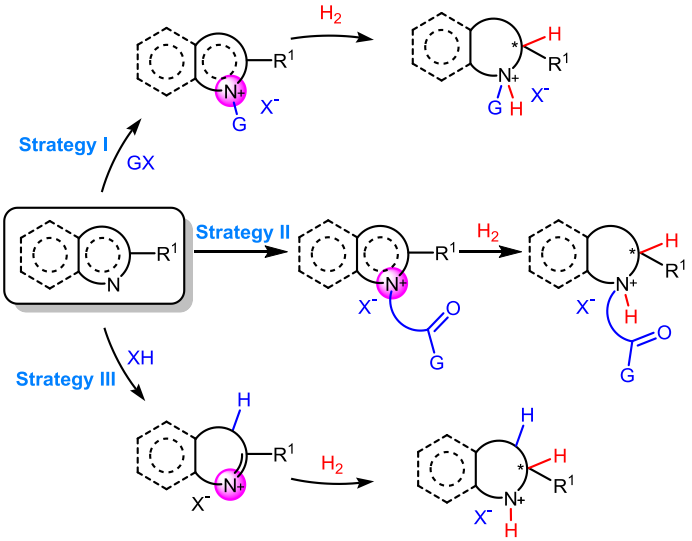

Scheme 1. General representation of the substrate manipulation strategies for improving the reactivity of heteroarenes in asymmetric hydrogenation.

As previously indicated, several reviews deal with ligand design in the asymmetric hydrogenation of heteroaromatic compounds and highlight the different additives that increase the activity of a given catalytic system or use the concept of relay catalysis for hydrogenating heteroaromatic

compounds, but none of these reviews provide a comprehensive and timely overview on the different methods for transforming the substrate into a more reactive derivative towards asymmetric hydrogenation. This microreview will therefore focus on the progress of synthetically manipulating heteroaromatic compounds in order to increase their reactivity in asymmetric hydrogenation mediated by enantiomerically pure transition-metal complexes.[11] The discussion is divided into three sections corresponding to these three different strategies.

2A.3.1 Strategy I: Activation by formation of positively charged derivatives of the substrate

In this strategy, the hydrogenation process is facilitated by the formation of positively charged derivatives of the heteroarene. One of the main problems to overcome in the hydrogenation of heteroarenes is catalyst deactivation due to substrate coordination to the metal center during the whole catalytic cycle. Those working on asymmetric catalysis have therefore sought to eliminate the ability of the substrate and product to bind to the catalytic metal by removing the lone pair of electrons from the ligating groups. In this strategy a dative covalent bond is formed between the lone pairs of electrons from the substrate and a suitable derivatization agent forming positively charged species. Moreover, these substrates are activated toward hydrogenation by quaternization of the nitrogen groups. Transition metal-mediated asymmetric hydrogenations of nitrogen containing heteroarenes proceed in many cases by stepwise proton transfer followed by the addition of a hydride.[12] This later step should be better favored with an iminium motif (*i.e.* $C=N^+$ double bond) rather than with the neutral C=N group present in the original heteroarene.

Thus, two main strategies have been devised for favoring hydrogenation through the formation of positively charged substrate derivatives:

- Firstly, the formation of positively charged derivatives of the substrate prior to the hydrogenation in a reversible manner and subsequent neutralization of the hydrogenation products.
- Secondly, formation of positively charged derivatives based on covalent chemistry.

The following discussion is divided into two sections corresponding to these two substrategies for suppressing the binding ability of the substrate to the metal center. The reader is referred to Section 2A.3.2 for examples in which the formation of a positively charged derivative also involves introducing a ligating group that facilitates hydrogenation through chelation assistance.

2A.3.1.1 Reversible formation of positively charged derivatives of the substrate and subsequent neutralization

Substrate activation should ideally be achieved with easy chemistry and in a minimum number of synthetic steps. The activating agent should also be easily removable. With these ideas in mind, activation of C=N-containing heteroarenes by protonation with Brønsted acids as activators appeared an obvious strategy to follow. A wide variety of Brønsted acids are easily available and hydrogenated protonated products can easily be transformed into the neutral compounds by adjusting the workup conditions.

Significant progress has been made by Ohshima, Ratovelomanana, Mashima, *et al.*[13] in the area of asymmetric hydrogenation of quinoline derivatives by use of this activation approach.[14] These authors used the cationic dinuclear triply halogen bridged iridium complexes **C1** as catalysts in the hydrogenation of quinolines. Interestingly, the asymmetric hydrogenation of the challenging 2-phenylquinoline in the presence of **C1** led to lower enantioselectivities than those obtained from the quinolinium analogues (an increase of up to 9% in the ee), thus indicating that

formation of quinolinium salts prior to hydrogenation was beneficial for enantioinduction. With the optimal catalyst and hydrogenation conditions in hand, the authors extended their chemistry to an array of diversely substituted quinolinium salts (thirteen examples) with excellent levels of conversions and enantioselectivities (up to 95% conversion and 95% ee; Scheme 2a). Although the authors normally used the same halogen ligand in **C1** or in the substrate derivative, they demonstrated that the original halogen ligand in **C1** remained in the catalytically active complex (similar results were obtained in the hydrogenation of 2-phenylquinoline hydrobromide or hydrochloride with **C1**·Cl). A series of isoquinolinium salts were hydrogenated by Mashima *et al*. with outstanding results using the same catalytic system.[15] Interestingly, diverse substitution patterns in the isoquinolinium ring are tolerated (Scheme 2b): 1-substitution (11 examples, up to 99% conv., up to 99% ee), 3-substitution (seven examples, up to 99% conv., up to 95% ee), 1,3-disubstitution (10 examples, up to 99% conv., 99% ee, complete *syn*-selectivity), 1,4-disubstituted- (one example not represented in Scheme 2b, up to 99% conv., *syn*:*anti* = 4:1; ee up to 97% for the *anti* isomer) and 3,4-disubstituted- (one example not represented in Scheme 2b, up to 99% conv., *syn*:*anti* = >95:5; 43% ee) isoquinolinium derivatives.

Mashima *et al*. have also reported the hydrogenation of 2-aryl-substituted pyridinium salts with a second alkyl substituent at the 3- or 6-position in the presence of **C1** as the enantioselective catalyst.[16] Even though a higher catalyst amount was used in this case (5 mol %, Scheme 2c), enantioselectivities were lower (up to 82% ee) than those reported for the quinolinium and isoquinolinium salts already discussed.

More recently, Zhou *et al*. also reported the hydrogenation of 3-(trifluoromethyl)pyridinium hydrochloride derivatives in the presence of an iridium catalyst based on (*R*)-difluorphos ligand **L1**. A *cis* arrangement

in all three substituents was found in the corresponding piperidines after the basic work-up, with enantioselectivities up to 90% ee (Scheme 2d).[17]

Asymmetric hydrogenation of quinazolinium salts catalyzed by halide-bridged dinuclear iridium complexes has recently been described by Mashima *et al.* (Scheme 2e).[18] Although enantioselectivities are very high (ee values ranging from 96 to >99%), this method suffers from low chemoselectivity for certain substrates: for R^1 = *p*-$MeOC_6H_4$ significant amounts of the two partially reduced dihydroquinazolines (34%) were obtained.

As a conclusion, it is worth noting that protonation has activated a wide range of heteroarenes towards efficient asymmetric hydrogenation in the presence of well-established iridium catalysts.

Kuwano *et al.* have developed an analogous activation strategy for the hydrogenation of pyrimidines with the use of Lewis acids as activators.[19] A broad range of chiral phosphines and Lewis acids were assayed in the iridium-mediated asymmetric hydrogenation of 2,3-disubstituted pyrimidines. High enantioselectivities were obtained with use of ligand **L2**, [{Ir(μ-Cl)(cod)}$_2$], iodine as additive and an excess of Yb(OTf)$_3$ as the Lewis acid (Scheme 2f). Enantioselectivities were high (18 examples, up to 99% ee) and installing a substituent at the *ortho* position of R^2 was beneficial for enantioselection. Pyrimidines bearing R^2 substituents other than aryl also underwent hydrogenation with high enantioselection.

The previously discussed activation examples involve the use of preformed *N*-protonated heteroarene salts (Scheme 2a–e) or of an excess of a Lewis acid (Scheme 2f). Several groups have reported the use of catalytic amounts of Brønsted acids as activators in the hydrogenation of quinolines (CF_3COOH,[20, 21] piperidinium hydrochloride,[22] piperidinium triflate,[23] triflic acid[24] or HCl[25]) and quinoxalines (piperidinium

hydrochloride [26]). Despite the improvement in catalyst activity and/or selectivity induced by these additives, their role has not been elucidated until now. Because they were used in catalytic amounts with respect to the substrates, it is not possible that these Brønsted acids completely prevent the binding of the heteroarene to the metal center. Several hypotheses have been made regard to the role of these additives. Firstly, it has been proposed that ammonium salts (either directly added or formed *in situ* through reaction between the heteroarene and the additive) increase the stability of the metal catalyst with an overall increase in the catalyst activity.[22] Secondly, experimental and theoretical studies on the hydrogenation of nitrogen-containing heteroarene rings have revealed that successive additions of dihydrogen and double bond migrations take place during hydrogenation.[12] Thus, it is also conceivable that these Brønsted acid additives facilitate the migration of double bonds in partially reduced heteroarene rings with an overall increase in catalyst activity.[27]

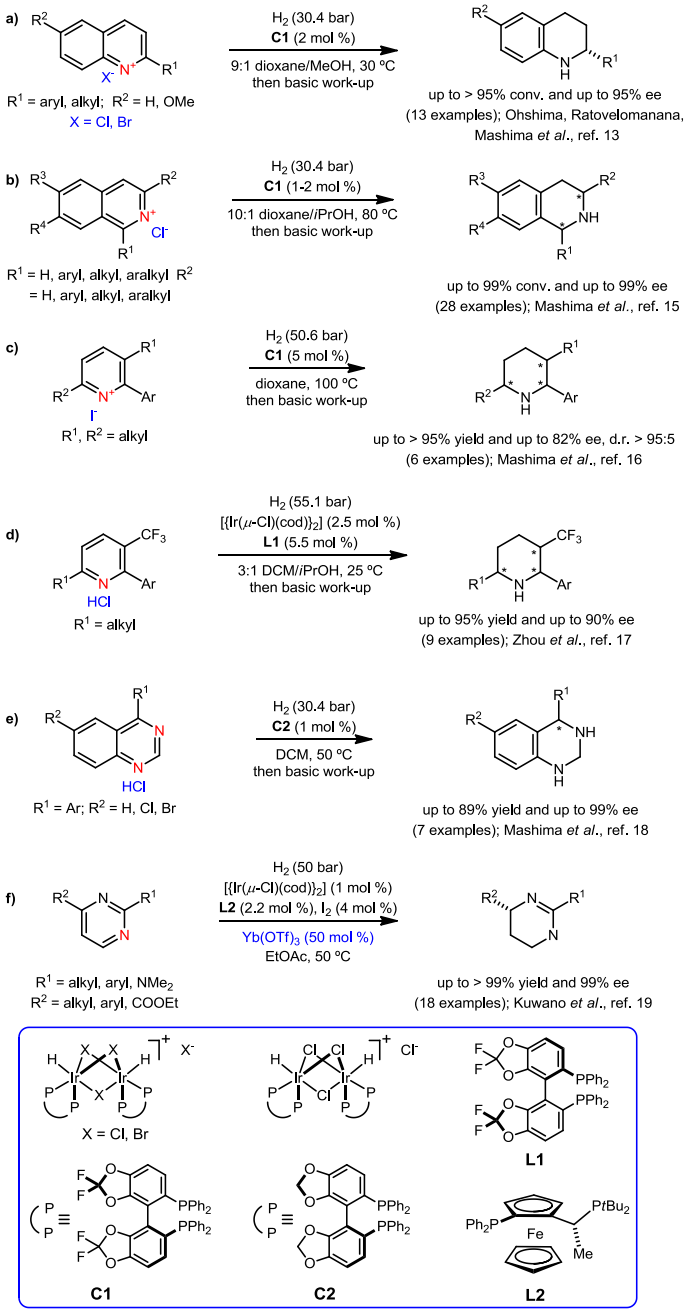

Scheme 2. Activation of C=N-containing heterocycles towards asymmetric hydrogenation by *N*-quaternization.

2A.3.1.2 Substrate *N*-derivatization

Several research groups have envisaged that the activation of simple pyridines might be achieved by derivatization at the nitrogen. Chen, Zhang, and co-workers recently reported the transformation of 2-substituted pyridines into *N*-benzylpyridinium bromides and their subsequent asymmetric hydrogenation in the presence of iridium(I) complexes derived from enantiomerically pure bisphosphines as catalysts.[28] After catalyst optimization, these authors identified that a combination of ligand **L3** and [{Ir(μ-Cl)(cod)}$_2$] (the standard iridium precursor in this chemistry) in a 1,2-dichloroethane (DCE)/acetone solvent mixture (1:1, *v/v*) provided very high levels of conversion and enantioselectivity (81–96% ee) in the hydrogenation of *N*-alkyl or *N*-aralkyl substituted pyridinium derivatives with aryl substituents in the 2-position (Scheme 3a). On the contrary, 2-alkylpyridinium substrates were obtained with low to moderate levels of enantioselection (24–69% ee). Zhou and coworkers have also reported the highly enantioselective iridium-catalyzed hydrogenation of *N*-benzylated pyrrolo[1,2–*a*]-pyrazinium systems (Scheme 3b).[29] The catalytic system consisted of [{Ir(μ-Cl)(cod)}$_2$] as iridium precursor and **L4** as ligand. Interestingly, **L4** incorporates central and axial stereogenic elements and provided up to 95% ee.

Enantioselectivities ranged from 80 to 95% ee in cases involving aryl-substituents in the pyrazinium ring (R^1 = substituted aryl groups), whereas the presence of alkyl substituents at the same position led to a significant drop in the enantioselectivity. The use of cesium carbonate increased the degree of conversion and inhibited racemization of the hydrogenated products.

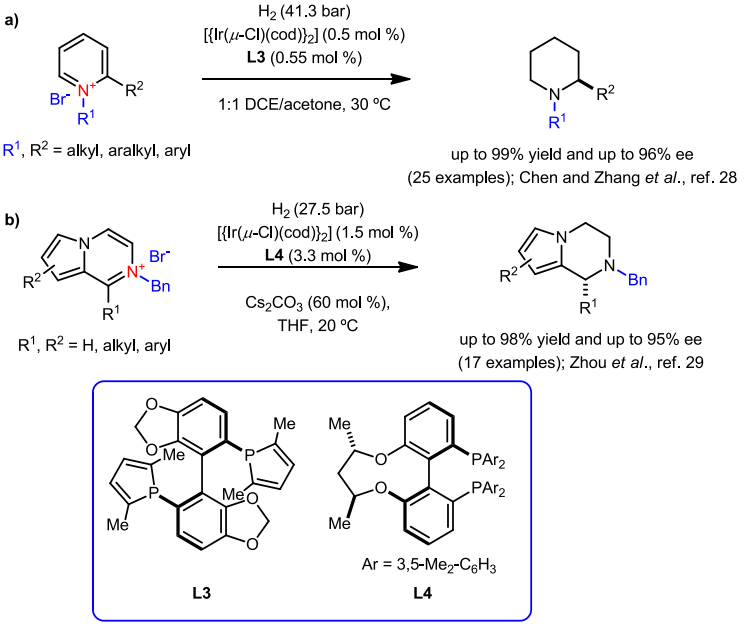

Scheme 3. Activation of heteroarenes by derivatization of the substrate.

2A.3.2 Strategy II: Chelation assistance during hydrogenation

Significant progress in the asymmetric hydrogenation of certain kinds of heteroarenes was already being made in the early 2000s. For instance, a number of efficient catalytic systems that mediate the hydrogenation of several heterocyclic systems, such as quinolines and quinoxalines, were developed. However, the hydrogenation of other kinds of relevant heterocycles such as pyridines, isoquinolines and indoles remained a challenge. Because the hydrogenation products of these heteroarenes (*i.e.* piperidines, isoquinolidines and indolines) are extremely important pharmacophores found in many bioactive compounds, chemists developed a conceptually elegant and practical synthesis of piperidines, isoquinolidines, and indolines based on chelation assistance during asymmetric hydrogenation.

The underlying principle in this strategy involved the attachment to the substrate of an auxiliary coordinating group capable of coordinating to the metal center. On the basis of the superb enantioselectivities obtained in chelation assisted asymmetric rhodium-mediated hydrogenations,[9] it was envisaged that coordination between the substrate and the metal center would be beneficial for controlling enantioselectivity. Because an acyl group is the classical model system for achieving high enantioselectivity and reactivity in rhodium-mediated hydrogenations, the groups led by Charette[30], Zhou[31,32,33], and Andersson[34] also attached acyl motifs to various six-membered heteroarenes to be hydrogenated in the presence of iridium-based enantioselective catalysts. Examples of this strategy are shown in Scheme 4.

Charette and co-workers transformed substituted pyridines into the corresponding *N*-acyliminopyridinium ylides, which were then subjected to asymmetric hydrogenation (Scheme 4a).[30] After screening different catalytic systems, the authors found that iridium cationic complexes derived from phosphinooxazoline ligands **-C3-** provided the highest levels of conversion and enantioselectivity. Conversion was essentially complete for all substrates tested (eight examples), although in some cases small quantities of partially hydrogenated compounds were detected. Enantioselectivities were generally high (up to 90%). Disubstituted pyridinium ylides were also studied. Whereas 2,3-disubstituted compounds afforded the *cis*-diastereoisomers with rather low enantioselectivities (it was observed that substitution at the 3-position was detrimental to enantioselectivities), 2,5-disubstituted pyridinium ylides were hydrogenated with high enantio- but lower diastereoselectivity. The final compounds could be efficiently converted into the corresponding piperidine derivatives by N–N bond cleavage.

An analogous strategy has been developed for the hydrogenation of quinolines and isoquinolines (Scheme 4b).[31] Quinolines were activated by

formation of the phenoxycarbonylquinolinium derivatives (R^3 = Bn) by derivatization *in situ* with benzyl chloroformate and a base. An array of substituted quinolines was efficiently hydrogenated with this activation strategy. 2-Alkyl substituted quinolines were hydrogenated with high enantioselectivity regardless of the length of the alkyl chain (*ca.* 90% ee) and the reaction did not prove to be very sensitive to the substituent in the 6-position.

Isoquinolines were also activated by the same authors with use of the same strategy (Scheme 4b). In this case, monohydrogenation took place and the corresponding 1,2-dihydroisoquinoline systems were obtained. Furthermore, conversions and enantioselectivities were lower than those observed for quinolines with the same catalytic system and activation strategy.

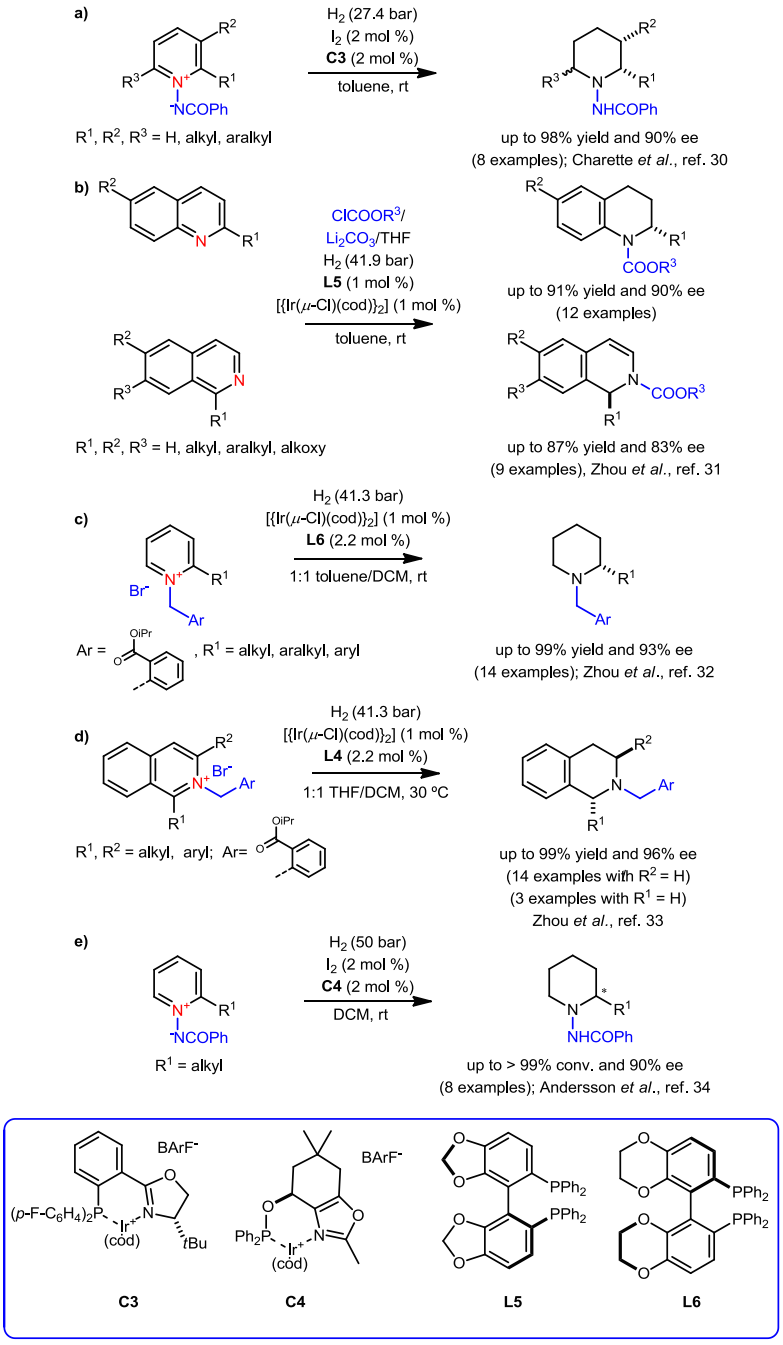

Scheme 4. Chelation-assistance during asymmetric hydrogenation of six-membered heteroarenes.

Enantioselectivities were close to 80% in most cases for monosubstituted isoquinolines (R^2 = H), although substitution in the carbocyclic ring (R^2 = OMe) led to a drop in enantioselectivity and conversion (*ca.* 64% ee). The authors did not provide any direct evidence of the participation of the acyl groups in the coordination sphere of the metal in the examples indicated in Scheme 4. However, the hydrogenation of analogous derivatives to the heterocycles indicated in Scheme 4a and 4b, but without a chelating substituent, did not proceed[30] or led to hydrogenated products with lower enantioselectivity.[35]

More recently, Zhou and co-workers reported the transformation of 2-substituted pyridines into *N*-aralkylpyridium bromides and subsequent asymmetric hydrogenation in the presence of iridium(I) complexes derived from enantiomerically pure bisphosphines as catalysts.[32] A benzyl group with a CO_2*i*Pr substituent at its *ortho*-position (Scheme 4c) was crucial in achieving high enantioselectivity, as the C=O group at the benzyl group is probably coordinated to the metal center of the catalyst, thus favoring control of enantioselectivity. After catalyst optimization, these authors demonstrated that the combination of ligand **L6** with the standard iridium precursors in this chemistry in a toluene/dichloromethane solvent mixture (1:1 *v/v*) provided very high conversions and enantioselectivities in the hydrogenation of *N*-substituted pyridinium derivatives with alkyl, benzyl and aryl substituents in the 2-position. Whereas iridium catalysts derived from **L6** enabled enantioselectivities ranging from 78 to 93% ee in the aryl substituted hydrogenated products, alkyl or benzyl substituents at the 2-position provoked a drop in enantioselectivity.

The same authors have described an analogous approach for the asymmetric hydrogenation of isoquinolinium salts.[33] The catalytic system involves ligand **L4**, which incorporates central and axial stereogenic elements. Excellent enantioselectivities are obtained for 1-aryl-substitued

substrates (up to 96% ee) and once again, the presence of a chelating C=O motif is crucial for controlling enantioselection (Scheme 4d). As observed for *N*-benzyl 2-alkylsubstituted pyridines, alkyl substituted isoquinolinium derivatives at the 1- and 3-positions (Scheme 4d) were hydrogenated with much lower ee values (43–74% ee).

Andersson *et al*. reported the hydrogenation of *ortho*-substituted *N*-iminopyridinium ylides mediated by the iridium complex **C4**. Eight substrates were explored and the ee values of the hydrogenated products ranged from 10 to 90% ee (Scheme 4e). Substrate chelation proved to be beneficial in achieving high levels of stereoselection.[34]

With regard to catalytic enantioselective hydrogenations of five-membered heteroaromatic rings, those long remained a challenge until Kuwano and coworkers reported that ruthenium complexes of enantiopure bisphosphines efficiently catalyzed the highly enantioselective hydrogenation of *N*-acyl indoles.[36] Although each of their hydrogenated indole derivatives contain a *N*-acyl group, which is *a priori* capable of coordinating to the metal center, Kuwano and coworkers do not attribute any effect of the potential coordination of the substrate to the metal center to the outstandingly high levels of conversion and enantioselectivity achieved. Further examples of successful hydrogenation of indole derivatives with *N*-Ac, *N*-Boc and *N*-Ts substituents were reported by the same research group,[37] by Pfaltz and coworkers[38] and by Feringa, de Vries and coworkers.[39] The results described for *N*-acetyl, *N*-Boc and *N*-tosylindoles by all these research groups demonstrate that the substituent at the nitrogen greatly influences the level of conversion and enantioselectivity achieved in the hydrogenation processes.[36–39] However, no conclusive evidences on the coordination of the *N*-substituents to the metal center is provided by the authors.

2A.3.3 Strategy III: Hydrogenation after breaking the aromaticity

The stability of these heteroaromatic compounds can result in the need for harsh hydrogenation conditions for breaking their aromaticity and low enantioselectivities of the hydrogenated products due to the high temperatures normally required. Breaking the aromaticity of the heteroarenes to be hydrogenated is not feasible for all kinds of substrates, but it was considered an intuitive step to undertake in order to facilitate hydrogenation, whenever aromaticity could be broken. For instance, it was known that simple unprotected indoles reacted with strong Brønsted acids to form iminium derivatives through protonation of the C=C double bond of the five-membered ring (Method A in Scheme 5).[40]

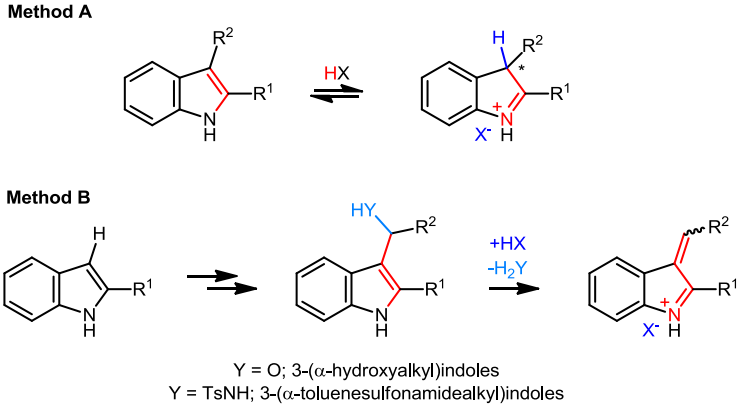

Scheme 5. Strategies for breaking the aromaticity in indoles.

Zhang, Zhou, and co-workers developed this idea and envisaged that the iminium compounds produced *in situ* according to Method A in Scheme 5 might be more prone to hydrogenation than the original indole derivatives. Catalyst screening studies in the hydrogenation of 2-methyl indole identified palladium complexes incorporating ligand **L7** as the most efficient catalyst. The combined use of these palladium complexes and L-camphorsulfonic acid (L-CSA) in a mixture of dichloromethane and

trifluoroethanol (TFE) as a solvent mediated the asymmetric hydrogenation of 2-methyl indole with a high levels conversion (>95%) and enantioselectivity (91% ee in favor of the (*R*)-enantiomer of the corresponding indoline).[41] Under the optimized reaction conditions, an array of diversely substituted indoles (13 examples), each possessing only one substituent in the five-membered ring, was hydrogenated with excellent yields (up to 99%) and enantioselectivities (up to 96% ee; Scheme 6a).[41,42]

Hydrogenation of 2,3-disubstituted indoles by this methodology deserves especial mention,[42] because it results in the formation of two contiguous stereogenic centers, one of which (the one corresponding to C3) should be formed during protonation and the other (the one relating to C2) during the hydrogenation process (Scheme 6b). The authors reasoned that if protonation could be made to take place at a higher rate than hydrogenation, the overall process could be driven under dynamic kinetic resolution conditions and might benefit from a reduction in the number of formed stereoisomers. The use of the palladium complexes incorporating ligand **L7** in combination with a protic acid different from that used for monosubstituted indoles (*p*-TsOH instead of L-CSA) at a higher reaction temperature in the same solvent mixture enabled the efficient preparation of 2,3-disubstituted indolines. Under these conditions, a variety of 2,3-substituted indoles (17 examples) were hydrogenated with excellent yields (up to 97%), diastereo- (only *cis*-diastereoisomers were obtained) and enantioselectivities (up to 98% ee; Scheme 6b). Alkyl, aryl and aralkyl substituents were tolerated in the indole ring, though enantioselectivities for 3-benzyl-substituted indoles were slightly lower than those for their 3-alkyl analogues. Fused-ring substrates were also satisfactorily hydrogenated (up to 96% ee). The effects of the substituents in the carbocycle were not extensively studied, although trisubstituted indoles with a 5-F substituent displayed slightly lower ee values than their F-

unsubstituted analogues (up to a 4% decrease in the ee). Combined experimental and theoretical studies suggest that the aforementioned bisphosphine-palladium complexes mediated the hydrogenations through an outer-sphere mechanism with stepwise proton and hydride transfers.[42] The authors reported the hydrogenation of unprotected indoles by the same strategy with ligand **L8** and $EtSO_3H$ as additive, although the results obtained in terms of enantioselectivity were not as good (up to 87% ee*;* Scheme 6c) as with *p*-TsOH (Scheme 6b).[43]

Liu, Wang and coworkers also reported the hydrogenation of indole systems with Pd(II) complexes derived from the BridgePhos ligand **L9**, which exhibits a large bite angle, with excellent enantioselectivities (up to 98% ee; 19 differently substituted indoles using D-CSA as activator; Scheme 6d).[44]

Although the above examples constituted efficient asymmetric hydrogenation of indoles, several practical challenges remained. First and foremost, stoichiometric amounts of a Brønsted acid are required, which calls for the recycling and reuse of the activator. Secondly, relatively high catalyst loadings (2 mol % of palladium precursor and 2.4 mol % of ligand) are used. Vidal-Ferran and coworkers reported the use of neutral iridium complexes of enantiomerically pure P–OP ligand **L10** (1 mol %) and (reusable) Brønsted acids for the efficient conversion of unprotected indoles into enantiomerically enriched indolines (six examples, up to 78% isolated yield and up to 91% ee; Scheme 6e).[45] Interestingly, the DOWEX™ resin used in this approach was recovered, recycled and reused up to twice, giving comparable catalytic activity.

A similar strategy combining enantiomerically pure palladium complexes derived from ligand **L11** and ethanesulfonic acid as activator enabled the efficient hydrogenation of 2-alkyl-5-aryl-substituted pyrroles (15 examples, up to 91% yield, up to 92% ee) to afford the corresponding 3,4-dihydro-2*H*-pyrrole derivatives (Scheme 6f).[46]

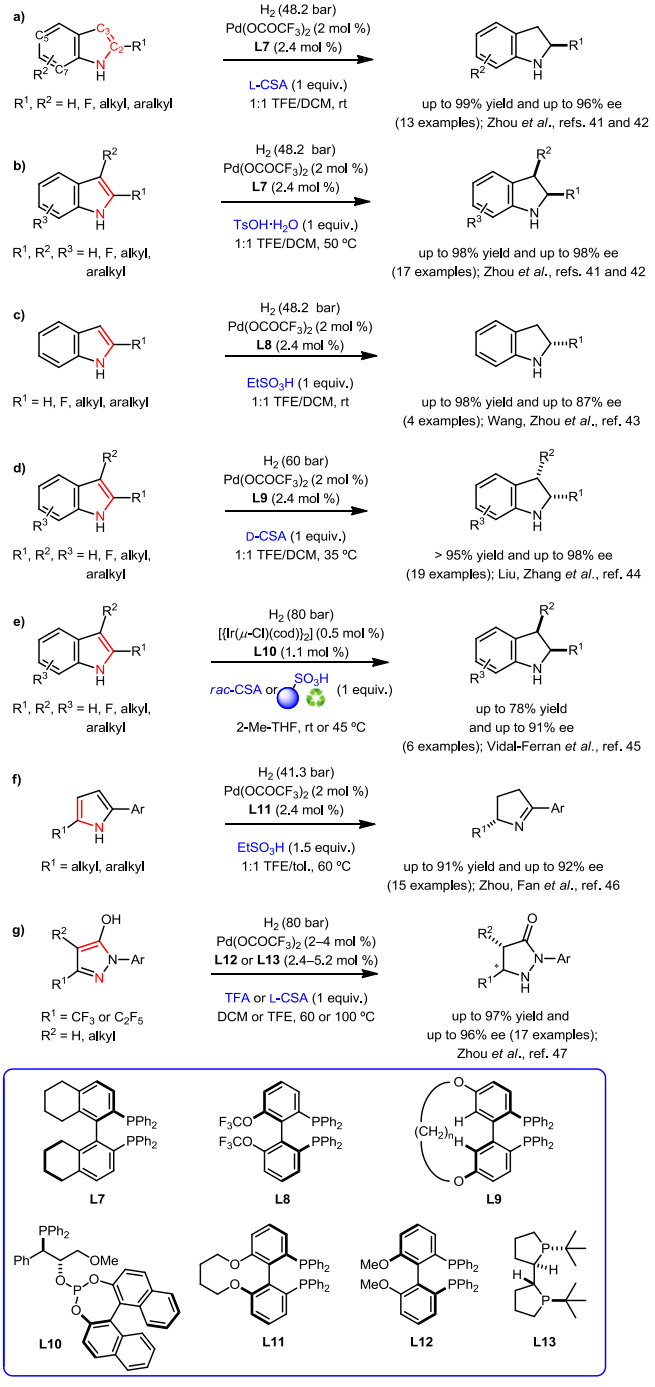

Scheme 6. Asymmetric hydrogenation of indoles and pyrroles.

Very recently, Zhou *et al*. reported the asymmetric hydrogenation of fluorinated pyrazol-5-ols by capturing one of the tautomers with the aid of a strong Brønsted acid as activator. Two catalytic systems were developed for 4-unsubstituted of 4-substituted pyrazol-5-ols, which based on the use of ligand **L12** or **L13** and TFA or L-CSA as activators, respectively (Scheme 6g).[47] The hydrogenation of up to 17 examples was reported, with overall enantioselectivity in the corresponding substituted hydrogenated compounds ranging from 82 to 96% ee.

Because partially saturated indoles represent an interesting class of organic molecules that can be found in many bioactive compounds, other activation methods for increasing the reactivity of indole derivatives towards hydrogenation involving C=C double bond migration have also been developed (Method B in Scheme 5). [48] Easily available 3-(α-hydroxyalkyl)indoles can readily be dehydrated in the presence of a Brønsted acid to form a conjugated iminium derivatives, in which the aromaticity has been partially broken.[49] Zhou, Jiang *et al*. took advantage of some of the palladium-based enantioselective catalytic systems described previously (see Scheme 7) for the hydrogenation of 3*H*-indol-1-ium derivatives.[48] In this case, the iminium derivatives (produced *in situ*) were efficiently hydrogenated in the presence of the standard palladium precursor and ligand **L7** in high yields (up to 99%) and with enantioselectivities ranging from 85 to 97% (Scheme 7a). This methodology provided an efficient route to enantiomerically enriched 2,3-disubstituted indolines (20 examples) all possessing relative *cis*-stereochemistry of the two substituents of the indoline ring. A wide variety of aryl and aralkyl substituents at the 2- and 3-positions of the indole system did not provoke major changes in the enantioselectivities (ee values ranged from 88 to 94% ee). Substitution at the 5-position of the indole with a fluoro group brought ee values to the lowest levels seen in the

series due to steric and electronic effects, whereas the highest enantioselectivities were obtained with a methyl group at the 7-position, probably due to steric effects.[48]

Zhou and co-workers[50] prepared a set of enantioenriched indolines analogous to that reported by Zhou, Jiang and coworkers[48] using an elegant tandem condensation and hydrogenation process. The tandem process involved a Brønsted-acid-promoted Friedel-Crafts reaction of the C3-unsubstituted indole to yield the corresponding 3-(α-hydroxyalkyl)indoles, which were directly hydrogenated in the presence of the catalytic system incorporating ligand **L7** (Scheme 7a). The overall selectivity of the process is similar regardless of how the 3-(α-hydroxyalkyl)indoles are prepared (preformed in Zhou's and Jiang's method[48] or generated *in situ* in Zhou's tandem process[50]).

Analogous 2,3-disubstituted indolines were obtained from 3-(tolylsulfonamidoalkyl)indoles (Scheme 7b), their asymmetric hydrogenation catalyzed by palladium complexes of ligand **L7** was triggered by acid-mediated elimination of toluenesulfonamide ($TsNH_2$). This method also proved to be highly efficient and fourteen di- or tri-substituted indolines were efficiently prepared (up to 97% yield and 97% ee) following this approach.[51]

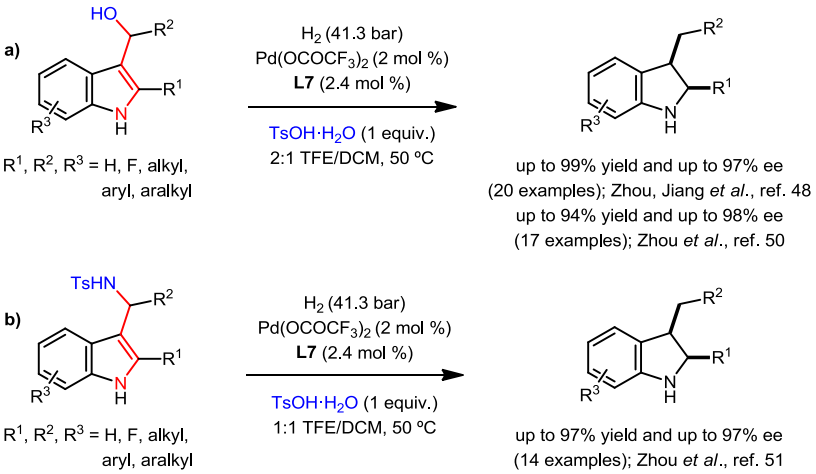

Scheme 7. Elimination-triggered asymmetric hydrogenation of indoles.

As a conclusion to this section, asymmetric hydrogenation of indoles triggered either by protonation or by double bond migration has enabled access to a wide variety of mono-, di-, or tri-substituted indolines with high enantioselectivities. Palladium- or iridium-based hydrogenation catalysts have been used for this transformation. A strategy for recovering, recycling, and reusing the stoichiometric amounts of the required Brønsted acids has also been developed. However, the main limitation lies in the fact that triggering hydrogenation by protonation or double bond migration can intrinsically only be applied to a reduced number of heteroarenes (for instance, indole, pyrrole, and pyrazole derivatives, as has been demonstrated to date).

2A.4 Conclusions and Future Outlook

In this review we have focused on the various strategies devised to activate heteroaromatic substrates towards asymmetric hydrogenation by manipulation of their structures. The published examples have been classified into three different strategies, and the most relevant experimental details (catalyst employed, reaction conditions used, type of

heteroarene, structural diversity, and catalyst activity in terms of conversion and enantioselectivity) have been highlighted in the different schemes throughout the text. These strategies include the formation of positively charged derivatives of the heteroarene (Strategy I), the introduction of a coordinating group that facilitates the hydrogenation by chelation assistance (Strategy II), and hydrogenation after breaking of the aromaticity (Strategy III). The use of an appropriate activation strategy for a given type of heteroarene has enabled access to a wide variety of fully and partially hydrogenated mono- and bi-cyclic heterocyclic compounds with excellent levels of conversion and enantioselectivity. In view of the wide repertoire of available ligand scaffolds and the ever-increasing number of reports on the application of substrate manipulation as a tool for improving the reactivity of heteroarenes in asymmetric hydrogenation, one can only imagine that the near future will witness several new examples of successful application of this methodology.

Subchapter B- Expansion of the scope of P–OP mediated iridium hydrogenations to new types of heterocycles

Asymmetric Hydrogenation of Seven-membered C=N-Containing Heterocycles and Rationalization of the Enantioselectivity[1]

Bugga Balakrishna,[†,] Antonio Bauzá,[§] Antonio Frontera,[,§]
Anton Vidal-Ferran*[,†,‡]

† Institute of Chemical Research of Catalonia (ICIQ) & Barcelona Institute of Science and Technology, Avinguda Països Catalans 16, E-43007, Tarragona, Spain.

‡ Catalan Institution for Research and Advanced Studies (ICREA), Passeig Lluís Companys 23, E-08010 Barcelona, Spain.

§ Departament de Química, Universitat de les Illes Balears (UIB), Cra. de Valldemossa, km 7.5. Palma, 07122 Palma de Mallorca, Spain..

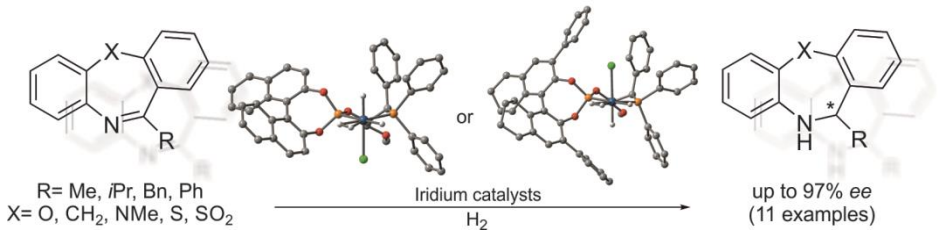

[1] The rationalization of the enantioselectivity by means of computational studies has been performed by Mr. Antonio Bauzá under the supervision of Prof. Dr. Antonio Frontera (Universitat de les Illes Balears). A summary of the main conclusions of these calculations have been included in this subchapter to aid discussion.

2B.1 Abstract

Iridium(I) complexes of phosphine-phosphite ligands efficiently catalyze the enantioselective hydrogenation of diverse seven-membered C=N-containing heterocyclic compounds (eleven examples; up to 97% ee). P–OP ligand **L3**, which incorporates an *ortho*-diphenyl substituted octahydrobinol phosphite fragment, provided the highest enantioselectivities in the hydrogenation of most of the *N*-heteroarenes that were studied. The observed sense of stereoselection was rationalized by means of DFT calculations.

2B.2 Introduction

Many biologically active compounds contain a chiral heterocyclic structural motif.[7] Method development to access partly or fully reduced enantiopure heterocycles has been growing in scope and importance in recent years. The enantioselective reduction of heterocyclic compounds is becoming more important in the preparation of their partly or fully reduced analogues, as this strategy benefits of a great diversity of starting materials and minimizes the need for manipulation of functional groups during the preparation of the target compounds.[8,10,11, 52] Transition metal-catalyzed asymmetric hydrogenation has been employed to reduce a large number of nitrogenated heterocyclic compounds (for instance pyridines and other monocyclic nitrogenated derivatives, quinolines, isoquinolines, quinoxalines and related compounds, benzoxazines and related derivatives, indoles, etc.) with high catalytic efficiencies and enantioselectivities. Although nitrogenated seven-membered heterocyclic motifs with stereogenic centers constitute an important pharmacophore,[53] examples of asymmetric reduction of seven-membered heterocyclic derivatives are scarce in the literature.[54]

We recently reported the hydrogenation of an array of structurally diverse five- and six-membered heterocyclic compounds **1** mediated by

iridium(I) complexes of phosphine-phosphite ligands[55] [Ir(Cl)(cod)(P–OP)] with high catalytic activity (Scheme 8).[25,27,45] Ligand **L1**, which incorporates an (R_a)-configured [1,1'-binaphthalene]-2,2'-diol phosphite group, provided the highest enantioselectivities in the asymmetric hydrogenation of heterocyclic compounds **1**. Interestingly, we described that the addition of a Brønsted acid (cat. amounts of HCl for 2-alkyl substituted quinolines[25] and quinoxalines[25] and stoichiometric amounts of *rac*-camphorsulfonic acid for indoles[45]) increased the conversion of the hydrogenation reaction and even positively affected the enantioselectivity.[25] Herein we report the development of efficient [Ir(P–OP)] complexes as catalysts for the enantioselective asymmetric hydrogenation of diversely substituted seven-membered C=N-containing heterocyclic compounds (see structures **3**, **5**, **7**, **9** and **11** in Scheme 8).

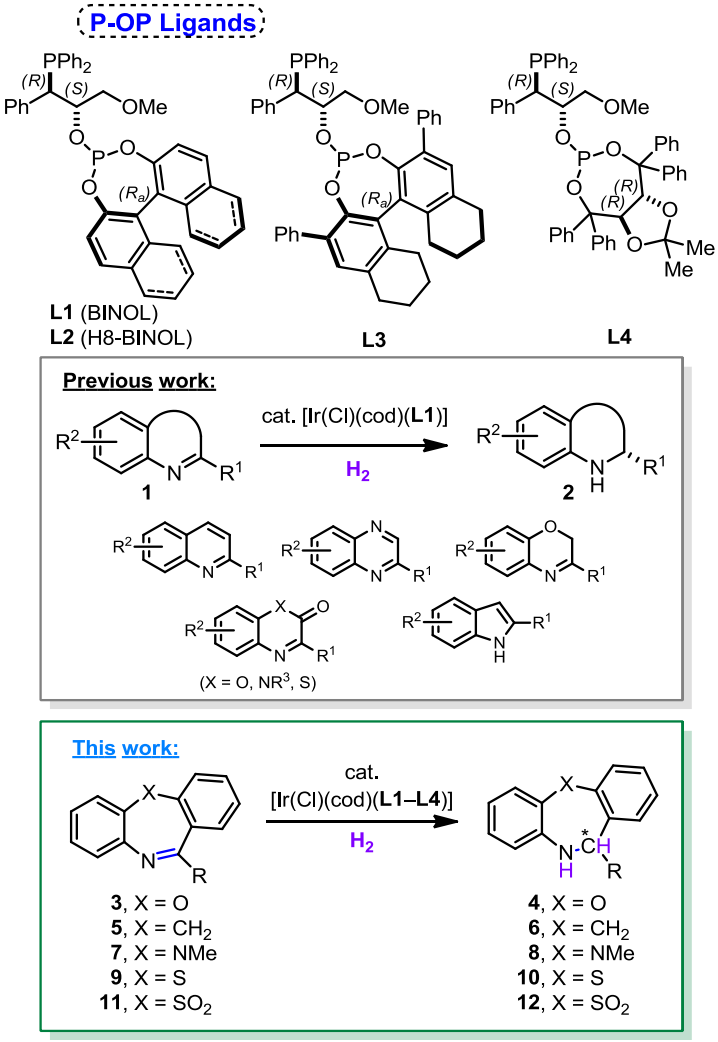

Scheme 8. Enantioselective partial hydrogenation of nitrogenated heterocyclic compounds.

2B.3 Results and Discussion

2B.3.1 Ir-catalyzed asymmetric hydrogenation. Initial screening and optimization

The present work began with the enantioselective hydrogenation of oxazepine **3a** as model substrate using well-established[25] *in situ* prepared iridium complexes of P–OP ligands **L1**–**L4** as precatalysts. The reaction conditions studied (1 mol % cat.; [**3a**] = 0.2 M in THF, 80 bar H_2, rt) efficiently led to the hydrogenated product **4a** with complete conversion in the absence of HCl as additive (see entries 1, 3, 5 and 7 in Table 1) with enantioselectivities ranging from 16% ee for **L4** to 79% ee for **L3**.[56] Enantioselectivities were improved by using 10 mol % of HCl in the case of ligands **L1**, **L2** and **L3** (compare entries 1, 3 and 5 with entries 2, 4 and 6 in Table 1), with ligand **L3** providing the highest enantioselectivities (86% ee, entry 6 in Table 1). The effects of a set of achiral and enantiomerically pure additives on the hydrogenation of substrate **3a** were also studied,[57] however the best results were obtained with HCl as the additive. Further attempts to optimize the hydrogenation conditions were aimed at varying the amount of HCl (see entry 9 in Table 1) and reducing the temperature (see entry 10 in Table 1). Increasing of the amount of additive did not have any effect on the catalytic activity (compare entries 6 and 9 in Table 1). The hydrogenation of **3a** was also run at lower temperature (0 ºC instead of rt), based on the premise that lowering the temperature normally offers higher enantioselectivity. As listed in entry 10 of Table 1, the ee at 0 ºC was 1% higher than at rt. However, further hydrogenation studies at this temperature were not considered, as conversion was not complete. The enantioselectivity of the hydrogenation of **3a** was solvent dependent, and 2-methyltetrahydrofuran (MeTHF), dichloromethane (DCM) or toluene lead to a noticeable increase in the ee of the reaction (compare entries 11, 12 and 13 with entry 6 in Table 1).

Table 1. Asymmetric hydrogenation[a] of **3a** mediated by [Ir(Cl)(cod)(**L1**–**L4**)]

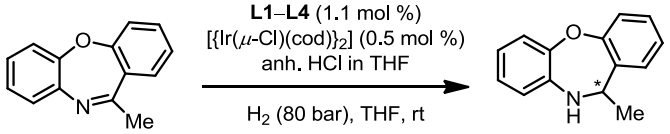

Entry	Ligand	Reaction conditions	Conv[b]	ee (%)[c] (config.)[d]
1	**L1**	No additive	99	42 (*S*)
2	**L1**	10 mol % of HCl	99	53 (*S*)
3	**L2**	No additive	99	29 (*S*)
4	**L2**	10 mol % of HCl	99	57 (*S*)
5	**L3**	No additive	99	79 (*R*)
6	**L3**	10 mol % of HCl	99	86 (*R*)
7	**L4**	No additive	99	16 (*S*)
8	**L4**	10 mol % of HCl	99[e]	8 (*S*)
9	**L3**	20 mol % of HCl	99	86 (*R*)
10	**L3**	10 mol % of HCl, 0 ºC	90	87 (*R*)
11	**L3**	10 mol % of HCl, DCM	99	91 (*R*)
12	**L3**	10 mol % of HCl, toluene	99	91 (*R*)
13	**L3**	10 mol % of HCl, MeTHF[f]	99	91 (*R*)

[a] Reaction conditions: [{Ir(μ–Cl)(cod)}$_2$]/P–OP ligand/substrate = 0.5:1.1:100 for precatalyst levels of 1 mol %, respectively, at rt, 20 h and a substrate concentration of 0.20 M in THF. If additive was present, the indicated amount of additive with respect to **3a** was added to a solution of the substrate before adding the catalyst. The values shown are the average of at least two runs. [b] Conversions were determined by ^{1}H NMR. [c] Determined by HPLC analysis using chiral stationary phases. [d] Absolute configuration was assigned by comparison with literature data (see ref. 54c). [e] The selectivity of the reaction towards **4a** was 35%. [f] MeTHF ≡ 2-methyltetrahydrofuran.

2B.3.2 Expanding the substrate scope

Once the optimal hydrogenation conditions for **3a** had been established, the hydrogenation of an array of seven-membered heterocycles was studied. 2-Methyltetrahydrofuran was chosen as the optimal solvent for further studies, given the overall good results in the hydrogenation of **3a**. The heterocycles studied and the optimal ligand (**L1** or **L3**) for achieving the highest ee's are summarized in Table 2. The results using 10 mol % of HCl are only indicated in Table 2 when this additive provided higher conversions and/or ee's. The reader is referred to the Supplementary Information (Table SI3) for the complete hydrogenation results employing **L1** or **L3** as ligands and in the absence or presence of anhydrous HCl as additive.

Several trends can be extracted from the results listed in Table 2. Firstly, **L3** was the ligand of choice for heterocycles with R = alkyl group (entries 1, 3–5, 7, 9 and 11 in Table 2). For these substrates, ee's ranged from 70 to 91%, with the highest ee's being obtained for oxazepine **4a** and thiazepine **9a** (91% ee; see entries 1 and 9 in Table 2). Secondly, the use of HCl as additive in the hydrogenation of substrates with R being an alkyl group had, with the exception of substrates **3c** and **5a** (see entries 3 and 5 in Table 2), a positive effect on the ee's.[58] Examples of the use of Brønsted acids as substrate activators in iridium-mediated hydrogenations are numerous[52j] but, despite the improvement in catalyst activity and/or selectivity induced by these additives, their role remains unclear.[52j] The third and last trend that can be extracted from the data summarized in Table 2, is that the hydrogenation of the substrates with R = Ph (compounds **3b**, **5b**, **7b** and **9b**) was more complicated than that of their alkyl substituted analogues. Though the hydrogenation of the *O*- and *S*-containing substrates took place efficiently in the absence of HCl (conversions up to 97%, ee's up to 97%, entries 2 and 10 in Table 2), the

hydrogenation of carbon and nitrogen-analogues **5b** and **7b** proceeded with low conversions and ee's (entries 6 and 8 in Table 2).

Table 2. Asymmetric hydrogenation[a] of seven-membered *N*-Heterocyclic compounds mediated by [Ir(Cl)(cod)(**L1** or **L3**)]

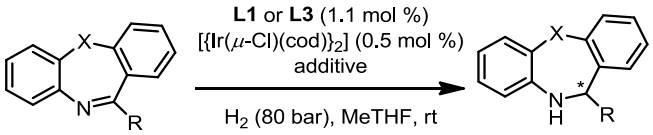

3, **5**, **7**, **9**, **11** — **4**, **6**, **8**, **10**, **12**

Entry	Substrate (X, R)	Ligand	Additive	Conv[b]	ee (%)[c] (config.)[d]
1	**3a** (O, Me)[e]	**L3**	10 mol % of HCl	99	91 (*R*)
2	**3b** (O, Ph)	**L1**	none	97	83 (*S*)
3	**3c** (O, *i*Pr)	**L3**	none	99	73 (*R*)
4	**3d** (O, Bn)	**L3**	10 mol % of HCl	99[f]	87 (*R*)
5	**5a** (CH_2, Me)	**L3**	none	99	70 (*R*)
6	**5b** (CH_2, Ph)	**L3**	10 mol % of HCl	33[g]	9 (*S*)
7	**7a** (NMe, Me)	**L3**	10 mol % of HCl	99	84 (*R*)
8	**7b** (NMe, Ph)	**L1**	none	24[g]	36 (*S*)
9	**9a** (S, Me)	**L3**	10 mol % of HCl	99	91 (*R*)
10	**9b** (S, Ph)	**L3**	none	72[f]	97 (*S*)
11	**11a** (SO_2, Me)	**L3**	10 mol % of HCl	99[f]	77 (*R*)

[a] Reaction conditions: [{Ir(μ–Cl)(cod)}$_2$]/P–OP ligand/substrate = 0.5:1.1:100 for precatalyst levels of 1 mol %, respectively, at rt, 20 h and a substrate concentration of 0.20 M in MeTHF. If additive was present, the indicated amount of additive with respect to substrate was added to a solution of the substrate before adding the catalyst. The values shown are the average of at least two runs. [b] Conversions were determined by ^{1}H NMR. Isolated yields after chromatography were >95%, unless otherwise stated. [c] Determined by HPLC analysis using chiral stationary phases. [d] Absolute configurations of **4a**, **4b**, **4d**, **10a** and **10b** were assigned by comparison with literature data (see ref. 54c for the oxazepines and ref. 54h for the thiazepines). The configurations of **4c**, **6a**, **6b**, **8a** and **8b** were assumed by analogy. The absolute configuration of **12a** was determined by X-ray analysis (see SI for details). [e] These results have been already summarized in Table 1, but are included here for comparison. [f] Isolated yields for **4d**, **10b** and **12a** were, 32%, 53% and 59%, respectively. [g] Isolation was not attempted due to low conversions and ee's.

Previous work from our group on asymmetric hydrogenations mediated by Ir- [25, 27, 45] or Rh-complexes [59] of P–OP ligands revealed that the phosphite group was the principal stereochemical director in the reaction (opposite configurations for the resulting hydrogenated products are obtained when the configuration of the phosphite moiety is inverted). Moreover, the introduction of substituents at the 3 and 3' positions of the [1,1'-biaryl]-2,2'-diol group did not change the configuration of the final product in Rh-mediated hydrogenations.[59] Interestingly, ligands **L1** (or **L2**) and **L3**, whose main difference is the presence or absence of substituents at the 3 and 3' positions of the binaphthyl motif, led to opposite enantiomers of **4**, **6** and **8** depending on the nature of the R substituent (alkyl or aryl groups; as an example, see Scheme 9 for the hydrogenation reactions leading to **4**).

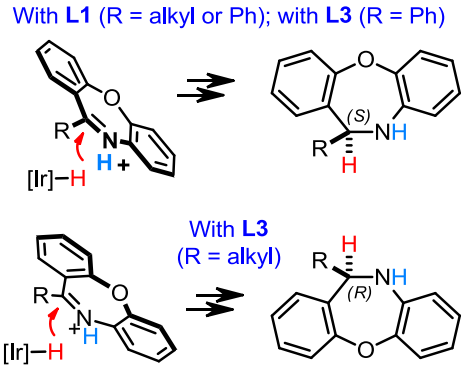

Scheme 9. Hydrogenation reactions of **3** leading to products **4**.

2B.3.3 Rationalization of the stereochemical outcome of the hydrogenations by DFT calculations

To shed light on the correlation between the features of the P–OP ligands and enantioselection in the hydrogenation towards alkyl-substituted products, we performed a theoretical investigation into the reactivity of the catalytic systems derived from ligands **L1** and **L3** with substrate **3a**. We considered this substrate to be suited to our purposes, as the configuration of the final product depends on whether the substituents at the 3 and 3' positions of the phosphite group are H (**L1**; *S*-configured product, see entries 1 and 2 in Table 1 and Scheme 9) or Ph groups (**L3**; *R*-configured product; see entries 5 and 6 in Table 1 and Scheme 9) and the absolute stereochemistry of its hydrogenated product was unequivocally assigned. The usual approach for theoretical studies on enantioselective processes is to focus on the stereo-determining step and compare the energy of transition states (TS's) for the paths leading to the (*R*) and (*S*) products.[60] The mechanism for the hydrogenation of iminic bonds is complex but has been explored at the experimental and theoretical level by a number of groups. Mechanistic studies from Pfaltz and co-workers have revealed that the employed iridium complexes react with the acyclic C=N-containing substrates to form a cyclometallated iridium complex that is the real hydrogenation catalyst.[61] On the contrary, a number of mechanistic studies from other research groups have revealed that the most favored process is the transfer of proton and hydride to the C=N bond of the heterocyclic derivative being non-coordinated to the metal center.[62]

We first explored the possibility of the hydrogenation pathway involving the formation of cyclometallated iridium complexes derived from **3a**. The stabilities of the plausible four-membered iridacycles derived from **3a** were computed at the BP86/def2-SVP level of theory (see Figure SI67), which is a good compromise between the size of the system (up to

139 atoms for the iridacycle involving **L3**) and the accuracy of the results. The energy content of the resulting four-membered iridacycles was very elevated indicating the highly strained nature of these compounds.[63] Therefore this hydrogenation pathway *via* the formation of such intermediates derived from **3a** was not further explored. As regards the hydrogenation pathway involving proton and hydride transfers to the C=N bond of heterocyclic derivatives, Crabtree and Eisenstein[62b] identified octahedral dihydrido mono-dihydrogen iridium complexes as crucial intermediates in the hydrogenation process, as hydrogen transfer from H_2 to the C=N bond starts with proton migration from the dihydrogen ligand to the nitrogen atom. Once the C=N bond is protonated,[64] the position alpha to nitrogen is activated for the subsequent hydride transfer, which is the stereo-determining step (see Scheme 9).

We[25] and others[55b] have demonstrated that the complexation of P–OP ligands with [{Ir(μ-Cl)(cod)}$_2$] quantitatively leads to compounds [Ir(Cl)(cod)(P–OP)], which correspond to the expected neutral pentacoordinated iridium(I) complexes. Removal of the cod ligand under hydrogenative conditions led to a complex mixture of [Ir(P–OP)] complexes. Unfortunately, neither NMR nor X-ray analysis allowed us to unequivocally establish the structure of the iridium complexes present in solution (no crystals suitable for X-ray analysis could be isolated from this mixture). For this reason, the relative stabilities of the plausible [Ir(Cl)(H)$_2$(H–H)(**L1** or **L3**)] complexes were computed at the BP86/def2-SVP level of theory. From among all the possible isomers in an octahedral iridium complex with one bidentate (**L1** or **L3**) and one chlorido ligand, only those with the two hydrido and dihydrogen ligands in a *fac*[65] (facial) geometry were considered[66] (hydrogen transfer from [Ir(Cl)(H)$_2$(H–H)(**L1** or **L3**)] complexes will lead to a trihydrido iridium complex and metal trihydrides have an intrinsic preference[62b] for a *fac* geometry to avoid

hydrido ligands that are mutually placed in a *trans* fashion). Interestingly, in [Ir(Cl)(H)$_2$(H–H)(**L1**)] the favorable *fac* isomers (see Figure 1) present the chlorido ligand pointing in the same direction and perpendicular to the plane that contains the P–OP and Ir atoms (see Figure 1a,b). The slightly more favored complex (difference 0.3 kcal·mol^{-1}) has the H–H ligand *cis* to the phosphite group. With regard to [Ir(Cl)(H)$_2$(H–H)(**L3**)], the lowest energy isomers also present the chlorido ligand perpendicular to the same plane but pointing in the opposite direction with respect to the [Ir(Cl)(H)$_2$(H–H)(**L1**)] complexes (see Figure 1c,d). This is due to the formation of intramolecular C–H···Cl bonds (see Figure 1 and SI69). This differentiating feature is very important for rationalizing the opposite enantioselectivity observed for **L1** and **L3** with methyl substituted substrates such as **3a** (*vide infra*).

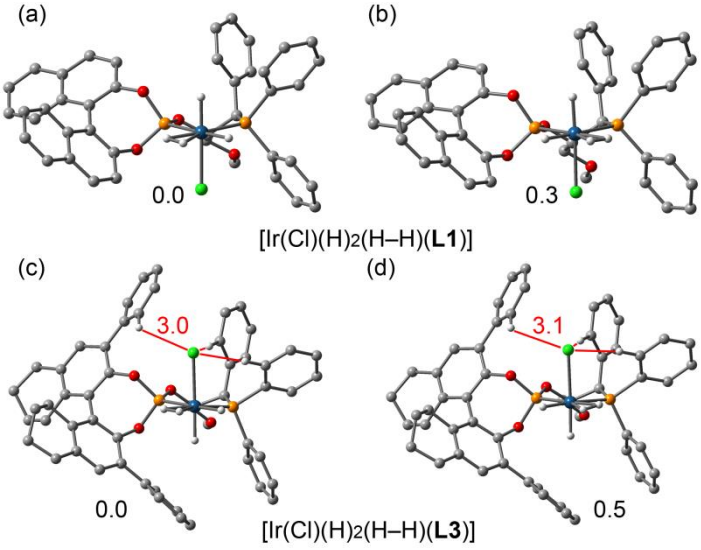

Figure 1. (a–d) Optimized geometries of the most stable isomers of [Ir(Cl)(H)$_2$(H–H)(**L1** or **L3**)] (some H atoms omitted for clarity; distances in Å, Relative energy profiles in kcal·mol^{-1}).

Protonation of **3a** by [Ir(Cl)$(H)_2$(H–H)(**L1** or **L3**)][64] leads to the [H**3a**][Ir(Cl)$(H)_3$(**L1** or **L3**)] assembly (see Figure 2a,b). Either isomer of complex [Ir(Cl)$(H)_2$(H–H)(**L1**)] (see Figure 1a,b) yields the same *fac* trihydrido iridium complex upon proton transfer (same behavior for **L3**), which simplifies the study. Proton transfer is not the stereo-determining step and the configuration of the final product is determined at later stages of the catalytic cycle. Therefore we started the calculations for understanding the stereochemical outcome of the reaction from the protonated substrate (H**3a**). Beginning from the initial geometry after proton transfer, where the N–H group points to the Ir–H motif (see Figure 2a,b), we examined different orientations for the protonated substrate (H**3a**) interacting with [Ir(Cl)$(H)_3$(**L1** or **L3**)]. Remarkably, we found a pre-TS complex for each ligand (see Figure 2c,d) that were lower in energy than the initial assembly due to the formation of favorable non-covalent interactions. In the case of **L1**, the preferred arrangement is governed by two interactions that fix the geometry of the substrate (H-bond and $CH_3\cdots\pi$ interactions, see Figure 2c). This preorganized complex facilitates the nucleophilic attack of the hydrido group that is located 3.0 Å away from the C atom in the C=N group (pro-(*S*) attack). In the case of **L3**, the presence of the chlorido ligand at the opposite position to the P–OP containing plane with respect to **L1** and the formation of a strong N–H···Cl interaction fixes the substrate in a different arrangement compared to **L1**. Moreover the formation of a C–H···H–Ir non-covalent interaction (see Figure 2b) fixes the position of the substrate, facilitating the pro-(*R*) attack of the hydrido ligand (located at 3.1 Å). The pre-TS complexes that would organize the protonated substrate towards the minor enantiomer (*i.e.* pro-(*R*) attack for **L1** and pro-(*S*) attack for **L3**) were not found in the potential hypersurface. The geometries of the TS's are shown in Figure 3 and Figure SI70. It is important to note the existence of strong

N–H···Cl hydrogen bonds in the favored TS's. These interactions are crucial in rationalizing the observed sense of stereoselection. The difference in energy between the two TS's states derived from **L1** ($\Delta\Delta G^{\#}$ = 2.2 kcal·mol^{-1}) is mainly governed by the different strength of two hydrogen-bond interactions: an N–H···Cl hydrogen-bond for the TS leading to the major enantiomer (TS_S; see Figure 3a) and an N–H···O hydrogen-bond for the TS leading to the minor enantiomer (TS_R; see Figure SI70a). Since the N–H···Cl interaction involves an anionic ligand, it is electrostatically favored with respect to the N–H···O interaction. As regards to **L3**, the transition state leading to the major enantiomer is also stabilized by an N–H···Cl hydrogen-bond (TS_R; see Figure 3b), whilst that leading to the minor enantiomer is only stabilized by a weaker N–H···π interaction involving a phenyl group (see Figure SI70b). Since this N–H···π interaction involving TS_S derived from **L3** is also weaker than the N–H···O hydrogen bond in TS_R derived from **L1** (both leading to the minor enantiomers of the hydrogenation product of **3a**), the $\Delta\Delta G^{\#}$ value for **L3** (4.3 kcal·mol^{-1}) is higher than that for **L1** (2.2 kcal·mol^{-1}). This observation is in agreement with the higher enantioselectivity observed experimentally in the hydrogenation of **3a** with **L3** than that with **L1** (compare entry 5 with entry 1 in Table 1, respectively).

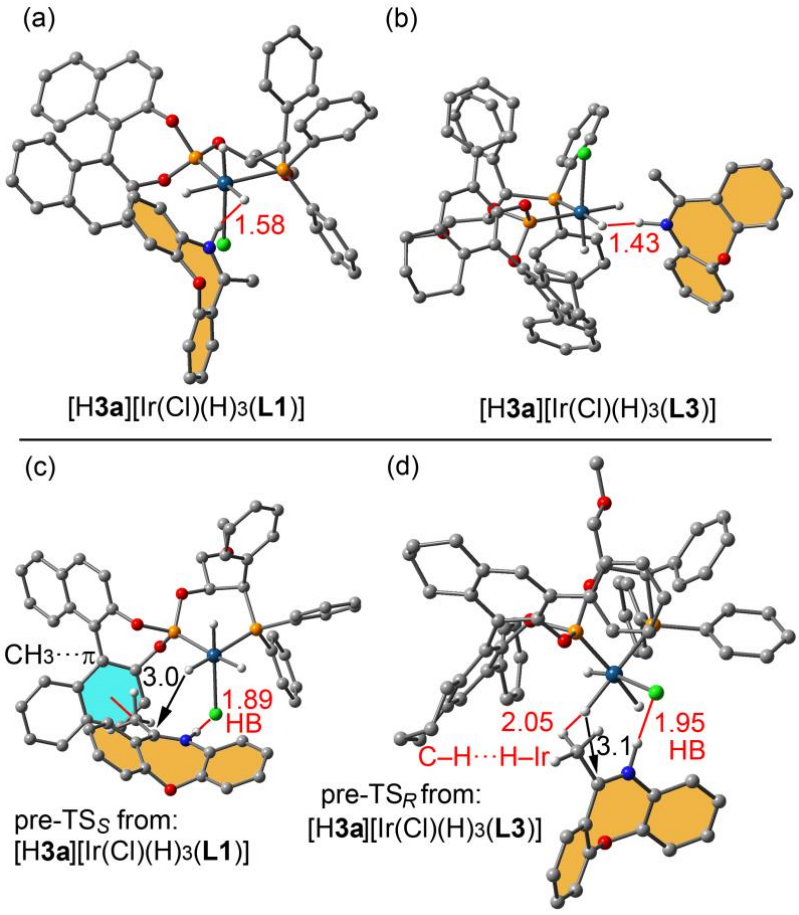

Figure 2. (a,b) Optimized geometries of [H**3a**][Ir(Cl)(H)$_3$(**L1** or **L3)]** assemblies. (c, d) Distances in Å of pre-TS complexes found for [H**3a**][Ir(Cl)(H)$_3$(**L1** or **L3**)] (some H atoms omitted for clarity).

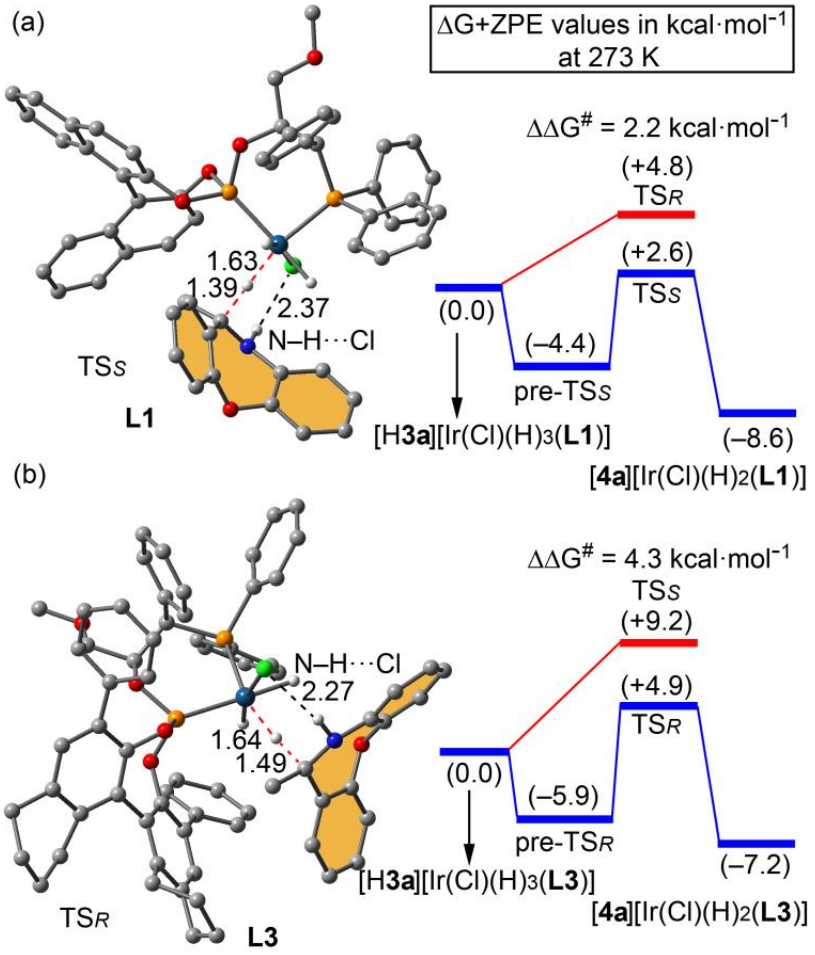

Figure 3. Optimized geometries of the transition states of **L1** (a) and **L3** (b) and their energetic profiles in kcal·mol^{-1} (some H atoms omitted for clarity).

2B.4 Conclusions

In conclusion, catalytic screening in enantioselective hydrogenation reactions revealed that the iridium complexes of chiral P–OP ligands **L1** and **L3** are excellent catalysts in the hydrogenation of various seven-membered heterocycles that contain C=N bonds. The "lead" precatalyst for alkyl-substituted seven-membered heterocycles (derived from ligand **L3**)

in combination with catalytic amounts of HCl exhibits excellent catalytic properties in this transformation. The hydrogenation of aryl-substituted seven-membered heterocycles was more complicated and highly efficient hydrogenation conditions could only be developed for phenyl substituted oxa- and thia-azepines employing **L1** without additive. The enantioselectivity has been rationalized by means of DFT calculations, which have identified the position of the Cl-ligand in catalytically relevant iridium structures and a number of non-covalent interactions (*i.e.* N–H···Cl, CH···π and CH···H–Ir interactions [67]) as key features in rationalizing the stereochemical outcome of the reactions with ligands **L1** and **L3**.

2B.5 Experimental Section

2B.5.1 General procedure for the Ir-catalyzed asymmetric hydrogenation

A solution of the required amount of [{Ir(μ-Cl)(cod)}$_2$] (5 μmol) and the P–OP ligand (0.011 mmol) in the corresponding dry and deoxygenated solvent (5.0 mL) was loaded into an autoclave under N_2, in which the required amounts of substrate (1 mmol) and additives (if necessary) were placed beforehand. The concentration of the substrate was adjusted to a final 0.20 M concentration. The autoclave was purged three times with H_2 (at a pressure not higher than the one selected) and finally, the autoclave was pressurized with H_2 to the desired pressure. The reaction mixture was stirred at the desired temperature for the stated reaction time. The autoclave was subsequently depressurized, the reaction mixture passed through a short pad of SiO_2 and further eluted with EtOAc (2 x 1 mL). The resulting solution was evaporated *in vacuo*. The conversion was determined by ^{1}H NMR and enantioselectivities were determined by HPLC analysis on chiral stationary phases.

2B.6 Supporting information

2B.6.1 General considerations

Air- and moisture-sensitive manipulations or reactions were done under inert atmosphere using anhydrous solvents, either in a glove box or with standard Schlenk techniques. Glassware was dried under vacuum and was heated with a hot air gun before use. All solvents were dried in a Solvent Purification System (SPS). Silica gel 60 (230-400 mesh) was used for column chromatography. NMR spectra were recorded on 400 MHz or 500 MHz spectrometers in $CDCl_3$, unless otherwise cited. ^{1}H NMR and ^{13}C{^{1}H} NMR chemical shifts are quoted in ppm relative to the residual

solvent peaks. $^{31}P\{^{1}H\}$ NMR chemical shifts are quoted in ppm relative to 85% phosphoric acid in water. High-resolution mass spectra (HRMS) were recorded using ESI ionization method in positive mode. GC-MS analyses were performed using EI as ionization method. Enantiomeric excesses were determined by HPLC analyses, using chiral stationary phases. HPLC analyses were performed on an instrument equipped with a diode array UV detector (DAD).

2B.6.2 General synthetic procedure for the P–OP ligands

The preparation of the P–OP ligands **L1**,[68] **L3**,[69] **L5**[68] and **L7**[69] has been previously reported by us in the literature. The preparation methods for **L2**, **L4** and **L6** are indicated below.

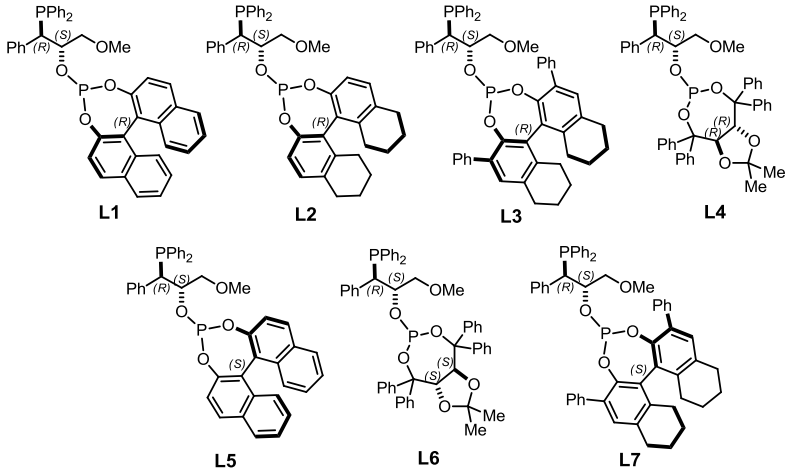

Figure SI1. Set of enantiomerically pure P–OP ligands.

Preparation of Ligand L2. The borane complex of (1*R*,2*S*)-1-(diphenylphosphanyl)-3-methoxy-1-phenylpropan-2-ol[68] (772 mg, 2.12 mmol) and diazabyciclo[2.2.2]octane (485 mg, 4.24 mmol) were charged in a flame-dried schlenk flask. The system was purged with three vacuum/Ar cycles and dry and deoxygenated toluene (12.0 mL) was added. A solution of the required chlorophosphite[70] (871 mg, 2.33 mmol) in THF

(12 mL) was then added dropwise. The mixture was stirred for 16 h at room temperature. The reaction mixture was filtered through celite under inert atmosphere and the filtrate was evaporated *in vacuo*. Rapid chromatography of the residue over SiO_2 (12 g) inside a glove box using dry and deoxygenated solvents (1:1; CH_2Cl_2:Hexane) gave the ligand **L2** as a white solid (824 mg, 58%). mp = 94–96 ºC; $[\alpha]_D^{25}$ = –235.1 (*c* 0.117, CH_2Cl_2); IR absorption (neat) ῡ 3053, 2925, 2856, 1583, 1467, 1433. ^{1}H NMR (500 MHz, $CDCl_3$) δ 7.82-7.72 (m, 2H), 7.53 (d, *J* = 8.2 Hz, 1H), 7.43-7.36 (m, 3H), 7.35-7.28 (m, 2H), 7.23-7.07 (m, 9H), 7.01 (d, *J* = 8.2 Hz, 1H), 6.86 (d, *J* = 8.1 Hz, 1H), 4.40-4.33 (m, 1H), 3.76 (dd, $^2J_{H\text{-}P}$ = 4.8 Hz, $^3J_{H\text{-}H}$ = 3.3 Hz, 1H), 3.20 (s, 3H), 3.20-3.16 (m, 1H), 2.96-2.66 (m, 7H), 2.38-2.26 (m, 2H), 1.86-1.79 (m, 6H), 1.62-1.57 (m, 2H). ^{13}C{^{1}H} NMR (125 MHz, $CDCl_3$) δ 146.86 (C), 146.84 (C), 138.5 (C), 137.5 (C), 137.4 (C), 137.2 (C), 137.1 (C), 136.4 (C), 136.2 (C), 135.3 (CH), 135.1 (CH), 134.5 (C), 133.8 (C), 133.2 (CH), 133.1 (CH), 131.3 (CH), 131.2 (CH), 130.0 (C), 129.9 (C), 129.8 (C), 129.2 (CH), 129.1 (CH), 129.02 (CH), 128.98 (CH), 128.3 (CH), 128.2 (CH), 128.11 (CH), 128.06 (CH), 126.9 (CH), 120.4 (CH), 120.3 (CH), 119.1 (CH), 74.5 (CH_2), 74.3 (dd, $^1J_{C\text{-}P}$ = 18.6 Hz, $^3J_{C\text{-}P}$ = 12.1 Hz, CH), 58.9 (CH_3), 48.2 (dd, $^1J_{C\text{-}P}$ = 15.0 Hz, $^3J_{C\text{-}P}$ = 6.4 Hz, CH), 29.6 (CH_2), 29.4 (CH_2), 28.1 (CH_2), 27.9 (CH_2), 23.1 (CH_2), 22.9 (CH_2), 22.8 (CH_2), 22.7 (CH_2); ^{31}P{^{1}H} NMR (202 MHz, $CDCl_3$) δ 149.5 (bs, P–O), –4.8 (bs, P–C); HRMS (ESI$^+$): calculated for $C_{42}H_{43}O_4P_2$ $(M+H)^+$ 673.2657; observed 673.2631.

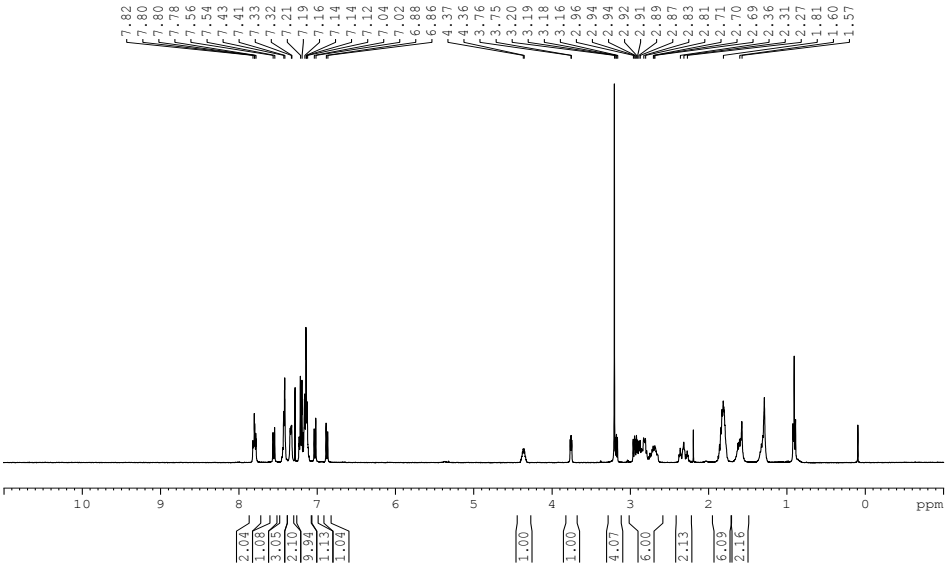

Figure SI2. ^{1}H NMR spectrum of **L2**.

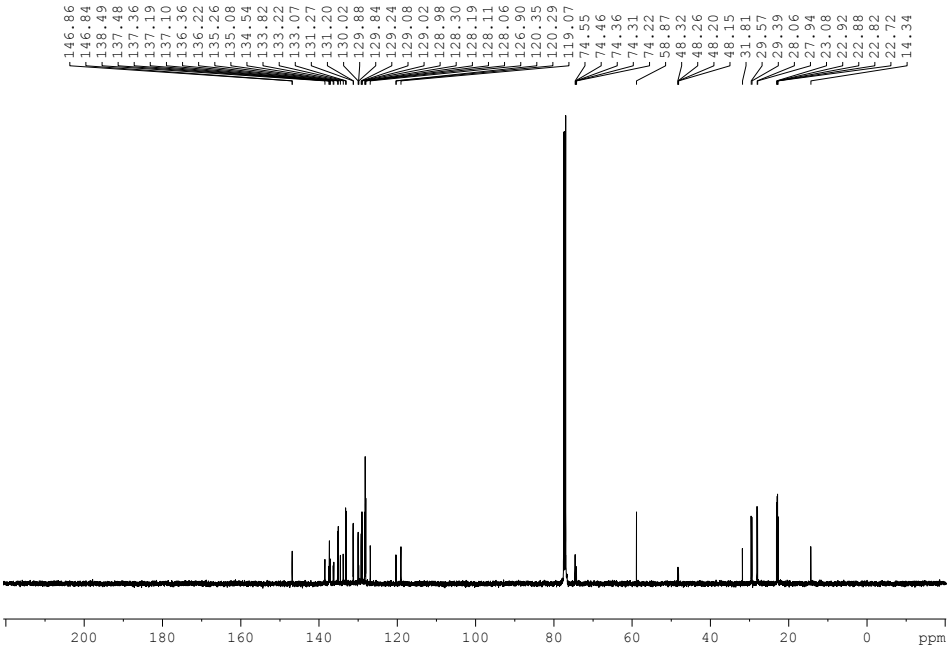

Figure SI3. ^{13}C{^{1}H} NMR spectrum of **L2**.

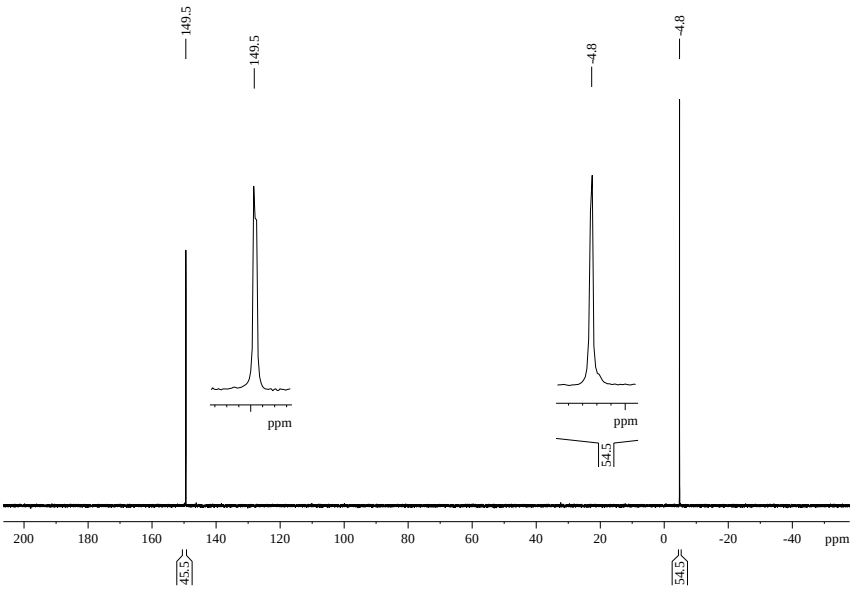

Figure SI4. $^{31}P\{^{1}H\}$ NMR spectrum of **L2**.

Preparation of Ligand L4. The borane complex of (1*R*,2*S*)-1-(diphenylphosphanyl)-3-methoxy-1-phenylpropan-2-ol[68] (354 mg, 0.972 mmol) and diazabyciclo[2.2.2]octane (223 mg, 1.94 mmol) were charged in a flame-dried schlenk flask. The system was purged with three vacuum/Ar cycles and dry and deoxygenated toluene (6.0 mL) was added. The reaction mixture was heated at 60 ºC and stirred for 2 h, allowed to cool down to room temperature, passed through a short SiO_2 pad under N_2 atmosphere and further eluted with dry and deoxygenated toluene (4.0 mL) giving a solution of (1*R*,2*S*)-1-(diphenylphosphanyl)-3-methoxy-1-phenylpropan-2-ol which was then dried under vacuum. The residue was dissolved in THF (5 mL) and NEt_3 (2.52 mL, 18.2 mmol) and DMAP (5.94 mg, 0.048 mmol) were added to the phosphino alcohol solution. A solution of the required chlorophosphite[71] (568 mg, 1.07 mmol) in THF (12 mL) was then added dropwise. The mixture was stirred for 16 h at room temperature. The reaction mixture was filtered through celite under inert atmosphere and the filtrate was evaporated *in vacuo*. Rapid

chromatography of the residue over SiO_2 (12 g) inside a glove box using dry and deoxygenated solvents (1:1; CH_2Cl_2:Hexane) gave the ligand **L4** as a white solid (598 mg, 73%). mp = 99–101 ºC; $[\alpha]_D^{25}$ = –242.1 (*c* 0.124, CH_2Cl_2); IR absorption (neat) ῡ 3056, 2986, 2926, 1599, 1492; ^{1}H NMR (400 MHz, $CDCl_3$) δ 7.68-7.47 (m, 8H), 7.35-6.95 (m, 27H), 5.06 (dd, $^3J_{H-H}$ = 8.2 Hz, $^4J_{H-P}$ = 2.3 Hz, 1H), 4.97 (d, $^3J_{H-H}$ = 8.2 Hz, 1H), 4.81-4.70 (m, 1H), 3.96 (dd, $^2J_{H-P}$ = 4.88 Hz, $^3J_{H-H}$ = 3.3 Hz, 1H), 3.36-3.29 (m, 1H), 3.18-3.11 (m, 1H), 3.04 (s, 3H), 1.04 (s, 3H), 0.33 (s, 3H); ^{13}C{^{1}H} NMR (125 MHz, $CDCl_3$) δ 146.4 (C), 146.0 (C), 142.02 (C), 142.00 (C), 141.0 (C), 137.6 (C), 137.5 (C), 137.03 (C), 136.97 (C), 136.8 (C), 134.3 (CH), 134.1 (CH), 133.9 (CH), 133.7 (CH), 131.6 (CH), 131.5 (CH), 129.32 (CH), 129.26 (CH), 129.2 (CH), 129.0 (CH), 128.8 (CH), 128.7 (CH), 128.3 (CH), 128.0 (CH), 127.84 (CH), 127.79 (CH), 127.76 (CH), 127.6 (CH), 127.50 (CH), 127.48 (CH), 127.4 (CH), 127.3 (CH), 127.1 (CH), 126.5 (CH), 112.7 (C), 84.7 (d, J_{C-P} = 5.8 Hz, C), 82.6 (d, J_{C-P} = 19.0 Hz, CH), 82.5 (d, J_{C-P} = 4.6 Hz, C), 81.6 (d, J_{C-P} = 3.7 Hz, CH), 73.5 (bs, CH_2), 72.8 (dd, $^1J_{C-P}$ = 16.6 Hz, $^3J_{C-P}$ = 8.3 Hz, CH), 58.8 (CH_3), 47.6 (dd, $^1J_{C-P}$ = 14.8 Hz, $^3J_{C-P}$ = 4.7 Hz, CH), 27.5 (CH_3), 25.9 (CH_3); ^{31}P{^{1}H} NMR (162 MHz, $CDCl_3$) δ 146.01 (d, $^4J_{P-P}$ = 13.9 Hz, P-O), –8.43 (d, $^4J_{P-P}$ = 13.9 Hz, P-C); HRMS (ESI^+): calculated for $C_{53}H_{50}NaO_6P_2$ $(M+Na)^+$ 867.2975; observed 867.2977.

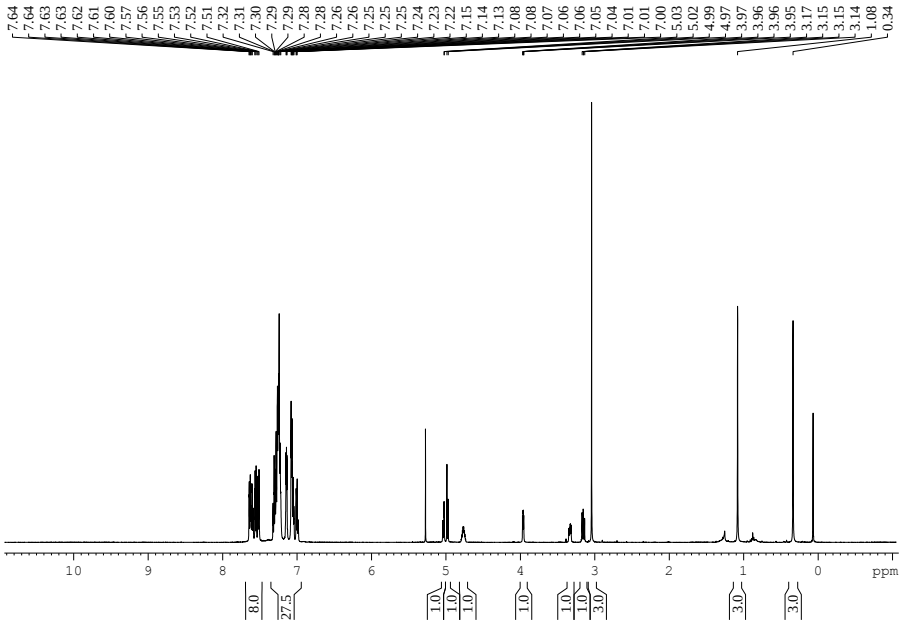

Figure SI5. ^{1}H NMR spectrum of **L4**.

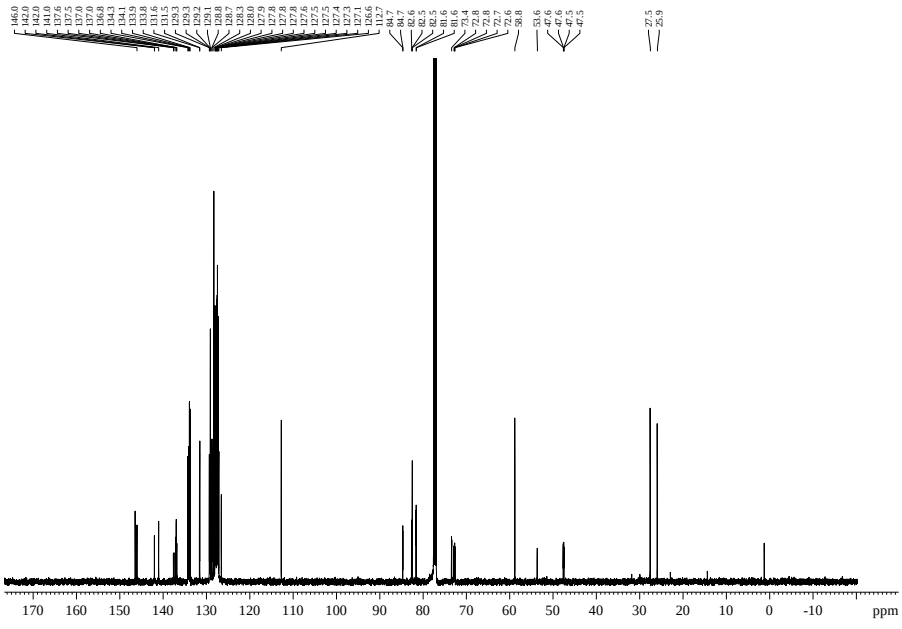

Figure SI6. ^{13}C{^{1}H} NMR spectrum of **L4**.

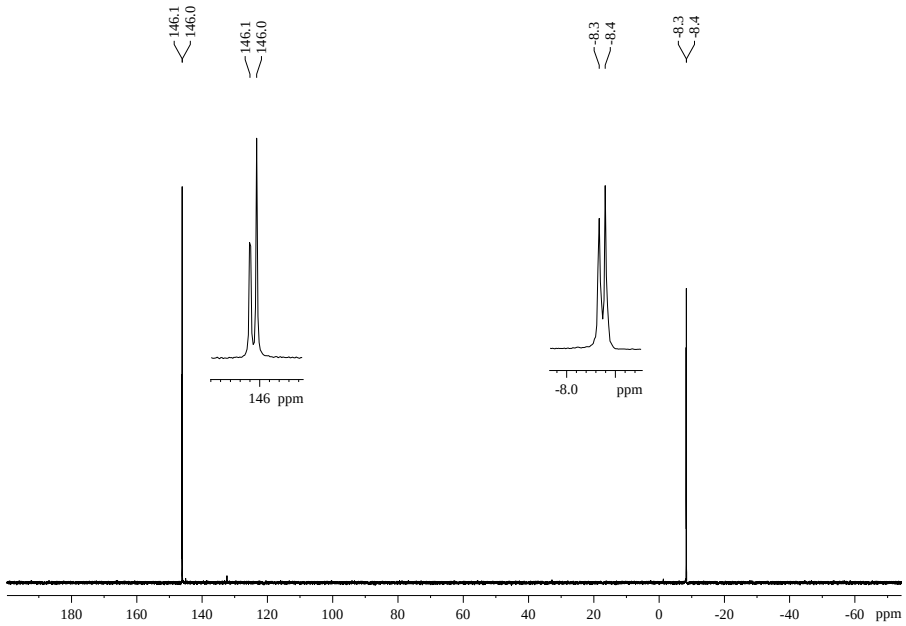

Figure SI7. $^{31}P\{^{1}H\}$ NMR spectrum of **L4**.

Preparation of Ligand L6. The same protocol as for **L4** was used, with the following amounts of reagents (solvent amounts were adapted so that concentrations were the same): borane complex of (1*R*,2*S*)-1-(diphenylphosphanyl)-3-methoxy-1-phenylpropan-2-ol (0.331 g, 0.908 mmol),[68] DABCO (0.208 g, 1.82mmol), NEt_3 (2.52 mL, 18.2 mmol), DMAP (5.94 mg, 0.0486 mmol) and chlorophosphite[71] (0.506 g, 0.045 mmol). **L6** was obtained as a white solid (0.527 g, 69%). mp = 186–189 ºC; $[\alpha]_D^{25}$ = 72.4 (*c* 0.155, CH_2Cl_2); IR absorption (neat) ῡ 3056, 2933, 1599, 1491, 1448; ^{1}H NMR (500 MHz, $CDCl_3$) δ 7.68-7.47 (m, 6H), 7.46-7.00 (m, 29H), 5.38 (d, $^{3}J_{H-H}$ = 8.2 Hz, 1H), 5.11 (d, $^{3}J_{H-H}$ = 7.8 Hz, 1H), 4.59-4.51 (m, 1H), 3.90 (dd, $^{2}J_{H-P}$ = 4.8 Hz, $^{3}J_{H-H}$ = 3.0 Hz, 1H), 3.09 (s, 3H), 2.96 - 2.90 (m, 1H), 2.84-2.81 (m, 1H), 0.85 (s, 3H), 0.48 (s, 3H); $^{13}C\{^{1}H\}$ NMR (126 MHz, $CDCl_3$) δ 146.0 (C), 145.7 (C), 142.1 (C), 141.5 (C), 137.0 (C), 136.9 (C), 136.8 (C), 136.7 (C), 134.7 (CH), 134.6 (CH),

133.7 (CH), 133.5 (CH), 131.6 (CH), 131.5 (CH), 129.4 (CH), 129.3 (CH), 128.8 (CH), 128.7 (CH), 128.4 (CH), 128.2 (CH), 128.0 (CH), 127.94 (CH), 127.88 (CH), 127.8 (CH), 127.61 (CH), 127.56 (CH), 127.5 (CH), 127.27 (CH), 127.25 (CH), 127.1 (CH), 126.5 (CH), 113.6 (C), 86.2 (d, J_{C-P} = 10.2 Hz, C), 83.3 (C), 82.3 (d, J_{C-P} = 13.0 Hz, CH), 80.1 (d, J_{C-P} = 4.6 Hz, CH), 73.0 (bs, CH_2), 72.8 (dd, $^{1}J_{C-P}$ = 17.5 Hz, $^{3}J_{C-P}$ = 13.9 Hz, CH), 58.7 (CH_3), 47.5 (dd, $^{1}J_{C-P}$ = 14.2 Hz, $^{3}J_{C-P}$ = 4.7 Hz, CH), 27.3 (CH_3), 26.2 (CH_3); $^{31}P\{^{1}H\}$ NMR (202 MHz, $CDCl_3$) δ 143.2 (d, $^{4}J_{P-P}$ = 25.2 Hz, P-O), –8.5 (d, $^{4}J_{P-P}$ = 25.0 Hz, P-C); HRMS (ESI^+): calculated for $C_{53}H_{50}NaO_6P_2$ $(M+Na)^+$ 867.2975; observed 867.2980.

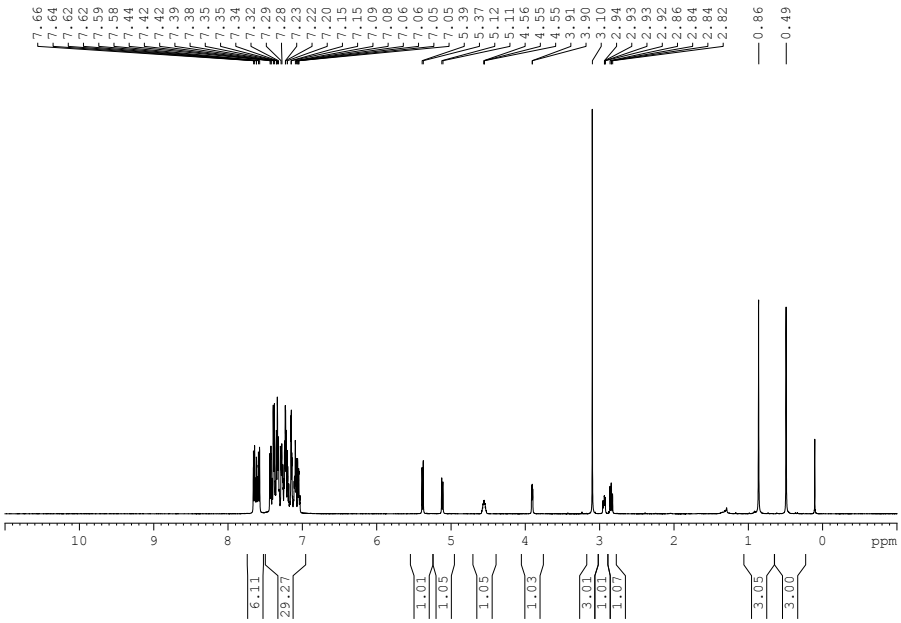

Figure SI8. ^{1}H NMR spectrum of **L6**.

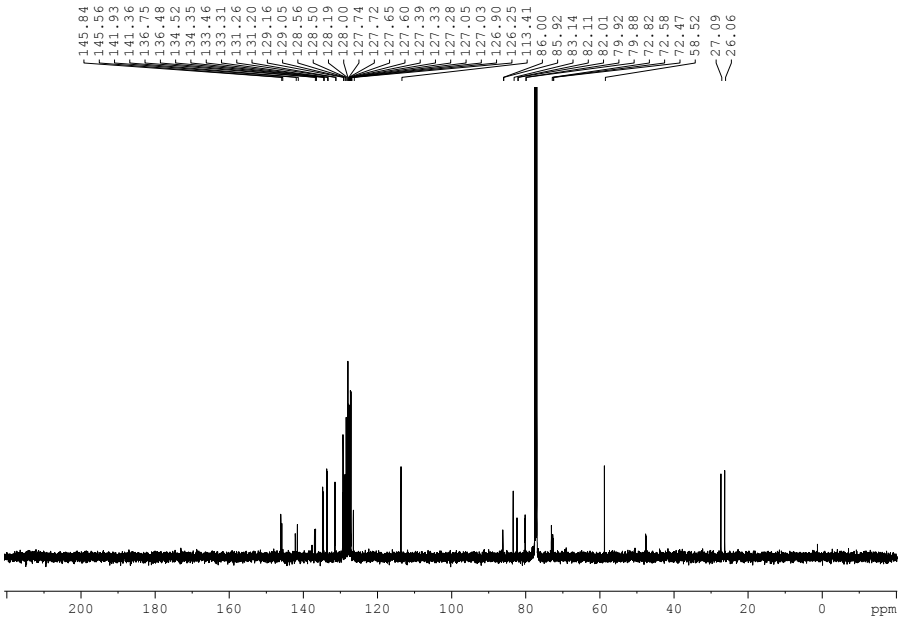

Figure SI9. $^{13}C\{^{1}H\}$ NMR spectrum of **L6**.

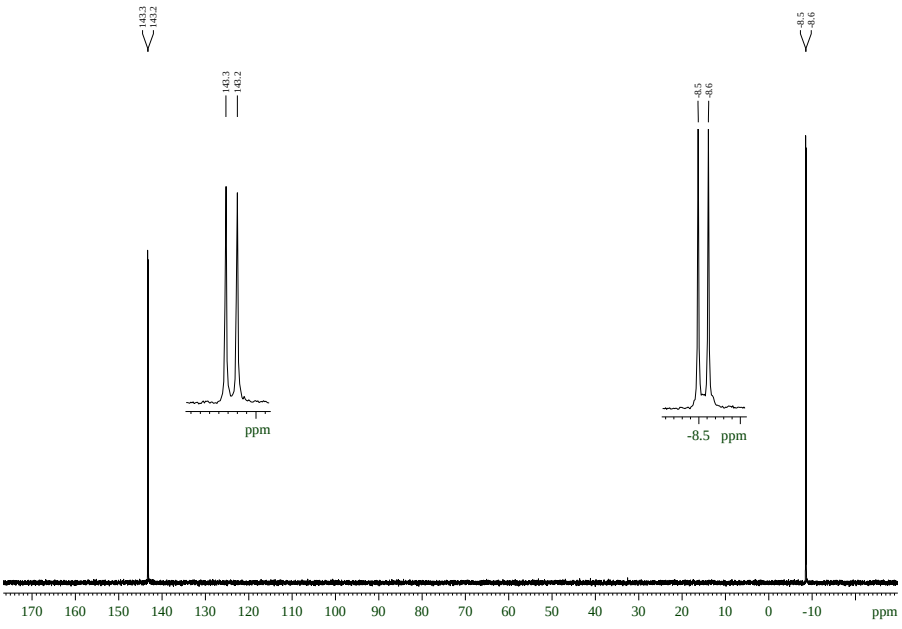

Figure SI10. $^{31}P\{^{1}H\}$ NMR spectrum of **L6**.

2B.6.3 Synthetic procedure for the preparation of heterocyclic compounds 3a–d, 5a, 5b, 7a, 7b, 9a, 9b and 11a.

Compounds **3a–d**, **5a**, **5b**, **9a** and **9b** were synthesized in 2 steps from the substituted anilines **SI-1** by following a known literature procedure.[54c]

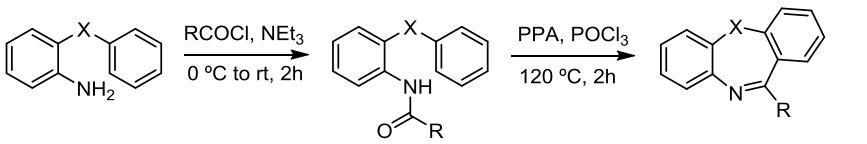

SI-1
X = O, S, CH_2

SI-2
X = O, S, CH_2
R = Me, Ph, *i*-Pr, Bn

3a; X = O, R = Me
3b; X = O, R = Ph
3c; X = O, R = *i*-Pr
3d; X = O, R = Bn
5a; X = CH_2, R = Me
5b; X = CH_2, R = Ph
9a; X = S, R = Me
9b; X = S, R = Ph

Scheme SI1. Synthetic procedure for the preparation of heterocyclic compounds **3a–d**, **5a**, **5b**, **9a**, and **9b**.

Commercially available aniline derivatives **SI-1** (5 mmol) were dissolved in 15 mL of CH_2Cl_2 and cooled to 0 ºC. The corresponding acetyl chloride (1.05 mmol) was added slowly to the solution. Then the temperature of the reaction mixture was allowed to reach rt and further stirred at this temperature. After the reaction was complete (TLC control, *ca.* 2 h), water (20 mL) was added to the reaction mixture. The organic layer was washed with brine (2 × 20 mL), dried over anhydrous $MgSO_4$ and concentrated *in vacuo*. The residue was purified by flash chromatography over SiO_2 using mixtures of *n*-hexane and EtOAc (90:10 to 70:30) to obtain the products **SI-2**. These derivatives were used in the synthetic protocol without any further purification. Thus, compounds **SI-2** (3 mmol) were added to a mixture of polyphosphoric acid (PPA) (18 mmol) and phosphorus oxychloride (18 mmol). The reaction mixture was heated at 120 ºC and the dense solution was stirred for 3 h. The reaction mixture was allowed to cool down to rt. DCM (6 mL) was added to the

original dense solution and the new solution was slowly poured onto iced water. The aqueous solution was neutralized with an ammonia solution (30%; *ca*. 10 mL), extracted with CH_2Cl_2 (30 mL). The organic solution was washed with brine (2 x 30 mL) and dried with anhydrous $MgSO_4$, concentrated under vacuum. The crude mixture was purified by column chromatography over SiO_2 eluting with mixtures of *n*-hexane and EtOAc (90:10 to 70:30) to give the desired products **3a–d**, **5a**, **5b**, **9a** and **9b**.

Compounds **3a**,[54c] **3b**,[54c] **3d**,[54c] **9a**[54h] and **9b**[54h] were previously reported and the obtained physical and spectroscopic data were in agreement with the reported ones. Compound **5a** was previously reported but complete spectroscopic data was not detailed in the corresponding publication.[72] These data is summarized below. Compounds **3c** and **5b** are new compounds and the spectroscopic data are indicated below.

Compound 3c: Yellow solid; 61% yield; mp = 64–66 ºC; IR absorption (neat) ῡ 3065, 2967, 1620, 1598, 1472; ^{1}H NMR (500 MHz, $CDCl_3$) δ 7.47–7.38 (m, 2H), 7.32–7.28 (m, 1H), 7.20 (ddd, *J* = 8.1, 6.9, 1.2 Hz, 2H), 7.17–7.11 (m, 3H), 3.29 (p, *J* = 6.8 Hz, 1H), 1.32 (d, *J* = 6.8 Hz, 6H); ^{13}C{^{1}H} NMR (126 MHz, $CDCl_3$) δ 174.7 (C), 161.9 (C), 152.6 (C), 141.1(C), 132.3 (CH), 128.8 (C), 127.9 (CH), 127.9 (CH), 127.0 (CH), 125.6 (CH), 125.2 (CH), 120.9 (CH), 120.6 (CH), 36.7 (CH), 21.2 (CH_3); HRMS (ESI$^+$): calculated for $C_{15}H_{14}N$ $(M+H)^+$ 238.1225; observed 238.1226.

Compound 5a:[72] Yellow Solid; 74% yield; mp = 97–99 ºC; IR absorption (neat) ῡ 3061, 2952, 1612, 1562; ^{1}H NMR (500 MHz, $CDCl_3$) δ 7.50 (dd, *J* = 8.1, 1.3 Hz, 1H), 7.39–7.34 (m, 1H), 7.29–7.17 (m, 6H), 7.10 (ddd, *J* = 7.8, 6.9, 1.5 Hz, 1H), 2.69 (s, 3H); ^{13}C{^{1}H} NMR (126 MHz, $CDCl_3$) δ 167.6 (C), 145.7 (C), 142.6 (C), 133.8 (C), 132.9 (C), 131.0 (CH), 127.3 (CH), 127.2 (CH), 126.8 (CH), 126.6 (CH), 126.0 (CH), 125.3

(CH), 39.3 (CH_2), 28.8 (CH_3); HRMS (ESI^+): calculated for $C_{15}H_{14}N$ $(M+H)^+$ 208.1118; observed 208.1121.

Compound 5b: Yellow solid; 89% yield; mp = 152–154 ºC; IR absorption (neat) ῡ 3053, 2958, 1588, 1441; ^1H NMR (500 MHz, $CDCl_3$) δ 7.90–7.82 (m, 2H), 7.51–7.38 (m, 5H), 7.35 (dd, *J* = 7.7, 1.2 Hz, 1H), 7.28–7.17 (m, 4H), 7.14 (td, *J* = 7.4, 1.3 Hz, 1H), 3.72 (q, *J* = 12.9 Hz, 2H); $^{13}C\{^1H\}$ NMR (126 MHz, $CDCl_3$) δ 167.1 (C), 145.9 (C), 143.9 (C), 141.3 (C), 133.1 (C), 131.8 (C), 131.3 (CH), 130.3 (CH), 130.1 (CH), 130.0 (CH), 128.3 (CH), 127.2 (CH), 127.1 (CH), 126.6 (CH), 126.2 (CH), 125.9 (CH), 125.8 (CH), 39.5 (CH_2); HRMS (ESI^+): calculated for $C_{20}H_{16}N$ $(M+H)^+$ 270.1266; observed 270.1277.

Compounds **7a** and **7b** were synthesized in 2 steps by Cu-mediated coupling of the corresponding aminophenones with *o*-iodo aniline [73] followed by *N*-alkylation.

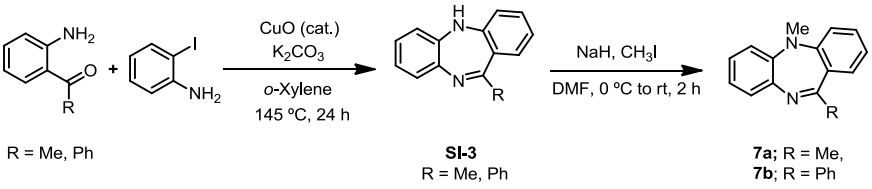

R = Me, Ph

SI-3
R = Me, Ph

7a; R = Me,
7b; R = Ph

Scheme SI2. Synthetic procedure for the preparation of heterocyclic compounds **7a** and **7b**.

A mixture of 2-aminoacetophenone or 2-aminobenzophenone (2.6 mmol), 2-iodoaniline (2.0 mmol), Cu_2O (0.2 mmol) and K_2CO_3 (5 mmol) in dry xylene (50 mL) was stirred at 145 °C under Ar until TLC analysis showed no starting material left (24 h). The reaction mixture was allowed to cool down to rt and the residue was washed with EtOAc (25 mL). The combined organic extracts were washed with H_2O (25 mL) and sat. NaCl

solution (25 mL). The organic layers were dried over $MgSO_4$, filtered and evaporated under reduced pressure. The residue was purified by chromatography over SiO_2 with hexanes:EtOAc mixtures of increasing polarity (10:1 to 10:3) to afford dibenzodiazepine derivatives **SI-3** as a yellow solids. These derivatives were used in the next step without any further purification. The unprotected dibenzodiazepine derivatives **SI-3** (2.0 mmol) were dissolved in dry DMF (15 mL) and the solution was cooled to 0 ºC. NaH (60% dispersion in mineral oil, 4.0 mmol) was then added and the reaction mixture allowed to stir for 10 min. Methyl iodide (4.0 mmol) was added, the reaction mixture was stirred at 0 ºC for another 2 h and then quenched with glacial acetic acid (16 mmol). The reaction mixture was poured into H_2O (30 mL) and extracted with EtOAc (3 × 30 mL). The organic layer was washed with saturated $NaHCO_3$ (2 x 30 mL) and brine (1 x 30 mL) and then dried over $MgSO_4$. The solvent was removed *in vacuo* to give a solid that was purified by flash chromatography over SiO_2 using hexanes/EtOAc mixtures of increasing polarity (up to a 1:1 mixture) as the eluent to give **7a** and **7b**.

Compound **7a** and **7b** was previously reported but complete spectroscopic data was not detailed in the corresponding publication.[74] These data is summarized below.

Compound 7a:[74] Brown compound; 24% yield; mp = 97–99 ºC; IR absorption (neat) ῡ 3058, 2950, 1627, 1590, 1469; ^{1}H NMR (500 MHz, $CDCl_3$) δ 7.37–7.28 (m, 2H), 7.15 (dd, *J* = 7.6, 1.7 Hz, 1H), 7.09 (td, *J* = 7.6, 1.8 Hz, 1H), 7.06–6.99 (m, 2H), 6.95 (ddd, *J* = 15.4, 8.1, 1.2 Hz, 2H), 3.22 (s, 3H), 2.58 (s, 3H);^{13}C{^{1}H} NMR (126 MHz, $CDCl_3$) δ 170.2 (C), 156.8 (C), 146.7 (C), 142.7 (C), 131.4 (CH), 131.0 (C), 128.5 (CH), 127.1 (CH), 126.2 (CH), 124.2 (CH), 123.3 (CH), 117.7 (CH), 117.2 (CH), 37.0 (CH_3), 28.7 (CH_3). HRMS (ESI$^+$): calculated for $C_{15}H_{15}N_2$ $(M+H)^+$ 223.1223; observed 223.1230.

Compound 7b:[74] Yellow solid; 89% yield; mp = 114–116 ºC; IR absorption (neat) ῡ 3058, 2808, 1627, 1734, 1609, 1468; ^{1}H NMR (500 MHz, $CDCl_3$) δ 7.80–7.75 (m, 2H), 7.48–7.37 (m, 4H), 7.32 (dd, *J* = 7.6, 1.8 Hz, 1H), 7.16–7.03 (m, 4H), 7.01–6.97 (m, 2H), 3.28 (s, 3H); ^{13}C{^{1}H} NMR (126 MHz, $CDCl_3$) δ = 169.5 (C), 158.1 (C), 146.8 (C), 143.0 (C), 141.1 (C), 131.6 (CH), 131.3 (CH), 130.2 (CH), 129.7 (CH), 129.1 (C), 128.1 (CH), 127.7 (CH), 126.4 (CH), 124.1 (CH), 122.8 (CH), 117.6 (CH), 117.4 (CH), 36.9 (CH_3); HRMS (ESI$^+$): calculated for $C_{20}H_{17}N_2$ $(M+H)^+$ 285.1390; observed 285.1386.

Compound **11a** was obtained by oxidation of **9a**.

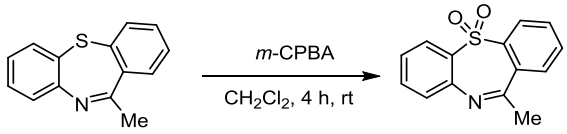

9a **11a**

Scheme SI3. Synthetic procedure for the preparation of heterocyclic compound **11a**.

Compound **9a** (1.35 mmol) was dissolved in DCM (20 mL) and 3-chloroperbenzoic acid (4.1 mmol) was added. After 5 hours stirring at room temperature the mixture was diluted with DCM (10 mL) and washed with saturated aq. $NaHCO_3$ (3 x 30 mL). The organic phase was dried over $MgSO_4$, filtered and evaporated to dryness. Purification by column chromatography over SiO_2 eluting with mixtures of cyclohexane:ethyl acetate of increasing polarity (from 90:10 to 50:50) afforded **11a** (189 mg, 54% yield). mp = 127–130 ºC; IR absorption (neat) ῡ 3059, 2925, 1622, 1585, 1456; ^{1}H NMR (400 MHz, $CDCl_3$) δ 8.06 (d, *J* = 7.7 Hz, 1H), 8.02–7.97 (m, 1H), 7.75–7.68 (m, 2H), 7.63 (ddd, *J* = 7.8, 4.8, 3.9 Hz, 1H), 7.56 (ddd, *J* = 8.1, 7.3, 1.5 Hz, 1H), 7.37 (dd, *J* = 8.1, 1.2 Hz, 1H), 7.30 (ddd, *J* = 7.9, 7.3, 1.2 Hz, 1H), 2.80 (s, 3H); ^{13}C{^{1}H} NMR (101 MHz, $CDCl_3$) δ 168.1 (C), 144.6 (C), 143.5 (C), 134.2 (C), 133.9 (CH), 133.7 (CH), 131.3

(CH), 131.1 (C), 128.3 (CH), 127.0 (CH), 125.7 (CH), 125.7 (CH), 124.6 (CH), 77.5 (CH), 77.2 (CH), 76.9 (CH), 29.8 (CH_3); HRMS (ESI^+): calculated for $C_{14}H_{11}NNaO_2S$ $(M+Na)^+$ 280.0400; observed 280.0403.

^1H and ^{13}C NMR spectra of compounds **3a–d**, **5a**, **5b**, **7a**, **7b**, **9a**, **9b** and **11a**

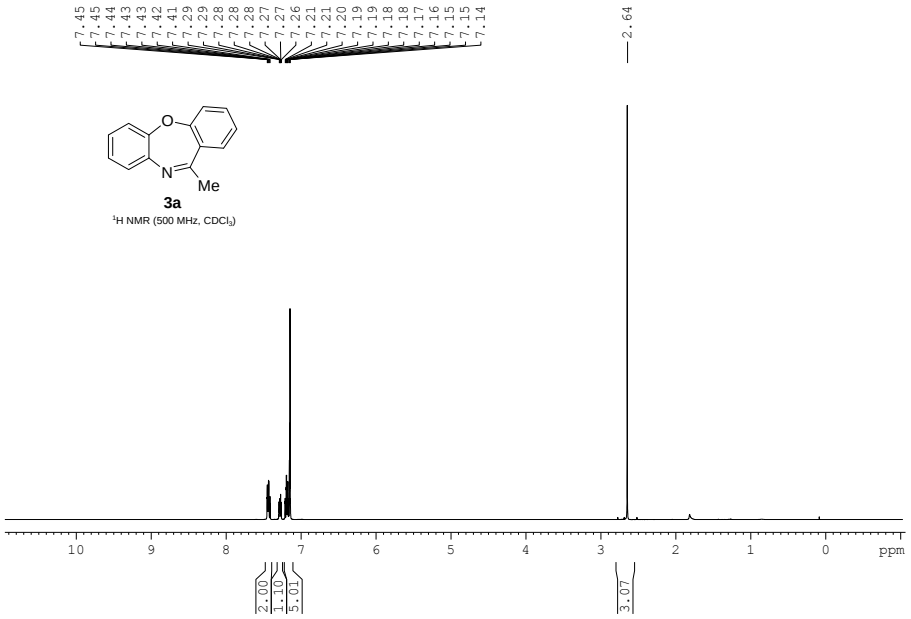

Figure SI11. ^{1}H NMR spectrum of **3a**.

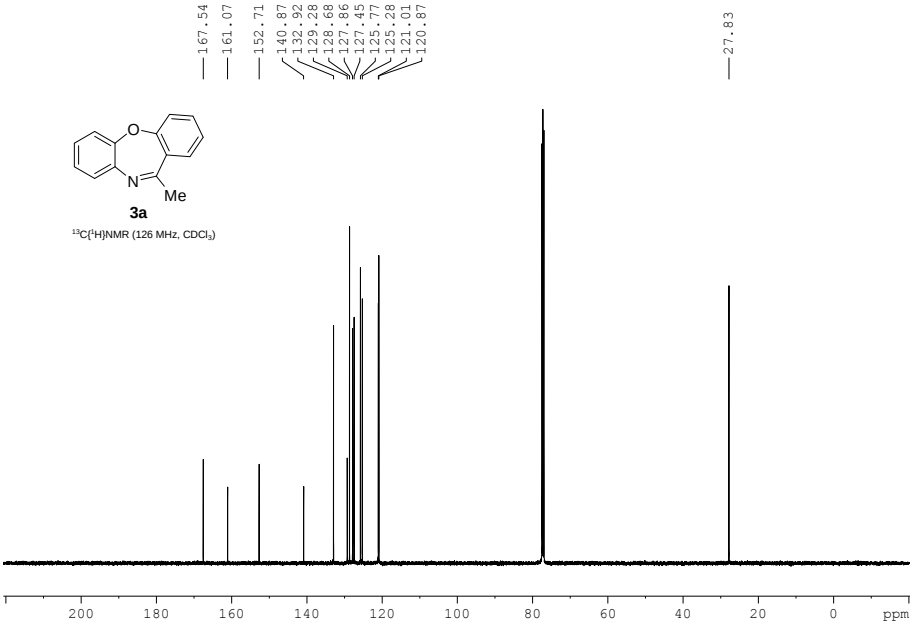

Figure SI12. ^{13}C{^{1}H} NMR spectrum of **3a**.

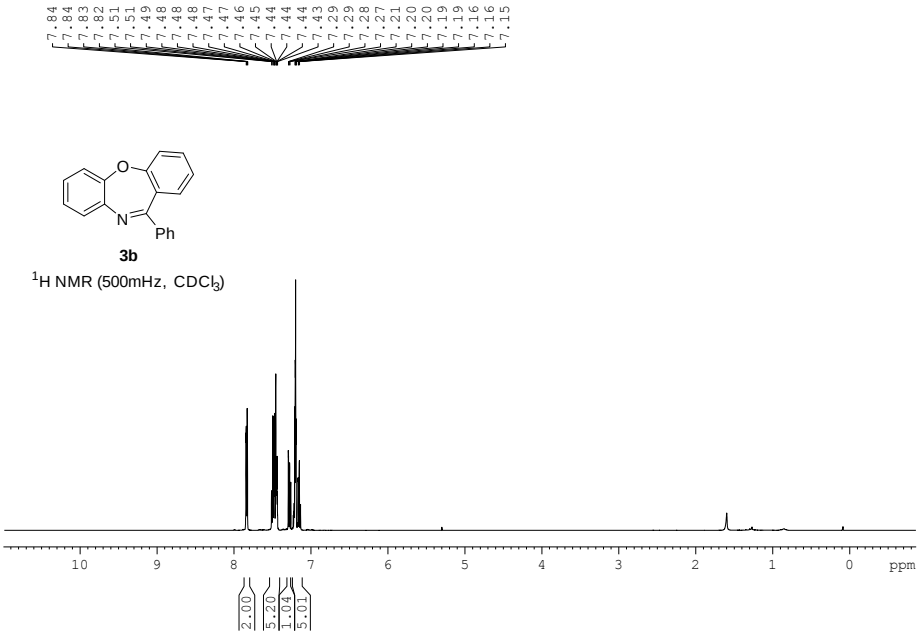

Figure SI13. ^{1}H NMR spectrum of **3b**.

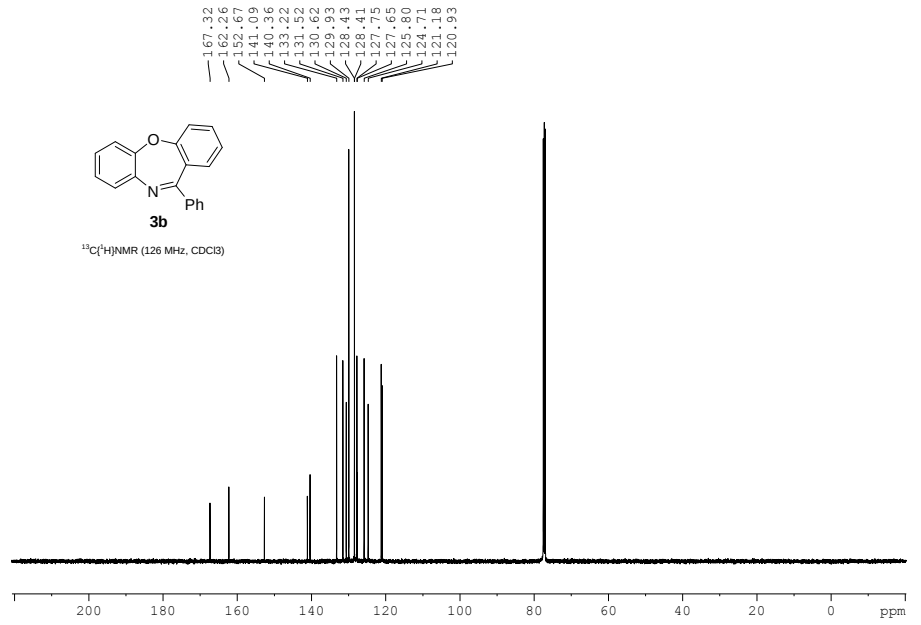

Figure SI14. ^{13}C{^{1}H} NMR spectrum of **3b**.

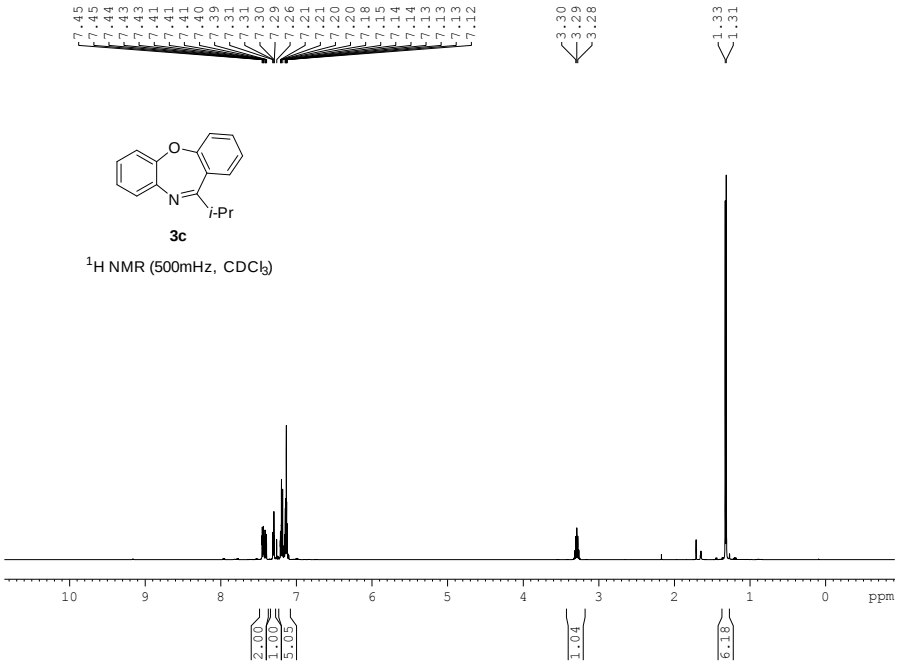

Figure SI15. ^{1}H NMR spectrum of **3c**.

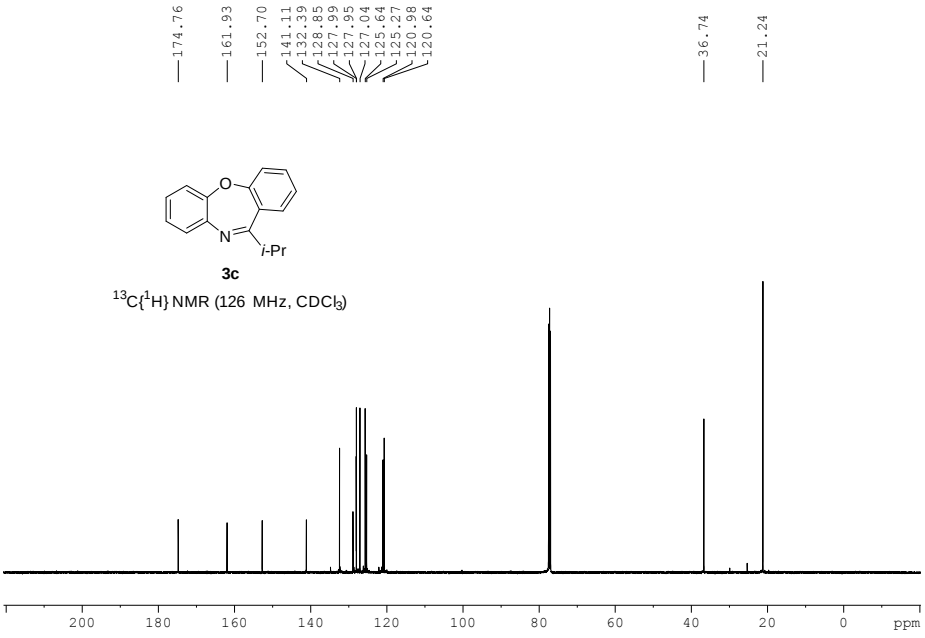

Figure SI16. ^{13}C{^{1}H} NMR spectrum of **3c**.

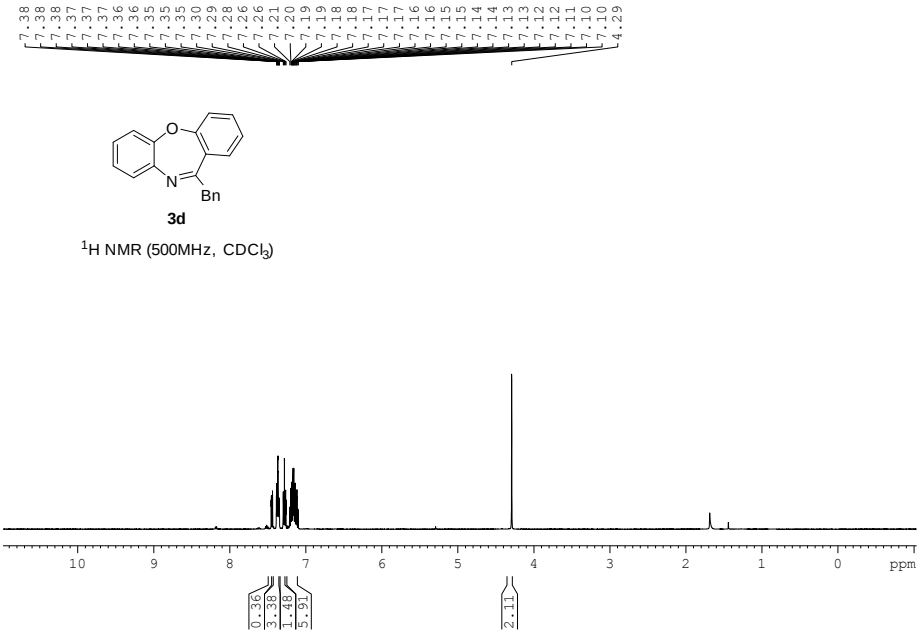

Figure SI17. 1H NMR spectrum of **3d**.

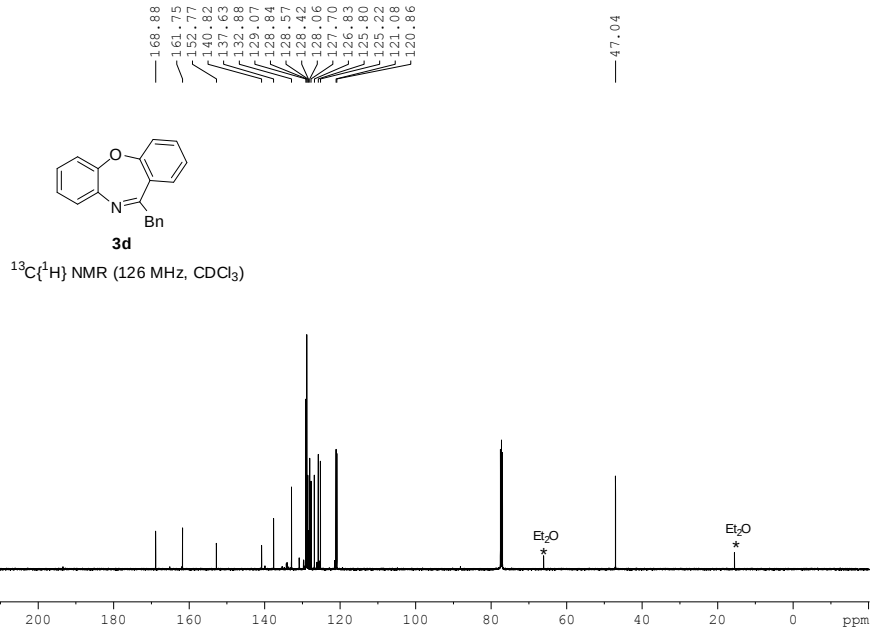

Figure SI18. ^{13}C{^{1}H} NMR spectrum of **3d**.

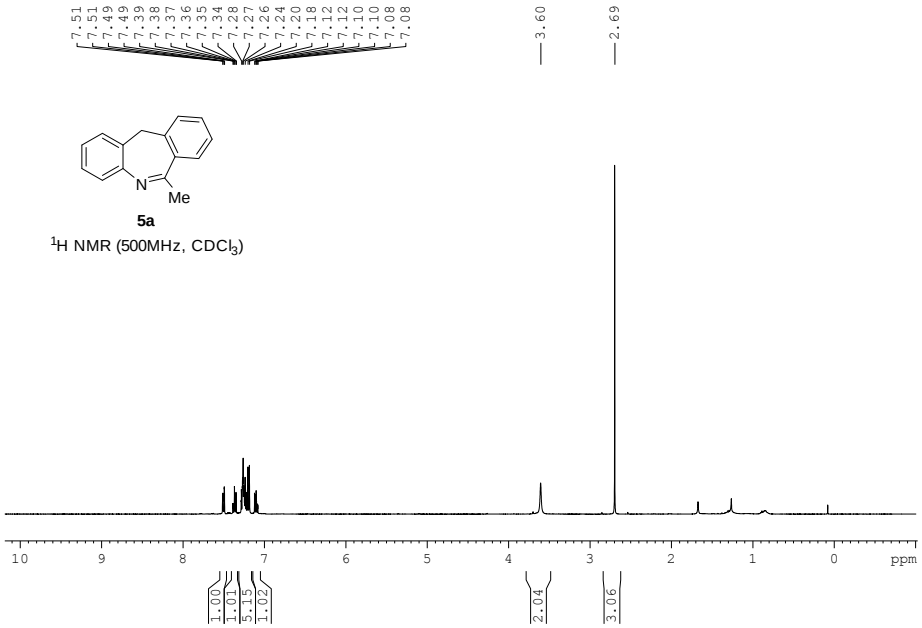

Figure SI19. ^{1}H NMR spectrum of **5a**.

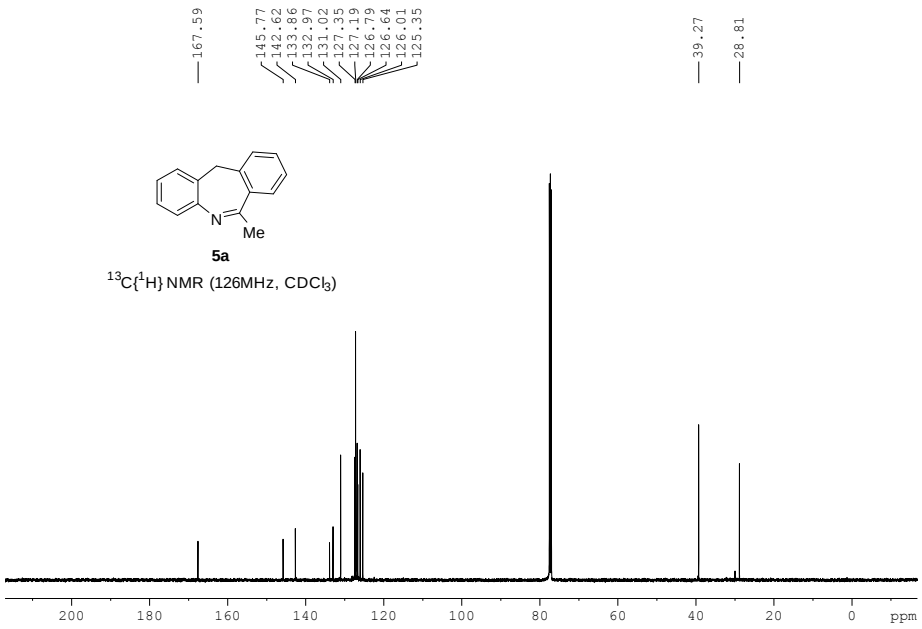

Figure SI20. ^{13}C{^{1}H} NMR spectrum of **5a**.

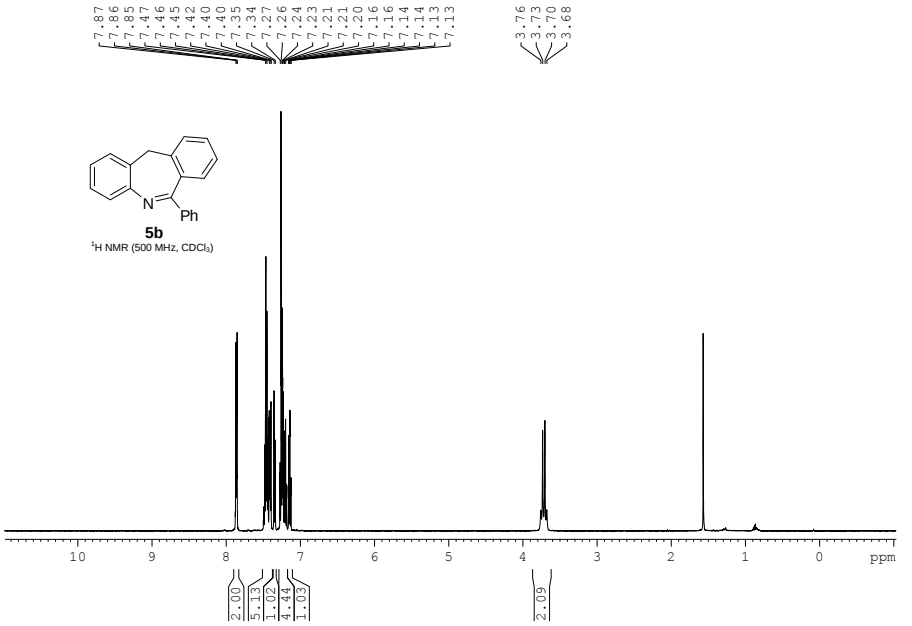

Figure SI21. ^{1}H NMR spectrum of **5b**.

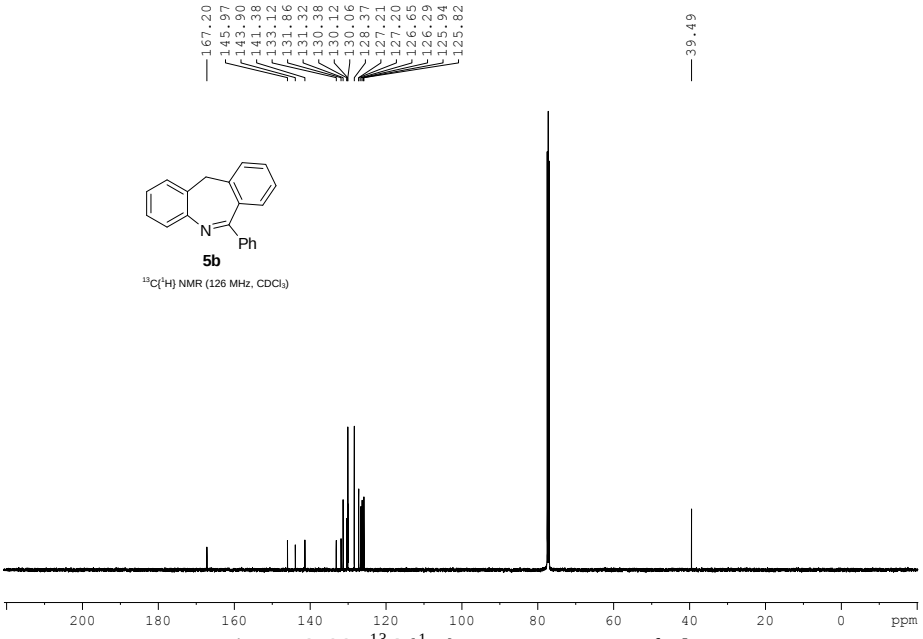

Figure SI22. ^{13}C{^{1}H} NMR spectrum of **5b**.

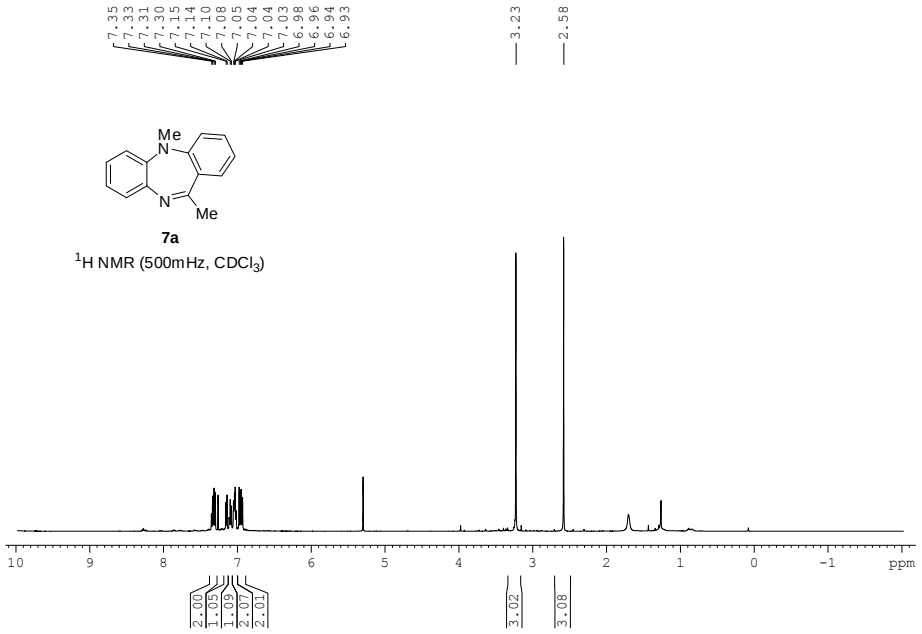

Figure SI23. ^{1}H NMR spectrum of **7a**.

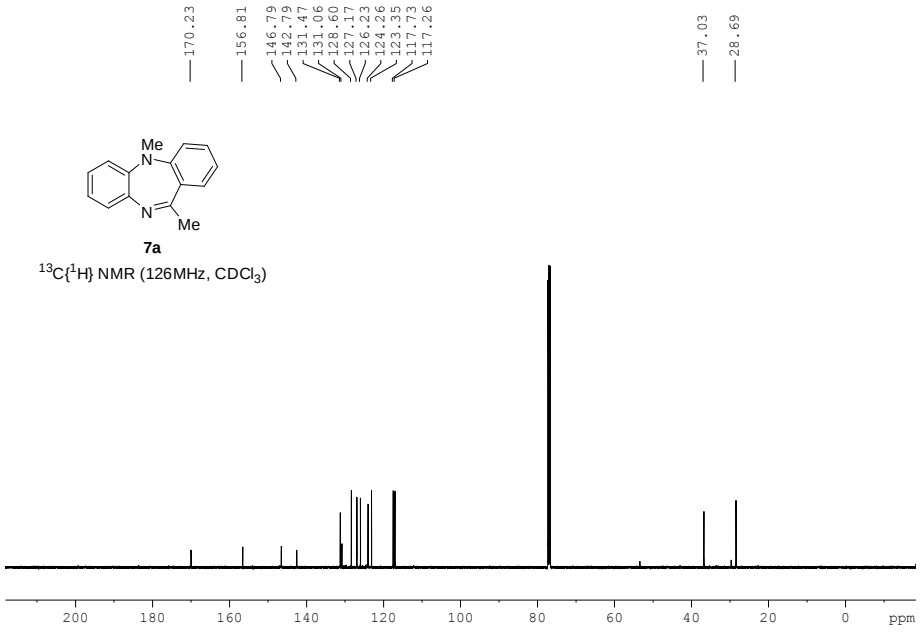

Figure SI24. ^{13}C{^{1}H} NMR spectrum of **7a**.

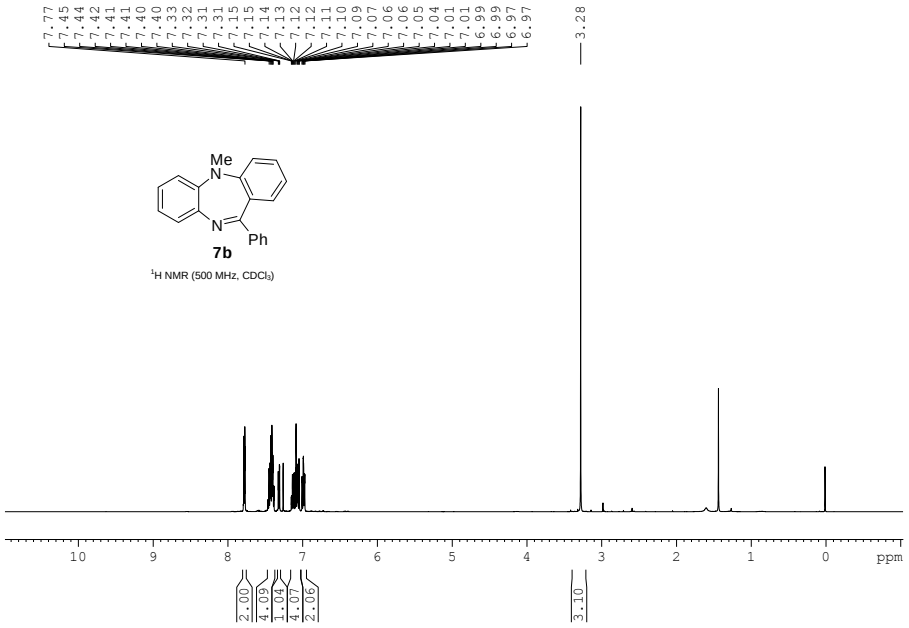

Figure SI25. ^{1}H NMR spectrum of **7b**.

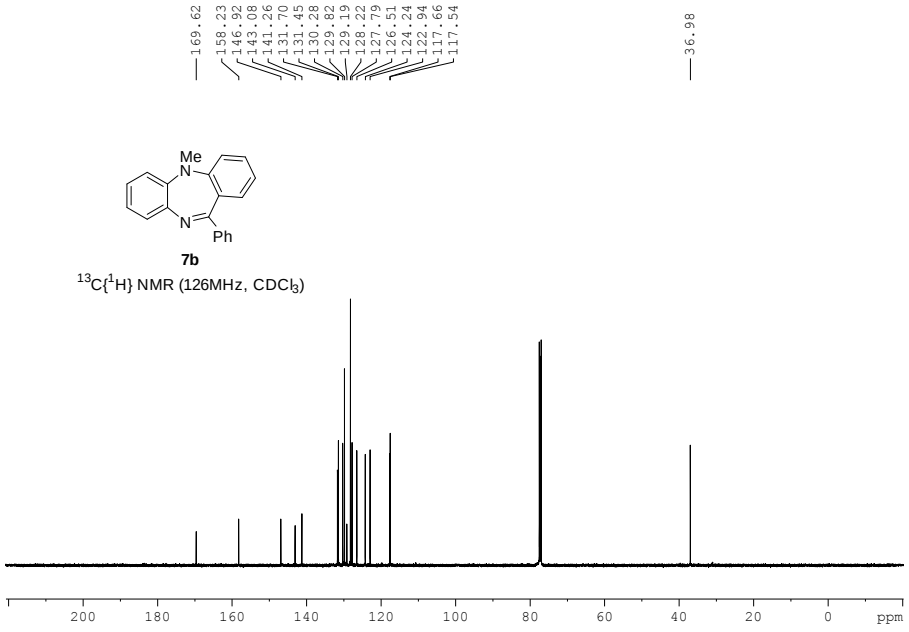

Figure SI26. $^{13}C\{^{1}H\}$ NMR spectrum of **7b**.

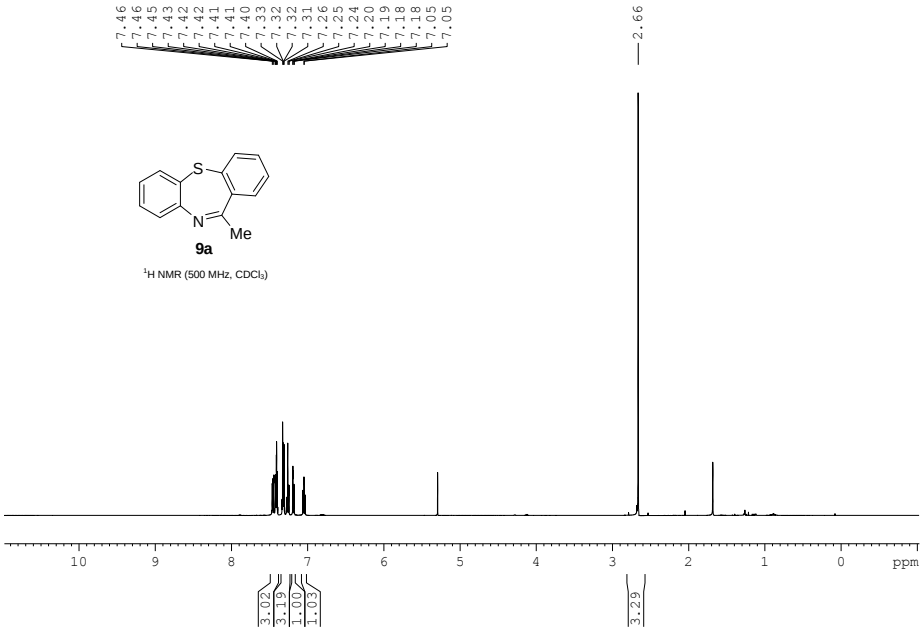

Figure SI27. ^{1}H NMR spectrum of **9a**.

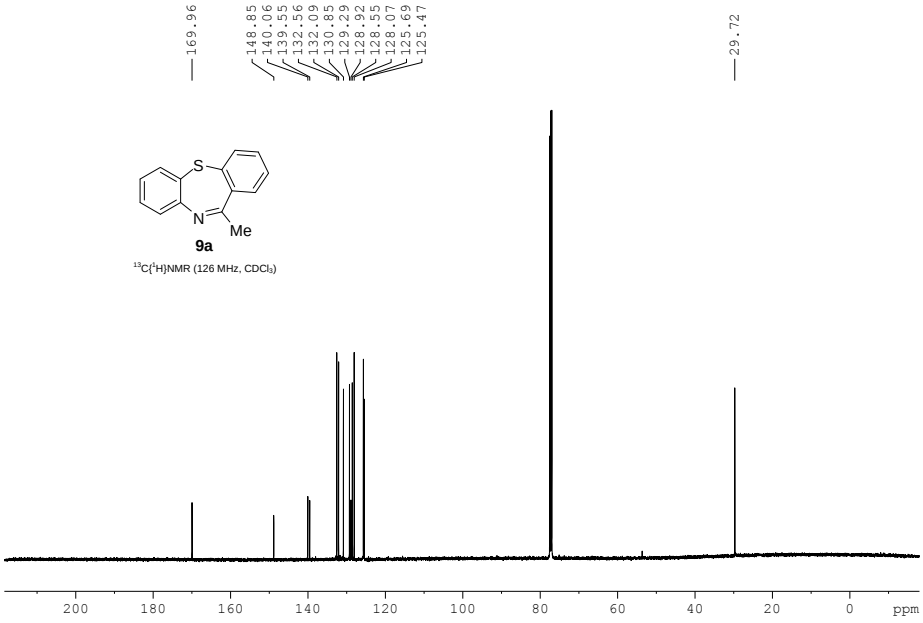

Figure SI28. ^{13}C{^{1}H} NMR spectrum of **9a**.

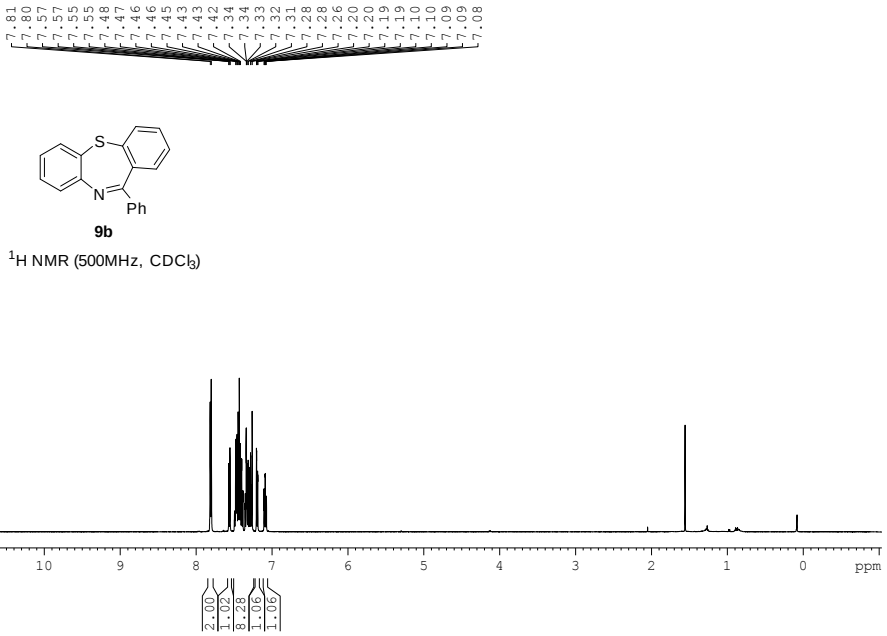

Figure SI29. ^{1}H NMR spectrum of **9b**.

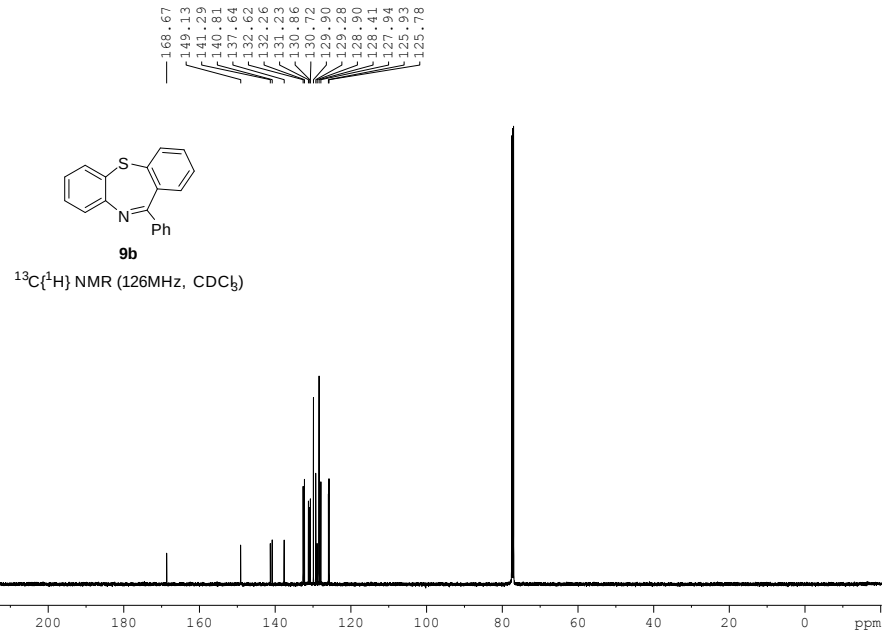

Figure SI30. ^{13}C{^{1}H} NMR spectrum of **9b**.

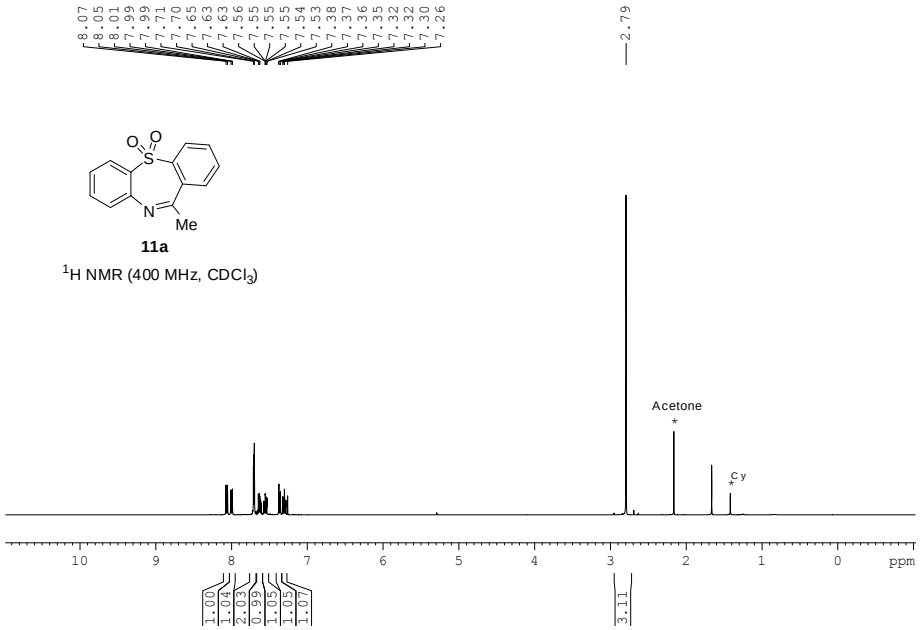

Figure SI31. ^{1}H NMR spectrum of **11a**.

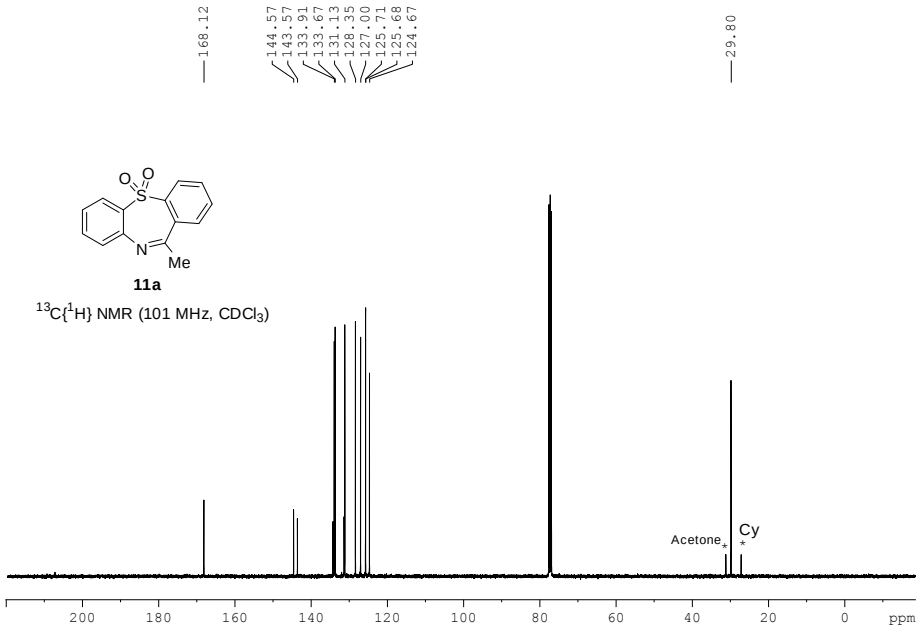

Figure SI32. ^{13}C{^{1}H} NMR spectrum of **11a**.

2B.6.4 General procedure for the Ir-mediated asymmetric hydrogenations

A solution of the required amount of iridium precursor ([{Ir(μ-Cl)(cod)}$_2$]) (0.005 mmol) and the P–OP ligand (0.011 mmol) in the corresponding dry and deoxygenated solvent (5.0 mL) was loaded into an autoclave under N_2 atmosphere, in which the required amounts of substrate (1 mmol) and additives (if necessary) were placed beforehand. In all cases, the molar concentration of the substrate in the reaction medium was adjusted to a final 0.20 M concentration. The autoclave was purged three times with H_2 (at a pressure not higher than the selected one) and finally, the autoclave was pressurized with H_2 to the desired pressure. The reaction mixture was stirred at the desired temperature for the stated reaction time. The autoclave was subsequently depressurized, the reaction mixture passed through a short pad of SiO_2 and further eluted with EtOAc (2 x 1 mL). The resulting solution was evaporated *in vacuo*. The conversion was determined by ^{1}H NMR and enantioselectivities were determined by HPLC analysis on chiral stationary phases.

2B.6.5 Complete set of hydrogenation results

Table SI1. Asymmetric hydrogenation[a] of compound **3a** mediated by complexes [Ir(Cl)(cod)(**L1**–**L7**)]

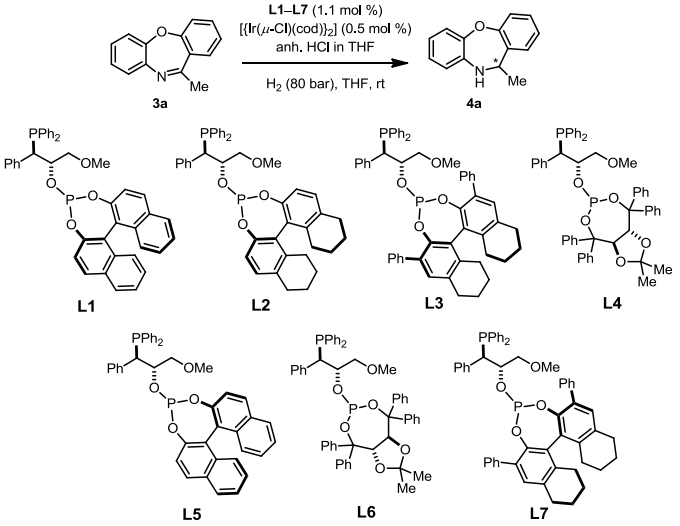

Entry	Ligand	Reaction conditions	Conv.[b]	ee (%)[c] (config.)[d]
1	**L1**	No additive, THF	99	42 (*S*)
2	**L1**	10 mol % HCl, THF	99	53 (*S*)
3	**L2**	No additive, THF	99	29 (*S*)
4	**L2**	10 mol % HCl, THF	99	57 (*S*)
5	**L3**	No additive, THF	99	79 (*R*)
6	**L3**	10 mol % HCl, THF	99	86 (*R*)
7	**L3**	20 mol % HCl, THF	99	86 (*R*)
8	**L3**	10 mol % HCl, THF, 0 ºC	99	87 (*R*)
9	**L3**	10 mol % HCl, DCM	99	91 (*R*)
10	**L3**	10 mol % HCl, toluene	99	91 (*R*)
11	**L3**	10 mol % HCl, MeTHF[e]	99	91 (*R*)
12	**L4**	No additive, THF	99	16 (*S*)
13	**L4**	10 mol % HCl, THF	99[f]	08 (*S*)
14	**L5**	10 mol % HCl, THF	99	27 (*R*)
15	**L6**	10 mol % HCl, THF	99[f]	*rac*
16	**L7**	10 mol % HCl, THF	99	65 (*S*)

[a] *Reaction conditions*: [{Ir(μ–Cl)(cod)}$_2$]/P–OP ligand/substrate = 0.5:1.1:100 for a precatalyst levels of 1 mol %, respectively, at rt, 20 h and a substrate concentration of 0.20 M in THF unless otherwise stated. If additive was present, the indicated amount of additive with respect to substrate was added to a solution of the substrate before adding the catalyst. The values shown are the average of at least two runs. [b] Conversions were determined by ^{1}H NMR. [c] Determined by HPLC analysis using chiral stationary phases. [d] Absolute configuration was assigned by comparison with literature data (see Table S3 and the following sections in this subchapter). [e] MeTHF = 2-methyltetrahydrofuran. [f] The selectivity of the reaction towards **4a** was *ca.* 30%.

The effects of a set of achiral and enantiomerically pure additives on the hydrogenation results of substrate **3a** were also studied. The best results were obtained with HCl as the additive. For a complete summary on the effects of the additives, see Table SI2.

Table SI2. Effect of the additives in the asymmetric hydrogenation[a] of compound **3a** mediated by complexes [Ir(Cl)(cod)(**L3**)]

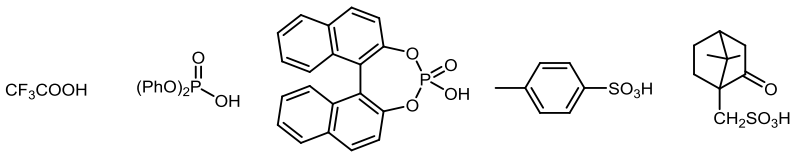

TFA **DPP** **BNP** **TsOH** **CSA**

Entry	Additive	Conv.[b]	ee (%)[c] (config.)[d]
1	TFA	99	88 (*R*)
2	DPP	99	89 (*R*)
3	(*R*)-BNP	99	87 (*R*)
4	(*S*)-BNP	99	89 (*R*)
5	TsOH	99	89 (*R*)
6	D-CSA	99	89 (*R*)
7	L-CSA	99	90 (*R*)
8	HCl	99	91 (*R*)

a, *b*, *c*, *d* See notes *a*, *b*, *c* and *d* in Table SI1.

Table SI3. Asymmetric hydrogenation[a] of compounds **3a–d**, **5a**, **5b**, **7a**, **7b**, **9a**, **9b** and **11a** mediated by complexes [Ir(Cl)(cod)(**L1** or **L3**)]

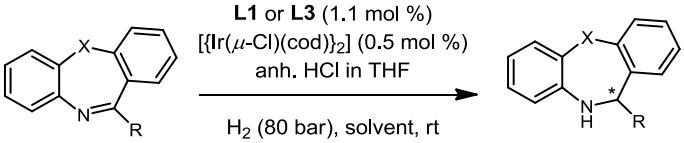

3, **5**, **7**, **9** and **11** → **4**, **6**, **8**, **10** and **12**

Entry	Substrate	Ligand	Reaction conditions	Conv.[b]	ee (%)[c] (config.)[d]
1	**3a** (X= O, R= Me)	**L1**	No additive, THF	99	42 (*S*)[e]
2	**3a** (X= O, R= Me)	**L1**	10 mol % HCl, THF	99	52 (*S*)[e]
3	**3a** (X= O, R= Me)	**L3**	No additive, THF	99	79 (*R*)[e]
4	**3a** (X= O, R= Me)	**L3**	10 mol % HCl, THF	99	86 (*R*)[e]
5	**3b** (X= O, R= Ph)	**L1**	No additive, THF	82	78 (*S*)[e]
6	**3b** (X= O, R= Ph)	**L1**	10 mol % HCl, THF	21	66 (*S*)[e]
7	**3b** (X= O, R= Ph)	**L3**	No additive, THF	18	4 (*S*)[e]
8	**3b** (X= O, R= Ph)	**L3**	10 mol % HCl, THF	5	5 (*S*)[e]
9	**3b** (X= O, R= Ph)	**L1**	No additive, MeTHF	97	83 (*S*)[e]
10	**3c** (X= O, R= *i*Pr)	**L1**	No additive, MeTHF	99	32 (*S*)[f]
11	**3c** (X= O, R= *i*Pr)	**L1**	10 mol % HCl, MeTHF	99	26 (*S*)[f]
12	**3c** (X= O, R= *i*Pr)	**L3**	No additive, MeTHF	99	73 (*R*)[f]
13	**3c** (X= O, R= *i*Pr)	**L3**	10 mol % HCl, MeTHF	99	65 (*R*)[f]
14	**3d** (X= O, R= Bn)	**L1**	No additive, MeTHF	99	8 (*S*)[e]
15	**3d** (X= O, R= Bn)	**L1**	10 mol % HCl, MeTHF	99	12 (*S*)[e]
16	**3d** (X= O, R= Bn)	**L3**	No additive, MeTHF	99	86 (*R*)[e]
17	**3d** (X= O, R= Bn)	**L3**	10 mol % HCl, MeTHF	99	87 (*R*)[e]
18	**5a** (X= CH_2, R= Me)	**L1**	No additive, MeTHF	99	32 (*S*)[f]
19	**5a** (X= CH_2, R= Me)	**L1**	10 mol % HCl, MeTHF	99	48 (*S*)[f]
20	**5a** (X= CH_2, R= Me)	**L3**	No additive, MeTHF	99	70 (*R*)[f]
21	**5a** (X= CH_2, R= Me)	**L3**	10 mol % HCl, MeTHF	99	25 (*R*)[f]
22	**5b** (X= CH_2, R= Ph)	**L1**	No additive, MeTHF	21	9 (*S*)[f]
23	**5b** (X= CH_2, R= Ph)	**L1**	10 mol % HCl, MeTHF	37	5 (*S*)[f]
24	**5b** (X= CH_2, R= Ph)	**L3**	No additive, MeTHF	67	4 (*S*)[f]
25	**5b** (X= CH_2, R= Ph)	**L3**	10 mol % HCl, MeTHF	33	9 (*S*)[f]
26	**7a** (X= NMe, R= Me)	**L1**	No additive, MeTHF	99	41(*S*)[f]
27	**7a** (X= NMe, R= Me)	**L1**	10 mol % HCl, MeTHF	99	60 (*S*)[f]
28	**7a** (X= NMe, R= Me)	**L3**	No additive, MeTHF	99	76 (*R*)[f]
29	**7a** (X= NMe, R= Me)	**L3**	10 mol % HCl, MeTHF	99	84 (*R*)[f]
30	**7b** (X= NMe, R= Ph)	**L1**	No additive, MeTHF	24	36 (*S*)[f]
31	**7b** (X= NMe, R= Ph)	**L1**	10 mol % HCl, MeTHF	<5	nd[g]
32	**7b** (X= NMe, R= Ph)	**L3**	No additive, MeTHF	25	12 (*S*)[f]
33	**7b** (X= NMe, R= Ph)	**L3**	10 mol % HCl, MeTHF	<5	nd[g]
34	**9a** (X= S, R= Me)	**L1**	No additive, MeTHF	99	7 (*R*)[h]
35	**9a** (X= S, R= Me)	**L1**	10 mol % HCl, MeTHF	99	25 (*R*)[h]
36	**9a** (X= S, R= Me)	**L3**	No additive, MeTHF	99	79 (*R*)[h]
37	**9a** (X= S, R= Me)	**L3**	10 mol % HCl, MeTHF	99	91 (*R*)[h]
38	**9b** (X= S, R= Ph)	**L1**	No additive, MeTHF	31	65 (*S*)[h]
39	**9b** (X= S, R= Ph)	**L1**	10 mol % HCl, MeTHF	41	23 (*S*)[h]
40	**9b** (X= S, R= Ph)	**L3**	No additive, MeTHF	72	97 (*S*)[h]
41	**9b** (X= S, R= Ph)	**L3**	10 mol % HCl, MeTHF	<5	nd[g]

Table SI3. Cont.

42	**11a** (X= SO_2, R= Me)	**L1**	No additive, MeTHF	99	56 (*R*)[i]
43	**11a** (X= SO_2, R= Me)	**L1**	10 mol % HCl, MeTHF	99	65 (*R*)[i]
44	**11a** (X= SO_2, R= Me)	**L3**	No additive, MeTHF	99	75 (*R*)[i]
45	**11a** (X= SO_2, R= Me)	**L3**	10 mol % HCl, MeTHF	99	77 (*R*)[i]

For *a*, *b*, *c*, *d* See notes *a*, *b*, *c* and *d* in Table **SI-1**. [e] The absolute configuration of compounds **4a**, **4b** and **4d** was established by comparison with reported values of specific optical rotations (see ref. 54c). [f] The absolute configuration of products **4c**, **6a**, **6b**, **8a**, **8b** and **10b** were tentatively assigned by analogy with the stereochemical outcome of the reactions leading to **4a**, **4b** and **4d**. [g] not determined. [h] The absolute configuration of compounds **10a** and **10b** was established by comparison with reported values of the specific optical rotation (see ref. 54h). [i] The absolute configuration could be unambiguously determined by X-ray analysis (see section 2B.6.7 of the SI), which is furthermore in agreement with the expected stereochemical outcome of the reaction by analogy with the results obtained for **4a**, **4d** and **10a**.

2B.6.6 Characterization and determination of the enantiomeric excesses of reaction products 4a–d, 6a, 6b, 8a, 8b, 10a, 10b and 12a

Enantiomerically enriched compounds **4a**,[54c] **4b**,[54c] **4d**,[54c] **10a**,[54h] and **10b**,[54h] were previously reported and the obtained physical and spectroscopic data obtained in the present work were in agreement with the reported ones. Measured optical rotation data and chromatographic data on chiral stationary phases are indicated below. Compounds **4c**, **6a**, **6b**, **8a**, **8b**, and **12a** are new compounds and the spectroscopic data, measured optical rotation data and chromatographic data on chiral stationary are indicated below.

(*R*)-11-methyl-10,11-dihydrodibenzo[*b,f*][1,4]oxazepine (4a): $[\alpha]_D^{27}$ = +42.7 (*c* 0.36, $CHCl_3$) for 91% ee, [Lit:[54c] $[\alpha]_D^{30}$ = –109 (*c* 1.26, $CHCl_3$) for 94% ee (*S*)]; HPLC conditions: Daicel Chiralcel® AD-H (25 cm x 0.46 cm), 80:20 *n*-hexane/2-propanol, 0.7 mL/min, 254 nm, t_1 (*S*) = 7.9 min, t_2 (*R*) = 9.2 min.

(*S*)-11-phenyl-10,11-dihydrodibenzo[*b,f*][1,4]oxazepine (4b): $[\alpha]_D^{27}$ = –20.6 (*c* 0.23, $CHCl_3$) for 83% ee, [Lit: [54c] $[\alpha]_D^{30}$ = –16.4 (*c* 0.2, $CHCl_3$) for 78% ee (*S*)]; HPLC conditions: Daicel Chiralcel® AD-H (25 cm x 0.46 cm),

70:30 *n*-hexane/2-propanol, 0.7 mL/min, 254 nm, t_1 (*S*) = 9.2 min, t_2 (*R*) = 12.4 min.

(*R*)-11-isopropyl-10,11-dihydrodibenzo[*b*,*f*][1,4]oxazepine (4c): White solid; mp = 60–63 ºC; IR absorption (neat) $\bar{\upsilon}$ 3398, 2958, 2867, 1607, 1486; ^{1}H NMR (400 MHz, $CDCl_3$) δ 7.26–7.20 (m, 1H), 7.14 (dd, *J* = 8.0, 1.3 Hz, 1H), 7.11–7.00 (m, 3H), 6.84 (ddd, *J* = 7.9, 7.2, 1.5 Hz, 1H), 6.62–6.66 (m, 1H), 6.56 (dd, *J* = 7.9, 1.6 Hz, 1H), 3.52 (d, *J* = 10.2 Hz, 1H), 2.71 (m, 1H), 1.11 (d, *J* = 6.6 Hz, 3H), 0.76 (d, *J* = 6.7 Hz, 3H); ^{13}C{^{1}H} NMR (101 MHz, $CDCl_3$) δ 156.7 (C), 143.5 (C), 137.3 (C), 133.8 (C), 129.4 (CH), 128.9 (CH), 124.5 (CH), 124.1 (CH), 121.8 (CH), 121.4 (CH), 118.5 (CH), 118.4 (CH), 66.9 (CH), 32.2 (CH), 20.9 (CH_3), 20.6 (CH_3). $[\alpha]_D^{27}$= –32 (*c* 0.15, $CHCl_3$) for 74% ee; HPLC conditions: Daicel Chiralcel® AD-H (25 cm x 0.46 cm), 80:20 *n*-hexane/2-propanol, 0.7 mL/min, 254 nm, t_1 = 6.96 min, t_2 = 8.17 min; HRMS (ESI$^+$): calculated for $C_{16}H_{18}NO$ $[M+H]^+$ 240.1380; observed 240.1383.

(*R*)-11-benzyl-10,11-dihydrodibenzo[*b*,*f*][1,4]oxazepine (4d): $[\alpha]_D^{27}$ = +27.1 (*c* 0.15, $CHCl_3$) for 87% ee, [Lit:[54c] $[\alpha]_D^{30}$= –100.3 (*c* 1.02, $CHCl_3$) for 52% ee (*S*); HPLC conditions: Daicel Chiralcel® AD-H (25 cm x 0.46 cm), 80:20 *n*-hexane/2-propanol, 0.7 mL/min, 254 nm, t_1 = 8.9 min (minor), t_2 = 10.4 min (major).

(*R*)-6-methyl-6,11-dihydro-5*H*-dibenzo[*b*,*e*]azepine (6a): IR absorption (neat) $\bar{\upsilon}$ 3396, 3018, 2965, 1602, 1477; ^{1}H NMR (400 MHz, $CDCl_3$) δ 7.30–7.15 (m, 4H), 7.04–6.98 (m, 1H), 6.98–6.90 (m, 1H), 6.61 (td, *J* = 7.4, 1.2 Hz, 1H), 6.42 (dd, *J* = 8.0, 1.2 Hz, 1H), 5.23 (q, *J* = 6.7 Hz, 1H), 4.84 (d, *J* = 15.0 Hz, 1H), 3.56 (d, *J* = 15.1 Hz, 1H), 1.63 (d, *J* = 6.7 Hz, 3H); ^{13}C{^{1}H} NMR (101 MHz, $CDCl_3$) δ 145.8 (C), 140.5 (C), 139.8

(C), 130.6 (CH), 128.3 (CH), 127.8 (CH), 127.7 (CH), 127.2 (CH), 123.7 (CH), 123.2 (CH), 118.3 (CH), 117.4 (CH), 49.8 (CH), 40.1 (CH_2), 20.3 (CH_3); $[\alpha]_D^{25}$ = +39.3 (*c* 0.14, $CHCl_3$) for 70% ee; HPLC conditions: Daicel Chiralcel® AD-H (25 cm x 0.46 cm), 80:20 *n*-hexane/2-propanol, 0.7 mL/min, 254 nm, t_1 = 9.8 min (major), t_2 = 10.6 min (minor); HRMS (ESI^+): calculated for $C_{15}H_{16}N$ $[M+H]^+$ 210.1270; observed 210.1277.

(*S*)-6-phenyl-6,11-dihydro-5*H*-dibenzo[*b*,*e*]azepine (6b): White solid; mp = 146–149 ºC; IR absorption (neat) ῡ 3410, 3016, 2924, 1597, 1488; ^{1}H NMR (400 MHz, MHz, $CDCl_3$) δ 7.42–7.15 (m, 8H), 7.06–6.99 (m, 3H), 6.68 (m, 1H), 6.60 (dd, *J* = 8.3, 1.2 Hz, 1H), 5.75 (s, 1H), 4.40 (s, 1H), 4.06–3.78 (m, 2H); ^{13}C{^{1}H} NMR (101 MHz, $CDCl_3$) δ 144.7 (C), 140.5 (C), 139.3 (C), 137.6 (C), 130.8 (CH), 130.7 (CH), 129.2 (CH), 129.0 (CH), 128.9 (CH), 128.7 (CH), 128.6 (CH), 127.7 (CH), 127.1 (CH), 126.9 (CH), 126.3 (CH), 124.5 (CH), 118.9 (CH), 115.8 (CH), 62.3 (CH) 39.5 (CH). $[\alpha]_D^{27}$ = –7.5 (*c* 0.16, $CHCl_3$) for 4% ee; HPLC conditions: Daicel Chiralcel® AD-H (25 cm x 0.46 cm), 80:20 *n*-hexane/2-propanol, 0.7 mL/min, 254 nm, t_1 = 13.4 min (major), t_2 = 14.1 min (minor). HRMS HRMS (ESI^+): calculated for $C_{20}H_{18}N$ $[M+H]^+$ 272.1432; observed 272.1434.

(*R*)-5,11-dimethyl-10,11-dihydro-5*H*-dibenzo[*b*,*e*][1,4]diazepine (8a): White solid; mp = 123–125 ºC, IR absorption (neat) ῡ 3387, 3049, 2979, 2887, 1586, 1478; ^{1}H NMR (500 MHz, $CDCl_3$) δ 7.29–7.22 (m, 1H), 7.18 (dd, *J* = 7.6, 1.6 Hz, 1H), 7.10 (dd, *J* = 8.1, 1.2 Hz, 1H), 7.01 (td, *J* = 7.5, 1.2 Hz, 1H), 6.92 (dd, *J* = 7.6, 1.9 Hz, 1H), 6.78 – 6.62 (m, 2H), 6.48 (dd, *J* = 7.4, 2.0 Hz, 1H), 5.27 (q, *J* = 6.8 Hz, 1H), 3.29 (s, 3H), 1.59 (d, *J* = 6.8 Hz, 3H); ^{13}C{^{1}H} NMR (126 MHz, $CDCl_3$) δ 150.6 (C), 139.5 (C), 137.3 (C), 136.4 (C), 128.1 (CH), 124.5 (CH), 122.9 (CH), 122.3 (CH), 120.0

(CH), 118.9 (CH), 118.0 (CH), 117.5 (CH), 50.2 (CH), 39.9 (CH_3), 20.5 (CH_3). $[\alpha]_D^{27}$= –71.3 (*c* 0.14, $CHCl_3$) for 83% ee; HPLC conditions: Daicel Chiralcel® AD-H (25 cm x 0.46 cm), 80:20 *n*-hexane/2-propanol, 0.7 mL/min, 254 nm, t_1 = 9.7 min (minor), t_2 = 10.3 min (major); HRMS (ESI^+): Calculated for $C_{15}H_{17}N_2$ $[M+H]^+$ 225.1382, found 225.1386.

(*S*)-5-methyl-11-phenyl-10,11-dihydro-5*H*-dibenzo[*b,e*][1,4]diazepine (8b): White solid. 36% ee; IR absorption (neat) ῡ 3407, 3024, 2943, 2799, 1597, 1488; ^1H NMR (400 MHz, $CDCl_3$) δ 7.42–7.23 (m, 6H), 7.12 (d, *J* = 8.0, 1H), 6.97–6.88 (m, 3H), 6.80–6.72 (m, 2H), 6.59 (dd, *J* = 7.2, 2.1 Hz, 1H), 5.92 (s, 1H). 3.16 (s, 3H).; $^{13}C\{^1H\}$ NMR (126 MHz, $CDCl_3$) δ 150.1 (C), 143.2 (C), 139.1 (C), 136.9 (C), 136.0 (C), 128.4 (CH), 128.3 (CH), 128.2 (CH), 127.2 (CH), 127.2 (CH), 122.5 (CH), 122.4 (CH), 120.2 (CH), 119.4 (CH), 118.5 (CH), 117.9 (CH), 61.4 (CH), 39.6 (CH_3); $[\alpha]_D^{27}$= –15.8 (*c* 0.09, $CHCl_3$) for 36% ee; HPLC conditions: Daicel Chiralcel® AD-H (25 cm x 0.46 cm), 80:20 *n*-hexane/2-propanol, 0.7 mL/min, 254 nm, t_1 = 17.26 min (major), t_2 = 19.54 min (minor); HRMS (ESI^+): calculated for $C_{20}H_{19}N_2$ $[M+H]^+$ 287.1549; observed 287.1543.

(*R*)-11-methyl-10,11-dihydrodibenzo[*b,f*][1,4]thiazepine (10a): $[\alpha]_D^{27}$= –89.0 (*c* 0.47, $CHCl_3$) for 92% ee; [Lit:[54h] $[\alpha]_D^{20}$ = –87.1 (*c* 0.48, $CHCl_3$) for 92% ee (*R*); HPLC conditions: Daicel Chiralcel® AD-H (25 cm x 0.46 cm), 80:20 *n*-hexane/2-propanol, 0.7 mL/min, 254 nm, t_1 = 15.9 min (minor), t_2 = 17.0 min (major).

(*S*)-11-phenyl-10,11-dihydrodibenzo[*b,f*][1,4]thiazepine (10b): Compound **10b** was isolated from the reaction mixture containing unreacted starting material by chromatography over SiO_2 (hexane: EtOAc, from 90:10 to 80:20), 53% isolated yield; $[\alpha]_D^{27}$ = +9.2 (*c* 0.25, $CHCl_3$) for

97% ee, [Lit:[54h] $[\alpha]_D^{20}$ = –9.5 (*c* 0.38, $CHCl_3$) for 56% ee (*R*); HPLC conditions: Daicel Chiralcel® AD-H (25 cm x 0.46 cm), 97:03 *n*-hexane/2-propanol, 0.7 mL/min, 254 nm, t_1 = 12.0 min (major), t_2 = 17.3 min (minor).

(*R*)-11-methyl-10,11-dihydrodibenzo[*b,f*][1,4]thiazepine 5,5-dioxide (12a): Compound **12a** was isolated from the reaction mixture containing unidentified by-products by preparative TLC over SiO_2 (hexane:DCM, 1:2), 59% isolated yield; pale yellow solid; mp = 167–169 ºC; IR absorption (neat) ῡ 3363, 3066, 2982, 1602, 1524, 1479; ^{1}H NMR (500 MHz, $CDCl_3$) δ 8.08 (dd, *J* = 7.8, 1.4 Hz, 1H), 7.99 (dd, *J* = 8.3, 1.6 Hz, 1H), 7.69 (td, *J* = 7.6, 1.4 Hz, 1H), 7.53–7.40 (m, 2H), 7.30–7.21 (m, 1H), 6.76 (dd, *J* = 8.2, 7.0 Hz, 1H), 6.54 (dd, *J* = 8.4, 1.1 Hz, 1H), 6.05 (q, *J* = 6.7 Hz, 1H), 4.38 (bs, 1H), 1.78 (d, *J* = 6.7 Hz, 3H); ^{13}C{^{1}H} NMR (126 MHz, $CDCl_3$) δ 143.6 (C), 140.0 (C), 136.8 (C), 134.8 (CH), 134.4 (CH), 128.4 (CH), 127.0 (CH), 126.5 (CH), 124.6 (CH), 122.2 (CH), 118.5 (CH), 117.1 (CH), 47.2 (CH), 19.0 (CH_3). $[\alpha]_D^{27}$ = –49.2 (*c* 0.13, $CHCl_3$) for 80% ee; HPLC conditions: Daicel Chiralcel® AD-H (25 cm x 0.46 cm), 80:20 *n*-hexane/2-propanol, 0.7 mL/min, 254 nm, t_1 = 12.6 min (minor), t_2 = 13.5 min (major). HRMS (ESI^+): calculated for $C_{14}H_{14}NO_2S$ $[M+H]^+$ 260.0738; observed 260.0740.

2B.6.7 X-ray crystallographic data of compound 12a

Crystals of **12a** were obtained by leaving a saturated solution of this compound in a Hexane/DCM mixture (3:1) stand overnight at –5 ºC. The measured crystals were stable under atmosphere conditions; nevertheless, they were prepared under inert conditions immersed in perfluoropolyether as protecting oil for manipulation.

***Data collection**:* Crystal structure determination for **12a** was carried out using a Apex DUO diffractometer equipped with a Kappa 4-axis goniometer, an APEX II 4K CCD area detector, a Microfocus Source E025 IuS using MoK_α radiation, Quazar MX multilayer Optics as monochromator and an Oxford Cryosystems low temperature device Cryostream 700 plus (T = –173 °C). Full-sphere data collection was used with ω and φ scans. *Programs used:* Data collection APEX-2[75], data reduction Bruker Saint[76] V/.60A and absorption correction SADABS[77]. Structure solution with

Structure Solution and Refinement: Crystal structure solution was achieved using SHELXS-97 as implemented in SHELXTL[78]. Visualization was performed with the program SHELXle[79]. Least-squares refinement on F^2 using all measured intensities was carried out using the program SHELXL 2015[80].

This compound crystallizes in the chiral space group $P2_1$. The absolute configuration of the product was determined to be *R*, according to a Flack value[81] of 0.12(14) and a Flack value based on Parsons' quotients[82] of 0.041(84).

CCDC 1452862 contains the supplementary crystallographic data for this paper. These data can be obtained free of charge from The Cambridge Crystallographic Data Centre via www.ccdc.cam.ac.uk/data_request/cif.

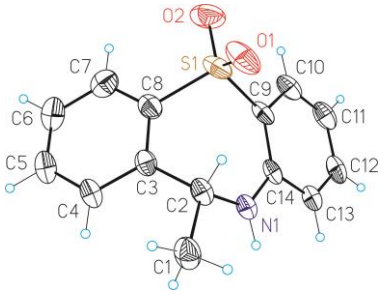

Figure SI33. ORTEP plot (thermal ellipsoids at 50% probability) showing the molecular structure of compound **12a**.

Chapter-2

Table SI4. Crystal data and structure refinement for **12a**

Empirical formula	$C_{14}H_{13}NO_2S$	
Formula weight	259.31	
Temperature	100(2) K	
Wavelength	0.71073 Å	
Crystal system	Monoclinic	
Space group	$P2_1$	
Unit cell dimensions	a = 7.1592(15) Å	α = 90°.
	b = 10.0169(16) Å	β = 98.587(8)°.
	c = 8.646(2)Å	γ = 90°.
Volume	613.1(2) $Å^3$	
Z	2	
Density (calculated)	1.405 Mg/m^3	
Absorption coefficient	0.256 mm^{-1}	
F(000)	272	
Crystal size	0.40 x 0.30 x 0.05 mm^3	
Theta range for data collection	2.382 to 31.059°	
Index ranges	-8<=h<=10,-14<=k<=8,-12<=l<=12	
Reflections collected	6695	
Independent reflections	3040 [R(int) = 0.0508]	
Completeness to theta = 31.059°	99.299995%	
Absorption correction	Multi-scan	
Max. and min. transmission	0.987 and 0.657	
Refinement method	Full-matrix least-squares on F^2	
Data / restraints / parameters	3040/ 1/ 164	
Goodness-of-fit on F^2	1.090	
Final R indices [I>2σ(I)]	R1 = 0.0667, wR2 = 0.1752	
R indices (all data)	R1 = 0.0729, wR2 = 0.1821	
Flack parameter	x = 0.04(8)	
Largest diff. peak and hole	1.207 and -0.473 e.$Å^{-3}$	

2B.6.8 NMR spectra of compounds and HPLC traces of hydrogenated products.

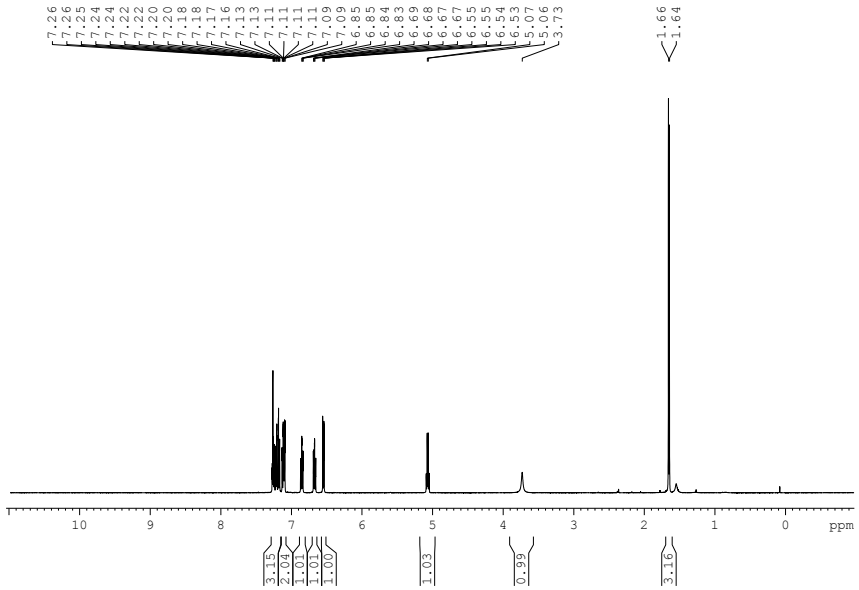

Figure SI34. ^{1}H NMR product **4a**.

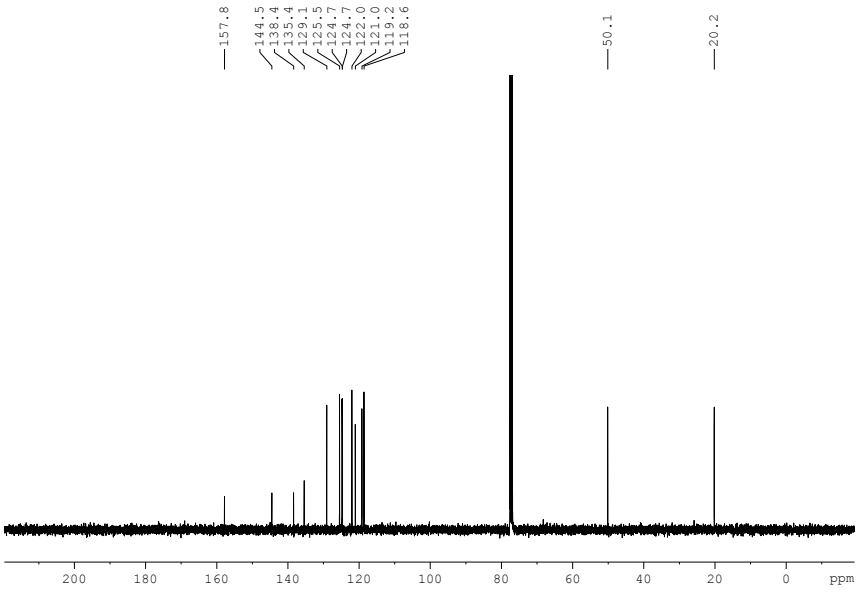

Figure SI35. ^{13}C{^{1}H} NMR product **4a**.

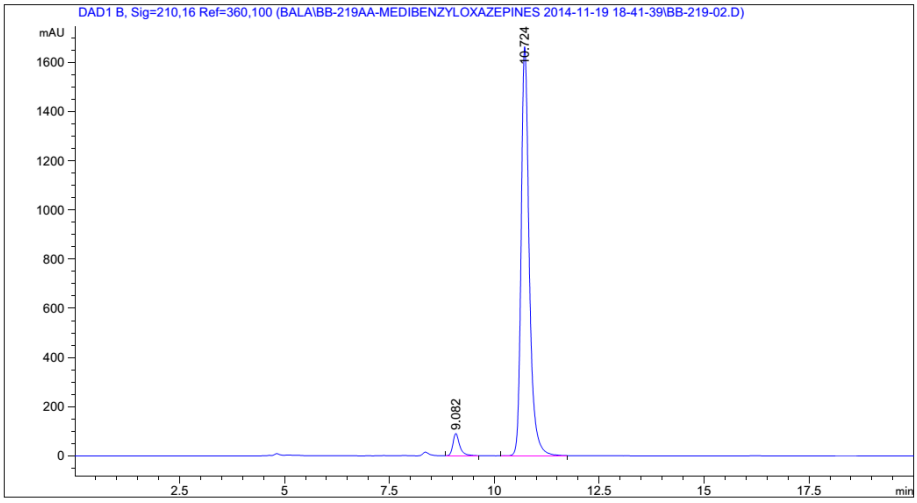


```
=====================================================================
                      Area Percent Report
=====================================================================

Sorted By             :      Signal
Multiplier:                   :      1.0000
Dilution:                     :      1.0000
Use Multiplier & Dilution Factor with ISTDs


Signal 1: DAD1 B, Sig=210,16 Ref=360,100

Peak RetTime Type  Width     Area      Height     Area
  #   [min]        [min]    [mAU*s]     [mAU]       %
----|-------|----|-------|----------|----------|--------|
   1   9.082 BB    0.1682 1025.39233   90.49195   4.3827
   2  10.724 BB    0.2049 2.23709e4  1663.64453  95.6173

Totals :                  2.33963e4  1754.13648
```

Figure SI36. HPLC trace product **4a**.

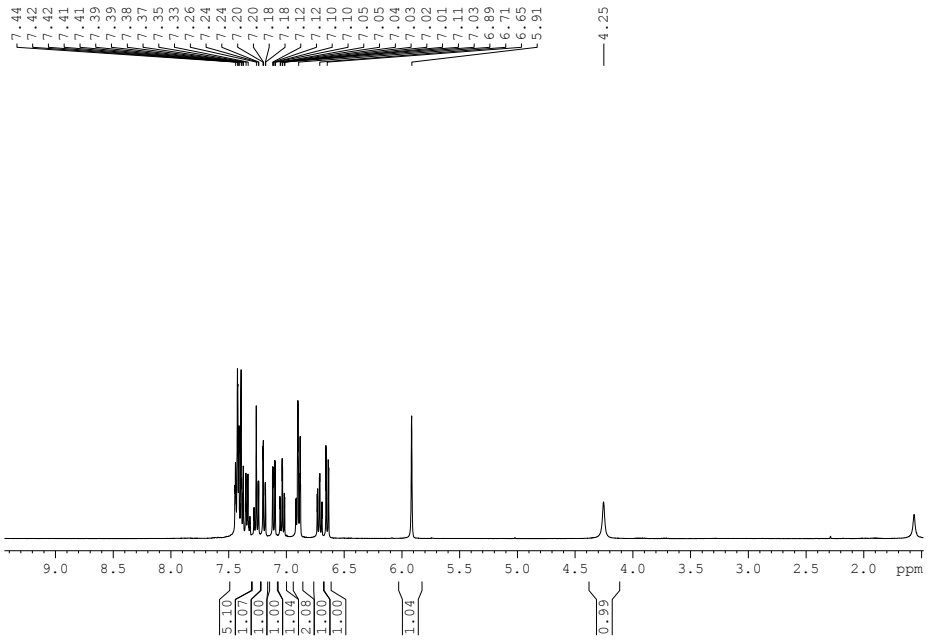

Figure SI37. ^{1}H NMR product **4b**.

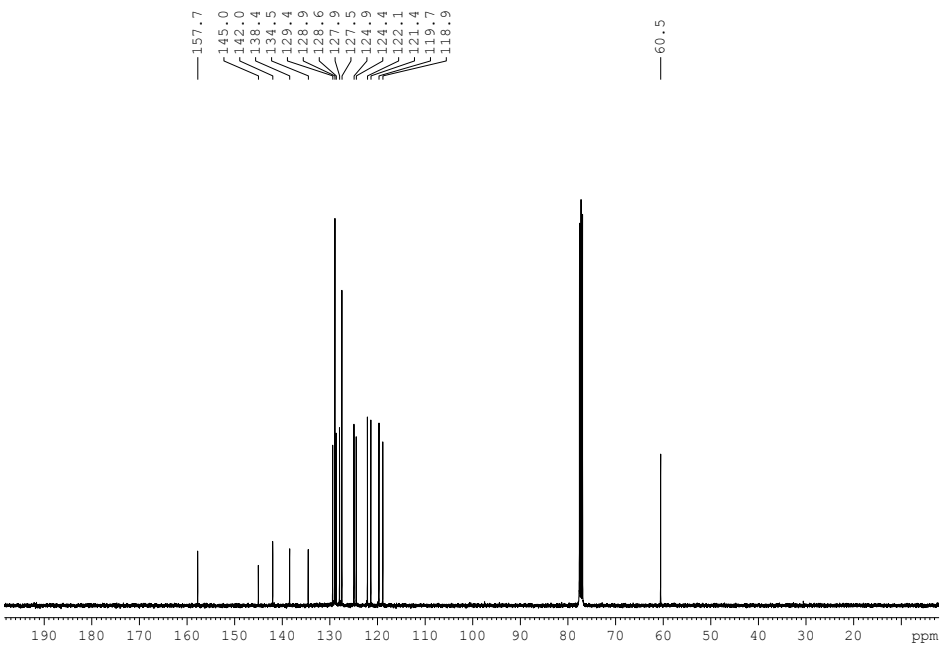

Figure SI38. ^{13}C{^{1}H} NMR product **4b**.

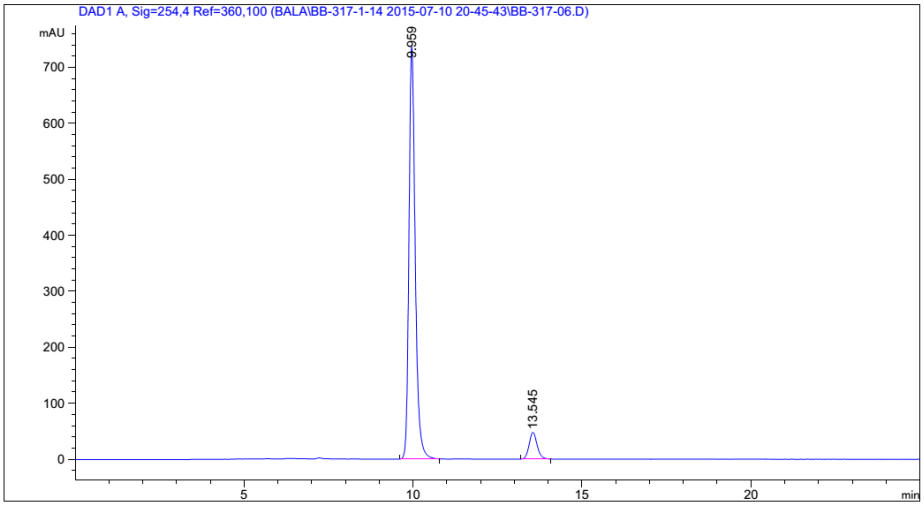


```
=====================================================================
                      Area Percent Report
=====================================================================

Sorted By             :      Signal
Multiplier:                   :      1.0000
Dilution:                     :      1.0000
Use Multiplier & Dilution Factor with ISTDs


Signal 1: DAD1 A, Sig=254,4 Ref=360,100

Peak RetTime Type  Width     Area      Height     Area
  #   [min]        [min]   [mAU*s]     [mAU]       %
----|-------|----|-------|----------|----------|--------|
   1   9.959 BB    0.1972 9550.35938  736.99359  92.2204
   2  13.545 BB    0.2581  805.65576   47.94289   7.7796

Totals :                 1.03560e4   784.93648
```

Figure SI39. HPLC trace product **4b**.

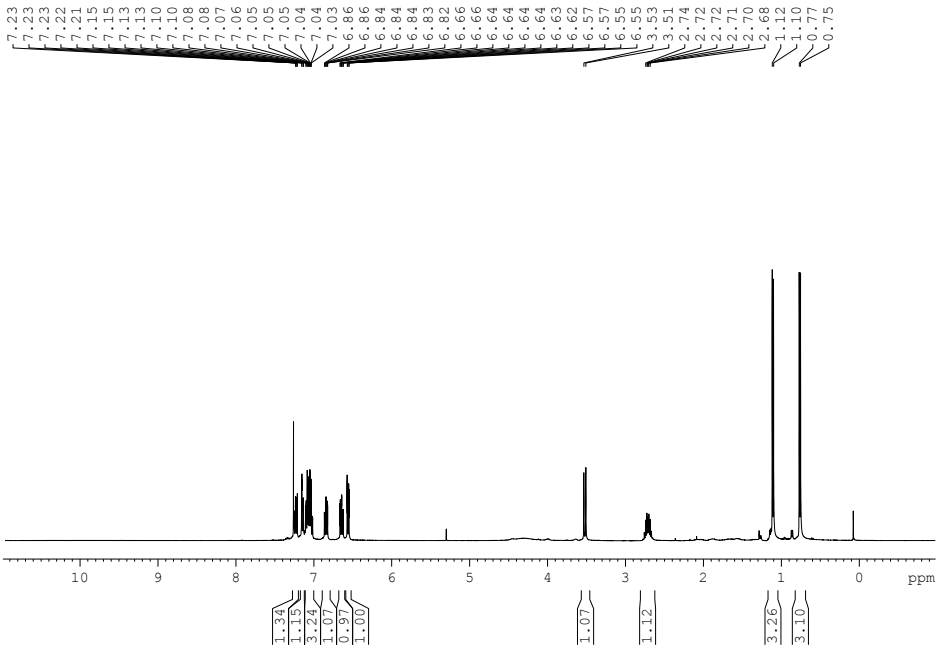

Figure SI40. ^{1}H NMR product **4c**.

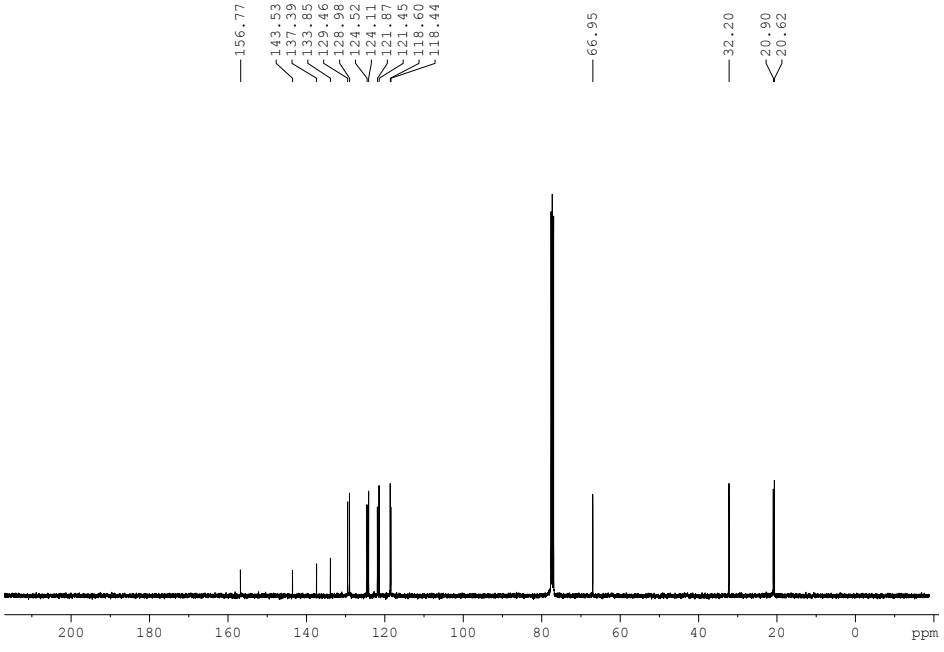

Figure SI41. ^{13}C{^{1}H} NMR product **4c**.

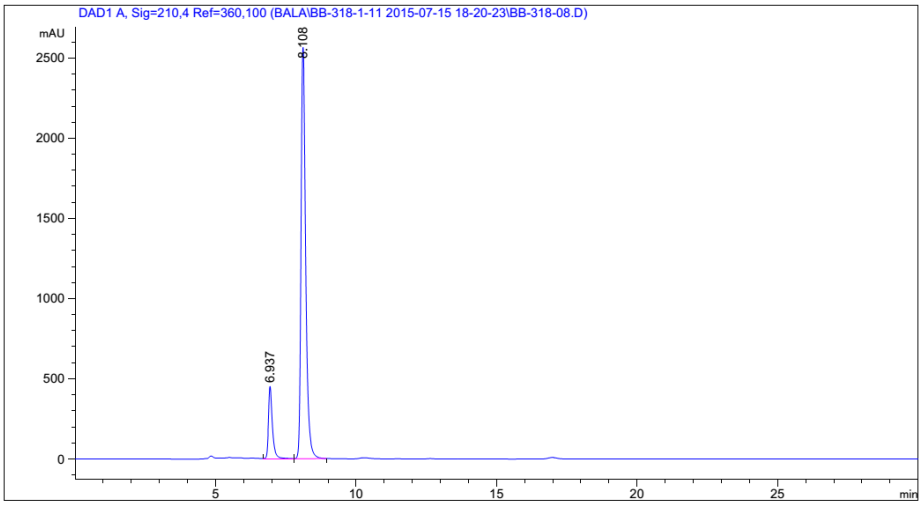


```
=====================================================================
                      Area Percent Report
=====================================================================

Sorted By             :      Signal
Multiplier:                   :      1.0000
Dilution:                     :      1.0000
Use Multiplier & Dilution Factor with ISTDs


Signal 1: DAD1 A, Sig=210,4 Ref=360,100

Peak RetTime Type  Width     Area      Height     Area
  #   [min]        [min]   [mAU*s]     [mAU]       %
----|-------|----|-------|----------|----------|--------|
   1   6.937 VB    0.1444 4428.13330  451.76270  13.0038
   2   8.108 BB    0.1767 2.96246e4   2565.26416  86.9962

Totals :                   3.40527e4   3017.02686
```

Figure SI42. HPLC trace product **4c**.

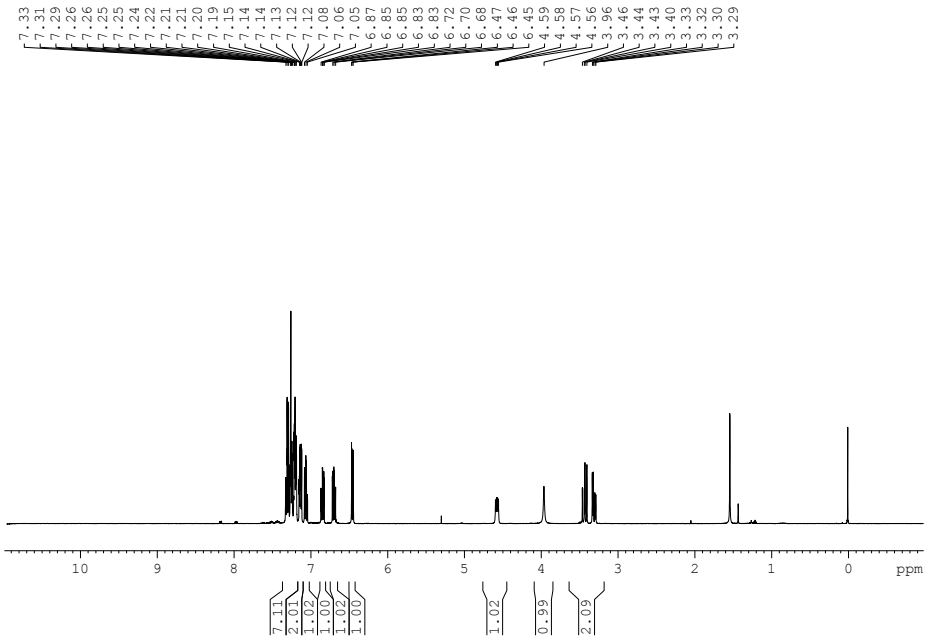

Figure SI43. ^{1}H NMR product **4d**.

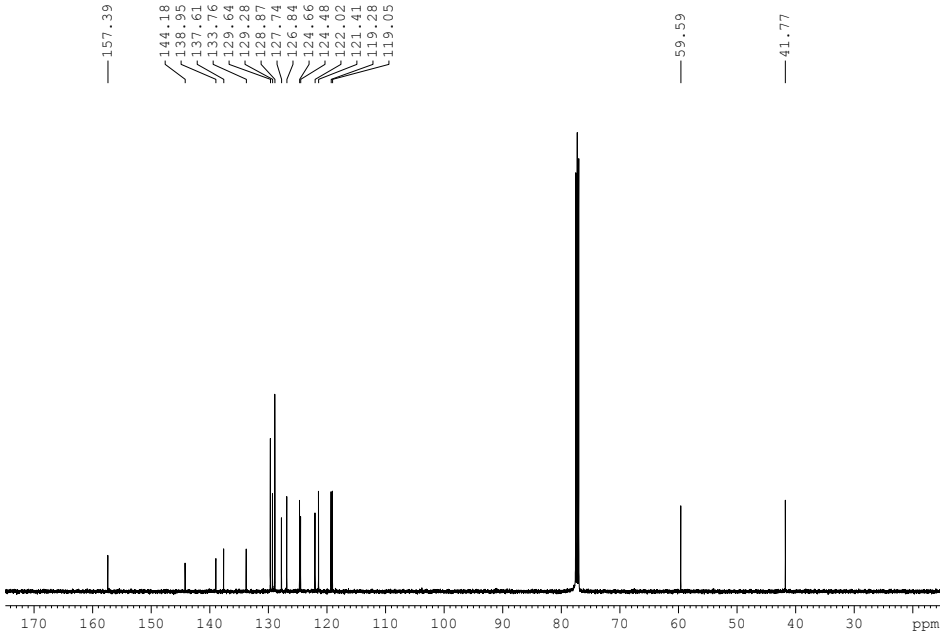

Figure SI44. ^{13}C{^{1}H} NMR product **4d**.

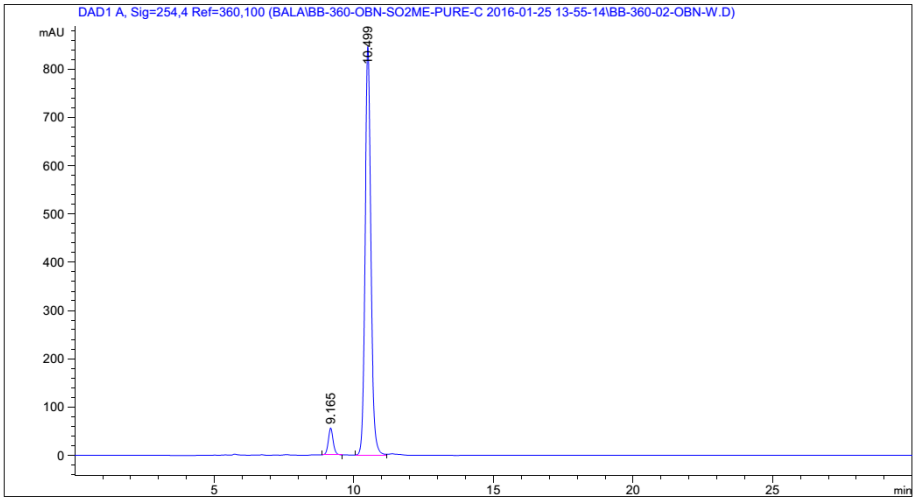


```
=====================================================================
                    Area Percent Report
=====================================================================

Sorted By             :      Signal
Multiplier:                   :      1.0000
Dilution:                     :      1.0000
Use Multiplier & Dilution Factor with ISTDs


Signal 1: DAD1 A, Sig=254,4 Ref=360,100

Peak RetTime Type  Width     Area      Height     Area
  #   [min]        [min]   [mAU*s]     [mAU]       %
----|-------|----|-------|----------|----------|--------|
   1   9.165 BB    0.1864  682.97333   55.97328   5.3088
   2  10.499 BB    0.2198 1.21821e4   846.89978  94.6912

Totals :                  1.28650e4   902.87306
```

Figure SI45. HPLC trace product **4d**.

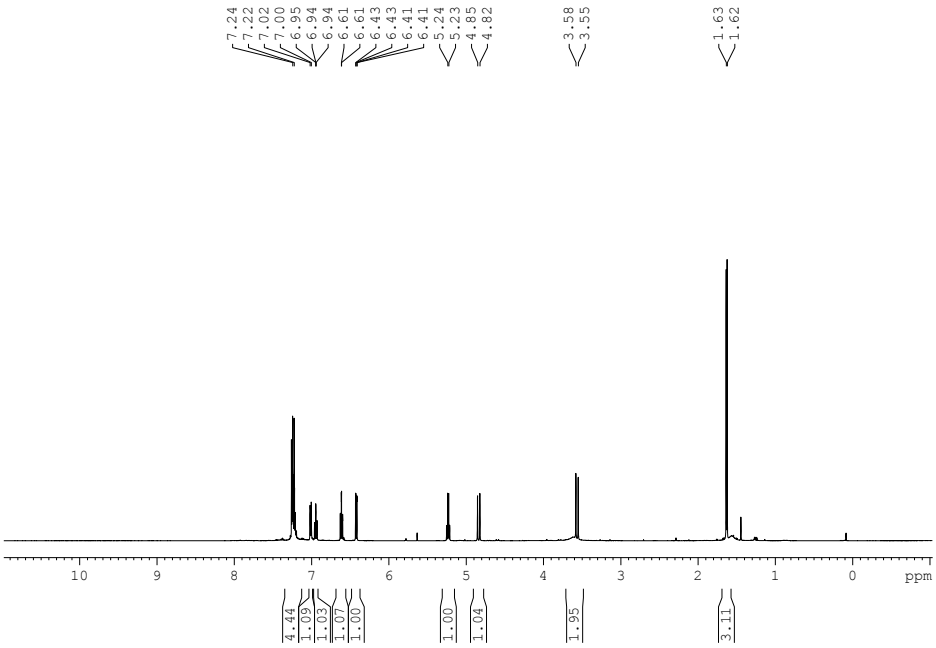

Figure SI46. ^{1}H NMR product **6a**.

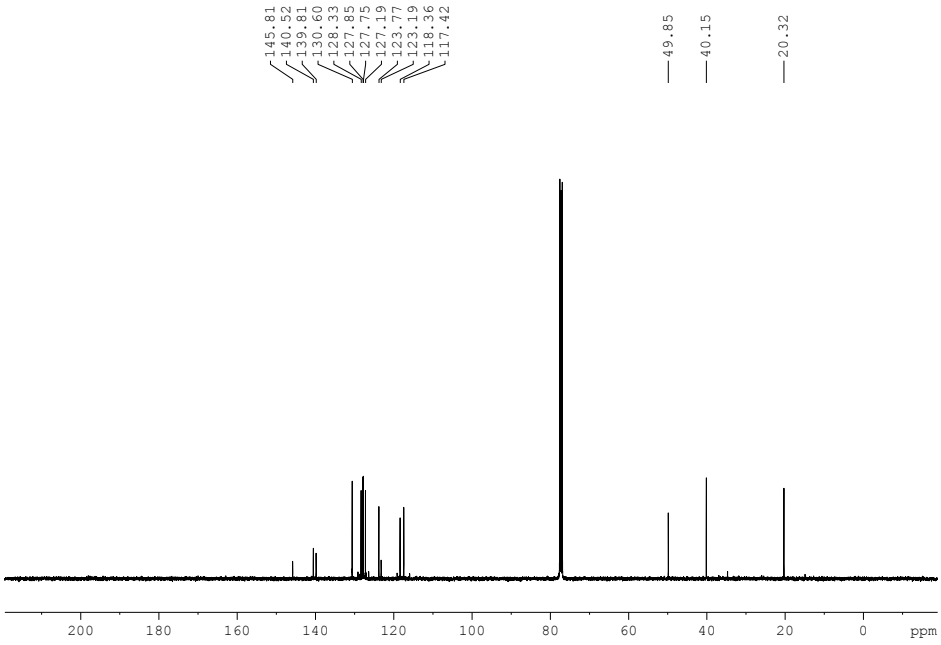

Figure 47. ^{13}C{^{1}H} NMR product **6a**.

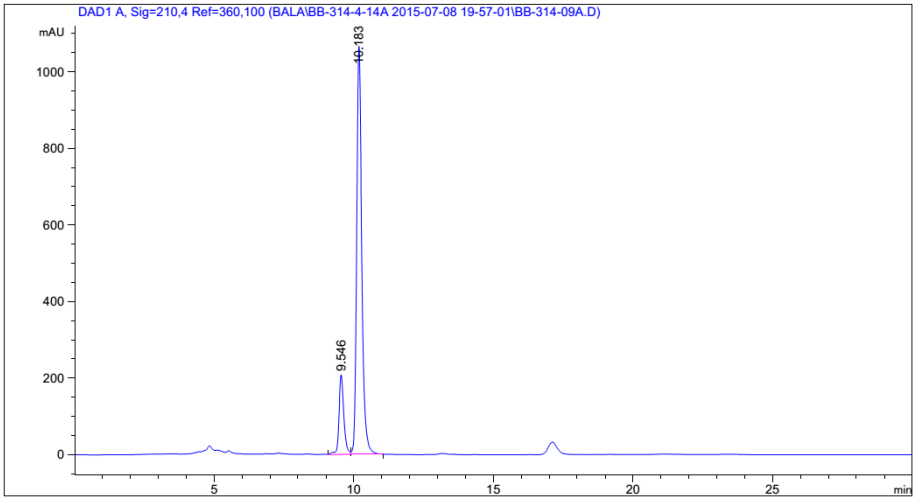


```
=====================================================================
                      Area Percent Report
=====================================================================

Sorted By             :      Signal
Multiplier:                   :      1.0000
Dilution:                     :      1.0000
Use Multiplier & Dilution Factor with ISTDs


Signal 1: DAD1 A, Sig=210,4 Ref=360,100

Peak RetTime Type  Width     Area      Height     Area
  #   [min]        [min]   [mAU*s]     [mAU]       %
----|-------|----|-------|----------|----------|--------|
   1   9.546 BV    0.1797 2490.25000  207.92662  15.6369
   2  10.183 VB    0.1909 1.34353e4  1067.10303  84.3631

Totals :                  1.59255e4  1275.02965

=====================================================================
                      *** End of Report ***
```

Figure SI48. HPLC trace product **6a**.

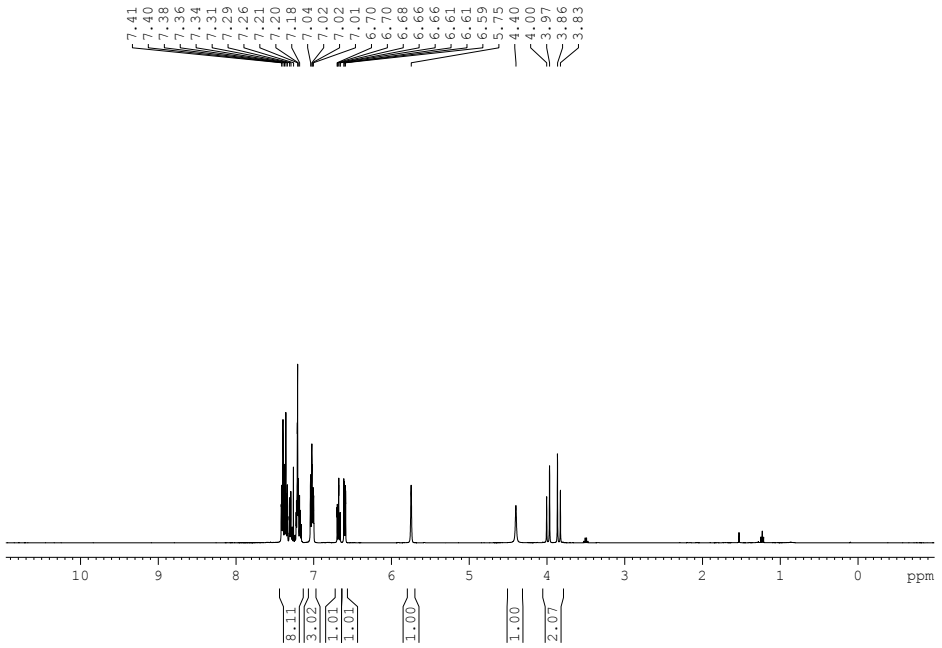

Figure SI49. ^{1}H NMR product **6b**.

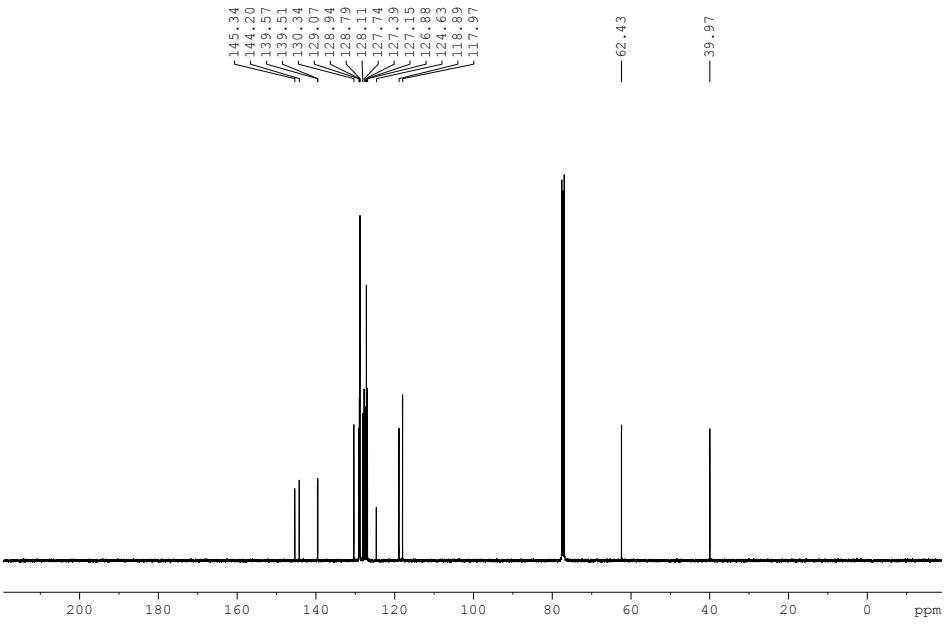

Figure SI50. ^{13}C{^{1}H} NMR product **6b**.

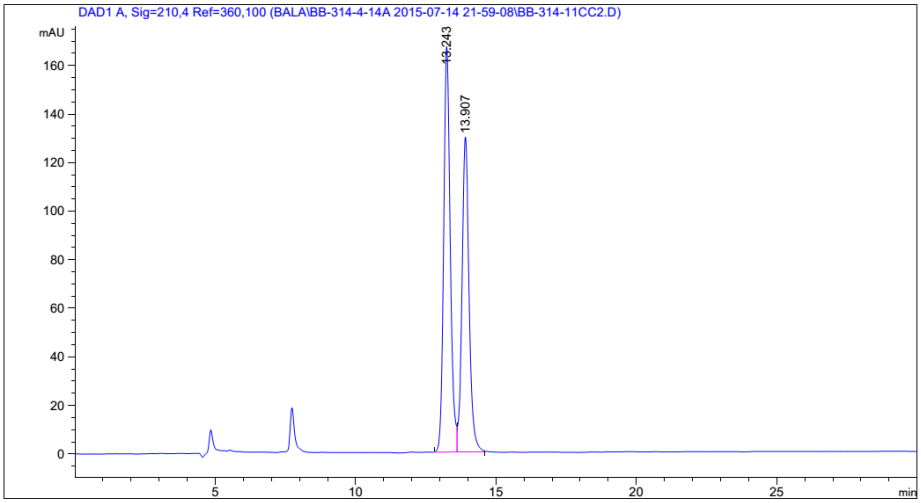


```
=====================================================================
                      Area Percent Report
=====================================================================

Sorted By             :      Signal
Multiplier:                   :      1.0000
Dilution:                     :      1.0000
Use Multiplier & Dilution Factor with ISTDs


Signal 1: DAD1 A, Sig=210,4 Ref=360,100

Peak RetTime Type  Width     Area      Height     Area
  #   [min]        [min]   [mAU*s]     [mAU]       %
----|-------|----|-------|----------|----------|--------|
   1  13.243 BV    0.2479 2717.64429  166.95212  54.4968
   2  13.907 VB    0.2641 2269.15308  129.71028  45.5032

Totals :                  4986.79736  296.66240

=====================================================================
                      *** End of Report ***
```

Figure SI51. HPLC trace product **6b**.

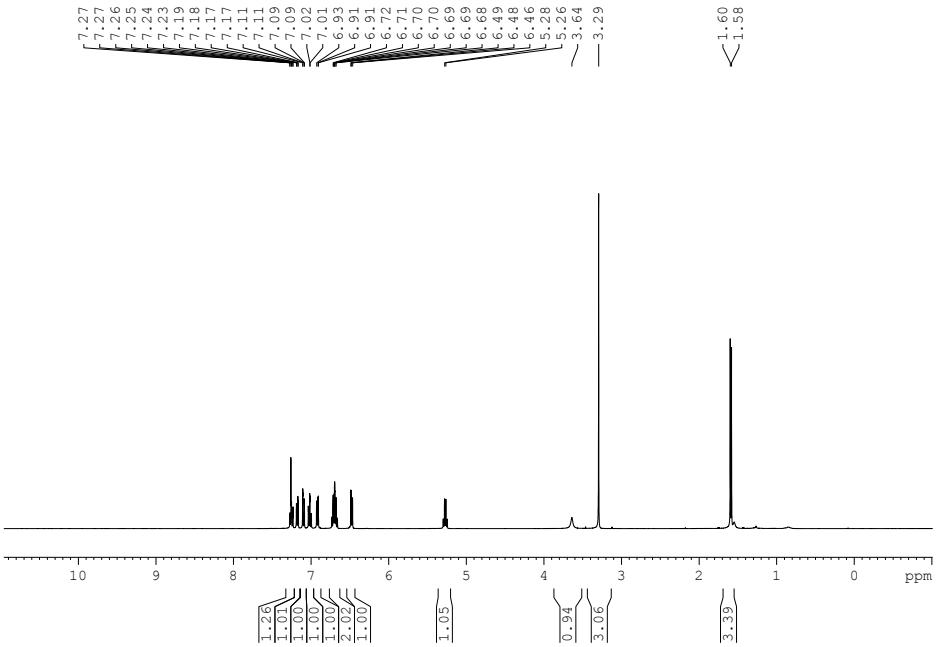

Figure SI52. ^{1}H NMR product **8a**.

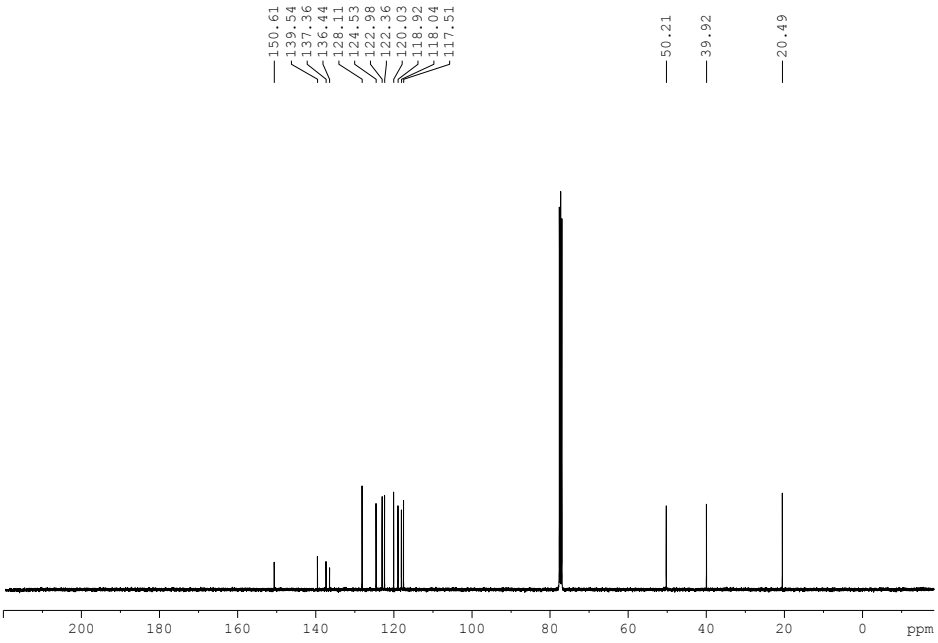

Figure SI53. ^{13}C{^{1}H} NMR product **8a**.

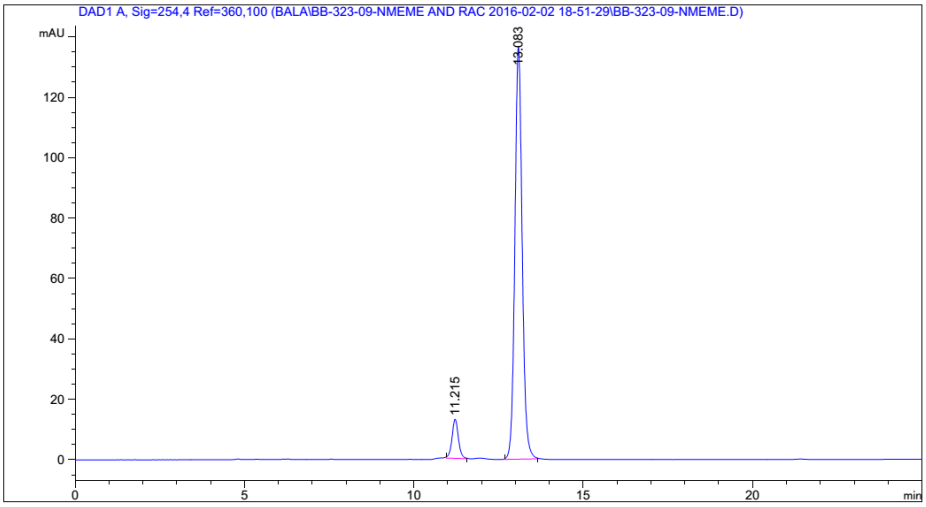


```
=====================================================================
                    Area Percent Report
=====================================================================

Sorted By             :      Signal
Multiplier:                   :      1.0000
Dilution:                     :      1.0000
Use Multiplier & Dilution Factor with ISTDs


Signal 1: DAD1 A, Sig=254,4 Ref=360,100

Peak RetTime Type  Width     Area      Height     Area
  #   [min]        [min]   [mAU*s]     [mAU]       %
----|-------|----|-------|----------|----------|--------|
   1  11.215 BB    0.2003  169.29102   12.96971   7.6280
   2  13.083 BB    0.2311 2050.05688  136.55611  92.3720

Totals :                  2219.34790  149.52581
```

Figure SI54. HPLC trace product **8a**.

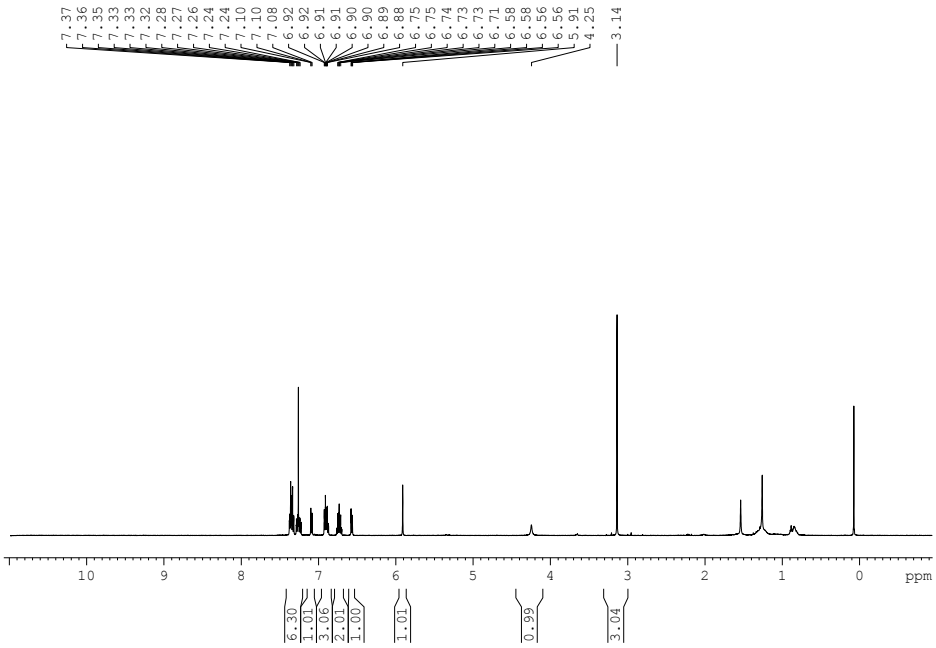

Figure SI55. ^{1}H NMR product **8b**.

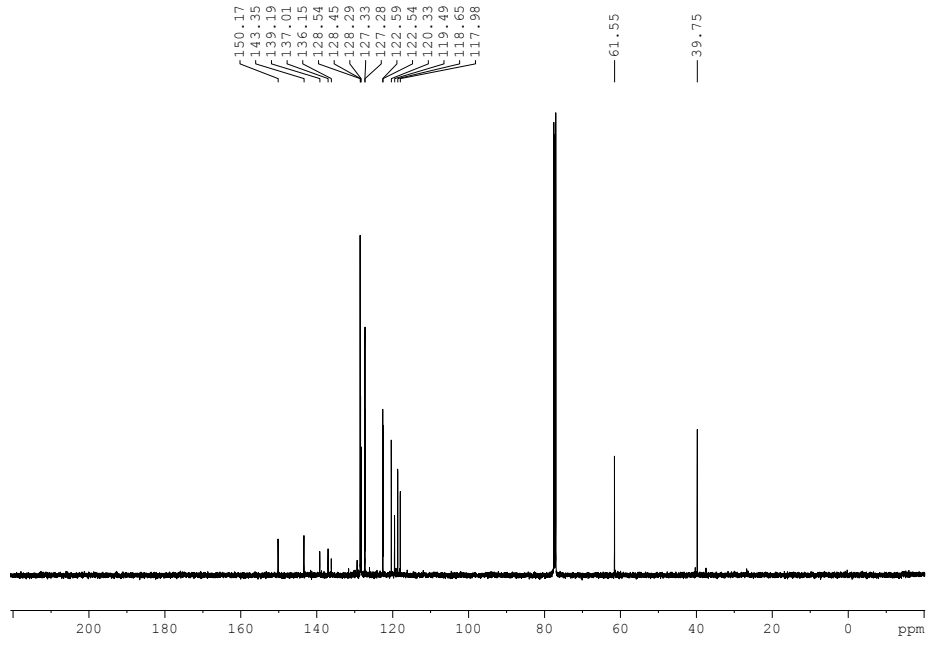

Figure SI56. ^{13}C{^{1}H} NMR product **8b**.

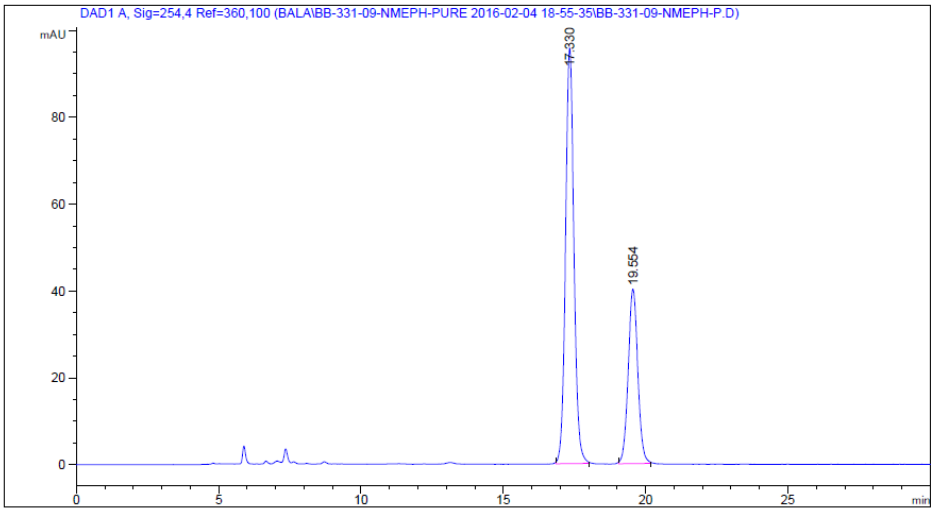


```
=====================================================================
                    Area Percent Report
=====================================================================

Sorted By             :      Signal
Multiplier:                   :      1.0000
Dilution:                     :      1.0000
Use Multiplier & Dilution Factor with ISTDs


Signal 1: DAD1 A, Sig=254,4 Ref=360,100

Peak RetTime Type  Width     Area      Height     Area
  #   [min]        [min]   [mAU*s]     [mAU]       %
----|-------|----|-------|----------|----------|--------|
   1  17.330 BB    0.3146 1957.84241   95.72030  67.5813
   2  19.554 BB    0.3627  939.17584   40.17785  32.4187

Totals :                  2897.01825  135.89815
```

Figure SI57. HPLC trace product **8b**.

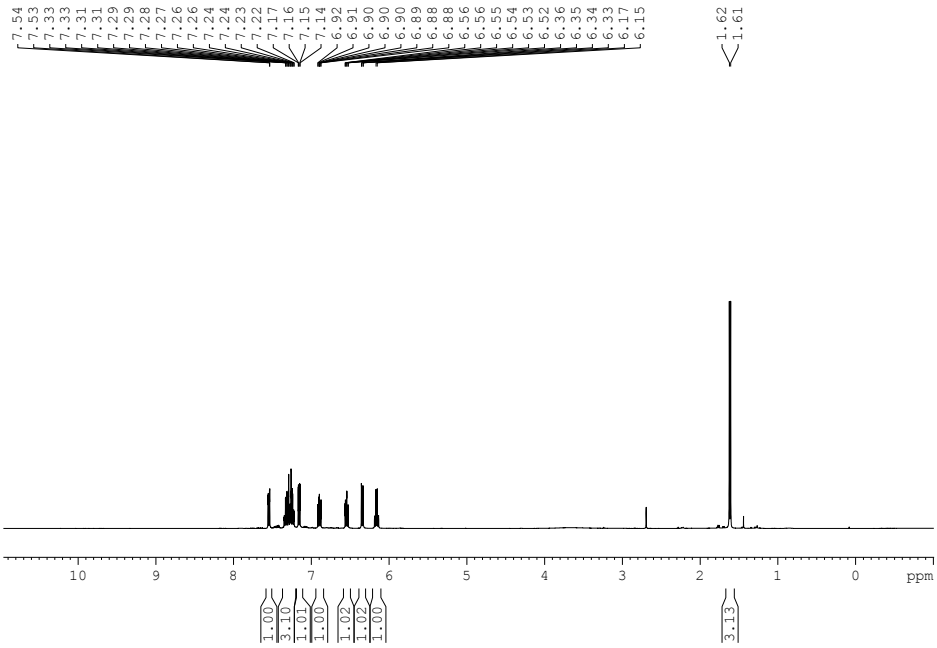

Figure SI58. ^{1}H NMR product **10a**.

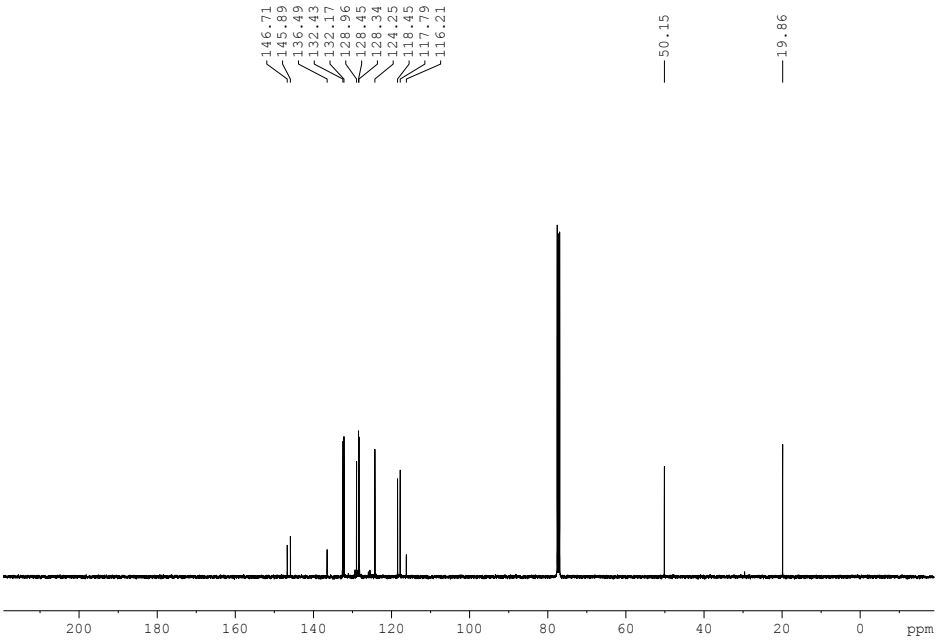

Figure SI59. ^{13}C{^{1}H} NMR product **10a**.

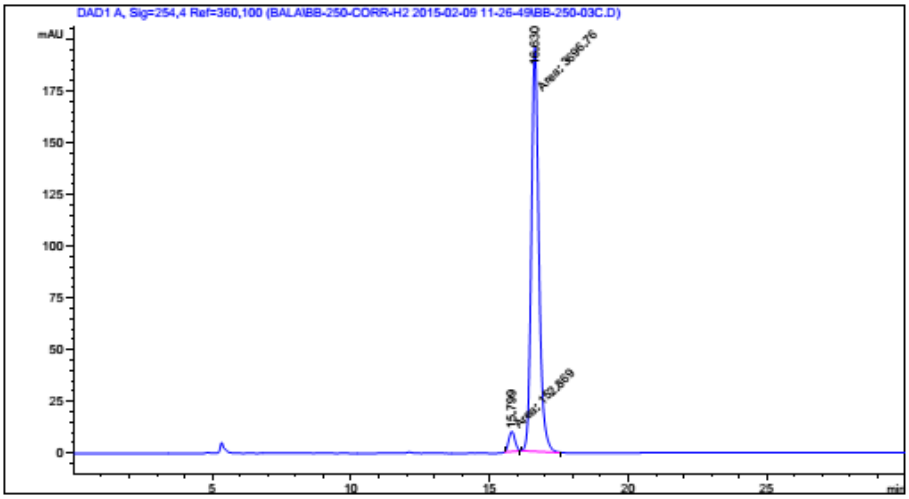


```
=====================================================================
                    Area Percent Report
=====================================================================

Sorted By             :      Signal
Multiplier:                   :      1.0000
Dilution:                     :      1.0000
Use Multiplier & Dilution Factor with ISTDs


Signal 1: DAD1 A, Sig=254,4 Ref=360,100

Peak RetTime Type  Width     Area      Height     Area
  #   [min]        [min]   [mAU*s]     [mAU]       %
----|-------|----|-------|----------|----------|--------|
   1  15.799 MM    0.2631  152.86937    9.68344   3.9710
   2  16.630 MM    0.3154 3696.75903  195.33446  96.0290

Totals :                  3849.62840  205.01789
```

Figure SI60. HPLC trace product **10a**.

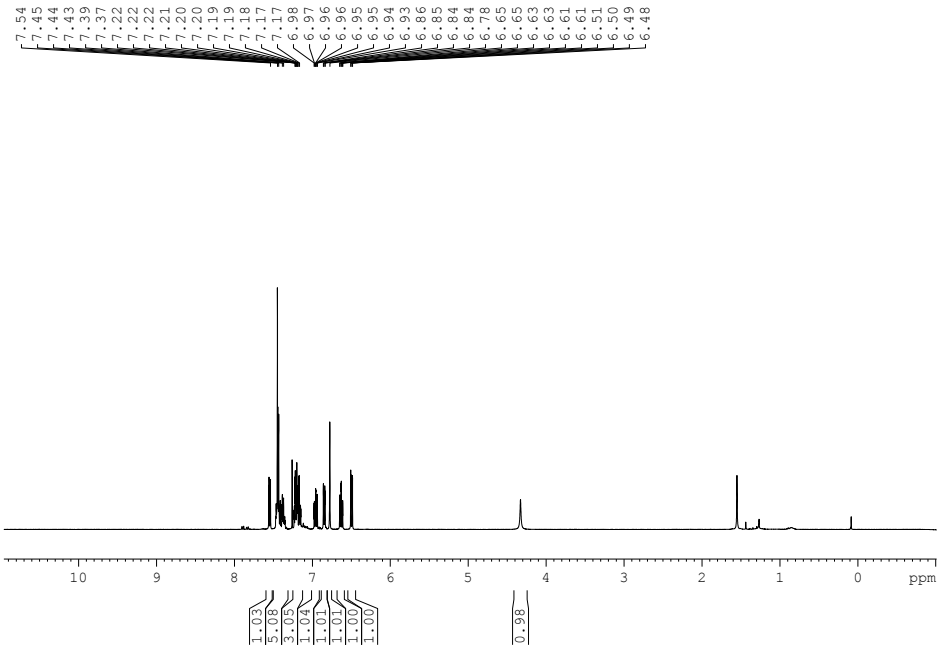

Figure SI61. ^{1}H NMR product **10b**.

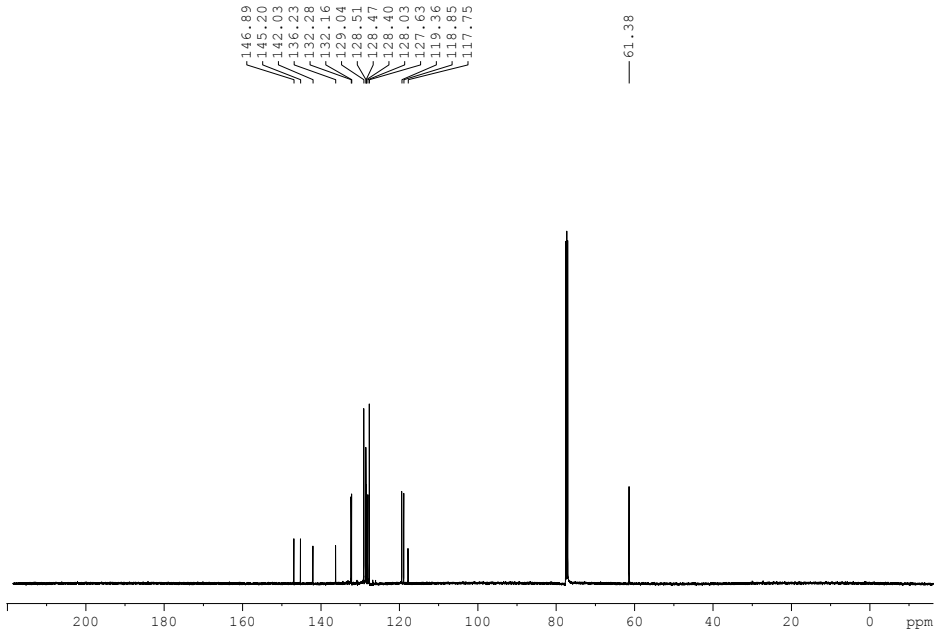

Figure SI62. ^{13}C{^{1}H} NMR product **10b**.

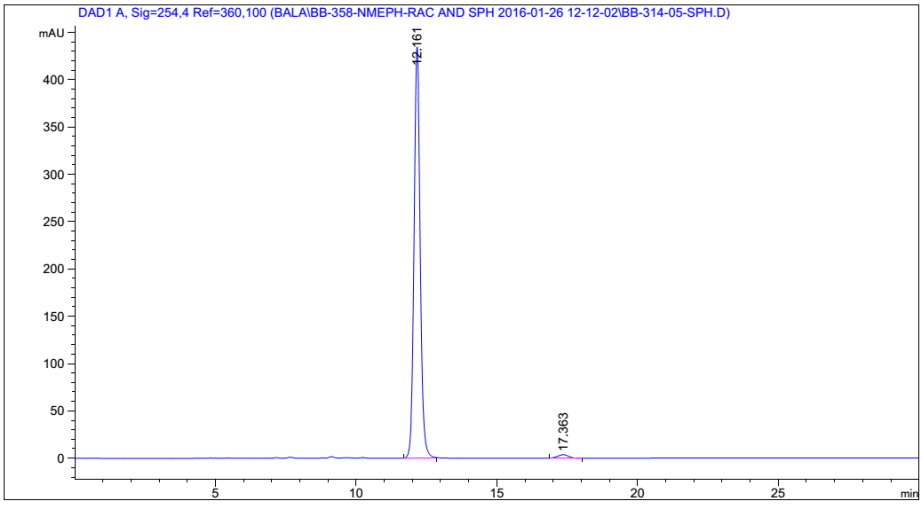


```
======================================================================
                      Area Percent Report
======================================================================

Sorted By             :      Signal
Multiplier:                   :      1.0000
Dilution:                     :      1.0000
Use Multiplier & Dilution Factor with ISTDs


Signal 1: DAD1 A, Sig=254,4 Ref=360,100

Peak RetTime Type  Width     Area      Height     Area
  #   [min]        [min]   [mAU*s]     [mAU]       %
----|-------|----|-------|----------|----------|--------|
   1  12.161 BB    0.2329 6588.28125  434.53781  98.5162
   2  17.363 BB    0.4112   99.22970    3.64939   1.4838

Totals :                  6687.51095  438.18720
```

Figure SI63. HPLC trace product **10b**.

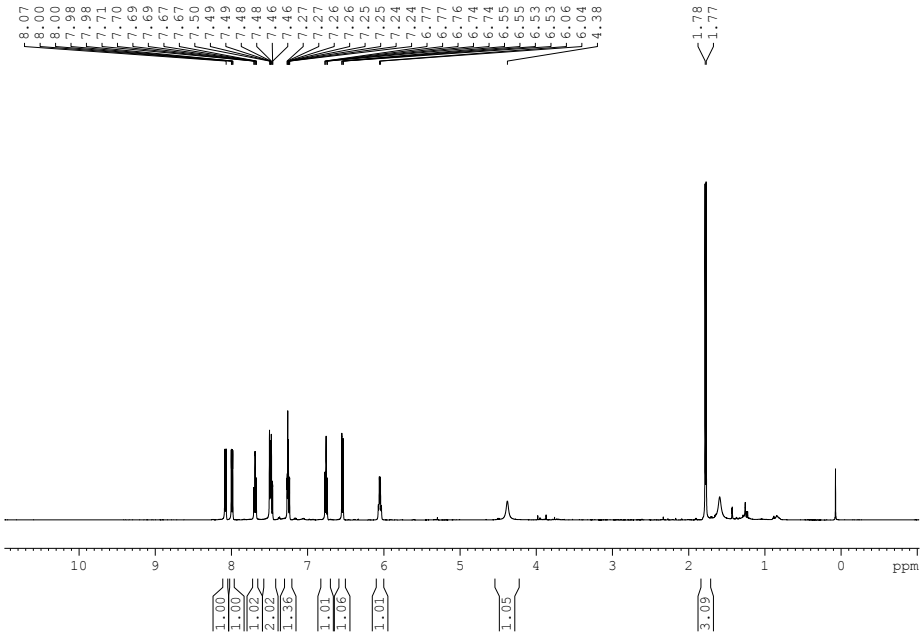

Figure SI64. ^{1}H NMR product **12a**.

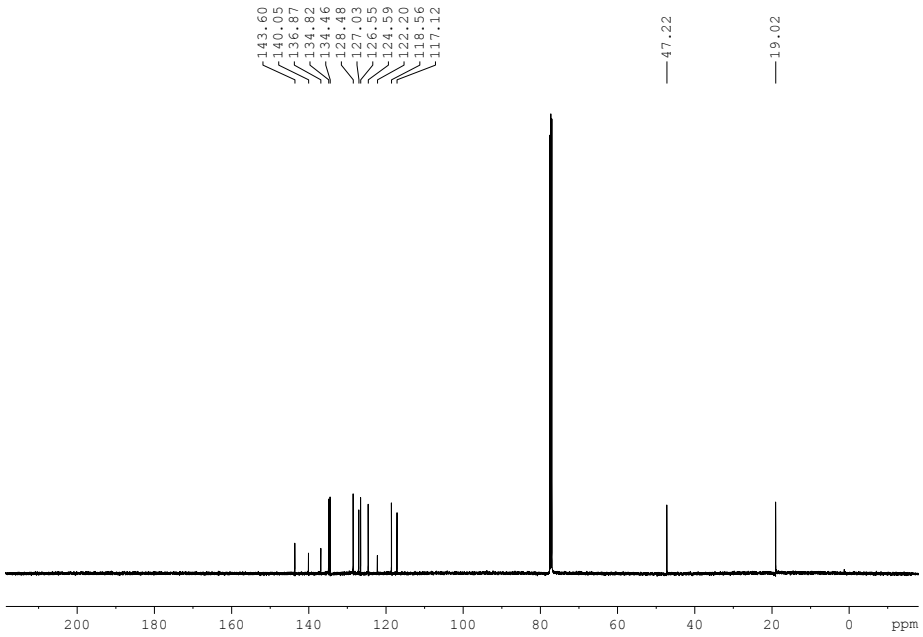

Figure SI65. ^{13}C{^{1}H} NMR product **12a**.

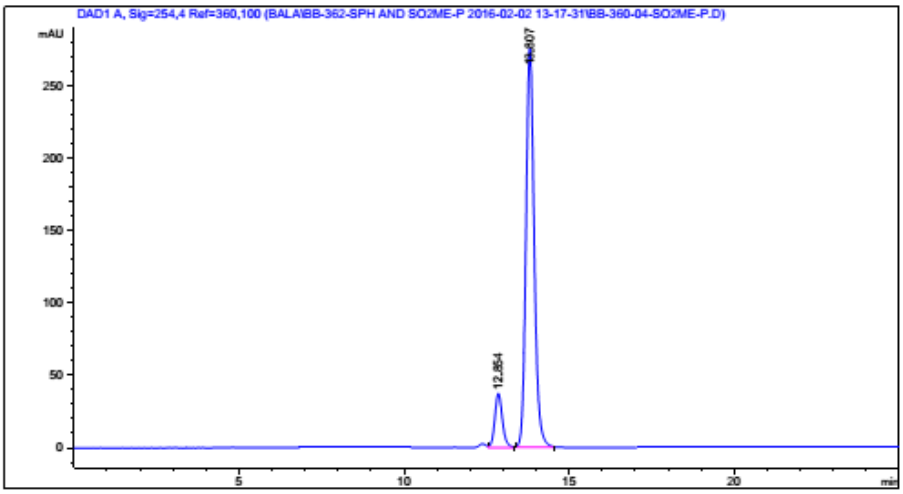


```
=====================================================================
                      Area Percent Report
=====================================================================

Sorted By             :      Signal
Multiplier:                   :      1.0000
Dilution:                     :      1.0000
Use Multiplier & Dilution Factor with ISTDs


Signal 1: DAD1 A, Sig=254,4 Ref=360,100

Peak RetTime Type  Width     Area      Height     Area
  #   [min]        [min]   [mAU*s]     [mAU]       %
----|-------|----|-------|----------|----------|--------|
   1  12.854 VB    0.2450  598.79120   37.36559  11.1432
   2  13.807 BB    0.2662 4774.79492  275.55667  88.8568

Totals :                  5373.58612  312.92226
```

Figure SI66. HPLC trace product **12a**.

2B.6.9 Details of the DFT computational studies on the stereochemical outcome of the Ir-mediated asymmetric hydrogenation

2B.6.9.1 Cyclometallated iridium complexes derived from **3a**:

As commented in the main text, we have explored the possibility of the hydrogenation pathway involving the formation of cyclometallated iridium complexes derived from **3a**. The geometries are shown in Figure SI67. We have computed two possible isomers for **L1** and one for **L3**. The relative energies of the four-membered iridacycles are much higher (>60 kcal·mol^{-1}) than the transition states computed for the mechanism shown in Figure 3 of the manuscript, thus this pathway was not further explored. A likely explanation for the high energy of the cyclometallated iridium complexes is the strain of the four membered ring, where the N–Ir–C angle is close to 60º.

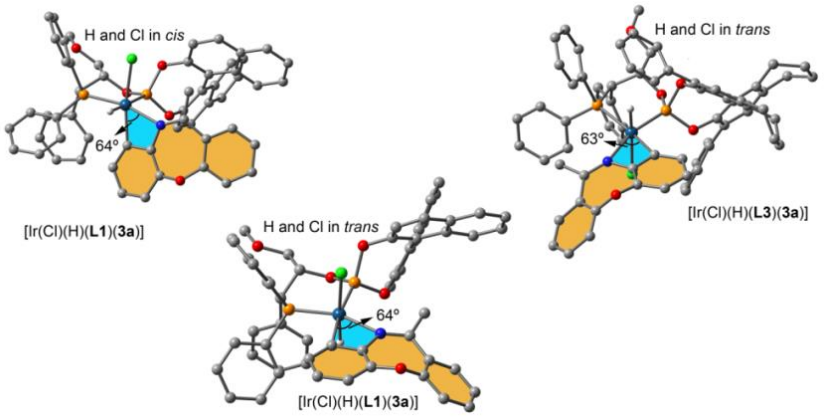

Figure SI67. Optimized geometries of the iridacycles [Ir(Cl)(H)(**L1**)(**3a**)] and [Ir(Cl)(H)(**L3**)(**3a**)].

2B.6.9.2 Geometric and energetic study of the isomers of complexes [Ir(Cl)(H)$_2$(H–H)(**L1**)] and [Ir(Cl)(H)$_2$(H–H)(**L3**)]:

The geometries of the six isomers considered for the octahedral complex [Ir(Cl)(H)$_2$(H–H)(**L1**)] are shown in Figure SI68 along with the relative energies. It can be observed that in the most favored isomers the chlorido ligand is located perpendicular to the plane that contains the P–OP and Ir atoms. In turn, the H–H ligand is occupying each of the two available positions in the aforementioned plane (in one case *cis* to the phosphine group and in the other *cis* to the phosphite motif). Figure SI69 shows the optimized geometries and relative energies of complex [Ir(Cl)(H)$_2$(H–H)(**L3**)]. In the most stable isomers, the chlorido ligand is located perpendicular to the plane that contains the P–OP and Ir atoms but with an opposite orientation to that observed for **L1**. The H–H ligand occupies each of the two possibilities in the aforementioned plane. This favored orientation with the Cl ligand pointing up, when the phosphite group is placed to the left, is due to the formation of an additional C–H···Cl interaction in these isomers of complex [Ir(Cl)(H)$_2$(H–H)(**L3**)] with respect to the same isomers of complex [Ir(Cl)(H)$_2$(H–H)(**L1**)] (see red lines in Figure SI69).

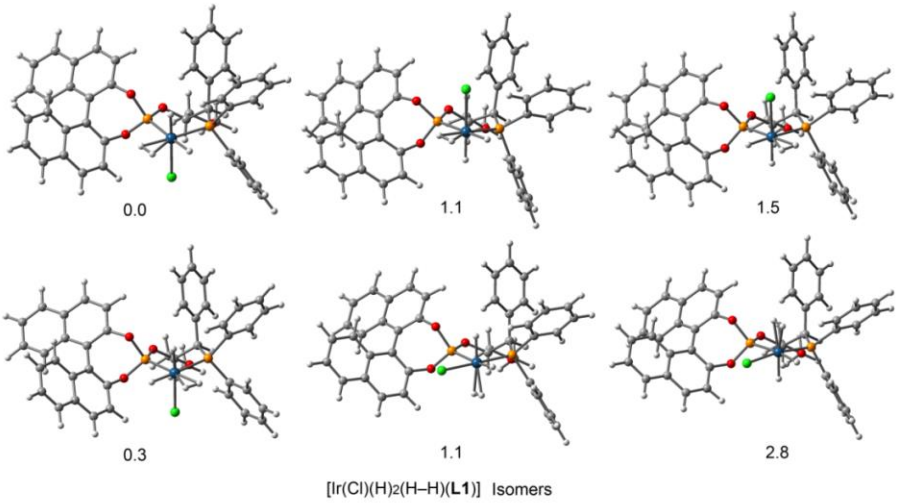

Figure SI68. Isomers of complex [Ir(Cl)(H)$_2$(H–H)(**L1**)] and the relative energies in kcal·mol^{-1}.

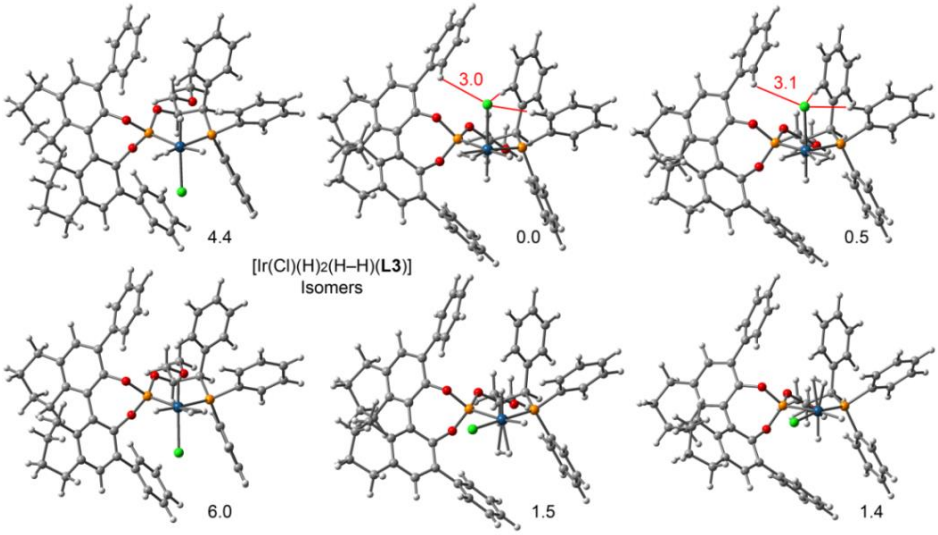

Figure SI69. Isomers of complex [Ir(Cl)(H)$_2$(H–H)(**L3**)] and the relative energies in kcal·mol^{-1}.

2B.6.9.3 TS_R derived from **L1** and TS_S of **L3** leading to the minor enantiomers of the hydrogenation products:

In Figure SI70 we show the transition states TS_R and TS_S computed for **L1** and **L3**. As commented in the main text, the transition states TS_S of **L1** is stabilized by a N–H···Cl hydrogen bond (see Figure 3a in the main text). The TS_R transition state (**L1**) is also stabilized by an N–H···O hydrogen bond (see black dashed line in Figure SI70a) involving the phosphite group. Therefore, the difference between both transition states (*i.e.* $\Delta\Delta G^{\#}$ = 2.2 kcal·mol^{-1}) is governed by the different strength of both H-bonds. Since the N–H···Cl hydrogen bond involves an anionic ligand, it is electrostatically favored with respect to the N–H···O hydrogen bond. Similarly for **L3**, the TS_R is stabilized by an N–H···Cl hydrogen bond (see Figure 3b in the main text). Instead, the TS_S transition state of **L3** is stabilized by an N–H···π interaction (see black dashed line in Figure SI70b) involving the phenyl group.

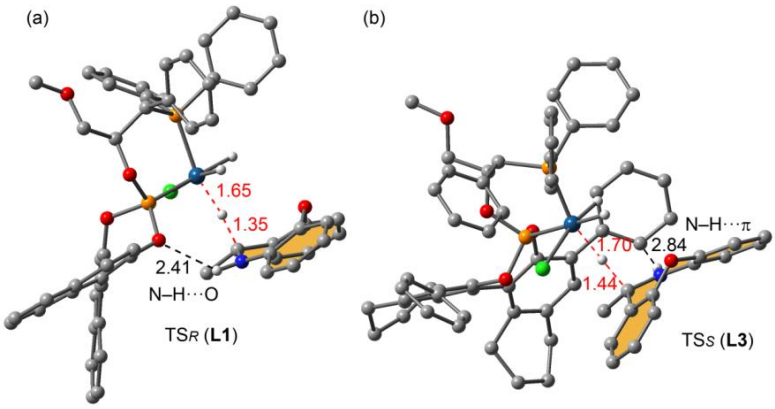

Figure SI70. Optimized geometries of TS_R (**L1**) and TS_S (**L3**) with indication of some interactions. Distances in Å.

2B.6.9.4 Final products:

Finally, in Figure SI71 we show the final products derived from the TS_S and TS_R computed for **L1** and **L3**, denoted as [**4a**][Ir(Cl)(H)$_2$(**L1**)] and [**4a**][Ir(Cl)(H)$_2$(**L3**)], respectively.

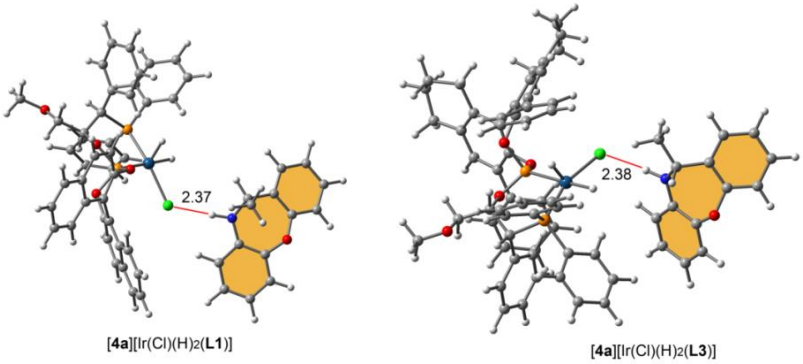

Figure SI71. Optimized geometries of [**4a**][Ir(Cl)(H)$_2$(**L1**)] and [**4a**][Ir(Cl)(H)$_2$(**L3**)] with indication of some interactions. Distances in Å.

2B.6.9.5 Computational methods:

The geometry of all the complexes included in this study was optimized at the BP86 /def2-SVP level of theory within the program TURBOMOLE version 7.0[83] without geometric constrains. The def2-SVP basis set was used for all atoms. It employs effective core potentials for Ir.[84] We initially used the M06-2X functional, however we encountered irresoluble convergence problems in the optimization of the largest systems. Consequently we decided to use the BP86 functional. The minimum/transition state nature of the complexes has been confirmed by means of frequency calculations using a fine grid. The imaginary frequency in the transition states connects the reactant to the product. The thermal analysis correction has been performed at 273 K. In order to validate the level of theory, the energies of all stationary points corresponding to the mechanism of **L1** have been also computed using the D3 correction[85] in order to account for dispersion effects. As a result, the

$\Delta\Delta G^{\#}$ value remains unaltered, giving reliability to the level of theory. This is likely due to the absence of π–π interactions in the proposed mechanism.

2B.7 Additional experiments

2B.7.1 Hydrogenation of quinoline and other six-membered *N*-heterocyclic derivatives mediated by [Ir(P–OP)] complexes derived from L1–L4

2B.7.1.1 Discussion:

Previous reports from the group,[25] demonstrated that the [Ir(P–OP)] complexes derived from ligand **L1** had been successfully applied to the asymmetric hydrogenation of 2-substituted quinolines. Within the present PhD thesis, we sought to expand the substrate scope and examine the hydrogenation of 3- and 4-, methyl- and phenyl-substituted quinolines (**13a–d**). Under the optimal reaction conditions developed for the hydrogenation of 2-substituted quinolines,[25] compounds **13a** and **13b** could only be hydrogenated in low conversions (*ca.* 15%) leading to small amounts of the corresponding hydrogenation products with low enantiopurity (see entries 1 and 3 in Table 3). Interestingly, substrates **13a** and **13b** were fully hydrogenated in the presence of catalytic amounts of HCl (10 mol %; see entries 2 and 4 in Table 3). Unfortunately, the enantiopurity of the hydrogenation products was again very low. In contrast to the previously mentioned results, substrates **13c** and **13d** could not be hydrogenated, not even in the presence of catalytic amounts of HCl (see entries 5–8 in Table 3) or at a higher pressure (160 bar of H_2; see entries 9–12 in Table 3).

Table 3. [Ir(P–OP)]-catalyzed asymmetric hydrogenation[a] of quinoline derivatives **13a–d**.

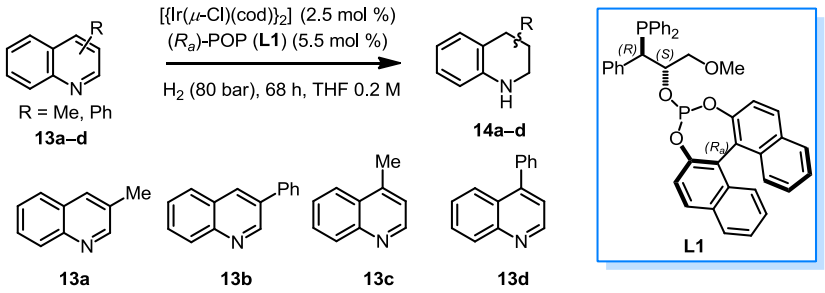

Entry	Substrate	Conditions	Additive (10 mol %)	Conv.[b]	ee[c]
1	**13a**	80 bar H_2	-	15	*rac*
2			HCl	>99	*rac*
3	**13b**	80 bar H_2	-	<10	*rac*
4			HCl	>99	*rac*
5	**13c**	80 bar H_2	-	<1	nd[d]
6			HCl	<2	nd
7	**13d**	80 bar H_2	-	nr[e]	nd
8			HCl	nr	nd
9	**13c**	160 bar H_2	-	<2	nd
10			HCl	<3	nd
11	**13d**	160 bar H_2	-	nr	nd
12			HCl	nr	nd

[a] Reaction conditions: [{Ir(μ-Cl)(cod)}$_2$]/**L1**/substrate = 2.5:5.5:100, respectively, for precatalyst amounts of 5 mol % at rt, 68 h and a substrate concentration of 0.20 M in THF. If additive was present, the indicated amount of additive with respect to substrate was added to a solution of the substrate before adding the catalyst. The values shown are the average of at least two runs. [b] Conversions were determined by ^{1}H NMR. [c] Enantiomeric excesses (ee) were determined by HPLC analysis on chiral stationary phases. [d] nd ≡ not determined. [e] nr ≡ no reaction.

We also turned our attention to the hydrogenation of quinolines containing two methyl or two phenyl groups. Under the optimal reaction conditions developed for the hydrogenation of 2-substituted quinolines,[25] substrate **13e** (2,3-dimethylquinoline) could be fully hydrogenated. The hydrogenation mediated by [Ir(P–OP)] complexes derived from ligand **L1** led to a mixture of the *cis*- and *trans*-diastereomers in a 10 to 1 ratio, respectively. The *cis*-product was obtained in 8% ee in favor of the (*S*,*S*)-configured product. The *trans*-product was obtained in 85% ee and the absolute configuration of the hydrogenation product could not be determined. In the presence of HCl, both the diastereoselectivity (6 to 1 in favor of the *cis*-product) and the enantioselectivity (6% ee for the *cis*-product and 71% ee for the *trans*-product; see entries 5–8 in Table 4) of the reaction worsened.

2,3-Diphenylquinoline (substrate **13f**) could completely converted to the corresponding hydrogenated product, under the optimal reaction conditions developed for the hydrogenation of 2-substituted quinolines.[25] Whilst the hydrogenation took place with perfect diastereoselectivity (dr = 99:1 in favor of the *cis*-compound), the enantioselectivity of the hydrogenations was low (10% ee in the absence of HCl, and 30% in the presence of catalytic amounts of this reagent) (see entries in 3 and 4 in Table 4).

As regards the hydrogenation of 2,4-dimethyl- and 2,4-diphenylquinoline (substrates **13g** and **13h**, respectively), the [Ir(P–OP)] complexes derived from ligand **L1** were not efficient in mediating the hydrogenations, as no conversion was observed (see entries 5–8 in Table 4).

Table 4. Ir-(P–OP)-mediated asymmetric hydrogenation[a] of disubstituted quinolines **13e–h**.

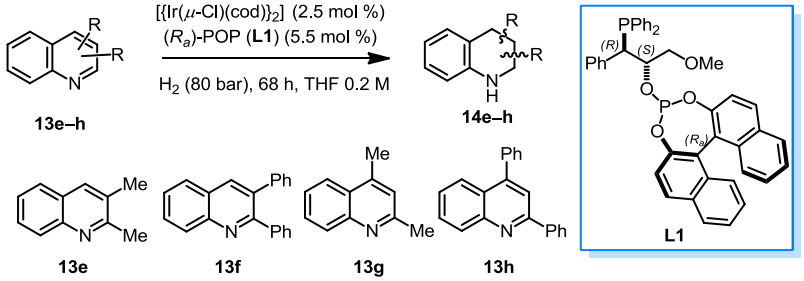

Entry	Substrate	Additive (10 mol %)	Conv.[b]	*dr* (*cis:trans*)[b]	ee of *cis* derivative [%][c]	ee of *trans* derivative [%][c]
1	**13e**	-	>99	9.8:1	8 (*S*,*S*)	85 (–)
2		HCl	>99	5.5:1	6 (*S*,*S*)	71 (–)
3	**13f**	-	>99	99:1	10 (–)	nd
4		HCl	>99	99:1	30 (–)	nd
5	**13g**	-	nr[d]	nd[e]	nd	nd
6		HCl	nr	nd	nd	nd
7	**13h**	-	nr	nd	nd	nd
8		HCl	nr	nd	nd	nd

[a] Reaction conditions: [{Ir(μ-Cl)(cod)}$_2$]/**L1**/substrate = 2.5:5.5:100, respectively, for precatalyst amounts of 5 mol % at rt, 68 h and a substrate concentration of 0.20 M in THF. If additive was present, the indicated amount of additive with respect to substrate was added to a solution of the substrate before adding the catalyst. The values shown are the average of at least two runs. [b] Conversions were determined by ^{1}H NMR. [c] Enantiomeric excesses (ee) were determined by HPLC analysis on chiral stationary phases. Absolute configurations were assigned by comparison with the reported data. [d] nr ≡ no reaction. [e] nd ≡ not determined.

With the extended P–OP ligand library that was available at the late stages of the present PhD thesis (see the structure of ligands **L2**–**L4** in Table 5), we turned our attention to the hydrogenation of an array six-membered *N*-heterocyclic derivatives (see the structure of substrates **13i–m** in Table 5) under the optimal reaction conditions developed by the group.[25,27] It should be mentioned at this point that the results of the hydrogenations of substrates **13i–m** employing ligand **L1** had already been reported,[27] however the results obtained with **L1** have also been included in Table 5 to aid comparison.

Ligand **L2**, whose main difference with respect to **L1** is a 5,5',6,6',7,7',8,8'-octahydro-[1,1'-binaphthalene]-2,2'-diol-derived phosphite group instead of the [1,1'-binaphthalene]-2,2'-diol-derived one in **L1**, provided similar results to **L1** in terms of conversion and enantioselectivity. Interestingly, ligand **L3**, incorporating a 3,3'-diphenyl-5,5',6,6',7,7',8,8'-octahydro-[1,1'-binaphthalene]-2,2'-diol-derived phosphite group, and ligand **L4**, incorporating a ((4*R*,5*R*)-2,2-dimethyl-1,3-dioxolane-4,5-diyl)bis(diphenylmethanol)-derived phosphite group, followed a different trend. In case of methyl-substituted substrates (**13i** and **13k**) opposite configurations for the hydrogenation products were obtained (compare entries 1 and 3 in Table 5) for ligands **L3** and **L4** and for **L2** (and **L1**). Ph-substituted substrates (**13j**, **13l** and **13m**) were hydrogenated in lower conversions with the [Ir(P–OP)] complexes derived from **L3** and **L4** than those observed for **L2** (and **L1**). In contrast to what was observed for methyl-substituted products, ligands **L1**–**L4** led to hydrogenation products with the same configuration. This behavior is in agreement with the results obtained in the hydrogenation of seven-membered C=N-containing heterocyclic derivatives, which have been previously discussed (see section 2B).

Table 5. Ir-(P–OP)-mediated asymmetric hydrogenation[a] of six-membered *N*-heterocyclic derivatives **13i–m**.

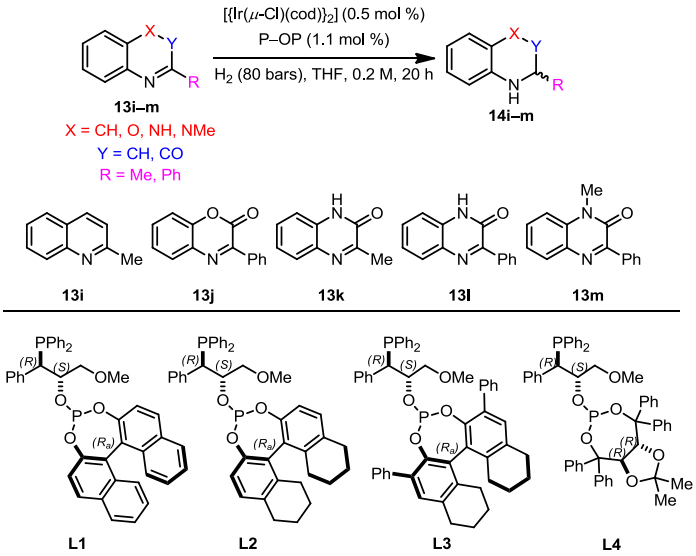

Entry	Sub \ Lig	L1 Conv.[b]; ee (*config.*)[c] (%)	L2 Conv.[b]; ee (*config.*)[c] (%)	L3 Conv.[b]; ee (*config.*)[c] (%)	L4 Conv.[b]; ee (*config.*)[c] (%)
1	**13i**	99; 92 (*S*)[d]	99; 88 (*S*)	99; 4 (*R*)	99; 5 (*R*)
2	**13j**	99; 95 (*S*)[d]	80; 94 (*S*)	6; 63 (*S*)	<1; nd[e]
3	**13k**	99; 85 (*S*)	99; 85 (*S*)	98; 38 (*R*)	4; 40 (*R*)
4	**13l**	98; 99 (*S*)[d]	96; 99 (*S*)	7; 83 (*S*)	<1; nd
5	**13m**	96; 99 (*S*)[d]	97; 99 (*S*)	65; 91 (*S*)	<2; nd

[a] Reaction conditions: [{Ir(μ-Cl)(cod)}$_2$]/P–OP ligand/substrate = 0.5:1.1:100, respectively, for precatalyst amounts of 1 mol % at rt, 20 h and a substrate concentration of 0.20 M in THF. If additive was present, the indicated amount of additive with respect to substrate was added to a solution of the substrate before adding the catalyst. The values shown are the average of at least two runs. [b] Conversions were determined by ^{1}H NMR. [c] Enantiomeric excesses (ee) were determined by HPLC analysis on chiral stationary phases. Absolute configurations were assigned by comparison with the reported data. [d] Published results; see ref. 25 for **13i** and ref. 27 for **13j**, **13l** and **13m**. [e] nd ≡ not determined.

Chapter-2

2B.7.1.2 Experimental section:

For the experimental procedure, see Section 2B.5.1.

The HPLC analytic conditions for determining the enantiomeric excesses of the hydrogenation products **14a–m** and their spectroscopic and characterization data are indicated below.

3-methyl-1,2,3,4-tetrahydroquinoline (14a): Known compound,[86] light yellow oil, HPLC conditions: Daicel Chiralcel® OJ-H (25 cm x 0.46 cm), 95:5 *n*-hexane/2-propanol, 0.5 mL/min, 254 nm, t_1 = 29.3 min, t_2 = 36.7 min.

3-phenyl-1,2,3,4-tetrahydroquinoline (14b): Known compound,[86] White solid, HPLC conditions: Daicel Chiralcel® OD-H (25 cm x 0.46 cm), 90:10 *n*-hexane/2-propanol, 0.6 mL/min, 254 nm, t_1 = 18.6 min, t_2 = 22.8 min.

4-methyl-1,2,3,4-tetrahydroquinoline (14c): Known compound, [87] HPLC conditions: Daicel Chiralcel® OD-H (25 cm x 0.46 cm), 98:2 *n*-hexane/2-propanol, 0.6 mL/min, t_1 = 17.2 min (major), t_2 = 18.6 min (minor).

4-phenyl-1,2,3,4-tetrahydroquinoline (14d): Known compound,[87] HPLC conditions: Daicel Chiralcel® OD-H column (25 cm x 0.46 cm), 90:10 *n*-hexane/2-propanol, 0.6 mL/min, t_1 = 14.6 min (minor), t_2 = 22.3 min (major).

***cis*- and *trans*-2,3-dimethyl-1,2,3,4-tetrahydroquinoline (14e):** Known compound,[88] HPLC conditions: Daicel Chiralcel® OD-H (25 cm x 0.46 cm), 98:2 *n*-hexane:2-propanol, 0.5 mL/min, 254 nm; *cis*-isomer: t_1 = 15.1 min (minor), t_2 = 16.3 min (major); *trans*-isomer: t_1 = 12.5 min (minor), t_2 = 19.2 min (major).

***cis*-2,3-diphenyl-1,2,3,4-tetrahydroquinoline (14f):** Known compound,[89] HPLC conditions: Daicel Chiralcel® OD-H (25 cm x 0.46 cm), 90:10 *n*-hexane/2-propanol, 0.5 mL/min, 254 nm, t_1 = 20.4 min (minor), t_2 = 25.2 min (major).

2-methyl-1,2,3,4-tetrahydroquinoline (14i): Known compound, [90] HPLC conditions: Daicel Chiralcel® OJ-H (25 cm x 0.46 cm), 95:5 *n*-hexane/2-propanol, 0.5 ml/min, 254 nm: t_1 (*S*) = 22.6 min, t_2 (*R*) = 25.2 min.

3-phenyl-3,4-dihydro-2*H*-benzo[*b*][1,4]oxazin-2-one (14j): Known compound,[91] HPLC conditions: Daicel Chiralcel® OD-H (25 cm x 0.46 cm), 80:20 *n*-hexane/2-propanol, 0.6 mL/min, 216 nm, t_1 (*R*) = 18.6 min, t_2 (*S*) = 24.6 min.

3-methyl-3,4-dihydroquinoxalin-2(1*H*)-one (14k): ^{1}H NMR (400 MHz, $CDCl_3$) δ 7.84–7.68 (m, 1H), 6.92–6.86 (m, 1H), 6.80–6.73 (m, 1H), 6.73–6.66 (m, 1H), 4.01 (q, *J* = 6.7 Hz, 1H), 3.82 (bs, 1H), 1.46 (d, *J* = 6.7 Hz, 3H); $^{13}C\{^1H\}$ NMR (100 MHz, $CDCl_3$) δ 133.7 (C), 125.8 (C), 124.0 (CH), 119.8 (CH), 115.3 (CH), 114.4 (CH), 52.2 (CH), 18.0 (CH_3). HRMS (ESI^+): calculated for $C_9H_{10}N_2NaO$ $(M+Na)^+$ 185.0685; found 185.0694. mp = 130–132 °C; $[\alpha]_D^{25}$= +51.7 (*c* 0.13, CH_2Cl_2) for 85% ee; HPLC conditions: Daicel Chiralcel® AD-H (25 cm x 0.46 cm), 90:10 *n*-hexane/2-propanol, 1.0 mL/min, 230 nm, t_1 (*S*) = 19.6 min, t_2 (*R*) = 21.2 min.

3-phenyl-3,4-dihydroquinoxalin-2(1*H*)-one (14l): Known compound,[92] HPLC conditions: Daicel Chiralcel® OD-H (25 cm x 0.46 cm), 80:20 *n*-hexane/2-propanol, 1.0 mL/min, 230 nm, t_1 (*S*) = 15.2 min, t_2 (*R*) = 23.3 min.

1-methyl-3-phenyl-3,4-dihydroquinoxalin-2(1*H*)-one (14m): Known compound,[93] HPLC conditions: Daicel Chiralcel® AD-H (25 cm x 0.46

cm), 80:20 *n*-hexane/2-propanol, 1.0 mL/min, 230 nm, t_1 (+) = 12.7 min, t_2 (–) = 16.3 min.

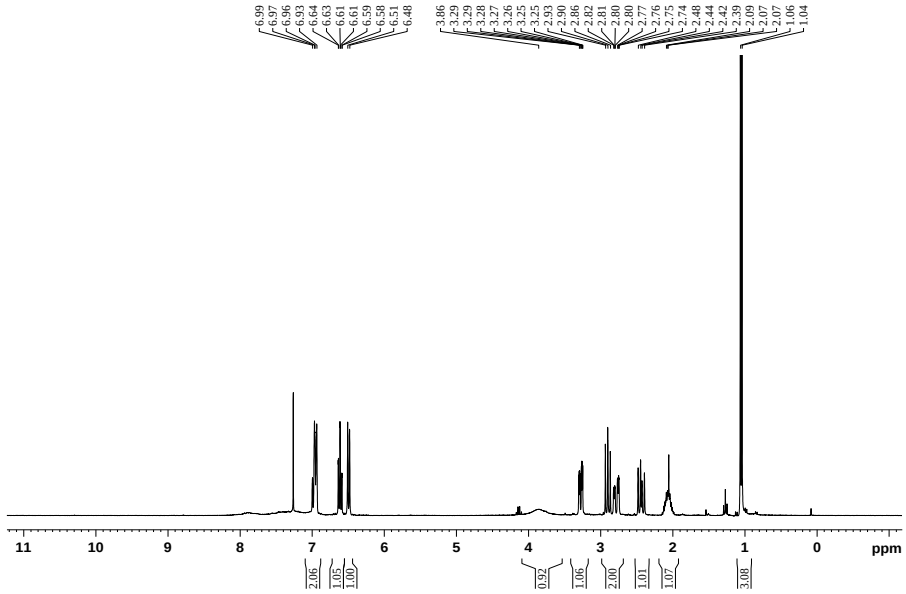

^{1}H NMR of **14a**

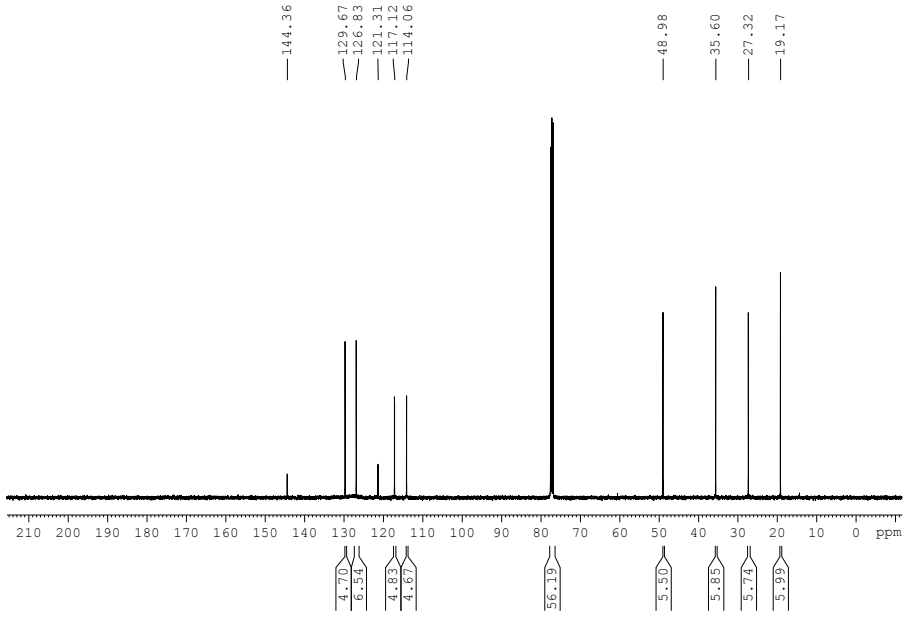

^{13}C{^{1}H} NMR of **14a**

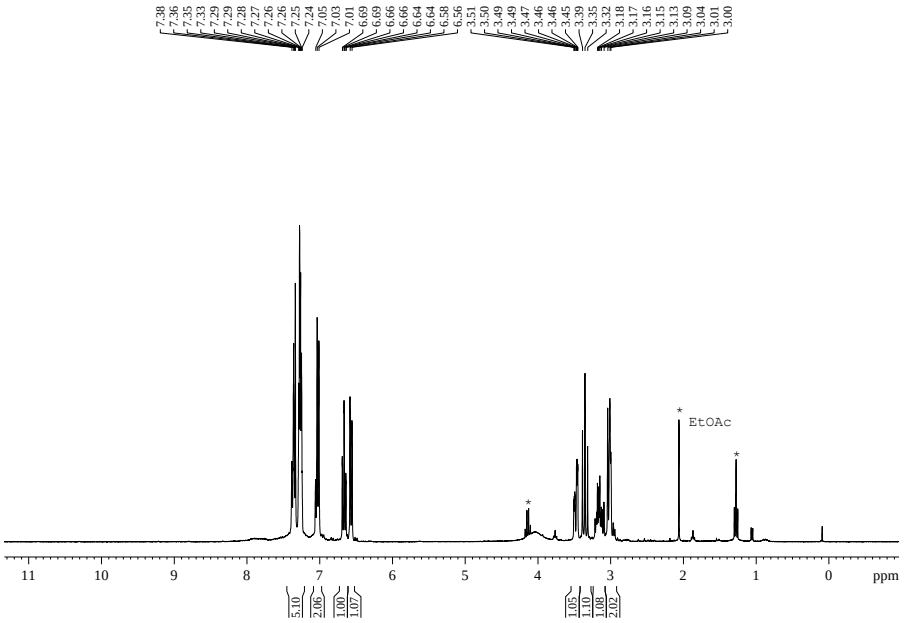

^{1}H NMR of **14b**

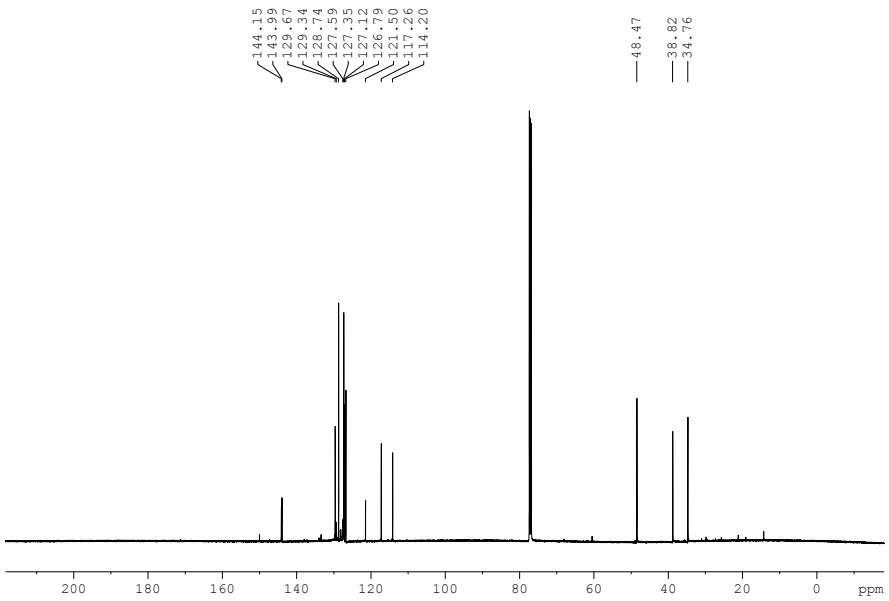

^{13}C{^{1}H} NMR of **14b**

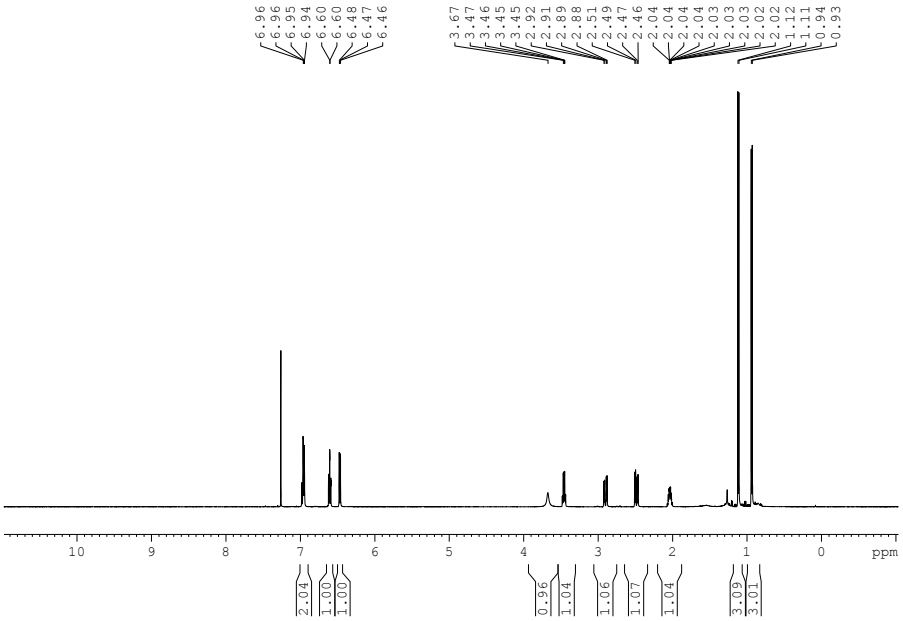

^{1}H NMR of *trans*-**14e**

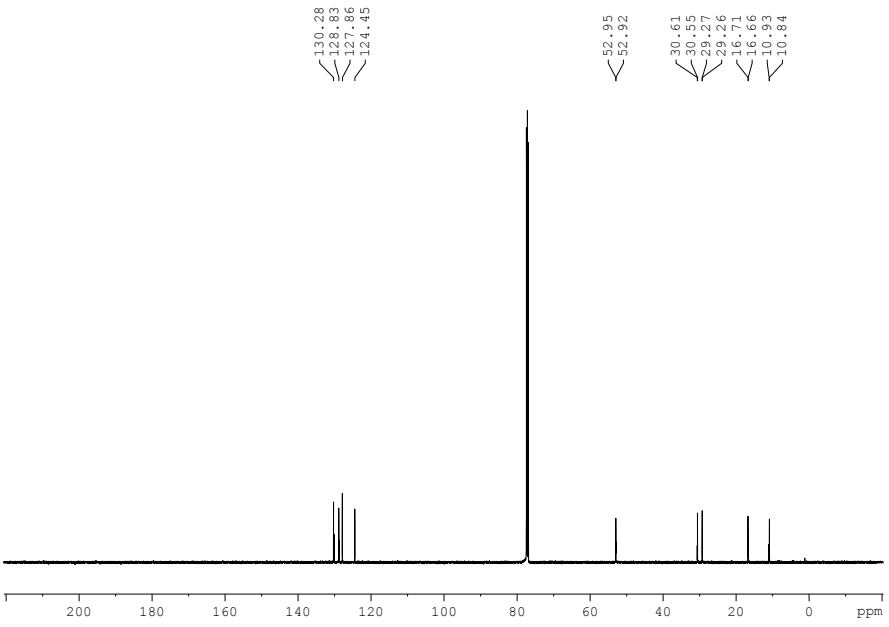

^{13}C{^{1}H} NMR of *trans*-**14e**

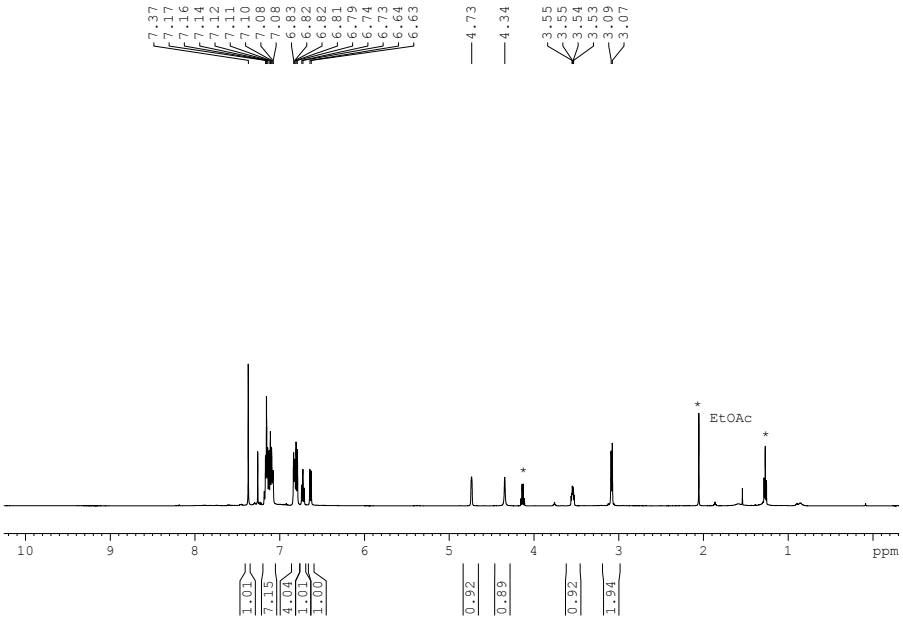

^{1}H NMR of **14f**

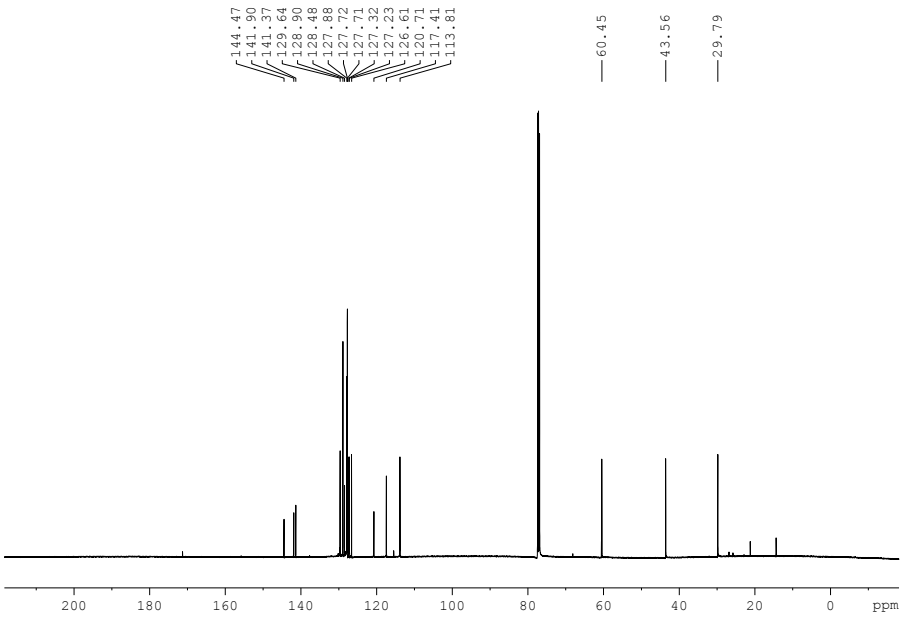

^{13}C{^{1}H} NMR of **14f**

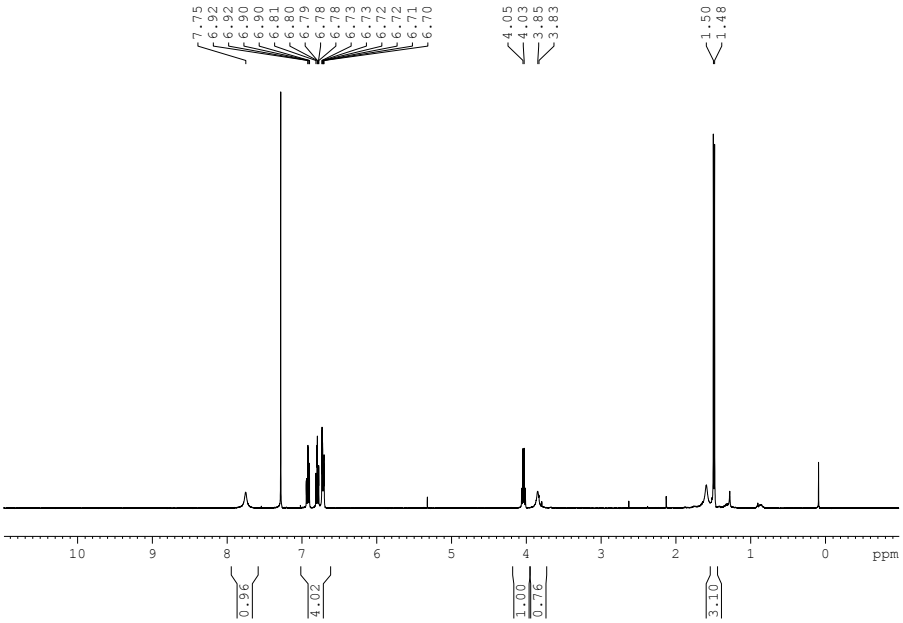

^{1}H NMR of **14k**

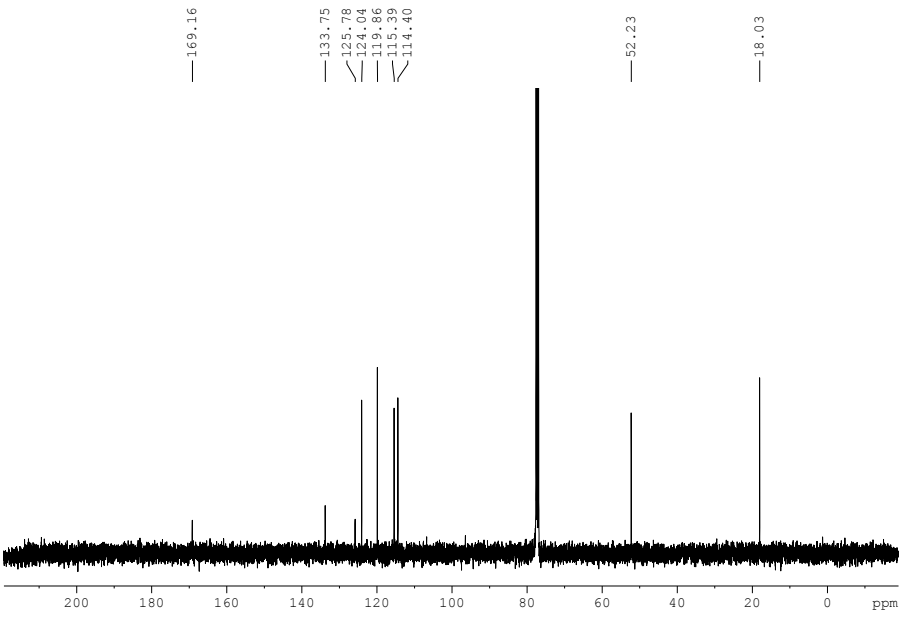

^{13}C{^{1}H} NMR of **14k**

2B.8 Summary on recent literature advances for substrate activation of *N*-heterocyclic compounds towards asymmetric hydrogenations

We identified in the literature up to 2015 three different strategies to activate *N*-heterocyclic compounds towards asymmetric hydrogenation. These strategies were published as a review in 2015[52a] and have been summarized in Subchapter 2A of the present thesis (see Scheme 1). The first strategy consists of facilitating hydrogenation by the formation of positively charged derivatives of the *N*-heterocyclic compounds. Catalyst deactivation processes arising upon binding of the substrate to the metal center can thus be prevented and, additionally, hydrogenation of positively charged *N*-heterocyclic compounds may also be more favored than that of their neutral analogues. The second strategy is based on introducing a ligating group onto the substrate to facilitate hydrogenation by chelation assistance to the metal center. The last strategy involves breaking the aromaticity of the *N*-heterocyclic compounds by inducing a double bond migration process. The above mentioned strategies have allowed the development of highly enantioselective catalytic hydrogenation methods of *N*-heterocyclic compounds for the production of fully or partially saturated chiral heterocycles. We summarize in the present section the latest and most relevant examples of substrate activation in asymmetric hydrogenation, which were not covered in Subchapter 2A of the present thesis.

An efficient enantioselective hydrogenation method for transforming isoxazolium triflates (**15** and **17**) into highly enantioenriched 4-isoxazolines (**16**) or isoxazolidines (**18**) has been reported by Kuwano *et al.*[94] This hydrogenation method belongs to substrate activation Strategy I (see in Subchapter 2A) and uses an enantioselective catalyst prepared from

[{Ir(μ-Cl)(cod)}$_2$], an enantiopure phosphino–oxazoline ligand and I_2. The iridium-catalyzed hydrogenations proceeded in high to good enantioselectivities. The 3-substituted 5-arylisoxazolium salts (**15** and **17**) were transformed into 4-isoxazolines (**16**) with up to 90% ee when phosphino–oxazoline ligand **L14** was used (Scheme 10a). 5-Alkylated substrates were also selectively converted into *cis*-3,5-disubstituted isoxazolidines (**18**) by using the iridium catalyst derived **L15** (Scheme 10b).

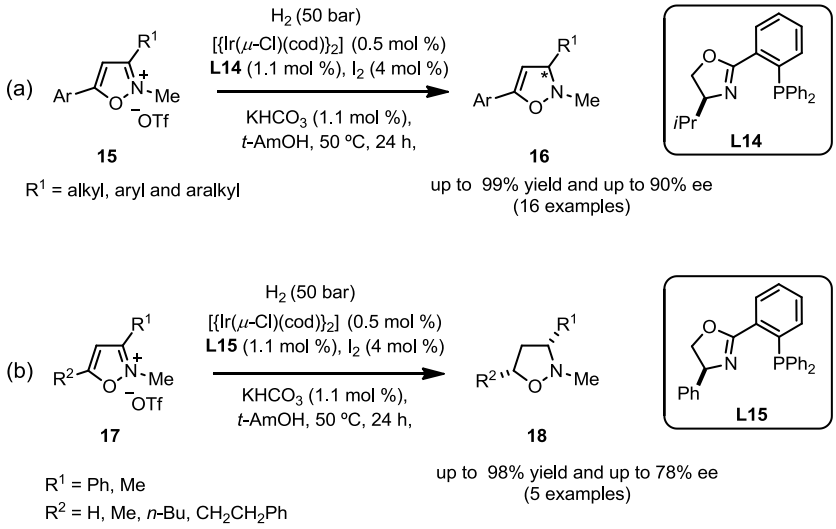

Scheme 10. Asymmetric hydrogenation of isoxazolium triflates with a chiral iridium catalyst.

The asymmetric hydrogenation of 3-amido-2-arylpyridinium salts (**19**) in the presence stoichiometric amounts of (–)-CSA catalyzed by halide-bridged dinuclear iridium complexes derived from the bisphosphine SEGPHOS (5 mol %, see Scheme 11 for the structure of the ligand) has recently been described by Mashima *et al.* (Scheme 11).[95] This hydrogenation method also belongs to substrate activation Strategy I.

Although high temperatures were required (60–80 ºC), high *cis*-diastereoselectivities (up to >95:5) and moderately high enantioselectivities were obtained (10 examples, ee's ranging from 70 to 86%). The pyridinium salt without any substituent at the 2-position was not hydrogenated. Moreover, a benzoyl protecting groups at the amino group improved the enantioselectivity.

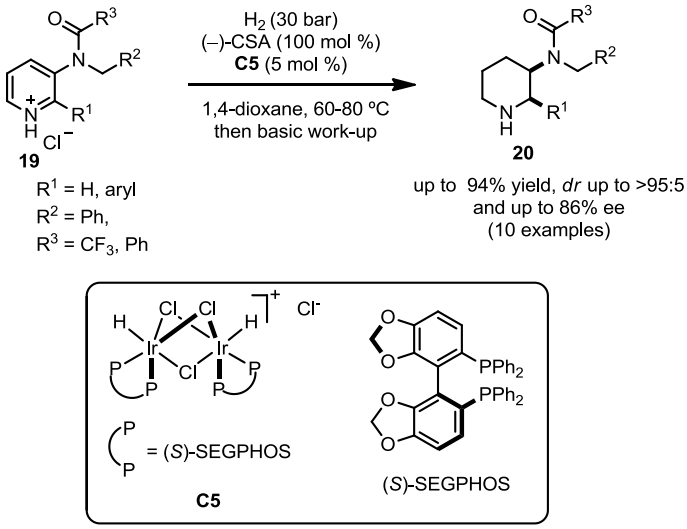

Scheme 11. Asymmetric hydrogenation of 3-amido-2-arylpyridinium salts.

Zhang, Zhao and coworkers have reported the Rh-mediated asymmetric hydrogenation of quinolones (**21**) and isoquinolines (**23**) to highly enantioenriched tetrahydroquinoline (**22**) and tetrahydroisoquinoline (**24**) derivatives (see Scheme 12).[96] The addition of stoichiometric amounts of anhydrous HCl facilitates the hydrogenation of the above mentioned substrates in agreement with the advantages provided by substrate activation Strategy I. Furthermore, the addition of HCl facilitates the formation of a non-covalent interaction between the urea motif of the ligand and the chloride anion of the protonated substrates. The enantioselective catalyst developed by Zhang, Zhao and coworkers was

very active in terms of catalytic activity (conversions up to 99%) and provided very high enantioselectivities (up to 99% ee).

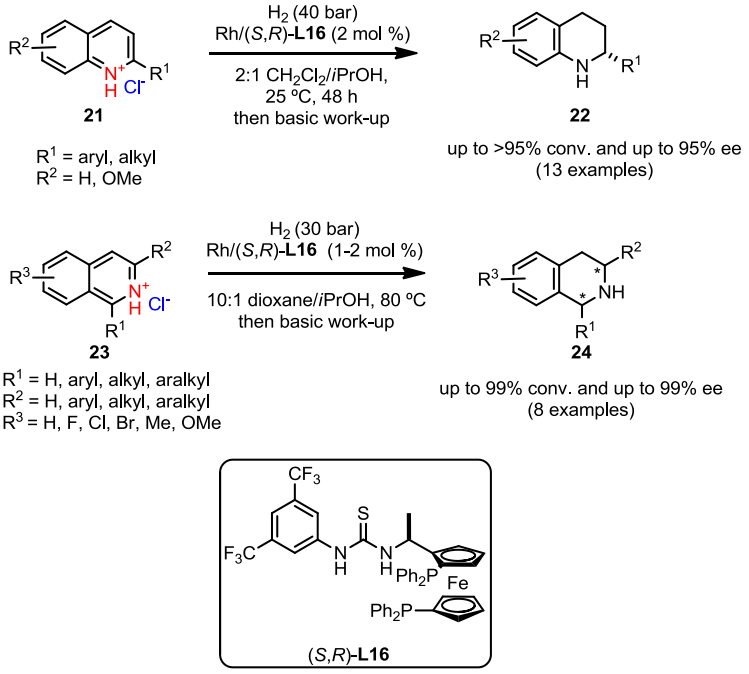

Scheme 12. Asymmetric hydrogenation of quinolines and isoquinolines.

Zhou *et al.* reported the highly enantioselective hydrogenation of quaternized heteroaromatic compounds bearing a hydroxyl group (*i.e.* 3-hydroxypyridinium salts (**25**)). The authors have successfully developed an enantiopure iridium complex derived from (*S*,*S*)-f-Binaphane (see Scheme 13 for the structure of the ligand; 3 mol %) as catalyst for this transformation. The combined used of the catalyst and stoichiometric amounts of $NaHCO_3$ provided a direct access to *trans*-6-substituted piperidin-3-ols (**26**) as the major diastereoisomers in up to 95% ee (13 examples, see Scheme 13).[97] This hydrogenation method also belongs to substrate activation Strategy I.

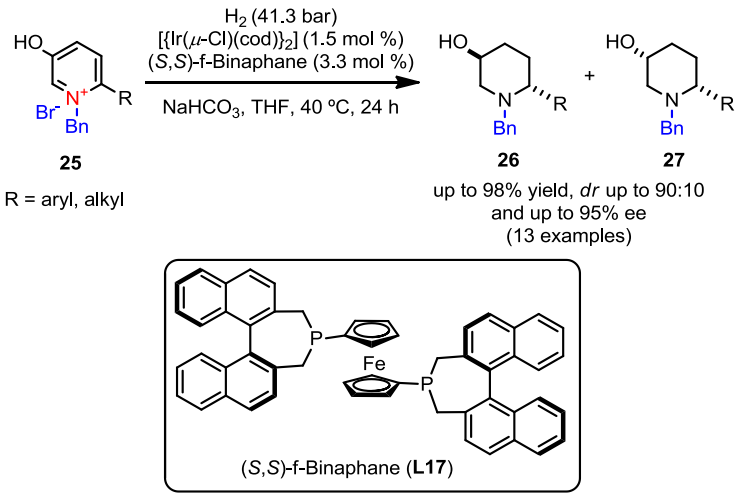

Scheme 13. Asymmetric hydrogenation of 3-hydroxypyridinium salts.

Following an analogous strategy (substrate activation Strategy I), Lefort *et al.* [98] reported the use of an enantiopure rhodium catalyst derived from **L18** (see Scheme 14 for the structure of the ligand) as an efficient catalyst for the asymmetric hydrogenation of *N*-benzylated 3-substituted pyridinium salts (**28**) into the corresponding piperidines (**29**) (ee values up to 90%; 10 examples, Scheme 14).

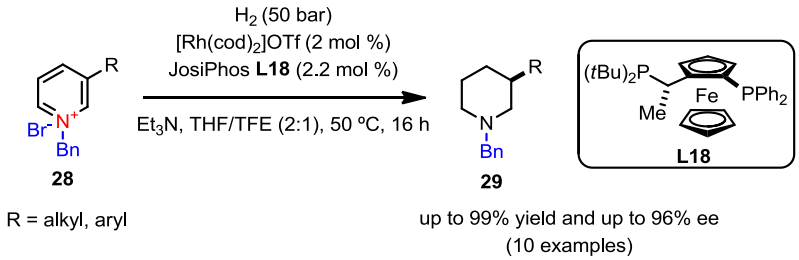

Scheme 14. Asymmetric hydrogenation of 3-substituted pyridinium salts.

References

(1) *Biological Significance – Pharmacology, Phamaceutical Agrochemical*, In *Comprehensive Chirality*, Carreira, E. M.; Yamamoto, H; Eds.; Elsevier B.V.: Oxford, UK, 2012; Vol. 1.

(2) (a) Noyori, R; in *Asymmetric Catalysis in Organic Synthesis*, Wiley, New York, USA, 1994. (b) Lin, G. Q.; Li, Y. M.; Chan, A. S. C.; in: *Principles and Applications of Asymmetric Synthesis*, Wiley: New York, USA 2001. (c) *Comprehensive Asymmetric Catalysis* Jacobsen, E. N.; Pfaltz, A.; Yamamoto, H; Eds.; Springer-Verlag: Heidelberg, Germany, 2012. (d) *Comprehensive Chirality*, Carreira, E. M.; and Yamamoto, H; Eds.; Elsevier B.V.: Oxford, UK, 2012; Vol. 1-9.

(3) (a) *Asymmetric Catalysis on Industrial Scale: Challenges, Approaches and Solutions*, Blaser, H.-U.; and Schmidt, E. Eds.; Wiley-VCH: Weinheim, Germany, 2004. (b) Blaser, H.-U.; Pugin, B.; Spindler, F.; Thommen, M. *Acc. Chem. Res.* **2007**, *40*, 1240. (c) *Asymmetric Catalysis on Industrial Scale: Challenges, Approaches and Solutions*, 2nd ed. Blaser, H.-U. and Federsel, H.-J. Eds.; Wiley-VCH, Weinheim, Germany, 2010.

(4) (a) *Handbook of Homogeneous Hydrogenation*, de Vries, J. G.; Elsevier, C. J. Eds.; Wiley-VCH: Weinheim, Germany, 2004. (b) Blaser, H.-U.; Pugin, B. and Spindler, F. in: *Asymmetric Hydrogenation* in *Organometallics as Catalysts in the Fine Chemical Industry* Beller, M. and Blaser, H.-U. Eds.; Springer-Verlag: Berlin, Heidelberg, Germany, 2012. (c) Etayo, P.; Vidal-Ferran, A. *Chem. Soc. Rev.* **2013**, *42*, 728. (d) Cadu, A.; Andersson, P. G. *Dalton Trans.* **2013**, *42*, 14345. (e) Bartoszewicz, A.; Ahlsten, N.; Martin-Matute, B. *Chem. –Eur. J.* **2013**, *19*, 7274.

(5) (a) *Phosphorus Ligands in Asymmetric Catalysis*, 1st ed.; Börner, A. Ed.; Wiley-VCH: Weinheim, Germany, 2008; Vols. I-III. (b) Fernández-Pérez, H.; Etayo, P.; Panossian, A.; Vidal-Ferran, A. *Chem. Rev.* **2011**, *111*, 2119.

(6) For selected references on the asymmetric hydrogenation of C=O bonds, see: (a) Xie, J.-H.; Bao, D.-H.; Zhou, Q.-L. *Synthesis* **2015**, *47*, 460. For selected references on the asymmetric hydrogenation of C=C bonds, see: (b) Roseblade, S. J.; Pfaltz, A. *Acc. Chem. Res.* **2007**, *40*, 1402. (c) Church, T. L.; Andersson, P. G. *Coord. Chem. Rev.* **2008**, *252*, 513. (d) Xie, J.-H.; Zhu, S.-F.; Zhou, Q.-L. *Chem. Rev.* **2011**, *111*, 1713. (e) Woodmansee, D. H.; Pfaltz, A. *Chem. Commun.* **2011**, *47*, 7912. For selected references on the asymmetric hydrogenation of C=N bonds, see reference [6e] and the following ones: (f) Fleury-Brégeot, N.; de la Fuente, V.; Castillón, S.; Claver, C. *ChemCatChem* **2010**, *2*, 1346. (g) Wang, C.; Villa-Marcos, B.; Xiao, J. *Chem. Commun.* **2011**, *47*, 9773. h) Hopmann, K. H.; Bayer, A. *Coord. Chem. Rev.* **2014**, *268*, 59.

(7) (a) Michael, J. P. *Nat. Prod. Rep.* **1997**, *14*, 605. (b) Daly, J. W. *J. Nat. Prod.* **1998**, *61*, 162. (c) O'Hagan, D. *Nat. Prod. Rep.* **2000**, *17*, 435. (d) Daly, J. W.; Spande, T. F.; Garraffo, H. M. *J. Nat. Prod.* **2005**, *68*, 1556. (e) Michael, J. P.

Nat. Prod. Rep. **2005**, *22*, 603. (f) *Pharmaceutical Substances*, 5th ed.; Kleemann, A.; Engel, J.; Kutscher, B. and Reichert, D. Eds., Georg Thieme Verlag: Stuttgart, Germany, 2008. (g) Samwel, S.; Odalo, J. O.; Nkunya, M. H. H.; Joseph, C. C.; Koorbanally, N. A. *Phytochemistry (Elsevier)* **2011**, *72*, 1826.

(8) (a) Glorius, F. *Org. Biomol. Chem.* **2005**, *3*, 4171. (b) Zhou, Y.-G. *Acc. Chem. Res.* **2007**, *40*, 1357. (c) Kuwano, R. *Heterocycles* **2008**, *76*, 909. (d) Wang, D.-S.; Chen, Q.-A.; Lu, S.-M.; Zhou, Y.-G. *Chem. Rev.* **2012**, *112*, 2557. (e) Chen, Q.-A.; Ye, Z.-S.; Duan, Y.; Zhou, Y.-G. *Chem. Soc. Rev.* **2013**, *42*, 497. (f) He, Y.-M.; Song, F.-T.; Fan, Q.-H. in: *Advances in Transition Metal-Catalyzed Asymmetric Hydrogenation of Heteroaromatic Compounds* in *Stereoselective Formation of Amines, Topics in Current Chemistry*, Li, W.; Zhang, X. Eds.; Springer-Verlag, Berlin Heidelberg, Germany, 2014, 145.

(9) (a) Brown, J. M.; Chaloner, P. A. *J. Am. Chem. Soc.* **1980**, *102*, 3040. (b) Landis, C. R.; Halpern, J. *J. Am. Chem. Soc.* **1987**, *109*, 1746.

(10) Rueping, M.; Dufour, J.; Schoepke, F. R. *Green Chem.* **2011**, *13*, 1084.

(11) For previous reviews on substrate activation, see reference 8b and: (a) Yu, Z.; Jin, W.; Jiang, Q. *Angew. Chem., Int. Ed.* **2012**, *51*, 6060. (b) Nagano, T.; Iimuro, A.; Yamaji, K.; Kita, Y.; Mashima, K. *Heterocycles* **2014**, *88*, 103.

(12) (a) Wang, T.; Zhuo, L.-G.; Li, Z.; Chen, F.; Ding, Z.; He, Y.; Fan, Q.-H.; Xiang, J.; Yu, Z.-X.; Chan, A. S. C. *J. Am. Chem. Soc.* **2011**, *133*, 9878. (b) Dobereiner, G. E.; Nova, A.; Schley, N. D.; Hazari, N.; Miller, S. J.; Eisenstein, O.; Crabtree, R. H. *J. Am. Chem. Soc.* **2011**, *133*, 7547.

(13) Tadaoka, H.; Cartigny, D.; Nagano, T.; Gosavi, T.; Ayad, T.; Genêt, J.-P.; Ohshima, T.; Ratovelomanana-Vidal, V.; Mashima, K. *Chem. –Eur. J.* **2009**, *15*, 9990.

(14) Seminal examples of activation of quinoline-type substrates by acids were reported by Chan, Fan and coworkers (see reference 12a and Zhou, H.; Li, Z.; Wang, Z.; Wang, T.; Xu, L.; He, Y.; Fan, Q.-H.; Pan, J.; Gu, L.; Chan, A. S. C. *Angew. Chem., Int. Ed.* **2008**, *47*, 8464.). However, as these examples involve using stoichiometric amounts of metal catalyst, they have not been summarized in this microreview dealing with catalytic methods.

(15) (a) Iimuro, A.; Yamaji, K.; Kandula, S.; Nagano, T.; Kita, Y.; Mashima, K. *Angew. Chem., Int. Ed.* **2013**, *52*, 2046. (b)Kita, Y.; Yamaji, K.; Higashida, K.; Sathaiah, K.; Iimuro, A.; Mashima, K. *Chem. –Eur. J.* **2015**, *21*, 1915.

(16) Kita, Y.; Iimuro, A.; Hida, S.; Mashima, K. *Chem. Lett.* **2014**, *43*, 284.

(17) Chen, M.-W.; Ye, Z.-S.; Chen, Z.-P.; Wu, B.; Zhou, Y.-G. *Organic Chemistry Frontiers* **2015**, *2*, 586.

(18) Kita, Y.; Higashida, K.; Yamaji, K.; Iimuro, A.; Mashima, K. *Chem. Commun.* **2015**, *51*, 4380.

(19) Kuwano, R.; Hashiguchi, Y.; Ikeda, R.; Ishizuka, K. *Angew. Chem., Int. Ed.* **2015**, *54*, 2393.

(20) Li, Z.-W.; Wang, T.-L.; He, Y.-M.; Wang, Z.-J.; Fan, Q.-H.; Pan, J.; Xu, L.-J. *Org. Lett.* **2008**, *10*, 5265.

(21) Cai, X.-F.; Huang, W.-X.; Chen, Z.-P.; Zhou, Y.-G. *Chem. Commun.* **2014**, *50*, 9588.
(22) Mrsic, N.; Lefort, L.; Boogers, J. A. F.; Minnaard, A. J.; Feringa, B. L.; de Vries, J. G. *Adv. Synth. Catal.* **2008**, *350*, 1081.
(23) Wang, D.-S.; Zhou, Y.-G. *Tetrahedron Lett.* **2010**, *51*, 3014.
(24) Wang, Z.-J.; Zhou, H.-F.; Wang, T.-L.; He, Y.-M.; Fan, Q.-H. *Green Chem.* **2009**, *11*, 767.
(25) Núñez-Rico, J. L.; Fernández-Pérez, H.; Benet-Buchholz, J.; Vidal-Ferran, A. *Organometallics* **2010**, *29*, 6627.
(26) Mrsic, N.; Jerphagnon, T.; Minnaard, A. J.; Feringa, B. L.; de Vries, J. G. *Adv. Synth. Catal.* **2009**, *351*, 2549.
(27) Núñez-Rico, J. L.; Vidal-Ferran, A. *Org. Lett.* **2013**, *15*, 2066.
(28) Chang, M.; Huang, Y.; Liu, S.; Chen, Y.; Krska, S. W.; Davies, I. W.; Zhang, X. *Angew. Chem., Int. Ed.* **2014**, *53*, 12761.
(29) Huang, W. X.; Yu, C. B.; Shi, L.; Zhou, Y. G. *Org. Lett.* **2014**, *16*, 3324.
(30) a) Legault, C. Y.; Charette, A. B. *J. Am. Chem. Soc.* **2005**, *127*, 8966. b) Legault, C. Y.; Charette, A. B.; Cozzi, P. G. *Heterocycles* **2008**, *76*, 1271.
(31) Lu, S.-M.; Wang, Y.-Q.; Han, X.-W.; Zhou, Y.-G. *Angew. Chem., Int. Ed.* **2006**, *45*, 2260.
(32) Ye, Z.-S.; Chen, M.-W.; Chen, Q.-A.; Shi, L.; Duan, Y.; Zhou, Y.-G. *Angew. Chem., Int. Ed.* **2012**, *51*, 10181.
(33) Ye, Z.-S.; Guo, R.-N.; Cai, X.-F.; Chen, M.-W.; Shi, L.; Zhou, Y.-G. *Angew. Chem., Int. Ed.* **2013**, *52*, 3685.
(34) Cadu, A.; Upadhyay, P. K.; Andersson, P. G. *Asian J. Org. Chem.* **2013**, *2*, 1061.
(35) Maj, A. M.; Suisse, I.; Hardouin, C.; Agbossou-Niedercorn, F. *Tetrahedron* **2013**, *69*, 9322.
(36) Kuwano, R.; Sato, K.; Kurokawa, T.; Karube, D.; Ito, Y. *J. Am. Chem. Soc.* **2000**, *122*, 7614.
(37) a) Kuwano, R.; Kaneda, K.; Ito, T.; Sato, K.; Kurokawa, T.; Ito, Y. *Org. Lett.* **2004**, *6*, 2213. b) Kuwano, R.; Kashiwabara, M. *Org. Lett.* **2006**, *8*, 2653. c) Kuwano, R.; Kashiwabara, M.; Sato, K.; Ito, T.; Kaneda, K.; Ito, Y. *Tetrahedron: Asymmetry* **2006**, *17*, 521.
(38) Baeza, A.; Pfaltz, A. *Chem. –Eur. J.* **2010**, *16*, 2036.
(39) Mršić, N.; Jerphagnon, T.; Minnaard, A. J.; Feringa, B. L.; de Vries, J. G. *Tetrahedron: Asymmetry* **2010**, *21*, 7.
(40) Chen, C.-B.; Wang, X.-F.; Cao, Y.-J.; Cheng, H.-G.; Xiao, W.-J. *J. Org. Chem.* **2009**, *74*, 3532.
(41) Wang, D.-S.; Chen, Q.-A.; Li, W.; Yu, C.-B.; Zhou, Y.-G.; Zhang, X. *J. Am. Chem. Soc.* **2010**, *132*, 8909.
(42) Duan, Y.; Li, L.; Chen, M.-W.; Yu, C.-B.; Fan, H.-J.; Zhou, Y.-G. Ibid.**2014**, *136*, 7688.
(43) Zhang, D.-Y.; Yu, C.-B.; Wang, M.-C.; Gao, K.; Zhou, Y.-G. *Tetrahedron Lett.* **2012**, *53*, 2556.

(44) Li, C.; Chen, J.; Fu, G.; Liu, D.; Liu, Y.; Zhang, W. *Tetrahedron* **2013**, *69*, 6839.
(45) Núñez-Rico, J. L.; Fernández-Pérez, H.; Vidal-Ferran, A. *Green Chem.* **2014**, *16*, 1153.
(46) Wang, D.-S.; Ye, Z.-S.; Chen, Q.-A.; Zhou, Y.-G.; Yu, C.-B.; Fan, H.-J.; Duan, Y. *J. Am. Chem. Soc.* **2011**, *133*, 8866.
(47) Chen, Z.-P.; Chen, M.-W.; Shi, L.; Yu, C.-B.; Zhou, Y.-G. *Chem. Sci.* **2015**, *6*, 3415.
(48) Wang, D.-S.; Tang, J.; Zhou, Y.-G.; Chen, M.-W.; Yu, C.-B.; Duan, Y.; Jiang, G.-F. *Chem. Sci.* **2011**, *2*, 803.
(49) 3-(α-Hydroxyalkyl)indoles were synthesized by formylation of 2-substituted indoles followed by nucleophilic addition of Grignard reagents to the formyl group (see reference 48).
(50) Duan, Y.; Chen, M.-W.; Ye, Z.-S.; Wang, D.-S.; Chen, Q.-A.; Zhou, Y.-G. *Chem.–Eur. J.* **2011**, *17*, 7193.
(51) Duan, Y.; Chen, M.-W.; Chen, Q.-A.; Yu, C.-B.; Zhou, Y.-G. *Org. Biomol. Chem.* **2012**, *10*, 1235.
(52) (a) Balakrishna, B.; Núñez-Rico, J. L.; Vidal-Ferran, A. *Eur. J. Org. Chem.* **2015**, *2015*, 5293. (b) Chen, Z.-P.; Zhou, Y.-G. *Synthesis* **2016**, *48*, 1769.
(53) For general reviews, see for example: (a) Smith, J. A.; Molesworth, P. P.; Ryan, J. H. Seven-Membered Rings. In *Progress in Heterocyclic Chemistry*, Gribble, G. W.; Joule, J. A., Eds.; Elsevier Ltd.: Oxford, Amsterdam, 2009; Vol. 21, pp 491. (b) Ryan, J. H.; Smith, J. A.; Hyland, C.; Meyer, A. G.; Williams, C. C.; Bissember, A. C.; Just, J. Seven-Membered Rings. In *Progress in Heterocyclic Chemistry*, Gribble, G. W.; Joule, J. A., Eds.; Elsevier: Oxford, Amsterdam, 2014; Vol. 26, pp 521.
(54) (a) Han, Z. Y.; Xiao, H.; Gong, L. Z. *Bioorg. Med. Chem. Lett.* **2009**, *19*, 3729. (b) Rueping, M.; Merino, E.; Koenigs, R. M. *Adv. Synth. Catal.* **2010**, *352*, 2629. (c) Gao, K.; Yu, C.-B.; Li, W.; Zhou, Y.-G.; Zhang, X.-M. *Chem. Commun.* **2011**, *47*, 7845. (d) Chen, X.; Zheng, Y.; Shu, C.; Yuan, W.; Liu, B.; Zhang, X. *J. Org. Chem.* **2011**, *76*, 9109. (e) Ding, Z.-Y.; Chen, F.; Qin, J.; He, Y.-M.; Fan, Q.-H. *Angew. Chem., Int. Ed.* **2012**, *51*, 5706. (f) Gao, K.; Wu, B.; Yu, C.-B.; Chen, Q.-A.; Ye, Z.-S.; Zhou, Y.-G. *Org. Lett.* **2012**, *14*, 3890. (g) Ma, B.; Ding, Z.; Liu, J.; He, Y.; Fan, Q.-H. *Chem. – Asian J.* **2013**, *8*, 1101. (h) Wang, J. *Tetrahedron Lett.* **2013**, *54*, 5956. (i) Guo, R.-N.; Gao, K.; Ye, Z.-S.; Shi, L.; Li, Y.; Zhou, Y.-G. *Pure Appl. Chem.* **2013**, *85*, 843. (j) Cowan, D. J.; Collins, J. L.; Mitchell, M. B.; Ray, J. A.; Sutton, P. W.; Sarjeant, A. A.; Boros, E. E. *J. Org. Chem.* **2013**, *78*, 12726. (k) Guo, C.; Sun, D.-W.; Yang, S.; Mao, S.-J.; Xu, X.-H.; Zhu, S.-F.; Zhou, Q.-L. *J. Am. Chem. Soc.* **2015**, *137*, 90. (l) Li, W.; Schlepphorst, C.; Daniliuc, C.; Glorius, F. *Angew. Chem., Int. Ed.* **2016**, *55*, 3300.
(55) Phosphine-phosphites ligands are also referred to as P–OP ligands (see for example: (a) Robert, T.; Velder, J.; Schmalz, H.-G. *Angew. Chem., Int. Ed.*

2008, *47*, 7718. (b) Suárez, A.; Méndez-Rojas, M. A.; Pizzano, A. *Organometallics* **2002**, *21*, 4611. and reference 56).

(56) The ligands with opposite configuration at the phosphite fragment were also studied in this transformation and led in all cases to lower enantioselectivities than those obtained with the corresponding diastereomeric ligand **L1**–**L4**. See the SI for details (Table SI1).

(57) For a complete summary on the effects of the additives, see Table SI2 in the Supporting Information.

(58) See Table SI3 from the Supporting Information for the hydrogenation conditions assayed.

(59) (a) Fernández-Pérez, H.; Donald, S. M. A.; Munslow, I. J.; Benet-Buchholz, J.; Maseras, F.; Vidal-Ferran, A. *Chem. –Eur. J.* **2010**, *16*, 6495. (b) Fernández-Pérez, H.; Benet-Buchholz, J.; Vidal-Ferran, A. *Chem. –Eur. J.* **2014**, *20*, 15375. (c) Lao, J. R.; Benet-Buchholz, J.; Vidal-Ferran, A. *Organometallics* **2014**, *33*, 2960.

(60) (a) Balcells, D.; Maseras, F. *New J. Chem.* **2007**, *31*, 333. (b) Brown, J. M.; Deeth, R. J. *Angew. Chem., Int. Ed.* **2009**, *48*, 4476.

(61) Schramm, Y.; Barrios-Landeros, F.; Pfaltz, A. *Chem. Sci.* **2013**, *4*, 2760.

(62) For seminal work on the concept of stepwise proton and hydride transfer to iminic C=N bonds see: (a) Martin, M.; Sola, E.; Tejero, S.; Andres, J. L.; Oro, L. A. *Chem.–Eur. J.* **2006**, *12*, 4043. For experimental and theoretical mechanistic studies on the iridium-mediated hydrogenation of cyclic iminic bonds by an outer-sphere coordination pathway, see: (b) Nagano, T.; Iimuro, A.; Schwenk, R.; Ohshima, T.; Kita, Y.; Togni, A.; Mashima, K. *Chem. –Eur. J.* **2012**, *18*, 11578. and 12b. For experimental and theoretical mechanistic studies on the ruthenium-mediated hydrogenation of cyclic iminic bonds by an outer-sphere coordination pathway, see: 12a.

(63) For the calculated energy contents of the four-membered iridacyles derived from **3a** and their structures, see the Supporting Information (Figure SI67).

(64) The use of catalytic amounts of HCl as additive translates to partial protonation of the substrate (HCl is added to the substrate before the catalyst). However, it should be recalled at this point that dihydrogen ligands in iridium complexes might certainly play a role in the protonation of the substrate: most of the heterocycles studied are fully hydrogenated with high enantioselectivities employing substoichiometric amounts of HCl, or even in the absence of HCl (see Tables 1, SI1, SI2 and SI3).

(65) Nomenclature of Inorganic Chemistry, IUPAC recommendations 2005; Connelly, N. G., Damhus, T., Hartshorn, R. M., Hutton, A. T., Eds.; RSC Publishing, Northampton, 2005.

(66) In fact, for each ligand we have optimized six possible isomeric iridium complexes (including *mer* complexes, see Figures SI68 and SI69) and the most favorable ones are *fac* isomers.

(67) See for example: Zhao, Y.; Benz, S.; Sakai, N.; Matile, S. *Chem. Sci.* **2015**, *6*, 6219.
(68) Fernández-Pérez, H.; Pericàs, M. A.; Vidal-Ferran, A. *Adv. Synth. Catal.* **2008**, *350*, 1984.
(69) Lao, J. R.; Fernández-Pérez, H.; Vidal-Ferran, A. *Org. Lett.* **2015**, *17*, 4114.
(70) Bakos, J.; Cserepi-Szucs, S.; Gomory, A.; Hegedus, C.; Marko, L.; Szollosy, A. *Can. J. Chem.* **2001**, *79*, 725.
(71) Wassenaar, J.; de Bruin, B.; Reek, J. N. H. *Organometallics* **2010**, *29*, 2767.
(72) Hunziker, F.; Kuenzel, F.; Schindler, O.; Schmutz, J. *Helv. Chim. Acta* **1964**, *47*, 1163.
(73) Yang, M.; Wu, L.; She, D.; Hui, H.; Zhao, Q.; Chen, M.; Huang, G.; Liang, Y. *Synlett* **2008**, 448.
(74) Hirobe, M.; Ozawa, T. *Tetrahedron Lett.* **1971**, *12*, 4493.
(75) Data collection with APEX II version v2013.4-1. Bruker (2007). Bruker AXS Inc., Madison, Wisconsin, USA.
(76) Data reduction with Bruker SAINT Version V8.30c. Bruker (2007). Bruker AXS Inc., Madison, Wisconsin, USA.
(77) SADABS: V2012/1 Bruker (2001). Bruker AXS Inc., Madison, Wisconsin, USA. Blessing, R. H. *Acta Crystallogr., Sect. A: Found. Crystallogr.* **1995**, *A51*, 33.
(78) Sheldrick, G. M. Ibid.**2008**, *64*, 112. SHELXTL version V6.14.
(79) SHELXle; Huebschle, C. B.; Sheldrick, G. M.; Dittrich, B. *J. Appl. Crystallogr.* **2011**, *44*, 1281.
(80) SHELXL; Sheldrick, G. M. *Acta Crystallogr., Sect. C: Struct. Chem.* **2015**, *71*, 3.
(81) Flack, H. D. *Acta Crystallogr., Sect. A: Found. Crystallogr.* **1983**, *A39*, 876.
(82) Parsons, S.; Flack, H. D.; *Acta Cryst.* **2004**, *A39*, S61.
(83) Ahlrichs, R.; Bär, M.; Häser, M.; Horn, H.; Kölmel, C. *Chem. Phys. Lett.* **1989**, *162*, 165.
(84) Andrae, D.; Häußermann, U.; Dolg, M.; Stoll, H.; Preuß, H. *Theor. Chim. Acta* **1990**, *77*, 123.
(85) Grimme, S.; Antony, J.; Ehrlich, S.; Krieg, H. *J. Chem. Phys.* **2010**, *132*, 154104/1.
(86) Yan, M.; Jin, T.; Chen, Q.; Ho, H. E.; Fujita, T.; Chen, L.-Y.; Bao, M.; Chen, M.-W.; Asao, N.; Yamamoto, Y. *Org. Lett.* **2013**, *15*, 1484.
(87) Rueping, M.; Theissmann, T.; Stoeckel, M.; Antonchick, A. P. *Org. Biomol. Chem.* **2011**, *9*, 6844.
(88) Wang, C.; Li, C.; Wu, X.; Pettman, A.; Xiao, J. *Angew. Chem., Int. Ed.* **2009**, *48*, 6524.
(89) Archer, D. A.; Booth, H.; Crisp, P. C. *J. Chem. Soc.* **1964**, 249.
(90) Wang, W.-B.; Lu, S.-M.; Yang, P.-Y.; Han, X.-W.; Zhou, Y.-G. *J. Am. Chem. Soc.* **2003**, *125*, 10536.
(91) Chen, Q.-A.; Chen, M.-W.; Yu, C.-B.; Shi, L.; Wang, D.-S.; Yang, Y.; Zhou, Y.-G. *J. Am. Chem. Soc.* 2011, *133*, 16432.

(92) Xue, Z.-Y.; Jiang, Y.; Peng, X.-Z.; Yuan, W.-C.; Zhang, X.-M. *Adv. Synth. Catal.* **2010**, *352*, 2132.
(93) Rueping, M.; Tato, F.; Schoepke, F. R. *Chem.–Eur. J.* **2010**, *16*, 2688.
(94) Ikeda, R.; Kuwano, R. *Chem. –Eur. J.* **2016**, *22*, 8610.
(95) Iimuro, A.; Higashida, K.; Kita, Y.; Mashima, K. *Adv. Synth. Catal.* **2016**, *358*, 1929.
(96) Wen, J.; Tan, R.; Liu, S.; Zhao, Q.; Zhang, X. *Chem. Sci.* **2016**, *7*, 3047.
(97) Huang, W.-X.; Yu, C.-B.; Ji, Y.; Liu, L.-J.; Zhou, Y.-G. *ACS Catal.* **2016**, *6*, 2368.
(98) Renom-Carrasco, M.; Gajewski, P.; Pignataro, L.; de Vries, J. G.; Piarulli, U.; Gennari, C.; Lefort, L. *Chem. –Eur. J.* **2016**, *22*, 9528.

CHAPTER-3

[Rh(P–OP)] Precatalysts Incorporating New Phosphite Fragments for Asymmetric Hydrogenation of Functionalized Alkenes

Table of Contents:

[Rh(P–OP)] Precatalysts Incorporating New Phosphite Fragments for Asymmetric Hydrogenation of Functionalized Alkenes

Bugga Balakrishna,[†] Anton Vidal-Ferran*[,†,‡]

† Institute of Chemical Research of Catalonia (ICIQ) & The Barcelona Institute of Science and Technology; Avinguda Països Catalans 16, E-43007, Tarragona, Spain, E-mail: avidal@iciq.cat

‡ Catalan Institution for Research and Advanced Studies (ICREA), Passeig Lluís Companys 23, E-08010 Barcelona, Spain.

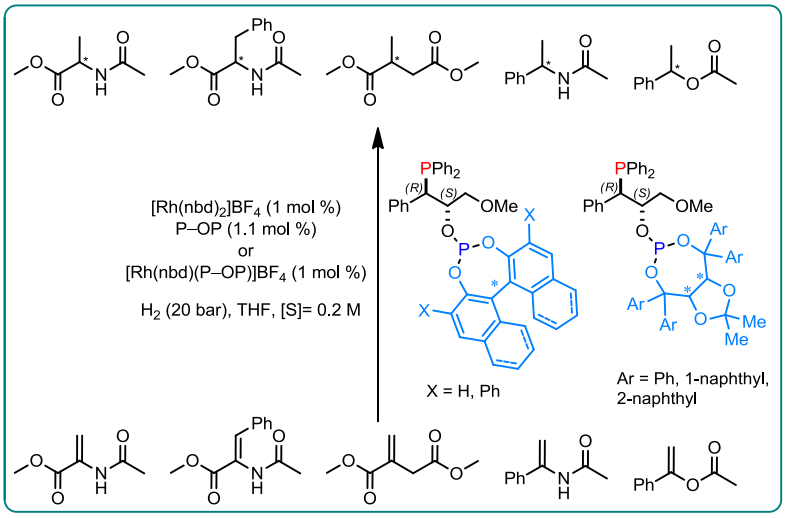

3.1 Abstract

Rhodium(I) complexes of a series of enantiopure phosphine-phosphite ligands were evaluated in the enantioselective hydrogenation of functionalized olefins. High activities (>99%) and moderate to excellent enantioselectivities (up to 99%) have been achieved. The effects on the enantioselectivities of TADDOL-derived phosphite groups (TADDOL = (2,2-dimethyl-1,3-dioxolane-4,5-diyl)bis(diphenylmethanol)) and 3,3'-diphenyl substituted H8-BINOL-derived phosphite motifs (H8-BINOL = 5,5',6,6',7,7',8,8'-octahydro-[1,1'-binaphthalene]-2,2'-diol) were comparatively studied. H8-BINOL-based ligands proved to be superior to the corresponding TADDOL-based ones in the current study and provided the highest enantioselectivities in the rhodium-mediated hydrogenation of functionalized alkenes within the whole series of P–OP ligands developed by the group.

3.2 Introduction

The design and development of efficient enantiopure phosphorus ligands and their potential application in several transition metal-mediated asymmetric transformations of interest constitute an expanding research area within academia and industry. [1] From a practical perspective, enantioselective hydrogenation offers several advantages for the asymmetric synthesis of enantiomerically pure compounds (optimal atom economy, broad substrate scope, high reactivity and selectivity, and operational simplicity). As a consequence, the asymmetric hydrogenation of prochiral substrates (alkenes, imines, ketones, heteroaromatic compounds), mostly catalyzed by chiral Ir, Rh or Ru complexes, is certainly amongst the most efficient and reliable methodologies in catalytic asymmetric synthesis.[2] Consequently, many industrial approaches for the production of optically active pharmaceuticals, agrochemicals,

fragrances, fine chemicals, and natural products rely on catalytic asymmetric hydrogenation reactions. Enantiopure bidentate ligands have become a crucial tool in the development of new metal-catalyzed asymmetric transformations[3] and a broad variety of such ligands have been described and optimized over the last few decades.[4] Among those, non-symmetrical ligands with two electronically different coordinating functionalities have proven to be superior in certain cases to C_2-symmetric ligands, as they have allowed for a better adjustment to the specific requirements of a given transformation.[5] In this context, enantiopure phosphine–phosphites have attracted much interest due to the different electronic properties of the two phosphorus functionalities.[6] Ligands of this type have been successfully applied in Rh-catalyzed hydrogenation and hydroformylation reactions, amongst other transformations.[7]

Despite the remarkably advanced state of the field, numerous research groups are still actively pursuing new catalytic systems that show higher activity and/or improved enantioselectivity for challenging substrates or for recently discovered pharmacologically active compounds. In this regard, our research group has employed a highly modular ligand design in combination with a fine-tuning methodology guided by computational analysis of the diastereomeric transition states in order to improve the performance of the catalytic systems. In this way, an array of enantiopure 1,2-P–OP derivatives (mostly phosphine-phosphite ligands) have been developed and successfully applied in Pd-mediated asymmetric allylic substitutions,[8] Ir-mediated asymmetric hydrogenation of heteroaromatic compounds[9] and Rh-mediated asymmetric hydrogenation of functionalized olefins.[10] As regards the Rh-mediated asymmetric hydrogenation, our group recently reported the highly enantioselective hydrogenation of a structurally diverse range of substrates catalyzed by cationic Rh complexes of ligands **3a** and **3b** (Scheme 1). Furthermore, very recently, Rh-catalysts

derived from P–OP ligands containing the 3,3'-disubstituted H8-BINOL-(H8-BINOL = 5,5',6,6',7,7',8,8'-octahydro-[1,1'-binaphthalene]-2,2'-diol]) and TADDOL-derived (TADDOL = (2,2-dimethyl-1,3-dioxolane-4,5-diyl)bis(diphenylmethanol)) phosphite fragments have been efficiently employed in the hydrogenative kinetic resolution of racemic vinyl sulfoxides[11] and the hydrogenative desymmetrization of achiral dienes,[12] respectively. However, the effects of these phosphite fragments (*i.e.* H8-BINOL and TADDOL groups) in the performance of the corresponding P–OP ligands in the Rh-mediated asymmetric hydrogenation of prochiral functionalized olefins had not been assessed. Hence, we sought herein to study the effects of these phosphite fragments in the asymmetric hydrogenation of an array of model functionalized olefins.

3.3 Results and Discussion

3.3.1 Ligand synthesis

Our group has previously synthesized a library of structurally diverse P–OP ligands based on the use of enantiomerically pure Sharpless epoxy ether **1** as a starting material. This compound was transformed into the final ligands in two steps: ring-opening of the epoxide with a nucleophilic trivalent phosphorus derivative followed by *O*-phosphorylation of the phosphino alcohol intermediate with trivalent phosphorus electrophiles (*i.e.* a chlorophosphite derived from an enantiomerically pure diol; see Scheme 1). The first step involved the opening of the epoxide ring, which proceeded smoothly at –30 ˚C to room temperature, and then *in situ* generation of corresponding borane protected adduct **2**. The free phosphino alcohol was subsequently obtained by cleavage of the borane adduct **2**, using 1,4-diazabicyclo[2.2.2]octane (DABCO; 2.2 equiv.) at 60 ˚C in toluene for two hours, and the *in situ* generated phosphino alcohol was subsequently derivatized with the corresponding chlorophosphite (1.1

equiv.). As previously mentioned (see pages 28-29 in Chapter 1 and the corresponding references cited therein), the phosphorylations of phosphino alcohol **2** with the chlorophosphites leading to ligands **3a**–**d** did not require the use of additional amounts of an auxiliary base:[13] the excess of DABCO from the borane-cleavage step in the reaction media served for quantitatively mediating the reaction between the free phosphino alcohol and the chlorophosphite.[10] However, the reaction of the free compound **2** with TADDOL-derived chlorophosphites leading to ligands **3e–i** proceeded at a slower rate. In order to increase the reaction rate, catalytic amounts of *N*,*N*-dimethylpyridin-4-amine (DMAP; 5 mol %) and an excess of NEt_3 as auxiliary base (20 equiv. with respect to the chlorophosphite) were used.[14,16] Under these reaction conditions, ligands **3e–i** were prepared in yields ranging from 39% (for ligand **3g**) to 73% (for ligand **3e**). It should be mentioned at this point, that ligand **3i** was obtained together with an unidentified by-product (the purity of **3i** was determined to be *ca.* 58%, based on integration of the ^{31}P NMR spectrum), which could not be completely removed. This by-product was efficiently removed in the following synthetic step (*i.e.* the complexation of the P–OP ligand with $[Rh(nbd)_2]BF_4$; section 3.5.2).

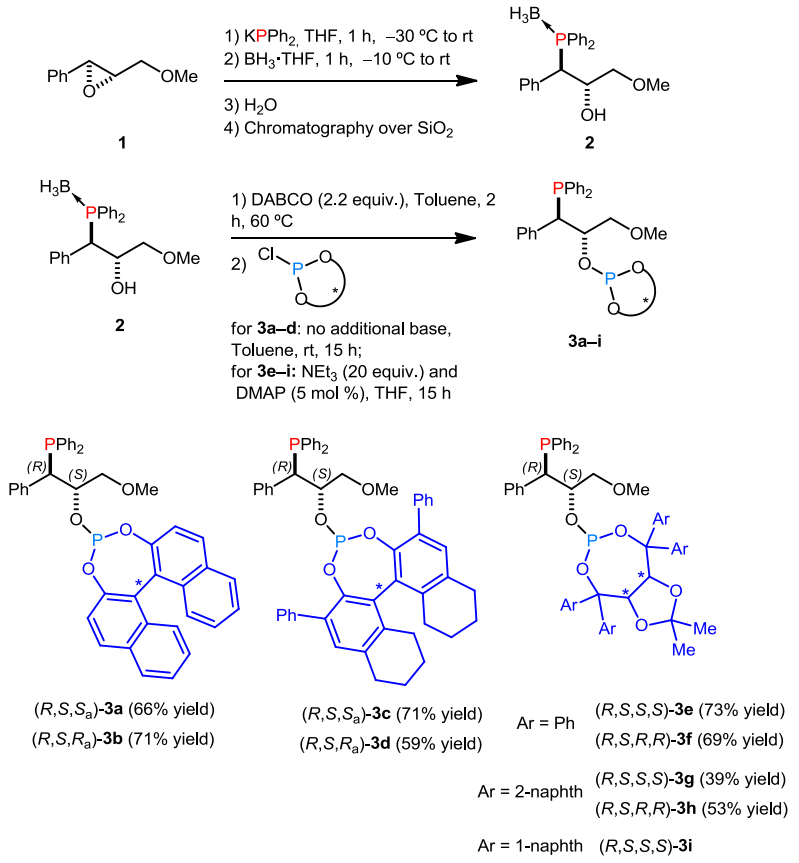

Scheme 1. Synthesis of phosphine-phosphite (P–OP) ligands.

3.3.2 Complexation Studies of H8-BINOL- and TADDOL-containing ligands with rhodium precursors

To demonstrate the general ability of bidentate P–OP ligands to form stable, well-defined complexes with the rhodium precursor normally used in hydrogenation reactions (*i.e.* $[Rh(nbd)_2]BF_4$), we performed complexation studies using enantiopure ligands **3c-i** [15] and the rhodium precursor previously mentioned. Rhodium complexes $[Rh(nbd)(P–OP)]BF_4$ derived from P–OP ligands **3c–i** were efficiently synthesized using

stoichiometric amounts of ligand and $[Rh(nbd)_2]BF_4$ (Scheme 2). The corresponding $[Rh(nbd)(P–OP)]BF_4$ complexes were isolated in high yields by crystallization (from 81 to 91%, Scheme 2). The spectroscopic data (NMR and MS) of the resulting complexes was in agreement with the proposed structure. Furthermore, single crystals of the rhodium complexes derived from ligands **3c**–**g** and **3i** suitable for X-ray diffraction analysis could be grown and then analyzed to unambiguously confirm a six-membered chelate coordination mode of the P–OP ligands to a square planar rhodium center (see Figure 1). The X-ray structures of two representative [Rh(nbd)(P–OP)] complexes are shown in Figure 1 (see Section 3.6.3 for the graphical representation of the rest of structures).

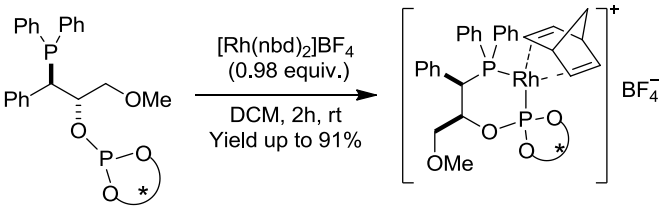

3c–i **4c–i**

Scheme 2. Complexation studies of the P–OP ligands **3c–i.**

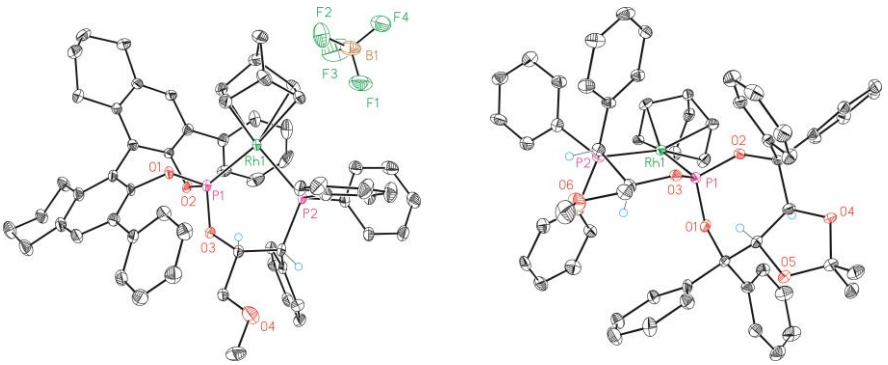

Figure 1. X-ray structures of the Rh-(P–OP) complexes. **4c** (*left*) and **4e** (*right*) (ORTEP drawings showing thermal ellipsoids at 50% probability; some H-atoms (and the BF_4 counterion for **4e**) have been omitted for clarity).

3.3.3 Catalytic performance of Rh complexes derived from H8-BINOL- and TADDOL-containing ligands in asymmetric hydrogenation of functionalized alkenes

Having studied the complexation properties of ligands **3c–i** with $[Rh(nbd)_2]BF_4$, we then investigated the performance of these ligands in the Rh-mediated enantioselective hydrogenation of various prochiral functionalized olefins: α-(acylamino)acrylates (**5a** and **5b**), dimethyl 2-methylenesuccinate (**5c**), *N*-(1-phenylvinyl)acetamide (**5d**) and 1-phenylvinyl acetate (**5e**). The hydrogenation reactions were run under standard screening conditions (1.0 mol % of preformed or *in situ* prepared $[Rh(nbd)(P–OP)]BF_4$ precatalyst, 20 bar of H_2, THF as solvent at room temperature during 18 h). The results of this comparative study are summarized in Table 1. Complete conversions were observed in almost all cases.

Although the results with ligands **3a** and **3b** have not been obtained within the present thesis,[10c] their hydrogenation results have been included in Table 1 in order to aid comparison. Previous hydrogenation studies had already revealed that the phosphite group is the principal stereodirector in the asymmetric hydrogenation of functionalized alkenes: opposite absolute configurations of the hydrogenation products **5a–e** were obtained with ligands **3a** and **3b**, whose only difference is the opposite configuration of the stereogenic axis in the phosphite fragment (compare entries 1 and 2 in Table 1).[10c] Thus, ligand **3a** contains the matched combination of stereogenic elements, which translates into higher enantioselectivities than those obtained with ligand **3b**.

The presence of sterically crowded phosphite groups (ligands **3c** and **3d,** see in Scheme 1) with phenyl substituents at the 3,3'-positions of the [1,1'-biaryl]-2,2'-diol motif led to an increase in the enantioselectivities for

all substrates tested (entries 3 and 4 in Table 1). Ligand **3c** incorporating an (S_a)-configured phosphite fragment provided perfect enantioselectivities (99% ee) for the four types of substrates tested (entry 3, Table 1) and should be considered the highest performing P–OP ligand developed by the group for the rhodium-mediated asymmetric hydrogenation of functionalized olefins. Interestingly, its diastereomeric ligand (**3d**) incorporating an (R_a)-configured phosphite fragment also provided excellent enantioselectivities for substrates **5a**, **5c** and **5e** (99% ee; see entry 4 in Table 1).

Ligands with TADDOL-derived phosphite fragments (*i.e.* ligands **3e–i**) were also investigated in the asymmetric hydrogenation of the aforementioned functionalized olefins **5a–e**. Although all ligands tested showed high performance in terms of activity (conversions >99%), enantioselectivities were lower than those obtained for the (H8-)BINOL containing ligands **3a–d** (compare entries 1–4 with entries 5–9 in Table 1). The choice of the optimal ligand clearly depended on substrate. For instance, (*S*,*S*)-TADDOL derived P–OP ligands **3e** and **3g** performed better for substrates **5c**, **5d** and **5e** and provided higher enantioselectivities than those obtained with (*R*,*R*)-TADDOL-derived ligands (up to 91% ee for (*S*,*S*)-TADDOL derived P–OP ligands; compare the columns corresponding to substrates **5c**, **5d** and **5e** in entries 5 and 7 with those in entries 6 and 8). On the contrary, (*R*,*R*)-TADDOL-derived ligands **3f** and **3h** led to better results in the case of α-(acetamido)acrylates **5a** and **5b** (up to 86% ee for (*R*,*R*)-TADDOL derived P–OP ligands; compare the columns corresponding to substrates **5a** and **5b** in entries 5 and 7 with those in entries 6 and 8 in Table 1). Changing the phenyl substituents at the TADDOL-derived phosphite group (ligands **3e** and **3g**) by the bulkier 2-naphthyl substituent (ligands **3f** and **3h**) did not lead to any significant effect on the observed enantioselectivities. Whenever a comparison is

possible between the configuration of the hydrogenation products obtained with (*S*,*S*)- and (*R*,*R*)-TADDOL-derived P–OP ligands (ligands **3e** and **3g** and ligands **3f** and **3h**, respectively), the performed hydrogenation studies confirmed that the phosphite group is the principal stereodirector of the asymmetric hydrogenation. As observed for (H8-)BINOL-derived ligands (**3a-d**), opposite absolute configurations of the hydrogenation products are obtained upon changing the configuration of the stereogenic centers of the TADDOL unit (compare entries 5 and 7 with entries 6 and 8 in Table 1). The only exception to this observation is that the hydrogenation product **5e** employing ligands **3f** and **3g** (which contain phosphite fragments with opposite configurations; entries 7 and 8 in Table 1) had the same configuration. This observation would suggest a substrate- and ligand-dependent mechanistic scenario in the hydrogenations. However, any mechanistic rationalizations about processes with low enantioselectivity (*e.g.* lower than 20% ee), should be made judiciously. Lastly, TADDOL-derived P–OP ligand **3i** containing 1-naphthyl substituents at the phosphite group performed better in terms of enantioselectivities (54–99% ee, see entry 9 Table 1) than any other TADDOL-containing ligand (compare entries 5, 6, 7 and 8 with 9, Table 1), except for substrate **5d**.

This comparative study on the catalytic performance of P–OP ligands with new phosphite motifs in rhodium-mediated asymmetric hydrogenations has revealed that 3,3’-disubstituted H8-BINOL-containing ligands are superior in terms of enantioselection than the TADDOL-based ligands or those lacking substituents at the 3,3’-positions of the [1,1'-biaryl]-2,2'-diol fragment. Unfortunately, an accurate structure-activity relationship (SAR) between the structural features of the different ligands and the observed enantioselectivities for the studied substrates is not possible. Detailed theoretical studies at a high computational level of the oxidative addition transition states of the different reaction manifolds for

the different substrates and ligands would probably be required for performing accurate SAR studies and these studies fall beyond the scope and capabilities of the present Ph.D. thesis.

Table 1. Asymmetric hydrogenation[a] of functionalized olefins catalyzed by Rh complexes derived of P–OP ligands **3c–i**.

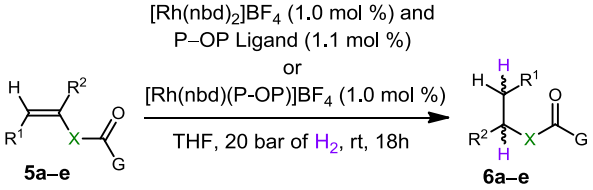

Entry	Ligand	Substrates				
		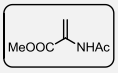 **5a**	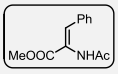 **5b**	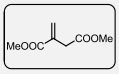 **5c**	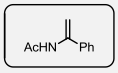 **5d**	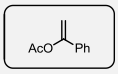 **5e**
		ee[b] (*Config*)[c]	ee[b] (*Config*)[c]	ee[b] (*Config*)[c]	ee[b] (*Config*)[c]	ee[b] (*Config*)[c]
1	**3a**	99% (*R*)[d]	99% (*R*)[d]	99% (*S*)[d]	98% (*R*)[d]	96% (*R*)[d]
2	**3b**	88% (*S*)[d]	86% (*S*)[d]	97% (*R*)[d]	94% (*S*)[d]	90% (*S*)[d]
3	**3c**	99% (*R*)	99% (*R*)	99% (*S*)	99% (*R*)	99% (*R*)[e]
4	**3d**	99% (*S*)	88% (*S*)	99% (*R*)	98% (*S*)	99% (*S*)
5	**3e**	36% (*R*)	76% (*R*)	84% (*S*)	80% (*R*)	32% (*R*)
6	**3f**	85% (*S*)	86% (*S*)	41% (*R*)	25% (*S*)	12% (*S*)
7	**3g**	29% (*R*)	77% (*R*)	91% (*S*)	71% (*R*)	24% (*R*)
8	**3h**	78% (*S*)	82% (*S*)	76% (*R*)	30% (*S*)	22% (*R*)
9	**3i**	99% (*R*)[f]	91% (*R*)[f]	91% (*S*)[f]	54% (*R*)[f]	64% (*R*)[f]

[a] The values shown are the average of at least two independent runs. Hydrogenations were run in a parallel reactor: *Reaction conditions*: $[Rh(nbd)_2]BF_4$/P–OP ligand/substrate = 1.0:1.1:100, rt, 20 bar H_2, substrate concentration = 0.20 M in THF, 18 h. Conversions were determined by ^1H NMR to be higher than 99%. [b] Enantiomeric excesses (ee) were determined by GC or HPLC analysis on chiral stationary phases, as indicated in the SI. [c] Absolute configurations were assigned by comparison of chromatographic elution orders with reported data. [d] Results published in ref. 10c and 10f. [e] Conversion was 96%. [f] Reaction conditions: $[Rh(nbd)(P–OP)]BF_4$/ substrate = 1.0:100.

3.4 Conclusions

In summary, we have expanded the structural diversity of the P–OP ligand library with 3,3'-diphenyl-H8-BINOL- and TADDOL-derived phosphite fragments. Efficient synthetic methods for the preparation of the new ligands have been developed. Complexation experiments between the P–OP ligands and the standard rhodium precursor for asymmetric hydrogenations afforded an array of [Rh(nbd)(P–OP)]BF_4 complexes, whose structures were unambiguosly confirmed by NMR and X-ray spectroscopic studies. The [Rh(nbd)(P–OP)]BF_4 complexes have been evaluated in the asymmetric hydrogenation of functionalized olefins. High activities (conversion >99%) and medium to excellent enantioselectivities (up to 99%) have been achieved for the studied substrates. The effects of different phosphite groups on the enantioselectivities of the rhodium-mediated asymmetric hydrogenations had been comparatively studied. H8-BINOL-based ligands proved to be superior to the corresponding TADDOL-based ones in the current study and provided the highest enantioselectivities in the rhodium-mediated hydrogenation of functionalized alkenes within the whole series of P–OP ligands developed by the group.

3.5 Experimental Section

All syntheses were carried out using chemicals as purchased from commercial sources, unless otherwise stated. Glassware was dried under vacuum and heated with a hot air gun before use. All manipulations and reactions were run under inert atmosphere using anhydrous solvents, in either a glove box or with standard Schlenk-type techniques. All solvents were dried by using a Solvent Purification System (SPS). Silica gel 60 (230–400 mesh) was used for column chromatography. NMR spectra were recorded in $CDCl_3$ unless otherwise cited, using a 400 MHz or 500 MHz spectrometer. ^{1}H NMR and $^{13}C\{^{1}H\}$ NMR chemical shifts are quoted in ppm relative to residual solvent peaks, whereas $^{31}P\{^{1}H\}$ and ^{31}P NMR chemical shifts are quoted in ppm relative to 85% phosphoric acid in water. $^{19}F\{^{1}H\}$ NMR chemical shifts are quoted in ppm relative to $BF_3{\cdot}OEt_2$ in $CDCl_3$. High resolution mass spectra (HRMS) were recorded by using an ESI ionization method in positive mode. Optical rotations were measured on a Jasco P-1030 polarimeter. Melting points were measured in open capillaries on a Büchi B-540 instrument and are uncorrected. Enantiomeric excesses were determined by GC or HPLC on using chiral stationary phases. GC analyses were performed on an Agilent 6890N chromatograph equipped with a FID detector. HPLC analyses were performed on an Agilent 1200 Series chromatograph equipped with a diode array UV detector.

3.5.1 General procedure for the synthesis of ligands

The phosphine-borane complex[10c] (1.0 mmol) and diazabyciclo[2.2.2]octane (2.0 mmol) were charged in a flame dried Schlenk flask. The system was purged three times with Ar. Dry and deoxygenated toluene (6.0 mL) was added. The reaction mixture was heated at 60 ºC and stirred for 2h, allowed to cool down to room temperature, passed through a short SiO_2 pad under N_2 atmosphere inside a glove box and further eluted with dry and deoxygenated toluene (4.0 mL) giving a solution of the corresponding phosphino alcohol, which was dried *in vacuo*. The residue was dissolved in THF (5.0 mL) and NEt_3 (20 mmol) and DMAP (0.05 mmol) were added to the previous solution. The appropriate amount of chlorophosphite[17] (1.1 mmol) in THF (12.0 mL) was added dropwise to the phosphino-alcohol solution. The mixture was stirred for 15 h at room temperature. The reaction mixture was filtered through Celite® inside the glove box and the filtrate was evaporated *in vacuo*. Rapid chromatography of the residue over a short column of silica gel (12 g) inside glove box using dry and deoxygenated solvents (2:1; DCM:Hexane) afforded the pure ligand. The syntheses and characterization data of ligands **3e**[16] and **3f**[16] have been already published.

Ligand 3g: Ligand **3g** was synthesized following the general procedure, starting from the required phosphino-alcohol-borane complex[10c] (0.387 g, 1.06 mmol), diazabyciclo[2.2.2]octane (0.243 g, 2.13 mmol), NEt_3 (2.95 mL, 21.3 mmol), DMAP (6.49 mg, 0.053 mmol) and chlorophosphite[17] (0.568 g, 1.07 mmol). It was obtained as a white solid (0.584 g, 53% isolated yield). R_F is 0.46 in 2:1 (DCM:Hexane) as an eluent. mp

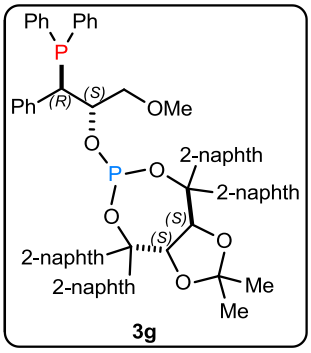

3g

139–142 ºC; $[\alpha]_D^{25}$ = +178 (*c* = 0.130 g/ 100 mL, DCM); IR absorption (neat) ῡ 3054, 2987, 2923, 1598, 1505, 1452; ^{1}H NMR (500 MHz, $CDCl_3$) δ 8.63–8.58 (m, 1H), 8.24–8.22 (m, 1H), 8.19–8.17 (m, 1H), 8.12–8.10 (m, 1H), 8.04–6.74 (m, 39H), 5.81 (d, $^3J_{H\text{-}H}$ = 8.1 Hz, 1H), 5.48 (d, $^3J_{H\text{-}H}$ = 8.1 Hz, 1H), 4.61–4.53 (m, 1H), 3.82 (dd, $^2J_{H\text{-}P}$ = 4.9 Hz, $^3J_{H\text{-}H}$ = 2.9 Hz, 1H), 3.00 (s, 3H), 2.91–2.85 (m, 1H), 2.74–2.68 (m, 1H), 0.81 (s, 3H), 0.53 (s, 3H); ^{13}C{^{1}H} NMR (100 MHz, $CDCl_3$) δ 143.0 (C), 142.8 (C), 139.45 (C), 139.41 (C), 139.2 (C), 136.7 (C), 136.6 (C), 136.5 (C), 134.6 (CH), 134.4 (CH), 133.6 (CH), 133.4 (CH), 133.2 (C), 133.1 (C), 133.0 (C), 132.9 (C), 132.7 (C), 132.6 (C), 131.0 (CH), 130.9 (CH), 129.3 (CH), 129.0 (CH), 128.9 (CH), 128.84 (CH), 128.79 (CH), 128.7 (CH), 128.6 (CH), 128.4 (CH), 128.2 (CH), 127.83 (CH), 127.76 (CH), 127.7 (CH), 127.6 (CH), 127.5 (CH), 127.48 (CH), 127.4 (CH), 127.2 (CH), 126.5 (CH), 126.42 (CH), 126.37 (CH), 126.20 (CH), 126.15 (CH), 126.1 (CH), 126.0 (CH), 125.8 (CH), 125.6 (CH), 125.2 (CH), 114.2 (C), 87.1 (d, $^2J_{C\text{-}P}$ = 12.2 Hz, C), 83.6 (C), 82.4 (d, $^3J_{C\text{-}P}$ = 11.1 Hz, CH), 80.2 (d, $^3J_{C\text{-}P}$ = 4.7 Hz, CH), 73.4–73.2 (m, CH_2), 73.2–72.8 (m, CH), 58.6 (CH_3), 47.5 (dd, $^1J_{C\text{-}P}$ = 14.1 Hz, $^3J_{C\text{-}P}$ = 4.5 Hz, CH), 27.3 (CH_3), 26.6 (CH_3); ^{31}P{^{1}H} NMR (202 MHz, $CDCl_3$) δ 142.7 (d, $^4J_{P\text{-}P}$ = 21.5 Hz, P–O), –9.0 (d, $^4J_{P\text{-}P}$ = 21.5 Hz, P–C); HRMS (ESI^+) [calculated for $C_{69}H_{59}O_6P_2$ $(M+H)^+$ 1045.3781; observed 1045.3772].

Ligand 3h: Ligand **3h** was synthesized following the general procedure, starting from the required phosphino-alcohol-borane complex[10c] (0.400 g, 1.08 mmol), diazabyciclo[2.2.2]octane (0.246 g, 2.15 mmol), NEt_3 (2.98 mL, 21.5 mmol), DMAP (6.57 mg, 0.0538 mmol) and chlorophosphite[17] (0.568 g, 1.07 mmol). It was obtained as a white solid (0.435 g, 39% isolated yield). R_F is 0.4 in 2:1 (DCM:Hexane) as an eluent. m.p. 133–135 ºC; $[\alpha]_D^{25}$ = –281.2 (*c* = 0.11 g/100 mL, DCM); IR absorption (neat) ῡ 3054, 2985, 2919, 1598, 1504, 1452, 1433; ^{1}H NMR (500 MHz, $CDCl_3$) δ 8.61 (bs, 1H), 8.19–8.16 (m, 2H), 8.02 (bs, 1H), 7.99–7.4 (m, 28H), 7.15–6.93 (m, 11H), 5.39 (s, 2H), 4.73–4.65 (m, 1H), 3.95 (dd, $^2J_{H\text{-}P}$ = 4.8 Hz, $^3J_{H\text{-}H}$ = 2.9 Hz, 1H), 3.41–3.34 (m, 1H), 3.21 (dd, $^2J_{H\text{-}H}$ = 9.2 Hz, $^3J_{H\text{-}H}$ = 7.9 Hz, 1H), 3.05 (s, 3H), 1.17 (s, 3H), 0.37 (s, 3H); ^{13}C{^{1}H} NMR (125 MHz, $CDCl_3$) δ 143.6 (C), 143.2 (C), 139.3 (C), 138.5 (C), 137.4 (C), 137.2 (C), 136.8 (C), 136.7 (C), 136.6 (C), 136.5 (C), 134.3 (CH), 134.1 (CH), 133.8 (CH), 133.7 (CH), 133.1 (C), 133.05 (C), 132.96 (C), 132.83 (C), 132.81 (C), 132.7 (C), 132.6 (C), 131.53 (CH), 131.47 (CH), 129.3 (CH), 128.99 (CH), 128.96 (CH), 128.9 (CH), 128.54 (CH), 128.49 (CH), 128.31 (CH), 128.28 (CH), 128.94 (CH), 127.91 (CH), 127.87 (CH), 127.81 (CH), 127.74 (CH), 127.68 (CH), 127.58 (CH), 127.51 (CH), 127.44 (CH), 126.9 (CH), 126.8 (CH), 126.6 (CH), 126.5 (CH), 126.4 (CH), 126.3 (CH), 126.2 (CH), 126.02 (CH), 125.99 (CH), 125.86 (CH), 125.5 (CH), 125.4 (CH), 113.1 (C), 85.3 (d, $^2J_{C\text{-}P}$ = 5.4 Hz, C), 83.0 (d, $^3J_{C\text{-}P}$ = 20.6 Hz, CH), 82.7 (d, $^2J_{C\text{-}P}$ = 4.7 Hz, C), 81.7 (d, $^3J_{C\text{-}P}$ = 4.0 Hz, CH), 73.5–73.4 (m, CH_2), 72.7 (dd, $^2J_{C\text{-}P}$ = 16.3 Hz, $^2J_{C\text{-}P}$ = 11.9 Hz, CH), 58.8 (CH_3), 47.7 (dd, $^1J_{C\text{-}P}$ = 14.4 Hz, $^3J_{C\text{-}P}$ = 4.3 Hz, CH), 27.7 (CH_3), 26.3 (CH_3); ^{31}P{^{1}H} NMR (202 MHz, $CDCl_3$) δ 147.6 (d, $^4J_{P\text{-}P}$ = 21.4 Hz, P–O),

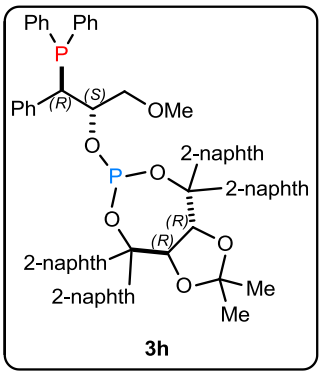

3h

–9.2 (d, $^4J_{P\text{-}P}$ = 21.4 Hz, P–C); HRMS (ESI$^+$) [calculated for $C_{69}H_{59}O_6P_2$ $(M+H)^+$ 1045.3781; observed 1045.3774].

Ligand 3i: Ligand **3i** was synthesized following the general procedure, starting from the required phosphino-alcohol-borane complex[10c] (0.231 g, 0.629 mmol), diazabyciclo[2.2.2]octane (0.144 g, 1.26 mmol), NEt_3 (1.75 mL, 12.6 mmol), DMAP (3.84 mg, 0.0314 mmol) and with corresponding chlorophosphite (0.631 g, 0.66 mmol). After careful column chromatography in glovebox using 2:1 (DCM:Hexane) as an eluent the ligand **3i** was obtained as a white solid. Though the TLC of the obtained compound shows single spot, the ligand is not in pure form (0.158 g, 58% pure by ^{31}P NMR). Hence the ligand was straightforwardly converted as its Rh precatalyst by treating with corresponding amount of Rh-precursor (*i.e.* $[Rh(nbd)_2]BF_4$) (see the preparation of Rh-complex **4i** in the following section 3.5.2).

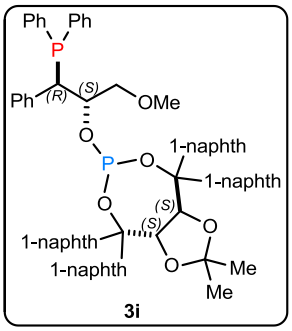

3i

3.5.2 General synthetic procedure for the preparation of Rh-complexes

A solution of the P–OP ligand (1 mmol) in anhydrous DCM (5.0 mL) was slowly added *via* cannula to a stirred solution of $[Rh(nbd)_2]BF_4$ (0.98 mmol) in anhydrous DCM (5.0 mL). The reaction was stirred for 2 h at room temperature under Ar atmosphere. The solvent was concentrated *in vacuo* to reach a final volume of *ca*. 2.5 mL. Anhydrous Et_2O (15.0 mL) was slowly added by syringe and the resulting solution was slowly stirred to yield an orange suspension. The solvent was filtered off under inert atmosphere by using a cannula filter and the resulting solid was washed with anhydrous Et_2O (2 x 12.0 mL) and dried *in vacuo* to afford the pure

Rh complex [Rh(nbd)(P–OP)]BF_4 as an orange powder. The syntheses and characterization data of complexes **4c** [18] and **4e**[18] has already been published.

[Rh(nbd)(3d)]BF_4 (4d): Rhodium complex **4d** was prepared by following the general procedure, starting from **3d** (197 mg, 0.239 mmol) and [Rh(nbd)$_2$]BF_4 (87.5 mg, 0.234 mmol). It was obtained as an orange powder (227.0 mg, 86% isolated yield). ^{1}H NMR (400 MHz, CD_2Cl_2) δ 7.84–7.74 (m, 2H), 7.62–7.39 (m, 9H), 7.37–7.14 (m, 5H), 7.10–6.85 (m, 7H), 6.76–6.71 (m, 2H), 6.35–6.24 (m, 2H), 5.93 (bs, 1H), 5.16 (bs, 1H), 4.52–4.44 (m, 1H), 4.02–3.96 (m, 2H), 3.86 (bs, 1H), 3.61 (bd, *J* = 14.5 Hz, 1H), 3.13–2.60 (m, 11H), 2.49–2.26 (m, 2H), 1.96–1.54 (m, 10H); ^{13}C{^{1}H} NMR (100 MHz, CD_2Cl_2) δ 143.4 (C), 143.3 (C), 142.5 (C), 142.4 (C), 139.8 (C), 138.3 (C), 137.9 (C), 137.5 (C), 137.1 (C), 136.7 (C), 135.3 (CH), 135.2 (CH), 132.70 (C), 132.68 (C), 132.4 (C), 132.3 (C), 132.09 (C), 132.07 (C), 131.89 (CH), 131.82 (CH), 131.82 (CH), 131.79 (CH), 131.69 (CH) 131.62 (CH), 131.59 (CH), 131.4 (CH), 130.74 (CH), 130.70 (CH), 130.4 (CH), 130.3 (CH), 129.9 (C), 129.8 (CH), 129.7 (CH), 129.5 (C), 129.4 (C), 129.3 (C), 129.2 (C), 129.1 (CH), 129.0 (CH), 128.94 (CH), 128.88 (CH), 128.77 (CH), 128.3 (CH), 128.2 (C), 128.1 (C), 127.64 (CH), 127.62 (CH), 103.3–102.9 (m, CH), 99.9–99.6 (m, CH), 93.0–92.8 (m, CH), 78.6 ($^2J_{C\text{-}P}$ = 8.1 Hz, CH), 75.5 (CH), 72.8 (CH_2), 71.7 (CH_2), 59.6 (CH_3), 56.3 (CH), 55.3 (CH), 43.7 (d, $^1J_{C\text{-}P}$ = 24.6 Hz, CH), 29.8 (CH_2), 29.7 (CH_2), 28.4 (CH_2), 28.3 (CH_2), 23.13 (CH_2), 23.1 (CH_2), 23.0 (CH_2); ^{31}P{^{1}H} NMR (162 MHz, CD_2Cl_2) δ 131.3 (dd, $^1J_{Rh\text{-}P}$ = 265.2 Hz, $^2J_{P\text{-}P}$ = 68.9 Hz, P–O), 27.7 (dd, $^1J_{Rh\text{-}P}$ =

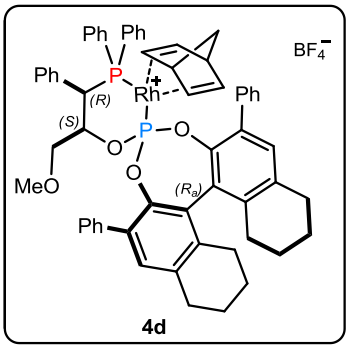

146.8 Hz, $^{2}J_{P\text{-}P}$ = 68.9 Hz, P–C). HRMS (ESI^{+}) [Calculated for $C_{61}H_{58}O_4P_2Rh$ $(M–BF_4)^{+}$ 1019.2860; observed 1019.2833].

[Rh(nbd)(3f)]BF_4 (4f): Rhodium complex **4f** was prepared by following the general procedure, starting from **3f** (59.3 mg, 0.0704 mmol) and [Rh(nbd)$_2$]BF_4 (25.0 mg, 0.0668 mmol). It was obtained as an orange powder (68.3 mg, 91% isolated yield). ^{1}H NMR (500 MHz, CD_2Cl_2) δ 8.12–8.09 (m, 2H), 7.72–6.89 (m, 31H), 6.35–6.26 (m, 2H), 6.11 (bs, 1H), 5.91 (bs, 1H), 5.86 (d, $^{3}J_{H\text{-}H}$ = 8.2 Hz, 1H), 5.36 (bs, 1H), 4.86 (d, $^{3}J_{H\text{-}H}$ = 8.2 Hz, 1H), 4.83 (bs, 1H), 4.31 (s, 1H), 4.22 (s, 1H), 3.77 (d, $^{2}J_{H\text{-}P}$ = 16.4 Hz, 1H), 3.67–3.58 (m, 1H), 2.91 (s, 3H), 2.06 (dd, $^{2}J_{H\text{-}H}$ = $^{3}J_{H\text{-}H}$ = 8.8 Hz, 1H), 2.03–1.96 (m, 1H), 1.79 (d, $^{2}J_{H\text{-}H}$ = 8.9 Hz, 1H), 1.75–1.71 (m, 1H), 1.29 (s, 3H), 0.17 (s, 3H); ^{13}C{^{1}H} NMR (125 MHz, CD_2Cl_2) δ 145.2 (C), 145.1 (C), 144.3 (C), 140.7 (C), 140.6 (C), 140.5 (C), 136.5 (CH), 136.4 (CH), 133.7 (CH), 132.2 (CH), 132.1 (CH), 131.8 (C), 131.31 (CH), 131.29 (CH), 130.6 (CH), 130.5 (CH), 129.6 (CH), 129.3 (CH), 129.2 (CH), 129.1 (CH), 129.03 (CH), 128.98 (CH), 128.85 (CH), 128.8 (CH), 128.74 (CH), 128.6 (CH), 128.55 (CH), 128.5 (CH), 128.34 (CH), 128.25 (CH), 127.4 (CH), 127.3 (CH), 114.4 (C), 96.7 (CH), 96.3 (CH), 90.2 (C), 90.1 (C), 88.8–88.6 (m, CH), 86.9–86.7 (m, CH), 82.0 (d, $^{3}J_{C\text{-}P}$ = 3.8 Hz, CH), 79.4 (d, $^{3}J_{C\text{-}P}$ = 3.8 Hz, CH), 75.0 (d, $^{2}J_{C\text{-}P}$ = 6.2 Hz, CH), 72.0 (CH_2), 70.5 (d, $^{3}J_{C\text{-}P}$ = 8.4 Hz, CH_2), 58.9 (CH_3), 56.4 (CH), 55.2 (CH), 42.2 (d, $^{1}J_{C\text{-}P}$ = 29.6 Hz, CH), 27.7 (CH_3), 25.5 (CH_3); ^{31}P{^{1}H} NMR (202 MHz, CD_2Cl_2) = 107.0 (dd, $^{1}J_{P\text{-}Rh}$ = 266.7 Hz, $^{2}J_{P\text{-}P}$ = 68.4 Hz, P–O), 26.4 (dd, $^{1}J_{P\text{-}Rh}$ = 148.0 Hz, $^{2}J_{P\text{-}P}$ = 68.4 Hz, P–C). HRMS (ESI^{+}) [calculated for $C_{60}H_{58}O_6P_2Rh$ $(M–BF_4)^{+}$ 1039.2758; observed 1039.2734].

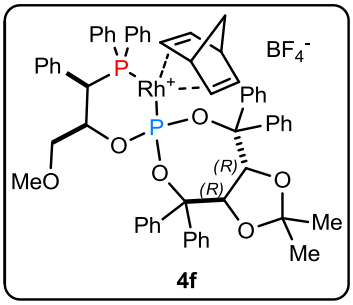

4f

[Rh(nbd)(3g)]BF_4 (4g): Rhodium complex **4g** was prepared by following the general procedure, starting from **3g** (145.0 mg, 0.138 mmol) and [Rh(nbd)$_2$]BF_4 (47.0 mg, 0.126 mmol). It was obtained as an orange powder (135.0 mg, 81% isolated yield). ^{1}H NMR (500 MHz, CD_2Cl_2) δ 8.17–6.80 (m, 41 H), 6.68–6.55 (m, 2H), 6.15 (bs, 1H), 5.68 (d, $^3J_{H\text{-}H}$ = 7.9 Hz, 1H), 5.64 (d, $^3J_{H\text{-}H}$ = 7.9 Hz, 1H), 5.36 (bs, 1H), 5.13 (bs, 1H), 4.78 (bs, 1H), 4.30 (bs, 1H), 3.95–3.81 (m, 2H), 3.33–3.23 (m, 1H), 2.44 (dd, $^2J_{H\text{-}H}$ = $^3J_{H\text{-}H}$, 1H), 2.07 (s, 3H), 1.77–1.61 (m, 2H), 1.48–1.39 (m, 1H), 1.01 (s, 3H), 0.42 (s, 3H); ^{13}C{^{1}H} NMR (125 MHz, CD_2Cl_2) δ 141.34 (C), 141.28 (C), 140.9 (C), 137.3 (C), 137.2 (C), 136.5 (C), 136.0 (CH), 135.9 (CH), 133.8 (C), 133.7 (CH), 133.6 (CH), 133.5 (C), 133.4 (C), 133.3 (C), 133.2 (C), 132.8 (C), 132.75 (C), 132.73 (CH), 132.65 (CH), 132.62 (C), 132.3 (C), 131.55 (CH), 131.53 (CH), 130.83 (C), 130.80 (CH), 130.7 (CH), 130.5 (C), 129.8 (CH), 129.6 (CH), 129.4 (CH), 129.34 (CH), 129.28 (CH), 129.2 (CH), 129.1 (CH), 129.0 (CH), 129.0 (C), 128.6 (C), 128.3 (CH), 128.2 (CH), 128.0 (CH), 127.9 (CH), 127.8 (CH), 127.75 (CH), 127.68 (CH), 127.6 (CH), 127.5 (CH), 127.3 (CH), 127.2 (CH), 127.0 (CH), 126.6 (CH), 126.3 (CH), 125.9 (CH), 125.6 (CH), 125.5 (CH), 115.5 (C), 96.7–96.5 (m, CH), 95.9–95.7 (m, CH), 93.7 (d, $^2J_{C\text{-}P}$ = 20.9 Hz, C), 91.1 (d, $^2J_{C\text{-}P}$ = 17.0 Hz, C), 89.2 (CH), 88.6 (CH), 80.5 (d, $^3J_{C\text{-}P}$ = 3.6 Hz, CH), 79.5 (d, $^3J_{C\text{-}P}$ = 4.5 Hz, CH), 75.0 (d, $^2J_{C\text{-}P}$ = 7.9 Hz, CH), 72.1 (CH_2), 69.1 (dd, $^3J_{C\text{-}P}$ = 8.8 Hz, CH_2), 58.0 (CH_3), 56.3 (CH), 55.2 (CH), 41.1 (d, $^1J_{C\text{-}P}$ = 30.2 Hz, CH), 27.7 (CH_3), 26.9 (CH_3); ^{31}P{^{1}H} NMR (202 MHz, CD_2Cl_2) δ 106.8 (dd, $^1J_{P\text{-}Rh}$ = 268.6 Hz, $^2J_{P\text{-}P}$ = 67.0 Hz, P–O), 26.2 (dd, $^1J_{P\text{-}Rh}$ = 149.5 Hz, $^2J_{P\text{-}P}$ = 67.0 Hz, P–C); HRMS

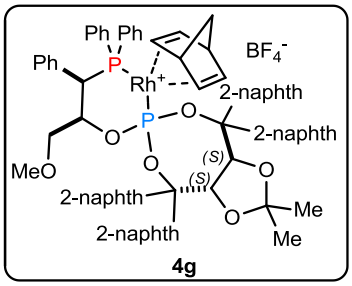

4g

(ESI$^+$) [calculated for $C_{76}H_{66}O_6P_2Rh$ $(M–BF_4)^+$ 1239.3384; observed 1239.3330].

[Rh(nbd)(3h)]BF_4 (4h): Rhodium complex **4h** was prepared by following the general procedure, starting from **3h** (124.0 mg, 0.119 mmol) and $[Rh(nbd)_2]BF_4$ (40.5 mg, 0.108 mmol). It was obtained as an orange powder (126.0 mg, 88% isolated yield). ^{1}H NMR (500 MHz, CD_2Cl_2) δ 8.46 (bs, 1H), 8.25–7.38 (m, 29H), 7.30–6.95 (m, 10 H), 6.42–6.25 (m, 5H), 6.16 (bs, 1H), 5.45 (bs, 1H), 5.20 (d, $^3J_{H-H}$ = 8.2 Hz, 1H), 4.84 (bs, 1H), 4.26 (bs, 1H), 4.24 (bs, 1H), 3.71–3.57 (m, 2H), 2.21 (s, 3H), 2.08–2.03 (m, 1H), 1.85–1.74 (m, 2H), 1.49 (s, 3H), 1.38–1.32 (m, 1H), 0.12 (s, 3H); ^{13}C{^{1}H} NMR (125 MHz, CD_2Cl_2) δ 142.2 (C), 142.1 (C), 141.1 (C), 137.9 (C), 137.8 (C), 137.2 (C), 136.5 (CH), 136.4 (CH), 133.9 (CH), 133.8 (CH), 133.6 (C), 133.41 (C), 133.37 (C), 133.31 (C), 133.28 (C), 132.9 (C), 132.8 (C), 132.6 (C), 132.2 (CH), 132.1 (CH), 131.4 (C), 131.3 (CH), 130.7 (CH), 130.6 (CH), 129.8 (C), 129.4 (C), 129.25 (CH), 129.20 (CH), 129.17 (CH), 129.12 (CH), 129.07 (CH), 128.9 (CH), 128.86 (CH), 128.77 (CH), 128.73 (CH), 128.67 (CH), 128.5 (C), 128.26 (CH), 128.16 (C), 128.10 (CH), 128.08 (CH), 128.06 (CH), 127.9 (CH), 127.8 (CH), 127.7 (CH), 127.6 (CH), 127.5 (CH), 127.31 (CH), 127.2 (CH), 127.0 (CH), 126.7 (CH), 126.2 (CH), 126.0 (CH), 125.8 (CH), 125.5 (CH), 114.6 (C), 97.2–96.7 (m, 2 x CH), 90.5 (d, $^2J_{C-P}$ = 5.6 Hz, C), 90.4 (d, $^2J_{C-P}$ = 4.3 Hz, C), 89.2–88.9 (m, CH), 86.4–86.2 (m, CH), 82.5 (d, $^3J_{C-P}$ = 3.8 Hz, CH), 79.3 (d, $^3J_{C-P}$ = 3.5 Hz, CH), 75.1 (d, $^2J_{C-P}$ = 6.1 Hz, CH), 72.2 (CH_2), 70.4 (dd, $^3J_{C-P}$ = 8.4 Hz, CH_2), 58.3 (CH_3), 56.4 (CH), 55.3 (CH), 42.2 (d, $^1J_{C-P}$ = 29.6 Hz, CH), 28.0 (CH_3), 25.8 (CH_3); ^{31}P{^{1}H} NMR (202 MHz, CD_2Cl_2) δ 109.6 (dd, $^1J_{P-Rh}$ = 264.3 Hz,$^2J_{P-P}$ = 72.8 Hz, P–O), 26.1

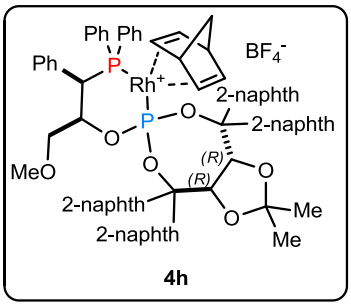

4h

(dd, $^{1}J_{P\text{-}Rh}$ = 147.7 Hz, $^{2}J_{P\text{-}P}$ = 72.8 Hz, P–C); HRMS (ESI^{+}) [calculated for $C_{69}H_{59}O_6P_2Rh$ $(M–BF_4)^{+}$1147.2758; observed 1147.2737].

[Rh(nbd)(3i)]BF_4 (4i): Rhodium complex **4i** was prepared by following the reported complexation procedure from the group,[18] the crude ligand **3i** (140.0 mg, 0.077 mmol, 58% pure by ^{31}P NMR) and $[Rh(nbd)_2]BF_4$ (40.5 mg, 0.108 mmol). It was obtained as an orange powder (87.0 mg, 88% isolated yield corresponds to Rh precursor). ^{1}H NMR (500 MHz, CD_2Cl_2) δ 8.52–8.48 (m, 1H), 8.44–8.34 (m, 2H), 8.29–8.22 (m, 3H), 8.15–6.72 (m, 35H), 6.54–6.33 (m, 4H), 6.06 (bs, 1H), 4.61 (bs, 1H), 4.57 (bs, 1H), 3.96 (bs, 2H), 3.67 (d, $^{2}J_{H\text{-}P}$ = 16.4 Hz, 1H), 3.19–3.06 (m, 1H), 2.98 (bs, 1H), 2.81 (s, 3H), 2.59 (dd, $^{2}J_{H\text{-}H}$ = $^{3}J_{H\text{-}H}$ = 9.5 Hz, 1H), 1.75–1.23 (m, 3H), –0.12 (s, 3H), –0.18 (s, 3H); ^{13}C{^{1}H} NMR (125 MHz, CD_2Cl_2) δ 141.0 (C), 140.9 (C), 139.3 (C), 136.5 (C), 136.4 (C), 135.7 (C), 135.1 (C), 135.0 (C), 134.4 (CH), 134.3 (CH), 133.4 (CH), 133.3 (CH), 133.2 (C), 132.40 (CH), 132.38 (CH), 132.2 (C), 132.15 (C), 132.07 (C), 132.05, 132.0 (CH), 131.71 (CH), 131.69 (CH), 131.5 (CH), 131.3 (C), 131.2 (CH), 130.3 (CH), 130.2 (CH), 130.1 (CH), 129.7 (CH), 129.1 (CH), 129.0 (CH), 128.9 (CH), 128.8 (CH), 128.6 (CH), 128.1 (CH), 127.8 (CH), 127.6 (CH), 127.2 (CH), 126.9 (CH), 126.8 (CH), 126.7 (CH), 126.6 (CH), 126.5 (CH), 126.23 (CH), 126.19 (CH), 126.1 (CH), 125.76 (CH), 125.73 (CH), 125.5 (CH), 125.3 (CH), 125.2 (CH), 125.1 (CH), 124.5 (CH), 116.7 (C), 98.4–98.1 (m, CH), 95.0 (d, $^{2}J_{C\text{-}P}$ = 19.7 Hz, C), 94.8–94.5 (m, CH), 92.0 (d, $^{2}J_{C\text{-}P}$ = 18.1 Hz, C), 89.8 (CH), 83.5 (CH), 80.8 (d, $^{3}J_{C\text{-}P}$ = 4.2 Hz, CH), 79.7 (d, $^{3}J_{C\text{-}P}$ = 4.3 Hz, CH), 74.9 (CH), 72.4 (CH_2), 68.8 (CH_2), 58.5 (CH_3), 55.6 (CH), 55.1 (CH), 41.3 (d, $^{1}J_{C\text{-}P}$ = 29.1 Hz, CH), 26.6 (CH_3), 26.3 (CH_3); ^{31}P{^{1}H} NMR (202 MHz, CD_2Cl_2) δ 106.8 (dd, $^{1}J_{Rh\text{-}P}$ = 269.3

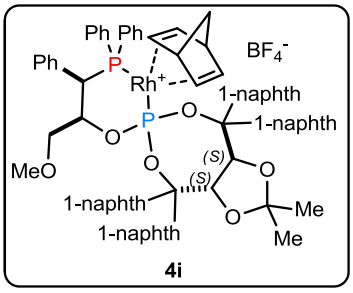

4i

Hz, $^{2}J_{P\text{-}P}$ = 68.0 Hz, P–O), 24.3 (dd, $^{1}J_{Rh\text{-}P}$ = 149.0 Hz, $^{2}J_{P\text{-}P}$ = 68.0 Hz, P–C); HRMS (ESI^{+}) [calculated for $C_{76}H_{66}O_6P_2Rh$ $(M–BF_4)^{+}$ 1239.3425; observed 1239.3384].

3.5.3 General procedure for the Rh-mediated asymmetric hydrogenation of substrates 5a–e

A solution of the required amount of $[Rh(nbd)_2]BF_4$ (1.0 mol %) and P–OP ligand **3c–i** (1.1 mol %) and the corresponding functionalized alkene **5a–e** (0.10 mmol) in anhydrous and degassed THF (0.50 mL) was prepared inside a glass vessel under N_2 atmosphere working in a glove box. In all cases, the molar concentration of a given substrate in the reaction medium was adjusted to 0.20 M. Once the reaction mixture had been loaded, the glass vessel was then placed into one of the positions of a steel autoclave reactor (HEL Cat-24 parallel pressure multireactor). The autoclave was purged three times with H_2 gas at 5 bar and finally, the autoclave was pressurized under 20 bar of H_2 gas. The reaction mixture was stirred at rt for 18 h (overnight reaction). The autoclave was then slowly depressurized. The reaction mixture was filtered through a short pad of SiO_2 and eluted with EtOAc (1.0 mL). The resulting solution was concentrated under vacuum and the conversion was determined by ^{1}H NMR. The enantiomeric excess was determined by GC or HPLC analysis on chiral stationary phases.

3.6 Supporting Information

3.6.1 NMR spectra of ligands 3c–i and rhodium complexes 4c–i:

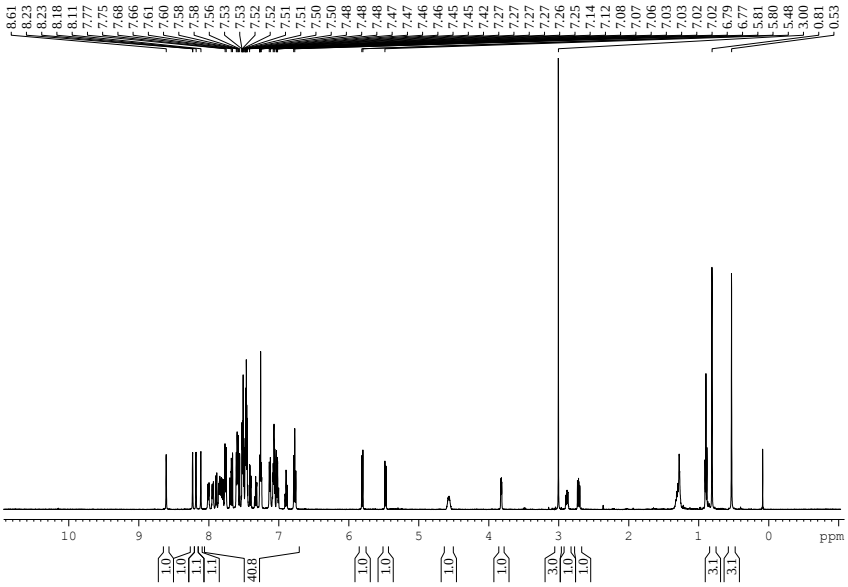

^{1}H NMR spectrum of **3g**

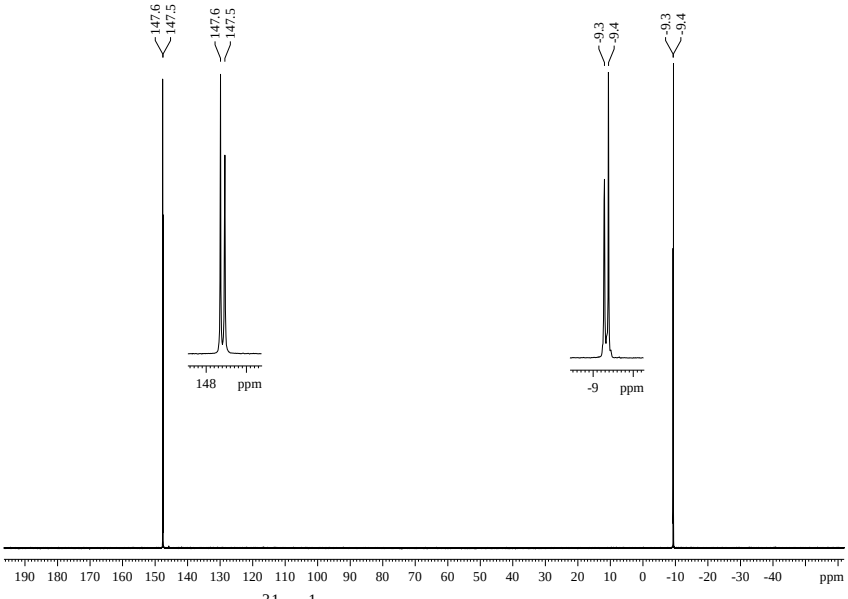

^{31}P{^{1}H} NMR spectrum of **3g**

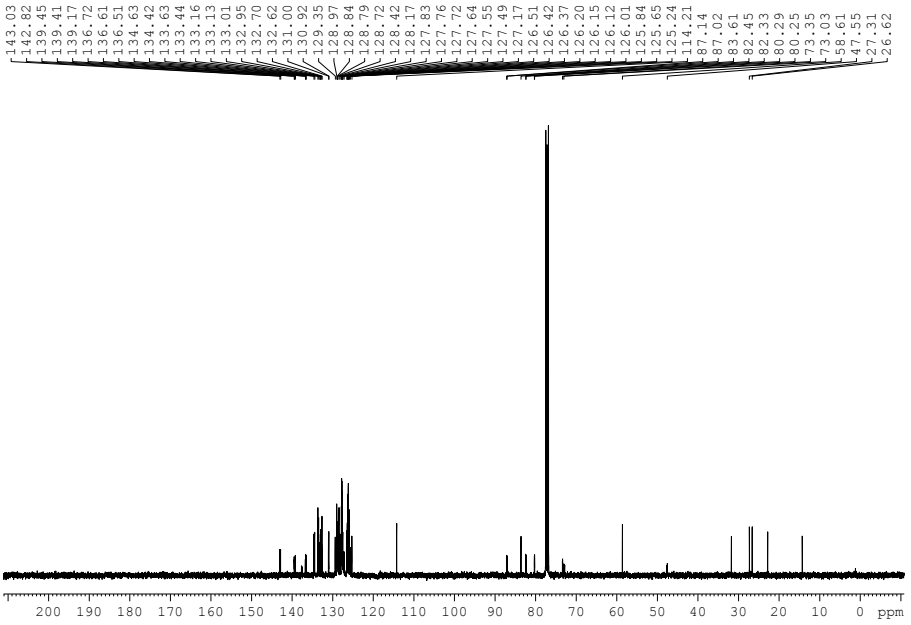

$^{13}C\{^{1}H\}$ NMR spectrum of **3g**

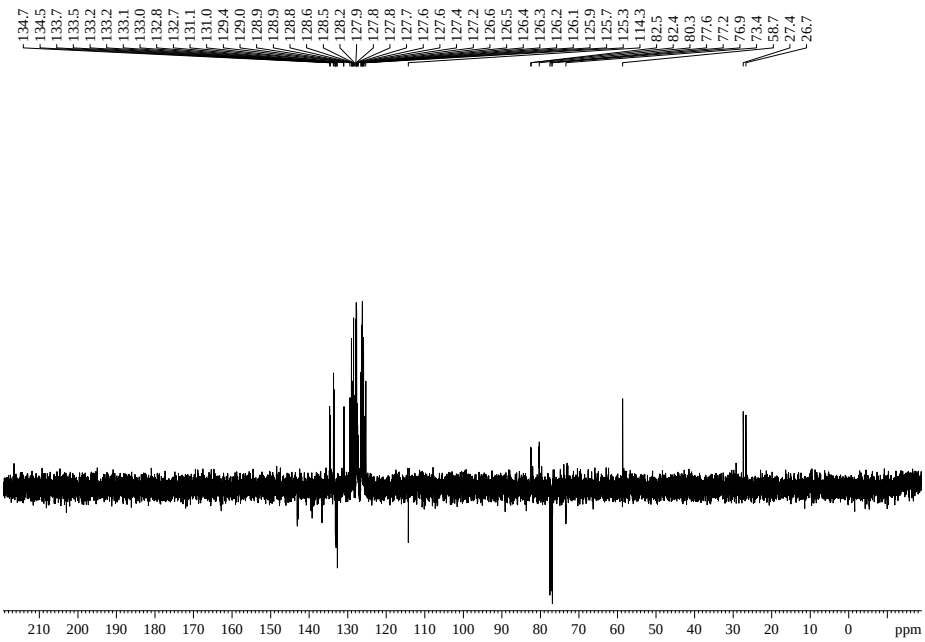

$^{13}C\{^{1}H\}$ Pendant NMR spectrum of **3g**

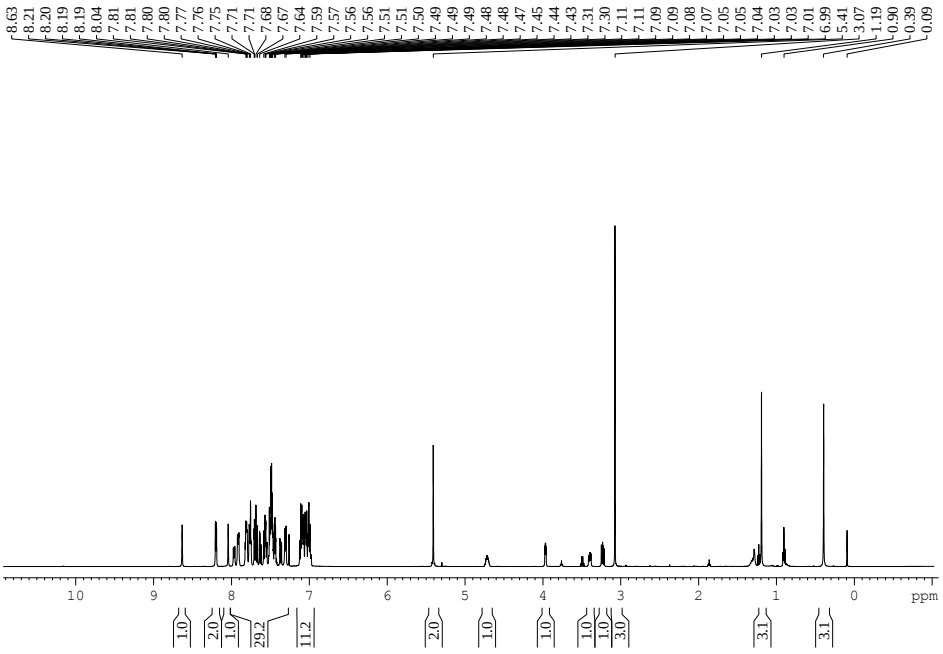

^{1}H NMR spectrum of **3h**

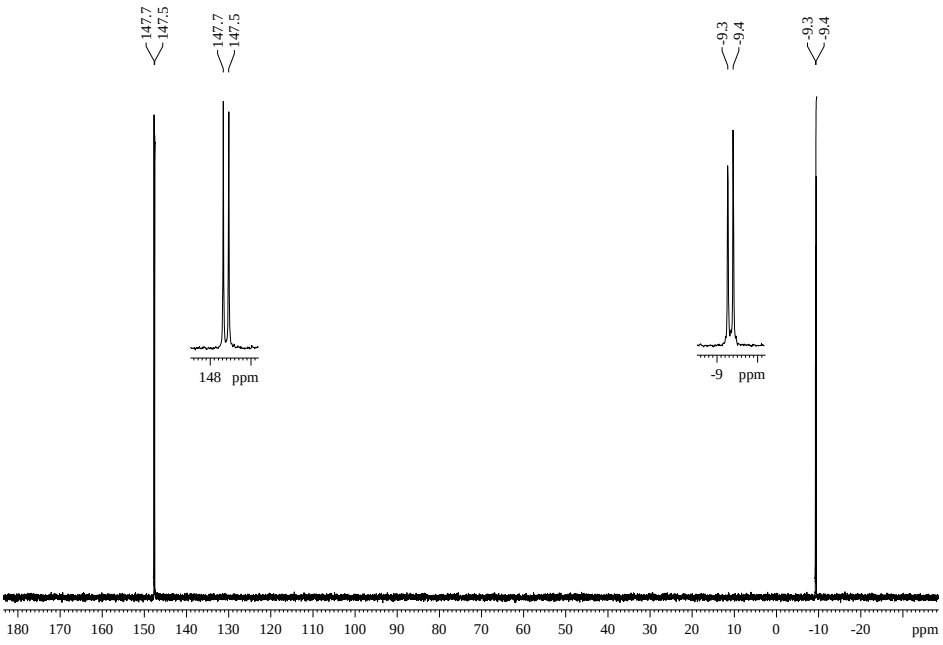

^{31}P{^{1}H} NMR spectrum of **3h**

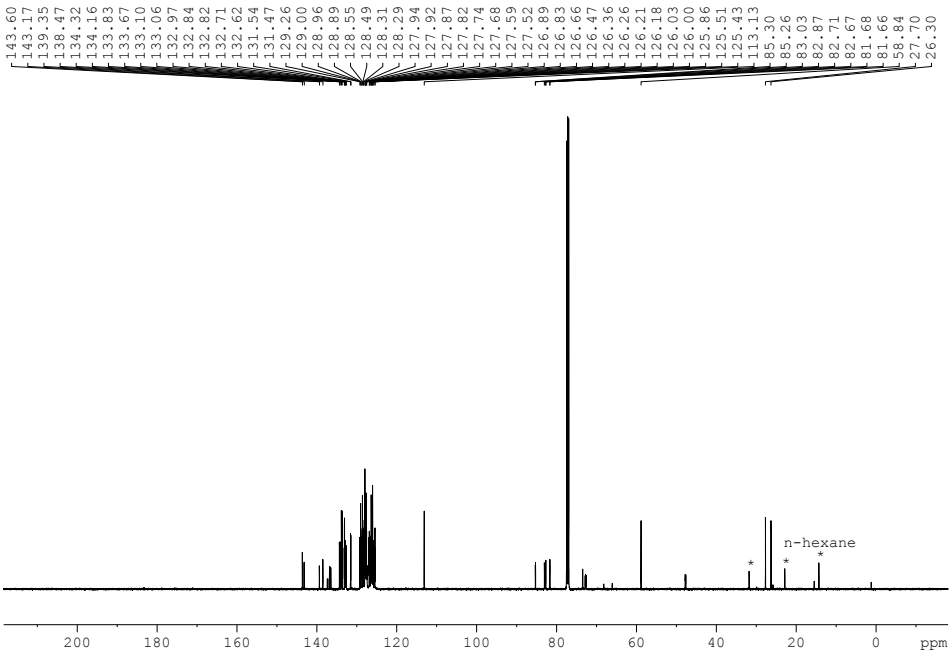

$^{13}C\{^{1}H\}$ NMR spectra of **3h**

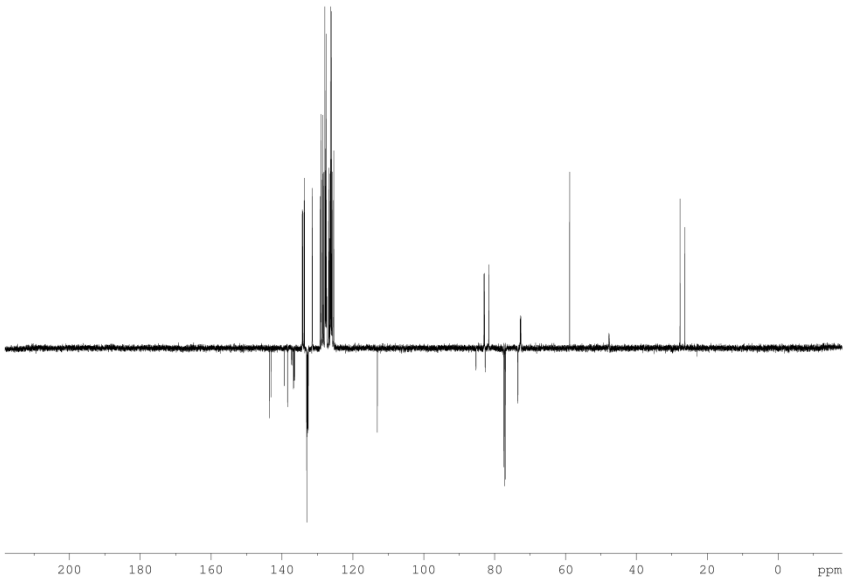

$^{13}C\{^{1}H\}$ Pendant NMR spectrum of **3h**

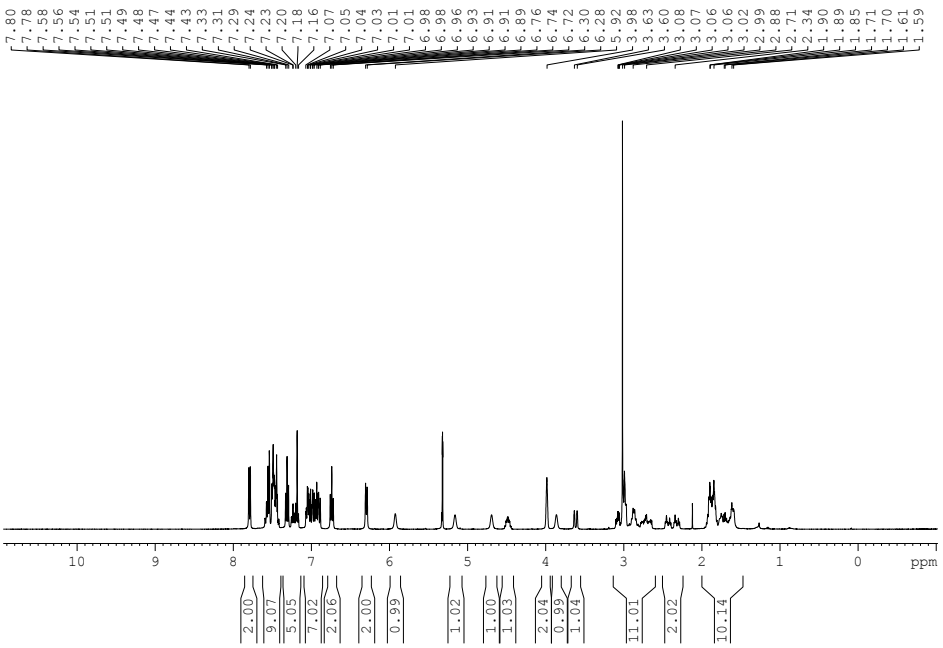

^{1}H NMR spectrum of **4d**

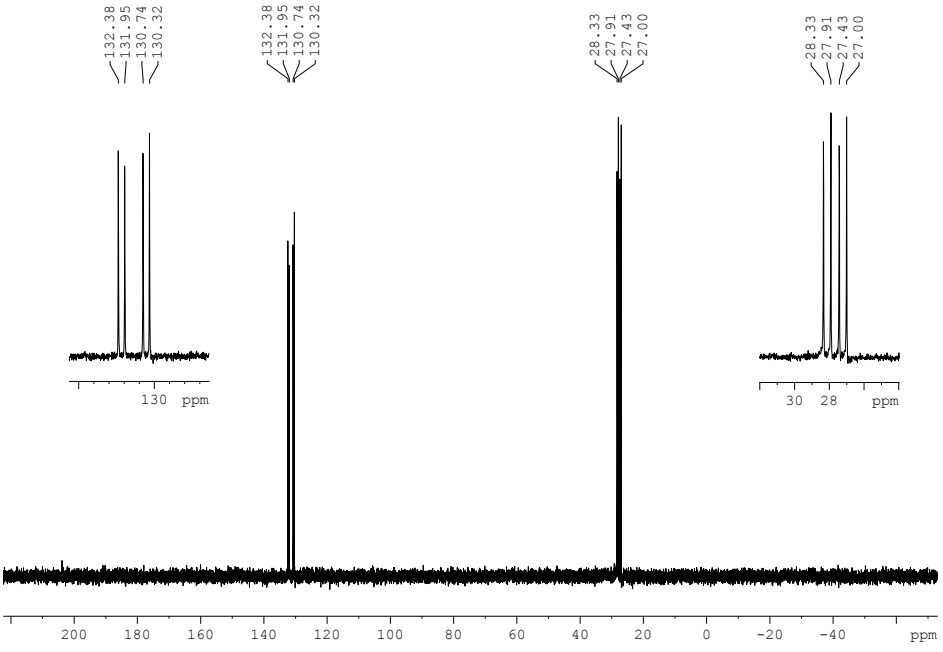

^{31}P{^{1}H} NMR spectrum of **4d**

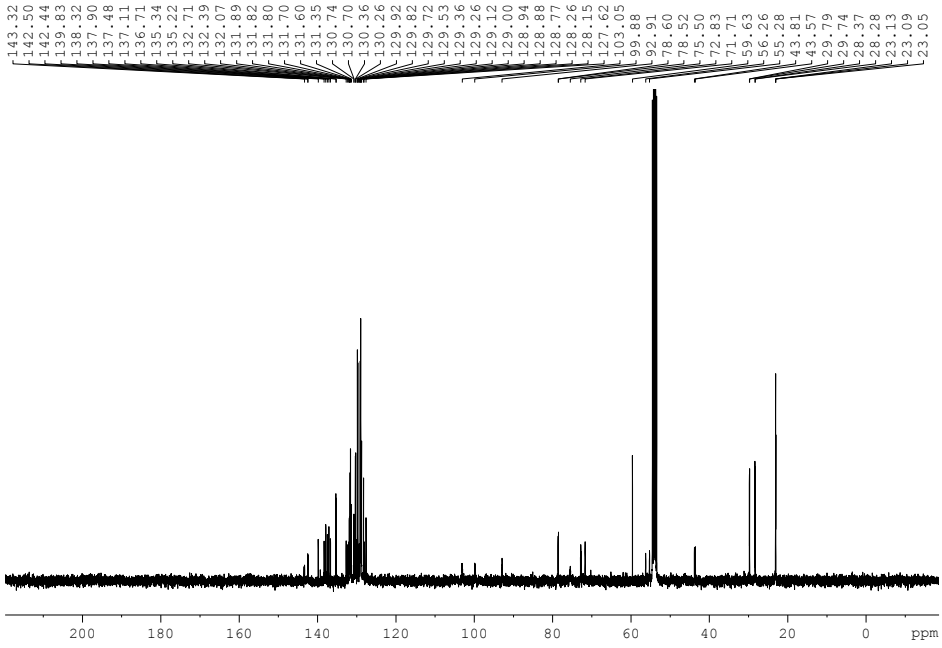

$^{13}C\{^{1}H\}$ NMR spectrum of **4d**

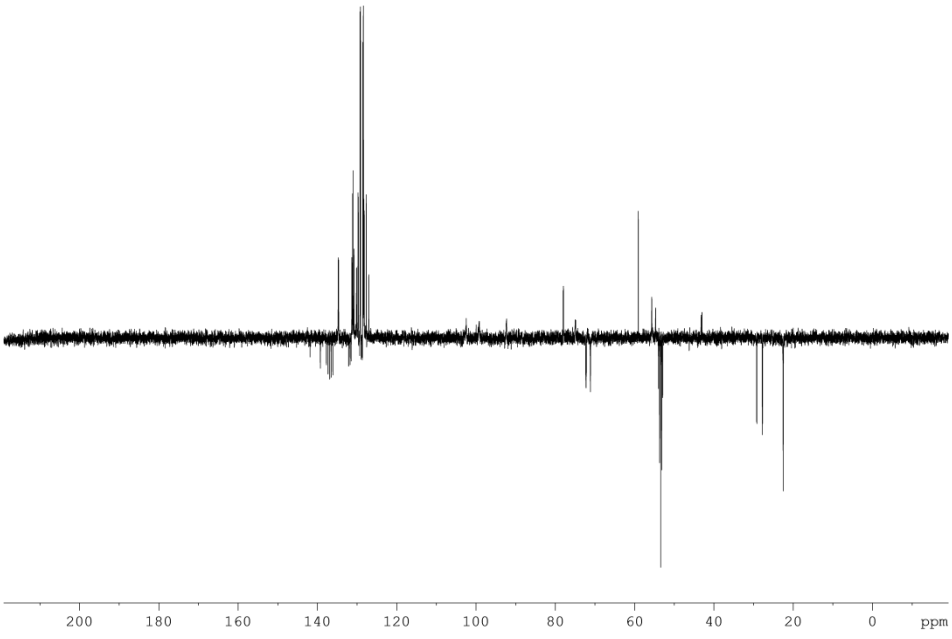

$^{13}C\{^{1}H\}$ Pendant NMR spectrum of **4d**

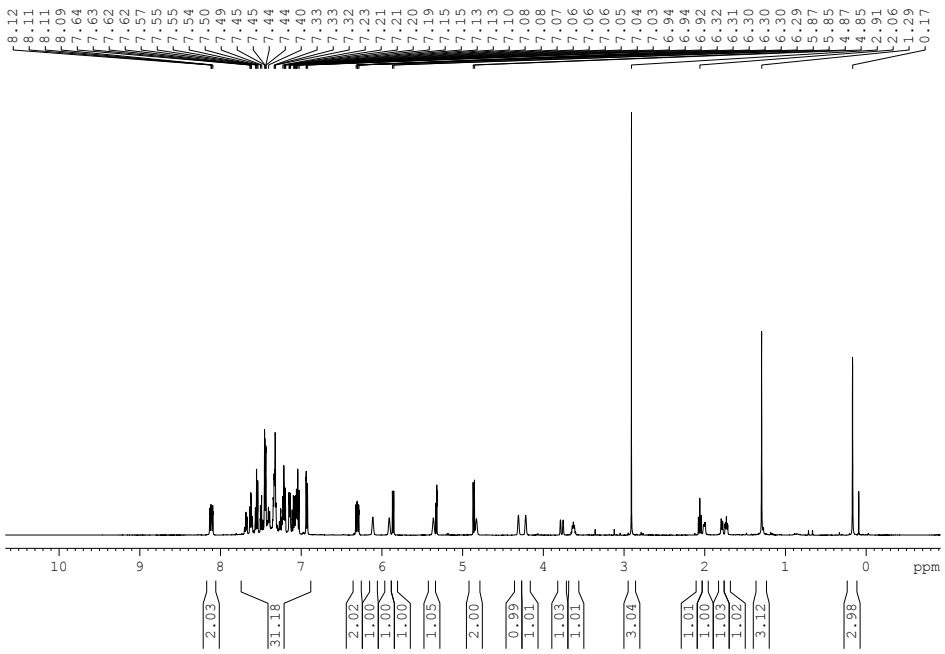

^{1}H NMR spectrum of **4f**

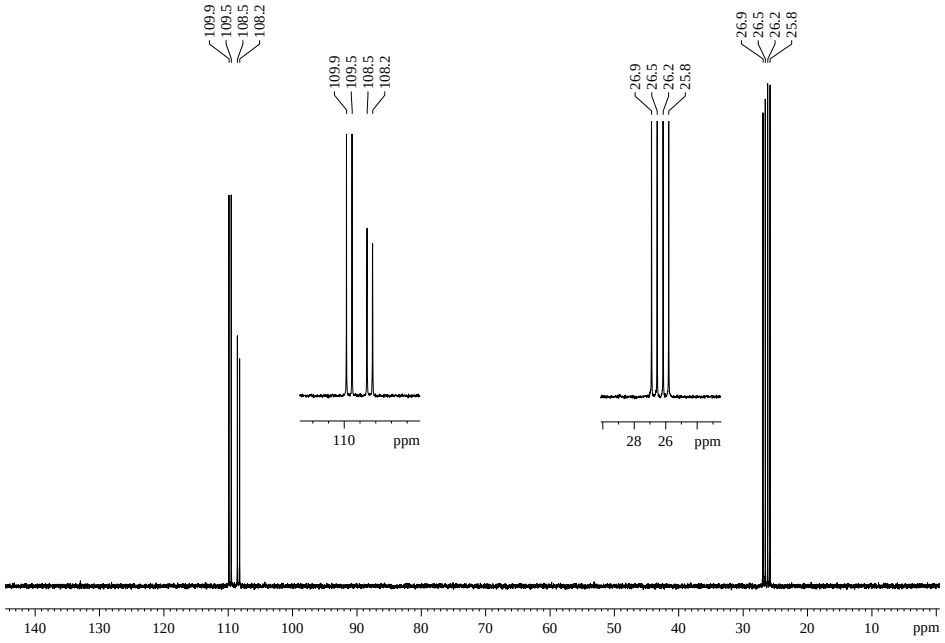

^{31}P{^{1}H} NMR spectrum of **4f**

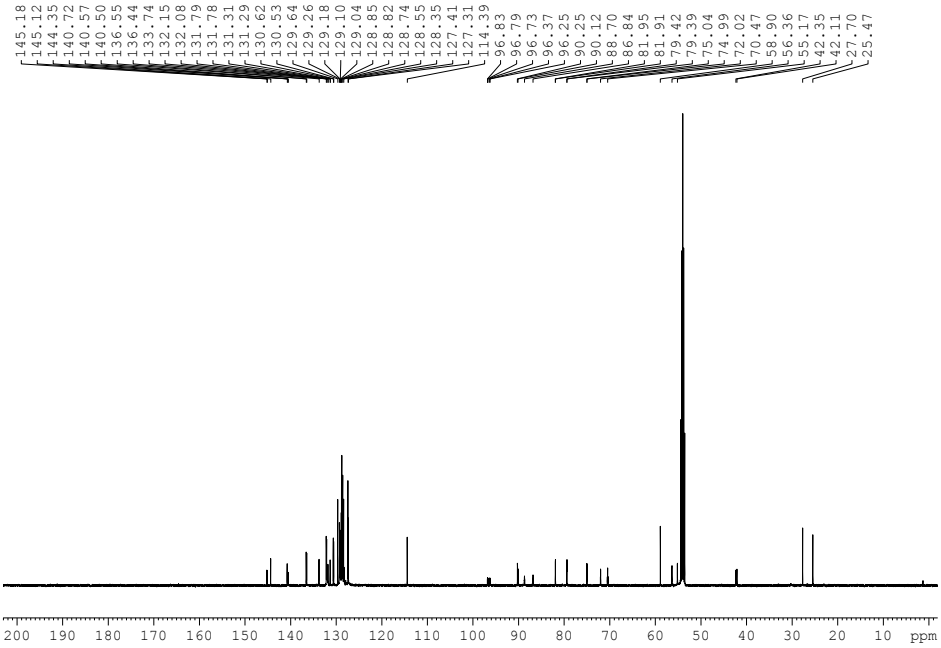

$^{13}C\{^{1}H\}$ NMR spectrum of **4f**

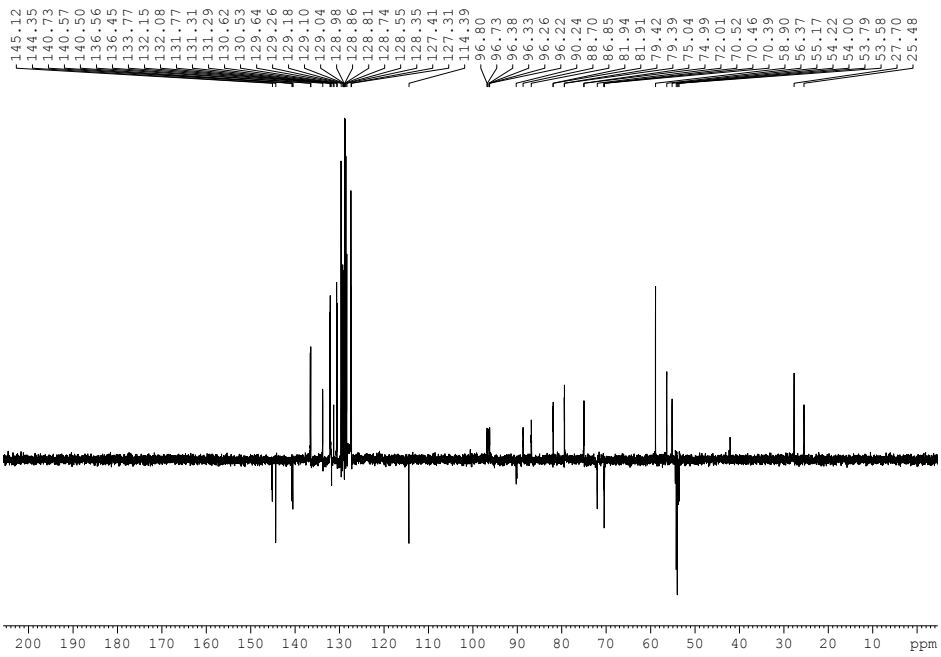

$^{13}C\{^{1}H\}$ Pendant NMR spectrum of **4f**

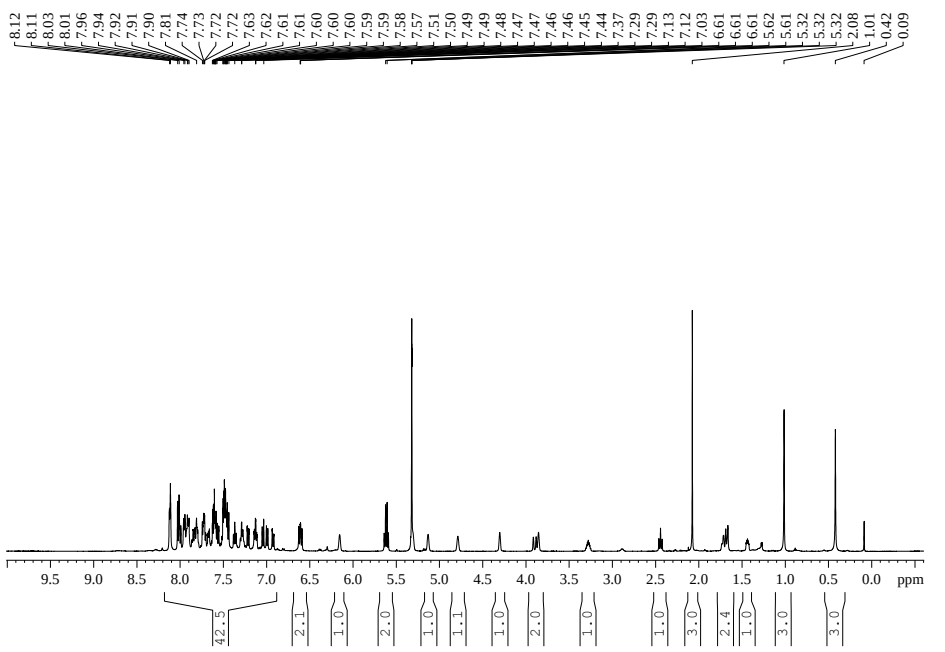

^{1}H NMR spectrum of **4g**

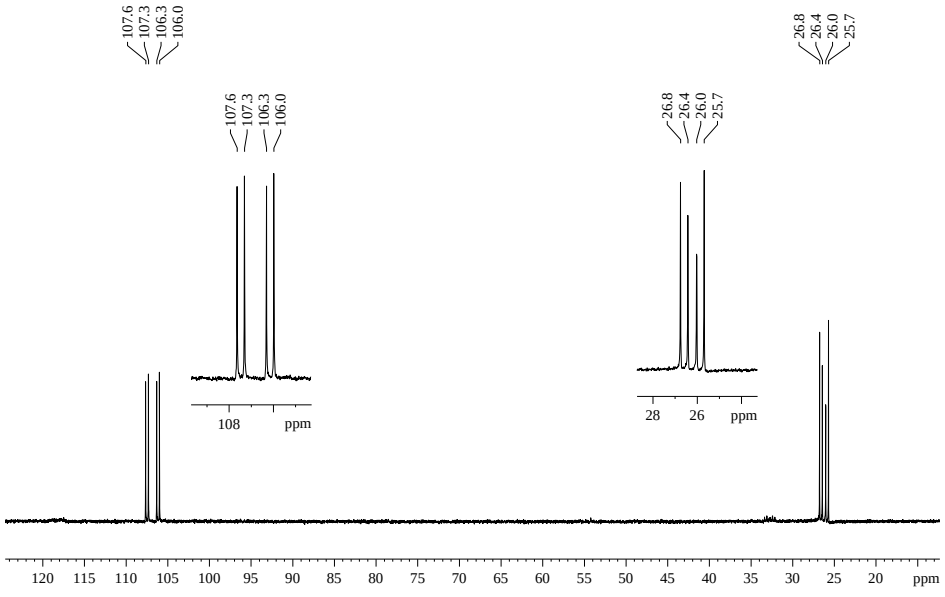

$^{31}P\{^{1}H\}$ NMR spectrum of **4g**

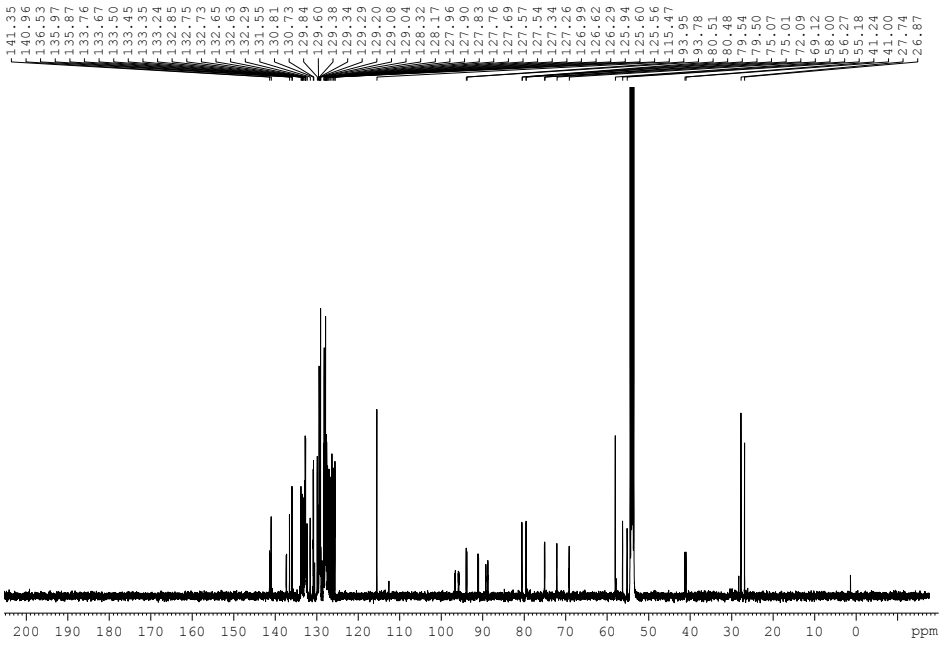

$^{13}C\{^{1}H\}$ NMR spectra of **4g**

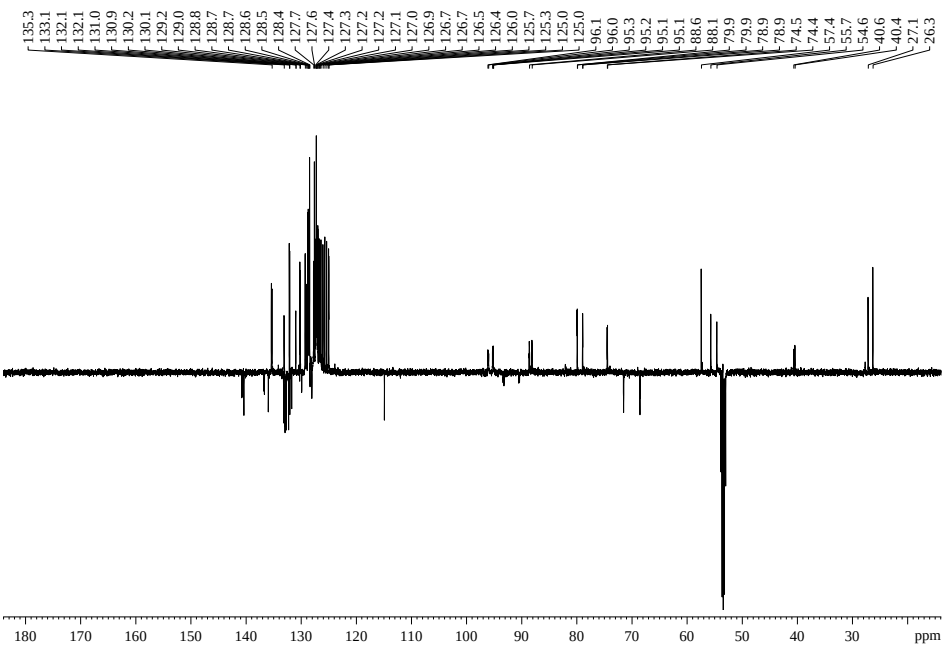

$^{13}C\{^{1}H\}$ Pendant NMR spectrum of **4g**

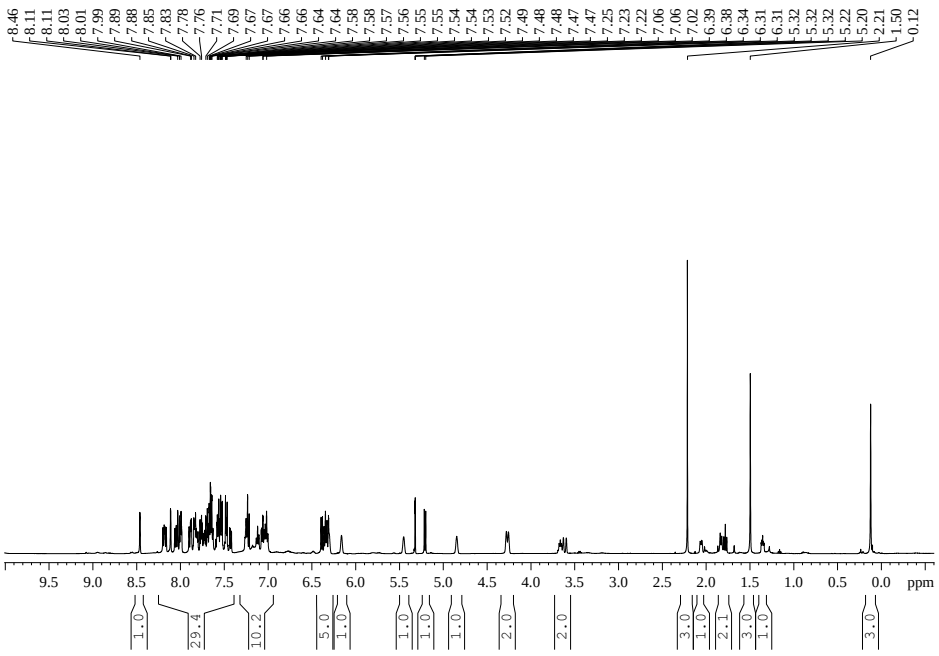

^{1}H NMR spectrum of **4h**

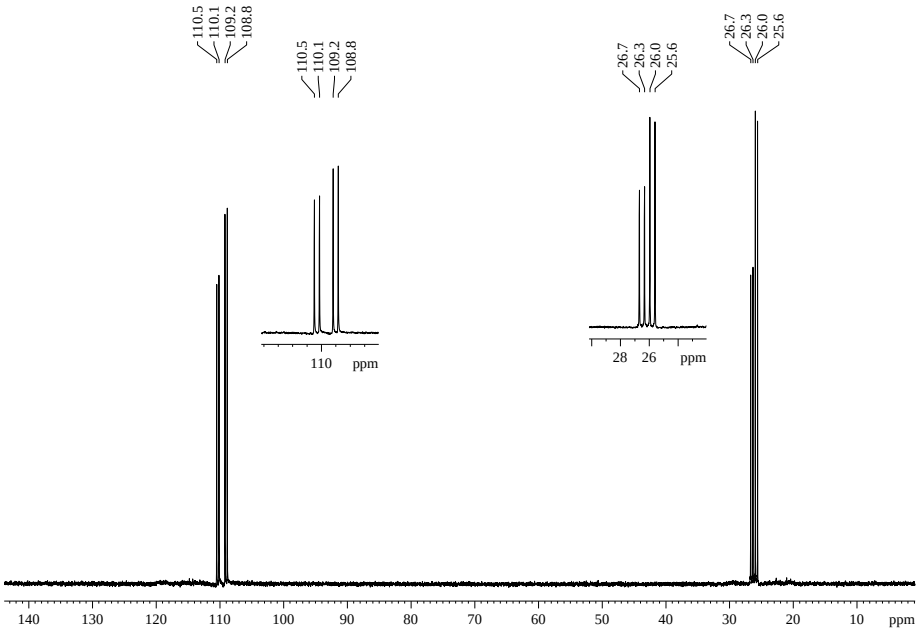

^{31}P{^{1}H} NMR spectrum of **4h**

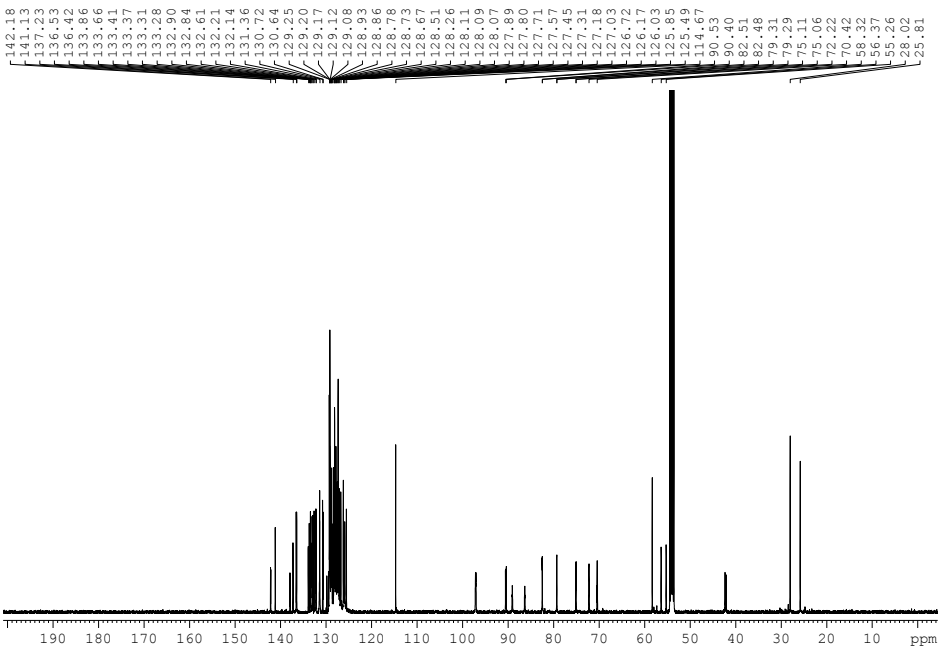

$^{13}C\{^{1}H\}$ NMR spectra of **4h**

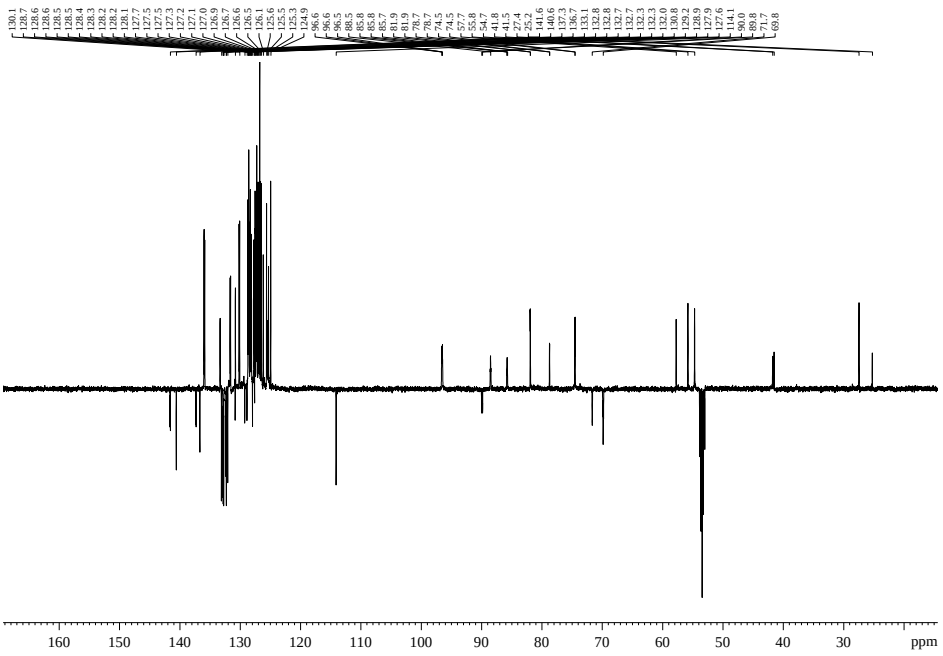

$^{13}C\{^{1}H\}$ Pendant NMR spectrum of **4h**

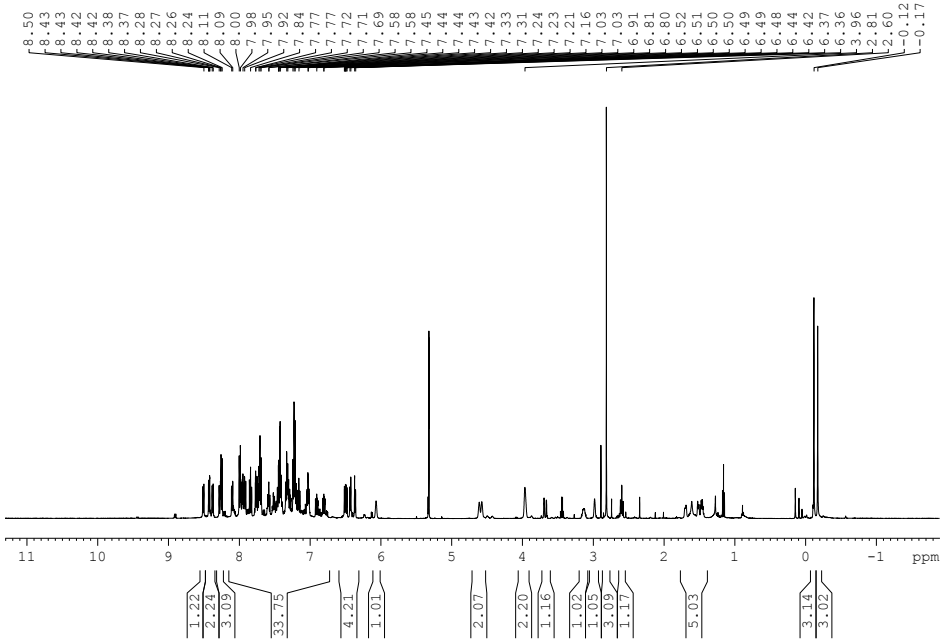

^{1}H NMR spectrum of **4i**

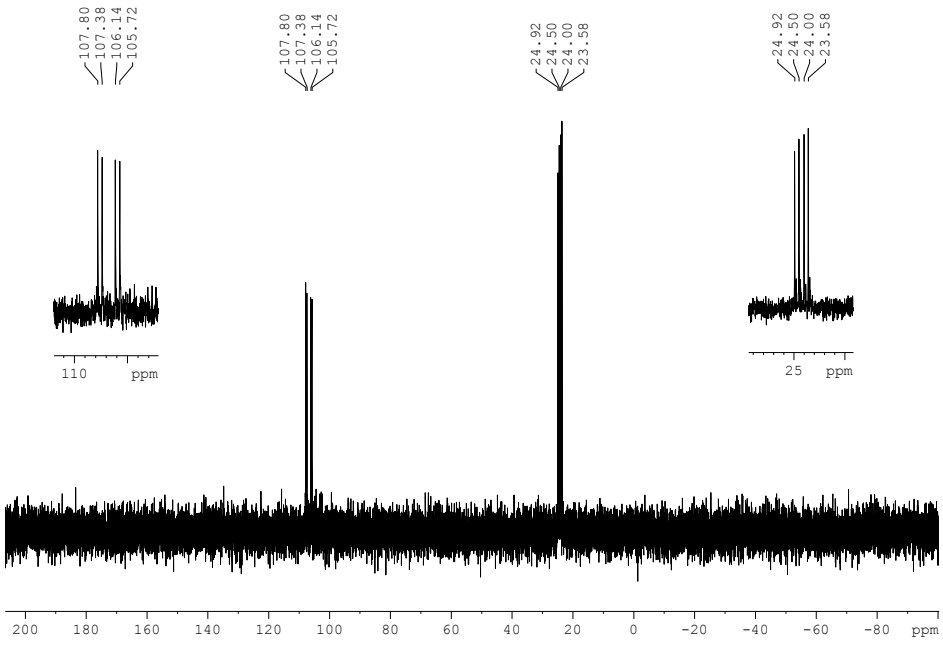

^{31}P{^{1}H} NMR spectrum of **4i**

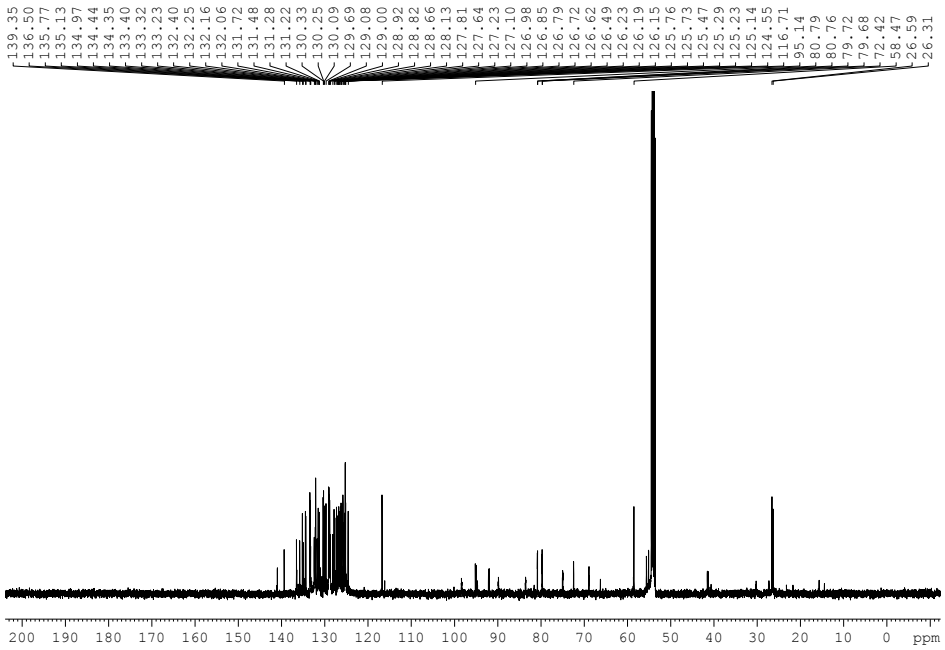

$^{13}C\{^{1}H\}$ NMR spectrum of **4i**

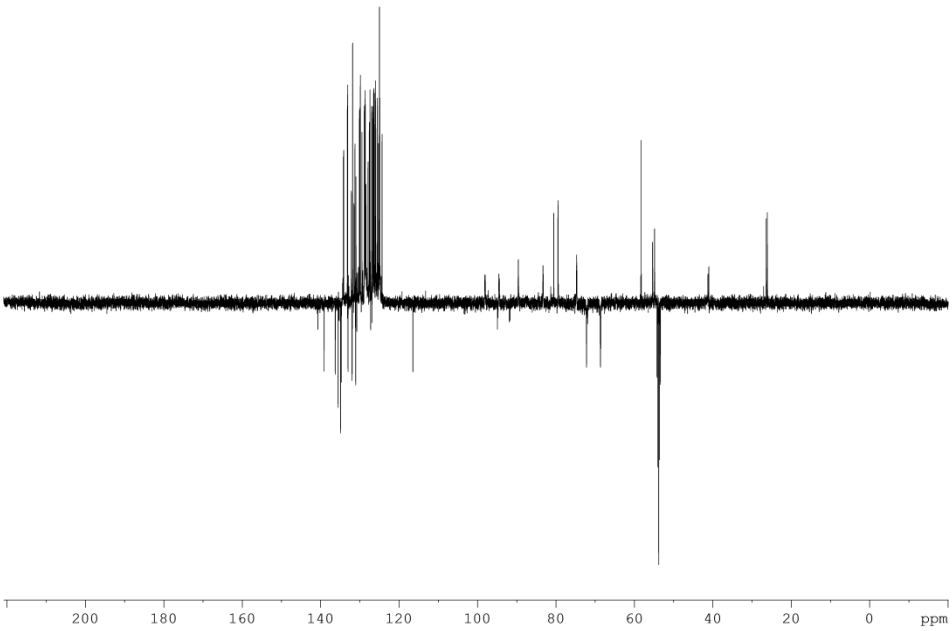

$^{13}C\{^{1}H\}$ Pendant NMR spectrum of **4i**

3.6.2 Determination of enantiomeric excesses:

Hydrogenation product of 5a:[19] GC conditions: Supelco Beta DEX™ 120 (30 m x 0.25 mm x 0.25 μm), isothermal 90 ºC, 15 psi He, t_1 (*S*) = 59.3 min, t_2 (*R*) = 61.9 min.

Hydrogenation product of 5b:[19] HPLC conditions: Daicel Chiralcel® OJ-H (25 cm x 0.46 cm), 93:7 *n*-hexane/2-propanol, 1.0 mL/min, 216 nm, t_1 (*R*) = 18.0 min, t_2 (*S*) = 29.1 min.

Hydrogenation product of 5c:[20] GC conditions: Supelco Beta DEX™ 225 (30 m x 0.25 mm x 0.25 μm), isothermal 70 ºC, 15 psi He, t_1 (*S*) = 46.4 min, t_2 (*R*) = 53.4 min.

Hydrogenation product of 5d:[20] HPLC conditions: Daicel Chiralcel ® AD-H (25 cm x 0.46 cm), 95:5 *n*-hexane/2-propanol, 1.0 mL/min, 210 nm, t_1 (*R*) = 10.0 min, t_2 (*S*) = 12.6 min.

Hydrogenation product of 5e:[21] HPLC conditions: Daicel Chiralcel® OD-H (25 cm x 0.46 cm), 99:1 *n*-hexane/2-propanol, 0.30 mL/min, 210 nm, t_1 (*R*) = 20.0 min, t_2 (*S*) = 21.8 min.

3.6.3 Single Crystal X-ray Structure Determinations:

Crystal preparation: Crystals of **4c, 4d, 4e, 4g** and **4i** were grown by slow diffusion of diethyl ether into solutions in dichloromethane. Crystals of **4f** were grown in toluene. The measured crystals were prepared under inert conditions immersed in perfluoropolyether as protecting oil for manipulation.

Data collection: Crystal structure determinations for samples **4f** was carried out using a Bruker-Nonius diffractometer equipped with an APEX II 4K CCD area detector, a FR591 rotating anode with MoK_α radiation, Montel mirrors as monochromator, a Kappa 4-axis goniometer and an Oxford Cryosystem plus low temperature device (T = -173 °C). Crystal structure determination for samples **4c**, **4d**, **4e**, **4g**, and **4i** were carried out using a Apex DUO Kappa 4-axis goniometer equipped with an APPEX 2 4K CCD area detector, a Microfocus Source E025 IuS using MoK_α radiation, Quazar MX multilayer Optics as monochromator and an Oxford Cryosystems low temperature device Cryostream 700 plus (T = -173 °C). Full-sphere data collection was used with ω and φ scans. *Programs used:* Data collection APEX-2,[22] data reduction Bruker Saint[23] V/.60A and absorption correction SADABS[24].

Structure Solution and Refinement: Crystal structure solution was achieved using the computer program SHELXT.[25] Visualization was performed with the program SHELXle.[26] Missing atoms were subsequently located from difference Fourier synthesis and added to the atom list. Least-squares refinement on F^2 using all measured intensities was carried out using the program SHELXL 2015.[27] All non-hydrogen atoms were refined including anisotropic displacement parameters. The crystal data parameters for **4c**, **4d**, **4e**, **4f**, **4g**, and **4i** are listed below.

X-ray Analyses:

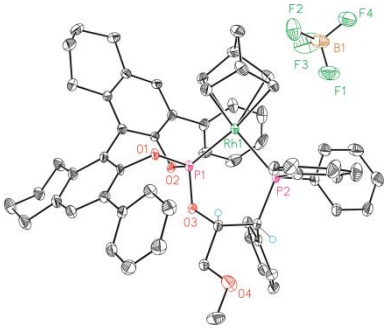

Figure 2. X-ray structure of the Rh-complex **4c** (ORTEP drawings showing thermal ellipsoids at 50% probability). Some H-atoms have been omitted for clarity. Selected bond lengths [Å] and angles [º]: Rh1-C55 = 2.170(6), Rh1-P1 = 2.1975(14), Rh1-C56 = 2.204(6), Rh1-C59 = 2.314(5), Rh1-C58 = 2.319(5), Rh1-P2 = 2.3286(14), P1-Rh1-P2 = 91.80(5).

Table 2. Crystal data and structure refinement for **4c**.

Empirical formula	$C_{65}H_{68}BF_4O_5P_2Rh$
Formula weight	1180.85
Temperature	100(2) K
Wavelength	0.71073 Å
Crystal system	Monoclinic
Space group	P2(1)
Unit cell dimensions	a = 9.691(2)Å α = 90°. b = 13.207(3)Å β = 95.977(5)°. c = 21.863(5)Å γ = 90°.
Volume	2783.1(10) $Å^3$
Z	2
Density (calculated)	1.409 Mg/m^3
Absorption coefficient	0.429 mm^{-1}
F(000)	1228
Crystal size	0.20 x 0.07 x 0.03 mm^3
Theta range for data collection	2.220 to 30.699°.
Index ranges	-7<=h<=13,-18<=k<=18,-30<=l<=30
Reflections collected	23737
Independent reflections	14822[R(int) = 0.0539]
Completeness to theta =30.699°	92.799995%
Absorption correction	Empirical
Max. and min. transmission	0.987 and 0.641
Refinement method	Full-matrix least-squares on F^2
Data / restraints / parameters	14822/ 8/ 706
Goodness-of-fit on F^2	1.008
Final R indices [I>2σ(I)]	R1 = 0.0534, wR2 = 0.1375
R indices (all data)	R1 = 0.0638, wR2 = 0.1434
Flack parameter	x = -0.03(3)
Largest diff. peak and hole	1.487 and -1.516 e.$Å^{-3}$

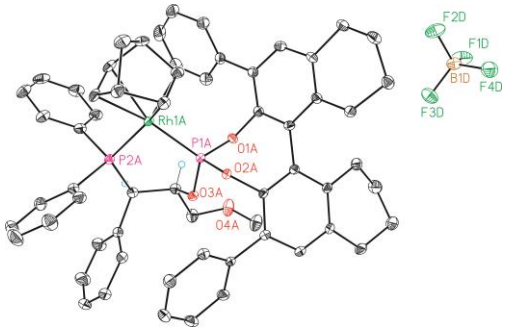

Figure 3. X-ray structure of the Rh-complex **4d** (ORTEP drawings showing thermal ellipsoids at 50% probability). Some H-atoms have been omitted for clarity. Selected bond lengths [Å] and angles [°]: Rh1A-P1A = 2.2015(8), Rh1A-P2A = 2.3218(9), Rh1A-C55A = 2.213(3), Rh1A-C56A = 2.178(3), Rh1A-C58A = 2.249(3), Rh1A-C59A = 2.260(3), P1A-Rh1A-P2A= 91.97(3).

Table 3. Crystal data and structure refinement for **4d**.

Empirical formula	$C_{62}H_{60}BCl_2F_4O_4P_2Rh$
Formula weight	1191.66
Temperature	100(2) K
Wavelength	0.71073 Å
Crystal system	Orthorhombic
Space group	P2(1)2(1)2(1)
Unit cell dimensions	a = 12.9435(8)Å α = 90° b = 20.8472(11)Å β = 90° c = 40.473(2)Å γ = 90°
Volume	10921.1(11) $Å^3$
Z	8
Density (calculated)	1.450 Mg/m^3
Absorption coefficient	0.532 mm^{-1}
F(000)	4912
Crystal size	0.04 x 0.04 x 0.01 mm^3
Theta range for data collection	1.006 to 32.429°.
Index ranges	-18<=h<=17, -21<=k<=30, -49<=l<=58
Reflections collected	93447
Independent reflections	34450[R(int) = 0.0398]
Completeness to theta =32.429°	91.2%
Absorption correction	Empirical
Max. and min. transmission	0.995 and 0.834
Refinement method	Full-matrix least-squares on F^2
Data / restraints / parameters	34450/ 312/ 1497
Goodness-of-fit on F^2	1.037
Final R indices [I>2σ(I)]	R1 = 0.0393, wR2 = 0.0840
R indices (all data)	R1 = 0.0484, wR2 = 0.0913
Flack parameter	x = -0.012(6)
Largest diff. peak and hole	1.087 and -0.795 e.$Å^{-3}$

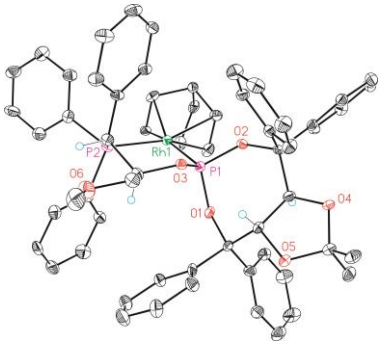

Figure 4. X-ray structure of the Rh-complex **4e** (ORTEP drawings showing thermal ellipsoids at 50% probability). Some H-atoms and the BF_4 counterion have been omitted for clarity. Selected bond lengths [Å] and angles [°]: Rh1-P1 = 2.2415(9), Rh1-P2 = 2.2880(9), Rh1-C54 = 2.242(3), Rh1-C55 = 2.212(3), Rh1-C57 = 2.217(3), Rh1-C58 = 2.225(3), P1-Rh1-P2 = 91.43(3).

Table 4. Crystal data and structure refinement for **4e**.

Empirical formula	$C_{62}H_{62}BCl_4F_4O_6P_2Rh$	
Formula weight	1296.58	
Temperature	100(2) K	
Wavelength	0.71073 Å	
Crystal system	Orthorhombic	
Space group	P2(1)2(1)2(1)	
Unit cell dimensions	a = 10.6530(6) Å	α = 90.00 °.
	b = 20.6711(11) Å	β = 90.00 °.
	c = 25.8364(13) Å	γ = 90.00 °.
Volume	5689.4(5) $Å^3$	
Z	4	
Density (calculated)	1.514 Mg/m^3	
Absorption coefficient	0.610 mm^{-1}	
F(000)	2664	
Crystal size	0.25 x 0.08 x 0.04 mm^3	
Theta range for data collection	1.58 to 29.61 °.	
Index ranges	-14<=h<=9, -27<=k<=28, -34<=l<=27	
Reflections collected	46051	
Independent reflections	15072 [R(int) = 0.0516]	
Completeness to theta = 29.61°	96.100006%	
Absorption correction	Empirical	
Max. and min. transmission	0.9760 and 0.8624	
Refinement method	Full-matrix least-squares on F^2	
Data / restraints / parameters	15072/0/724	
Goodness-of-fit on F^2	1.025	
Final R indices [I>2σ(I)]	R1 = 0.0451, wR2 = 0.1003	
R indices (all data)	R1 = 0.0570, wR2 = 0.1052	
Flack parameter	x =0.00(2)	
Largest diff. peak and hole	1.166 and -0.919 e.$Å^{-3}$	

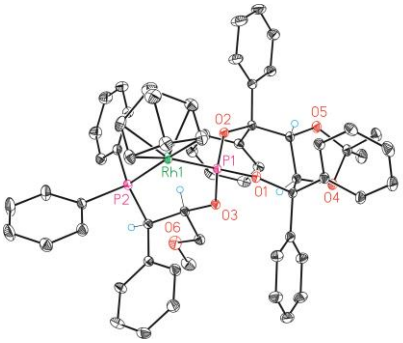

Figure 5. X-ray structure of the Rh-complex **4f** (ORTEP drawings showing thermal ellipsoids at 50% probability). Some H-atoms and the BF_4 counterion have been omitted for clarity. Selected bond lengths [Å] and angles [º]: Rh1-P1 = 2.2174(4), Rh1-P2 = 2.2966(4), Rh1-C1 = 2.2102(14), Rh1-C2 = 2.1941(14), Rh1-C4 = 2.2277(15), Rh1-C5 = 2.2580(15), P1-Rh1-P2 = 89.771(13)

Table 5. Crystal data and structure refinement for **4f**.

Empirical formula	$C_{74}H_{74}BF_4O_6P_2Rh$	
Formula weight	1310.99	
Temperature	100(2) K	
Wavelength	0.71073 Å	
Crystal system	Monoclinic	
Space group	P2(1)	
Unit cell dimensions	a = 10.7603(12) Å	α = 90.00°
	b = 23.165(3) Å	β = 98.810(2)°
	c = 12.7943(14) Å	γ = 90.00°
Volume	3151.6(6) $Å^3$	
Z	2	
Density (calculated)	1.382 Mg/m^3	
Absorption coefficient	0.388 mm^{-1}	
F(000)	1364	
Crystal size	0.25 x 0.12 x 0.08 mm^3	
Theta range for data collection	1.61 to 33.31°.	
Index ranges	-13<=h<=16,-35<=k<=35, -19<=l<=19	
Reflections collected	61802	
Independent reflections	23589 [R(int) = 0.0256]	
Completeness to theta = 33.31°	98.799995%	
Absorption correction	Empirical	
Max. and min. transmission	0.9696 and 0.9092	
Refinement method	Full-matrix least-squares on F^2	
Data / restraints / parameters	23589/160/862	
Goodness-of-fit on F^2	1.020	
Final R indices [I>2σ(I)]	R1 = 0.0313, wR2 = 0.0772	
R indices (all data)	R1 = 0.0337, wR2 = 0.0788	
Flack parameter	x = -0.030(8)	
Largest diff. peak and hole	1.300 and -0.441 e.$Å^{-3}$	

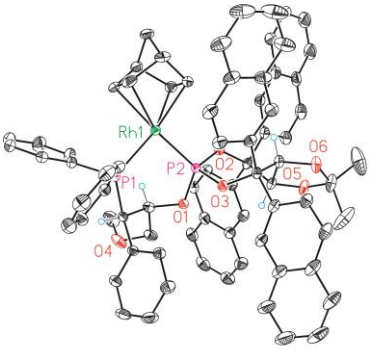

Figure 6. X-ray structure of the Rh-complex **4g** (ORTEP drawings showing thermal ellipsoids at 50% probability). Some H-atoms and the BF_4 counterion have been omitted for clarity. Selected bond lengths [Å] and angles [°]: Rh1-P1 = 2.3161(9), Rh1-P2 = 2.2132(8), Rh1-C1 = 2.270(3), Rh1-C2 = 2.277(3), Rh1-C4 = 2.200(3), Rh1-C5 = 2.190(3), P2-Rh1-P1 = 91.47(3).

Table 6. Crystal data and structure refinement for **4g**.

Empirical formula	$C_{92}H_{98}BF_4O_{14}P_2Rh$	
Formula weight	1679.36	
Temperature	100(2) K	
Wavelength	0.71073 Å	
Crystal system	Orthorhombic	
Space group	P2(1)2(1)2(1)	
Unit cell dimensions	a = 16.7357(4)Å	α = 90°
	b = 16.8281(5)Å	β = 90°
	c = 29.8634(10)Å	γ = 90°
Volume	8410.4(4) $Å^3$	
Z	4	
Density (calculated)	1.326 Mg/m^3	
Absorption coefficient	0.314 mm^{-1}	
F(000)	3512	
Crystal size	0.04 x 0.03 x 0.02 mm^3	
Theta range for data collection	1.364 to 31.007°.	
Index ranges	-20<=h<=23, -22<=k<=23, -43<=l<=24	
Reflections collected	89263	
Independent reflections	24092[R(int) = 0.0301]	
Completeness to theta = 31.007°	92.1%	
Absorption correction	Empirical	
Max. and min. transmission	0.994 and 0.919	
Refinement method	Full-matrix least-squares on F^2	
Data / restraints / parameters	24092/ 292/ 1094	
Goodness-of-fit on F^2	1.077	
Final R indices [I>2σ(I)]	R1 = 0.0404, wR2 = 0.1092	
R indices (all data)	R1 = 0.0479, wR2 = 0.1160	
Flack parameter	x = -0.021(4)	
Largest diff. peak and hole	0.884 and -0.740 e.$Å^{-3}$	

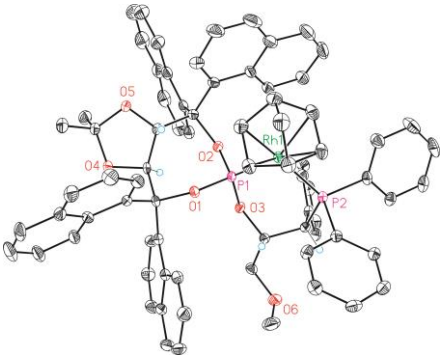

Figure 7. X-ray structure of the Rh-complex **4i** (ORTEP drawings showing thermal ellipsoids at 50% probability). Some H-atoms and the BF_4 counterion have been omitted for clarity. Selected bond lengths [Å] and angles [°]: Rh1-P1 = 2.2134(9), Rh1-P2 = 2.3235(10), Rh1-C1 = 2.200(4), Rh1-C2 = 2.152(4), Rh1-C4 = 2.273(4), Rh1-C5 = 2.332(4), P1-Rh1-P2 = 92.58(4).

Table 7. Crystal data and structure refinement for **4i**.

Empirical formula	$C_{78}H_{70}BCl_4F_4O_6P_2Rh$	
Formula weight	1496.80	
Temperature	100(2) K	
Wavelength	0.71073 Å	
Crystal system	Orthorhombic	
Space group	P2(1)2(1)2(1)	
Unit cell dimensions	a = 14.4966(7)Å	α = 90°
	b = 19.3144(9)Å	β = 90°
	c = 24.3219(10)Å	γ = 90°
Volume	6810.0(5) $Å^3$	
Z	4	
Density (calculated)	1.460 Mg/m^3	
Absorption coefficient	0.521 mm^{-1}	
F(000)	3080	
Crystal size	0.20 x 0.20 x 0.03 mm^3	
Theta range for data collection	1.635 to 28.976°	
Index ranges	-8<=h<=19,-26<=k<=26,-32<=l<=32	
Reflections collected	58133	
Independent reflections	18019[R(int) = 0.0427]	
Completeness to theta = 28.976°	99.7%	
Absorption correction	Empirical	
Max. and min. transmission	0.985 and 0.874	
Refinement method	Full-matrix least-squares on F^2	
Data / restraints / parameters	18019 / 112 / 899	
Goodness-of-fit on F^2	1.051	
Final R indices [I>2σ(I)]	R1 = 0.0400, wR2 = 0.0992	
R indices (all data)	R1 = 0.0492, wR2 = 0.1054	
Flack parameter	x = -0.044(8)	
Largest diff. peak and hole	0.909 and -0.937 e.$Å^{-3}$	

3.6.4 Selected GC/HPLC data from catalytic experiments:

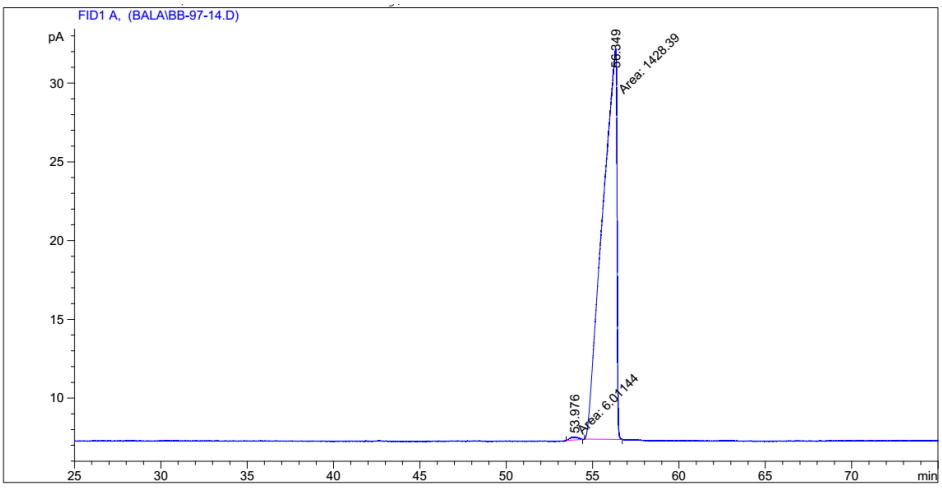


```
=====================================================================
                        Area Percent Report
=====================================================================

Sorted By             :      Signal
Multiplier            :      1.0000
Dilution              :      1.0000
Use Multiplier & Dilution Factor with ISTDs


Signal 1: FID1 A,

Peak RetTime Type  Width     Area      Height     Area
  #   [min]        [min]   [pA*s]      [pA]         %
----|-------|----|-------|----------|----------|--------|
   1  53.976 MM    0.5375    6.01144 1.86404e-1  0.41909
   2  56.349 MM    0.9619 1428.39124   24.74978 99.58091
```

HPLC trace of product **6a**

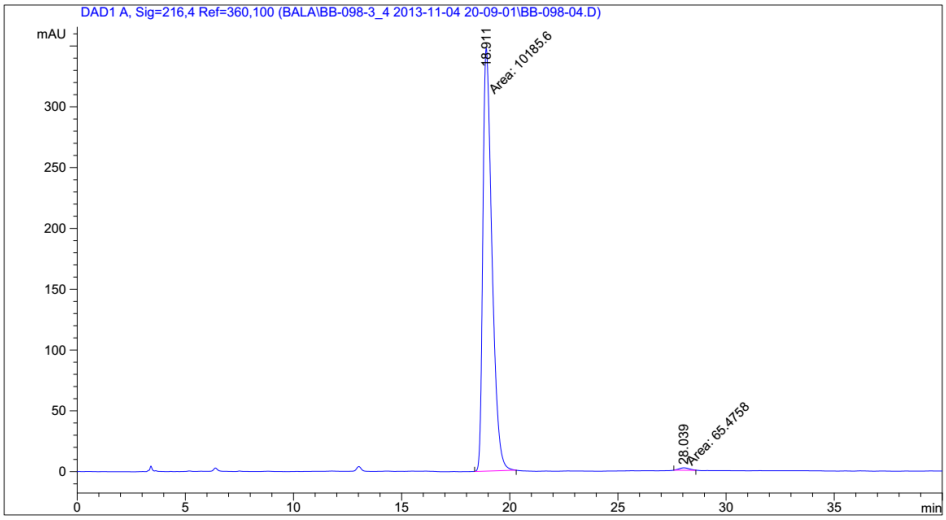


```
================================================================================
                          Area Percent Report
================================================================================

Sorted By             :      Signal
Multiplier            :      1.0000
Dilution              :      1.0000
Use Multiplier & Dilution Factor with ISTDs


Signal 1: DAD1 A, Sig=216,4 Ref=360,100

Peak RetTime Type  Width     Area      Height     Area
  #   [min]        [min]   [mAU*s]     [mAU]       %
----|-------|----|-------|----------|----------|--------|
   1  18.911 MM    0.4881 1.01856e4   347.79736  99.3613
   2  28.039 MM    0.5595   65.47579    1.95040   0.6387
```

HPLC trace of product **6b**

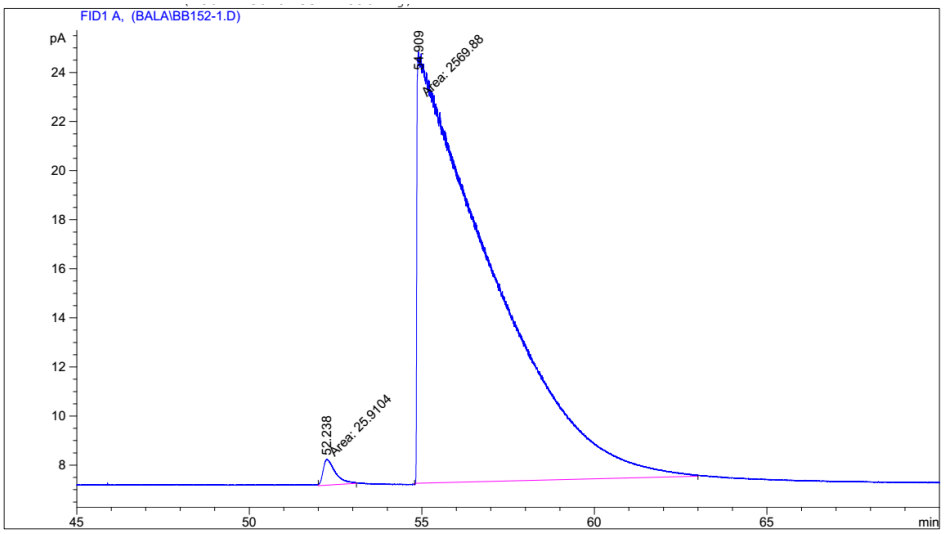


```
======================================================================
                        Area Percent Report
======================================================================

Sorted By             :      Signal
Multiplier            :      1.0000
Dilution              :      1.0000
Use Multiplier & Dilution Factor with ISTDs


Signal 1: FID1 A,

Peak RetTime Type  Width     Area      Height     Area
  #   [min]        [min]   [pA*s]      [pA]        %
----|-------|----|-------|----------|----------|-------|
   1  52.238 MM    0.4094   25.91044    1.05470  0.99817
   2  54.909 MM    2.4389 2569.87793   17.56209 99.00183
```

HPLC trace of product **6c**

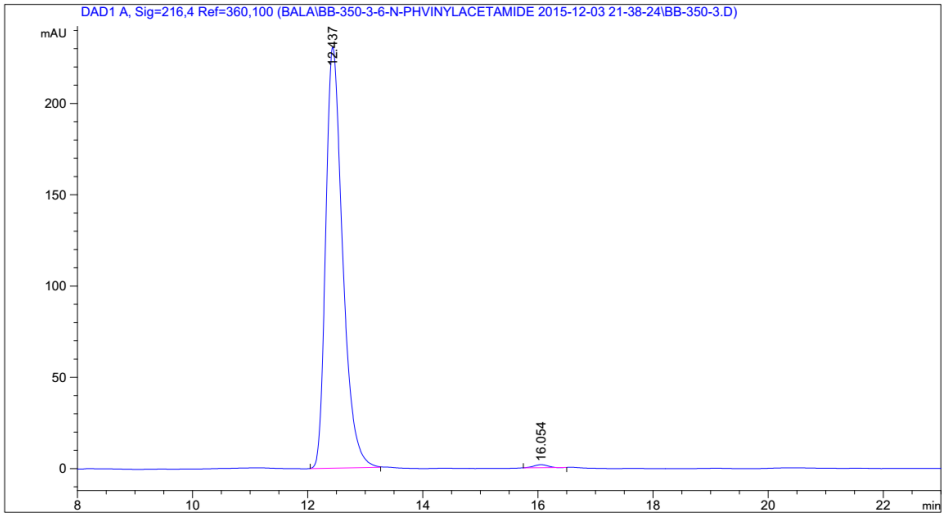


```
=====================================================================
                      Area Percent Report
=====================================================================

Sorted By             :      Signal
Multiplier:                   :      1.0000
Dilution:                     :      1.0000
Use Multiplier & Dilution Factor with ISTDs


Signal 1: DAD1 A, Sig=216,4 Ref=360,100

Peak RetTime Type  Width     Area      Height     Area
  #   [min]        [min]   [mAU*s]     [mAU]       %
----|-------|----|-------|----------|----------|--------|
   1  12.437 BB    0.3098 4700.19775  230.56055  99.4058
   2  16.054 BB    0.2625   28.09401    1.65093   0.5942
```

HPLC trace of product **6d**

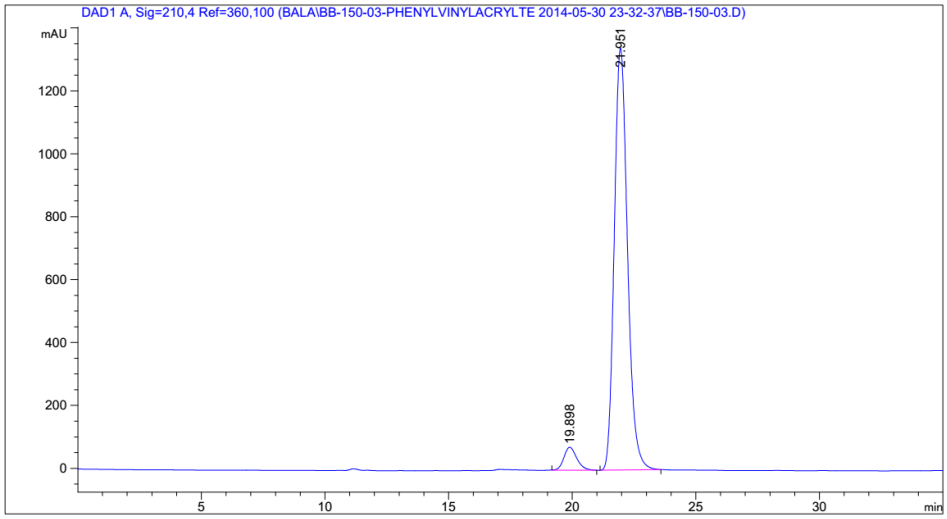


```
=====================================================================
                    Area Percent Report
=====================================================================

Sorted By             :      Signal
Multiplier:                   :      1.0000
Dilution:                     :      1.0000
Use Multiplier & Dilution Factor with ISTDs


Signal 1: DAD1 A, Sig=210,4 Ref=360,100

Peak RetTime Type  Width     Area      Height     Area
  #   [min]        [min]   [mAU*s]     [mAU]       %
----|-------|----|-------|----------|----------|--------|
   1  19.898 BB    0.5564 2656.14185   73.01383   5.0530
   2  21.951 BB    0.5721 4.99091e4  1341.35522  94.9470
```

HPLC trace of product **6e**

3.7 References

(1) For recent reviews, see for example: (a) *Phosphorus Ligands in Asymmetric Catalysis*, 1st ed.; Börner, A., Ed.; Wiley-VCH: Weinheim, 2008; Vol. I-III. (b) Teichert, J. F.; Feringa, B. L. *Angew. Chem., Int. Ed.* **2010**, *49*, 2486. (c) Gladiali, S.; Alberico, E.; Junge, K.; Beller, M. *Chem. Soc. Rev.* **2011**, *40*, 3744.

(2) See for example: (a) Shang, G.; Li, W.; Zhang, X. In *Transition Metal-Catalyzed Homogeneous Asymmetric Hydrogenation*; John Wiley & Sons, Inc.:NJ, USA, 2010; pp 343-436. (b) Fleury-Bregeot, N.; de la Fuente, V.; Castillón, S.; Claver, C. *ChemCatChem* **2010**, *2*, 1346. (c) Xie, J.-H.; Zhu, S.-F.; Zhou, Q.-L. *Chem. Rev.* **2011**, *111*, 1713. (d) Imamoto, T. In *Asymmetric Hydrogenation*; InTech: Japan, 2012; pp 3. (e) Etayo, P.; Vidal-Ferran, A. *Chem. Soc. Rev.* **2013**, *42*, 728.

(3) *Comprehensive Asymmetric Catalysis*; Jacobsen, E. N., Pfaltz, A., Yamamoto, H., Eds.; Springer: Heidelberg, 1999; Vols I–III.

(4) Yoon, T. P.; Jacobsen, E. N. *Science* **2003**, *299*, 1691.

(5) (a) Pfaltz, A.; Drury, W. J., III *Proc. Natl. Acad. Sci. U. S. A.* **2004**, *101*, 5723. (b) Atkinson, R. C. J.; Gibson, V. C.; Long, N. J. *Chem. Soc. Rev.* **2004**, *33*, 313.

(6) Fernández-Pérez, H.; Etayo, P.; Panossian, A.; Vidal-Ferran, A. *Chem. Rev.* **2011**, *111*, 2119.

(7) (a) Klosin, J.; Landis, C. R. *Acc. Chem. Res.* **2007**, *40*, 1251. (b) Claver, C.; Godard, C.; Ruiz, A.; Pàmies, O.; Diéguez, M. *Enantioselective Carbonylation Reactions*. In *Modern Carbonylation Reactions*; Wiley-VCH Verlag GmbH & Co. KGaA: 2008; pp 65. (c) Gual, A.; Godard, C.; Castillón, S.; Claver, C. *Tetrahedron: Asymmetry* **2010**, *21*, 1135. (d) Perandones Bernabe, F.; Godard, C.; Claver, C. *Asymmetric Hydroformylation*. In *Top. Curr. Chem.*, 2013; Vol. 342, pp 79. (e) Chikkali, S. H.; van der Vlugt, J. I.; Reek, J. N. H. *Coord. Chem. Rev.* **2014**, *262*, 1.

(8) Panossian, A.; Fernández-Pérez, H.; Popa, D.; Vidal-Ferran, A. *Tetrahedron: Asymmetry* **2010**, *21*, 2281.

(9) (a) Núñez-Rico, J. L.; Fernández-Pérez, H.; Benet-Buchholz, J.; Vidal-Ferran, A. *Organometallics* **2010**, *29*, 6627. (b) Núñez-Rico, J. L.; Vidal-Ferran, A. *Org. Lett.* **2013**, *15*, 2066. (c) Núñez-Rico, J. L.; Fernández-Pérez, H.; Vidal-Ferran, A. *Green Chem.* **2014**, *16*, 1153.

(10) (a) Fernández-Pérez, H.; Pericàs, M. A.; Vidal-Ferran, A. *Adv. Synth. Catal.* **2008**, *350*, 1984. (b) Donald, S. M. A.; Vidal-Ferran, A.; Maseras, F. *Can. J. Chem.* **2009**, *87*, 1273. (c) Fernández-Pérez, H.; Donald, S. M. A.; Munslow, I. J.; Benet-Buchholz, J.; Maseras, F.; Vidal-Ferran, A. *Chem. –Eur. J.* **2010**, *16*, 6495. (d) Fernández-Pérez, H.; Etayo, P.; Núñez-Rico, J. L.; Vidal-Ferran, A. *Chim. Oggi* **2010**, *28*, XXVI. (e) Etayo, P.; Núñez-Rico, J. L.; Vidal-Ferran, A. *Organometallics* **2011**, *30*, 6718. (f) Núñez-Rico, J. L.; Etayo, P.; Fernández-Pérez, H.; Vidal-Ferran, A. *Adv. Synth. Catal.* **2012**, *354*, 3025. (g) Fernández-Pérez, H.; Benet-Buchholz, J.; Vidal-Ferran, A. *Org. Lett.* **2013**, *15*, 3634. (h)

Fernández-Pérez, H.; Benet-Buchholz, J.; Vidal-Ferran, A. *Chem. –Eur. J.* **2014**, *20*, 15375. (i) Lao, J. R.; Benet-Buchholz, J.; Vidal-Ferran, A. *Organometallics* **2014**, *33*, 2960.

(11) Lao, J. R.; Fernández-Pérez, H.; Vidal-Ferran, A. *Org. Lett.* **2015**, *17*, 4114.

(12) Fernández-Pérez, H.; Lao, J. R.; Vidal-Ferran, A. *Org. Lett.* **2016**, *18*, 2836.

(13) The preparation of ligands **3a–d** employing this synthetic strategy has already been reported by the group (see references 10c and 11. Rhodium-mediated asymmetric hydrogenations of the standard model substrates employing ligands **3a–b** have also been previously reported (see ref. 10c, 10f).

(14) It has been reported that *O*-phosphorylations employing the chlorophosphite derived from ((4*S*,5*S*)-2,2-dimethyl-1,3-dioxolane-4,5-diyl)bis(diphenyl-methanol) are not so favored as those involving chlorophosphites from [1,1'-biaryl]-2,2'-diols and require a large excess of base (see for example: Kranich, R.; Eis, K.; Geis, O.; Mühle, S.; Bats, J. W.; Schmalz, H.-G. *Chem. –Eur. J.* **2000**, *6*, 2874.).

(15) The preparation of the rhodium complexes derived from ligands **3a** and **3b** and $[Rh(nbd)_2]BF_4$) has already been reported (see reference 10c).

(16) Balakrishna, B.; Bauzá, A.; Frontera, A.; Vidal-Ferran, A. *Chem. –Eur. J.* **2016**, *22*, 10607.

(17) Wassenaar, J.; de Bruin, B.; Reek, J. N. H. *Organometallics* **2010**, *29*, 2767.

(18) Balakrishna, B.; Vidal-Ferran, A. *Synthesis* **2016**, *48*, 997.

(19) Burk, M. J.; Feaster, J. E.; Nugent, W. A.; Harlow, R. L. *J. Am. Chem. Soc.* **1993**, *115*, 10125.

(20) Yu, L.; Wang, Z.; Wu, J.; Tu, S.; Ding, K. *Angew. Chem., Int. Ed.* **2010**, *49*, 3627.

(21) Paeivioe, M.; Mavrynsky, D.; Leino, R.; Kanerva, L. T. *Eur. J. Org. Chem.* **2011**, 1452.

(22) Data collection with APEX II version v2013.4-1. Bruker (2007). Bruker AXS Inc., Madison, Wisconsin, USA.

(23) Data reduction with Bruker SAINT version V8.30c. Bruker (2007). Bruker AXS Inc., Madison, Wisconsin, USA.

(24) SADABS: V2012/1 Bruker (2001). Bruker AXS Inc., Madison, Wisconsin, USA. Blessing, R. H. *Acta Crystallogr., Sect. A: Found. Crystallogr.* **1995**, *A51*, 33.

(25) SHELXT; Sheldrick, G. M. *Acta Crystallogr., Sect. A: Found. Adv.* **2015**, *A71*, 3.

(26) SHELXle; Huebschle, C. B.; Sheldrick, G. M.; Dittrich, B. *J. Appl. Crystallogr.* **2011**, *44*, 1281.

(27) SHELXL; Sheldrick, G. M. *Acta Crystallogr., Sect. C: Struct. Chem.* **2015**, *71*, 3.

CHAPTER-4

Conclusions

1. We optimized and developed a chromatography-free and practical preparation method for enantiopure [Rh(P–OP)] complexes. The synthetic route starts with the ring-opening of a Sharpless epoxy-ether, followed by *O*-phosphorylation, complexation of the *in situ* generated P–OP ligand with the corresponding Rh-precursor and crystallization, to provide the target [Rh(P–OP)] precatalyst in up to 95% yield in gram amounts.
2. We expanded the structural diversity of the library of enantiopure phosphine-phosphite (P–OP) ligands to new phosphite fragments derived from 3,3'-diphenyl-octahydro-[1,1'-binaphthalene]-2,2'-diol and TADDOL motifs (TADDOL = 2,2-dimethyl-1,3-dioxolane-4,5-diyl)bis(diarylmethanol).
3. We have identified in the literature three different strategies to activate *N*-heteroaromatic substrates towards asymmetric hydrogenation. The first strategy consists of facilitating hydrogenation by the formation of positively charged derivatives from the initial *N*-heteroaromatic compound. The second strategy is based on introducing a ligating group on the substrate to assist its coordination to the metal center and facilitate hydrogenation by chelation assistance. The last strategy involves breaking the aromaticity of the heteroarene by inducing double bond isomerization processes.
4. We have expanded the scope of [Ir(P–OP)]-mediated asymmetric hydrogenations to new C=N-containing heterocyclic systems. Studies on [Ir(P–OP)]-mediated asymmetric hydrogenations of a variety of seven-membered heterocycles containing C=N bonds have revealed

that our iridium complexes are excellent catalysts (up to full conversion; up to 97% ee).

5. An unexpected inversion of the configuration of the hydrogenated products in [Ir(P–OP)]-mediated asymmetric hydrogenations having equally configured stereogenic elements in the ligand, but differing in the substituents at the 3,3'-positions of the [1,1'-biaryl]-2,2'-diol-derived phosphite group, has been rationalized by means of DFT calculations. These studies have identified the position of the Cl-ligand in catalytically relevant iridium structures and a number of non-covalent interactions (*i.e.* N–H···Cl, CH···π and CH···H–Ir interactions) as key features in rationalizing the stereochemical outcome of the reactions.
6. We have investigated the performance of a series of P–OP ligands with new phosphite moieties in Rh-mediated asymmetric hydrogenation of functionalized olefins. High activities (up to >99%) and medium to excellent enantioselectivities (up to 99%) have been achieved for selected model substrates. Newly prepared ligands with substituents at the 3,3'-positions of the [1,1'-biaryl]-2,2'-diol-derived phosphite group proved to be superior to the corresponding TADDOL-based ligands. Particularly, the ligand incorporating the 3,3'-diphenyl-(S_a)-octahydro-[1,1'-binaphthalene]-2,2'-diol-derived phosphite fragment provided the highest performing enantioselective catalyst in this chemistry.

Resum del pla de recerca:

L'objectiu de la present tesi està focalitzat en la síntesi de lligands enantiopurs de tipus fosfina-fosfit (P–OP) incorporant nous fragments fosfit. També s'ha abordat l'estudi de les seves propietats de coordinació amb precursors de rodi i d'iridi. Els lligands sintetitzats han estat emprats de forma satisfactòria en hidrogenacions asimètriques catalitzades per rodi i iridi.

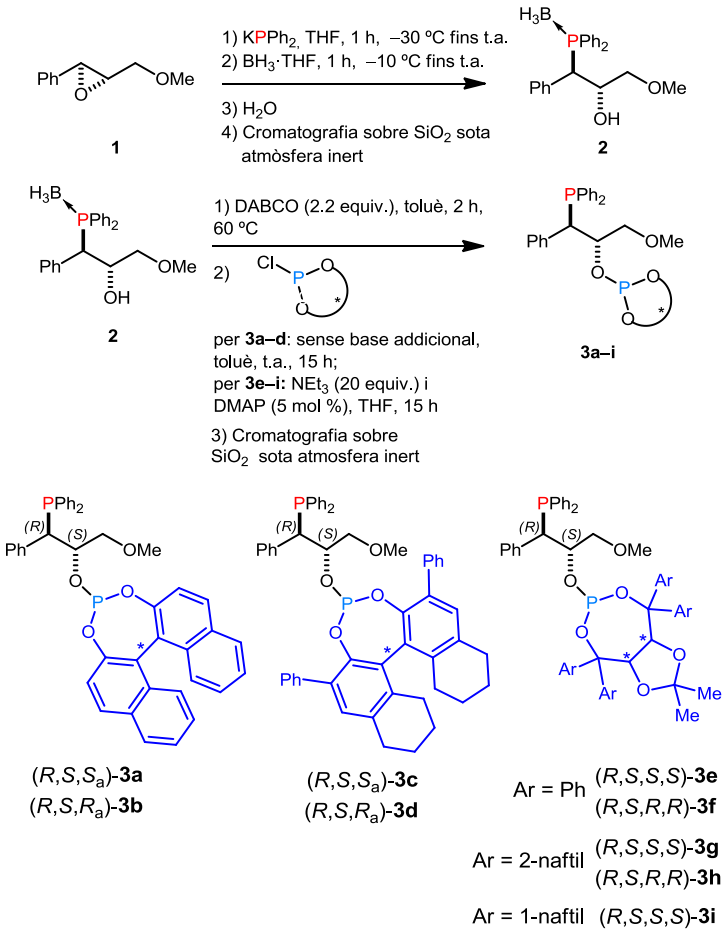

Esquema 1. Síntesi dels lligads fosfina-fosfit (P–OP).

Els lligands de tipus P–OP preparats han estat sintetitzats a través de rutes sintètiques prèviament desenvolupades pel grup, que, en primer lloc, es basen en l'apertura asimètrica d'epoxi-èters enantiopurs (de tipus Sharpless) mitjançant nucleòfils fosforats, seguit de l'addició de borà per obtenir els complexes de tipus fosfino-alcohol i, en segon lloc, l'eliminació del borà seguit d'una *O*-fosforilació amb els corresponents electròfils fosforats (clorofosfits) resultant en els lligands objectiu (veure Esquema 1).

En aquest context, s'ha desenvolupat una metodologia pràctica i sense purificacions cromatogràfiques per a la preparació de complexes de rodi(I) enantiopurs incorporant lligands del tipus P–OP, que actuen en general com a directors estereoquímics en la transformació asimètrica. Aquests precatalitzadors de rodi poden ser utilitzats eficientment com a catalitzadors en la hidrogenació asimètrica d'alquens funcionalitzats, la resolució cinètica de vinil sulfòxids i la desimetrització catalítica de diens aquirals. Aquesta metodologia està basada en l'apertura asimètrica d'epoxi-èters purs (mitjançant nucleòfils fosforats) seguit de l'adició de borà per rendir els complexes fosfino-alcohol, que són purificats i aïllats eficientment mitjançant un procés de cristal·lització. Posteriorment es realitza l'eliminació del borà, la fosforilació amb els corresponents clorofosfits (electròfils fosforats) i finalment, la complexació dels corresponents lligands (obtinguts *in situ*) amb$[Rh(nbd)_2]BF_4$ obtenint els precatalitzadors objectiu, els quals són aïllats mitjançant processos de cristal·lització (Esquema 2).

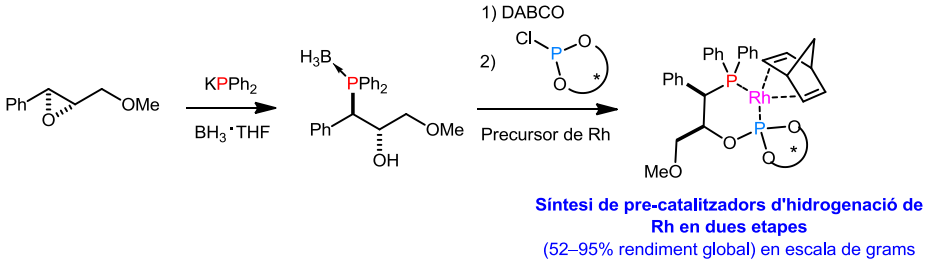

Esquema 2. Síntesi de complexes de Rh basats en lligands P–OP sense separacions cromatogràfiques.

La recerca realitzada al nostre grup també s'ha estès a l'estudi d'altres tipus de substrats de tipus heteroaromàtic, així com també al desenvolupament de possibles estratègies (a través de modificacions en la seva estructura) per a l'activació d'aquests tipus de compostos en hidrogenacions asimètriques. Els exemples prèviament descrits a la bibliografia s'han classificat en tres estratègies diferents, i els detalls experimentals més rellevants (catalitzador utilitzat, condicions de reacció, tipus d'heteroarè, diversitat estructural i l'activitat catalítica en termes de conversió i enantioselectivitat) han estat resumits. La primera estratègia consisteix en facilitar el procés d'hidrogenació per protonació o quaternització d'àtoms de nitrogen continguts a l'heteroarè. D'aquesta manera, la desactivació del catalitzador per part del substrat pot ser evitada i, addicionalment, la hidrogenació d'aquests compostos (carregats positivament) pot estar més afavorida respecte als seus anàlegs neutres. La segona estratègia, engloba els casos on l'activació es produeix mitjançant la introducció d'un grup lligant, que facilita (per assistència quelant) la coordinació amb el metall. Finalment, la tercera estratègia es basa en la ruptura de l'aromaticitat de l'heteroarè a través de processos d'isomerització de dobles enllaços. Aquest *microreview* resumeix els últims avanços en aquest tòpic, que han permès desenvolupar reaccions d'hidrogenació d'heteroarens altament enantioselectives per a la producció de sistemes heterocíclics total (o parcialment) saturats.

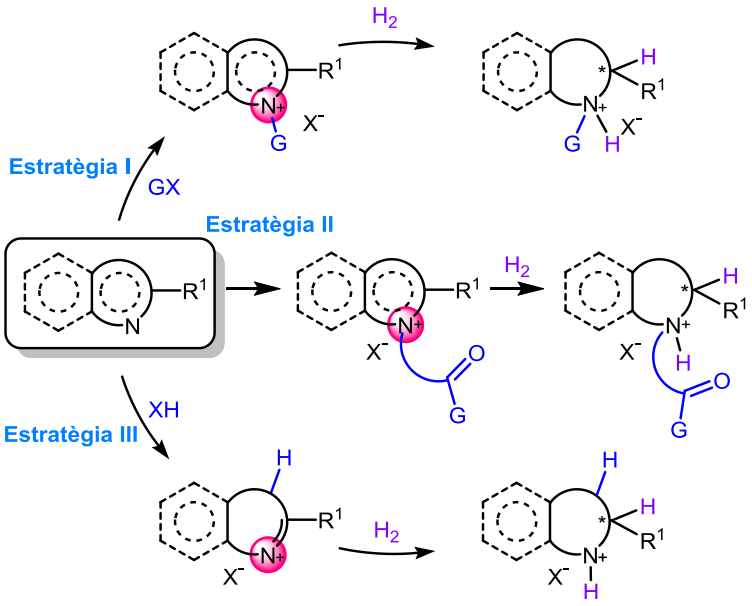

Esquema 3. Estratègies per a l'activació del substrat.

Per tal d'ampliar l'aplicació d'hidrogenacions asimètriques de compostos heterocíclics (contenint enllaços C=N) catalitzades per complexes d'iridi de tipus [Ir(P–OP)], els complexes derivats dels lligands P–OP **3b** i **3d** van ser satisfactòriament aplicats a la reacció d'hidrogenació asimètrica d'heterocicles de set membres (onze exemples, fins a 97% d'ee). El millor precatalitzador desenvolupat (derivat del lligand **3d**) junt amb quantitats catalítiques de HCl ha mostrat propietats catalítiques excel·lents en la hidrogenació d'heterocicles de set membres substituïts amb grups de tipus alquílic. Malgrat que la reacció d'hidrogenació de substrats substituïts amb grups de tipus arílic va tenir lloc amb més dificultat, es van poder trobar condicions de reacció altament efectives (sense la presència de HCl) per substrats del tipus oxa- o tia-azepina fenil substituïts. L'origen de l'enantioselectivitat ha estat racionalitzada amb l'ajut de càlculs DFT, que han permès identificar la posició del lligand clorur, així com una sèrie d'interaccions de tipus no covalent (*i.e.*

interaccions N–H···Cl, CH···π i CH···H–Ir), com a paràmetres clau en la racionalització de l'estereoquímica obtinguda a través de la reacció catalitzada per els complexes d'iridi derivats dels lligands **3a** i **3b**.

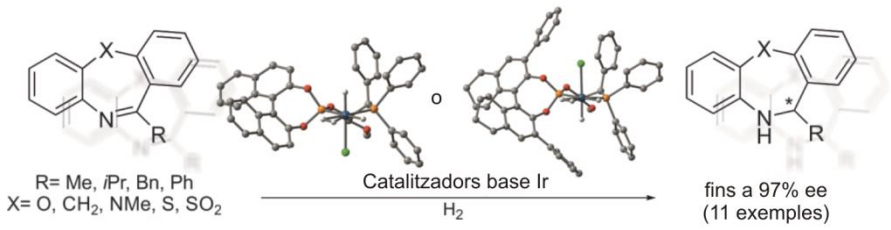

Esquema 4. Hidrogenació asimètrica d'imines cícliques catalitzada per complexes d'iridi.

Estudis de coordinació dels lligands P–OP (derivats de fosfits de tipus TADDOL o de 3,3'-difenil-octahidro-[1,1'-binaftalè]-2,2'-diol) amb precursors de rodi resultaren en la formació de complexes catiònics, l'estructura dels quals va ser determinada inequívocament mitjançant estudis de RMN i de difracció de rajos-X. Els complexes de rodi(I) derivats de una sèrie de lligands enantiopurs de tipus P–OP han estat avaluats en la reacció d'hidrogenació asimètrica d'alquens funcionalitzats. Els precatalitzadors resultants mostraren excel·lent comportament en termes d'activitat (99%) i d'enantioselectivitat (fins a 99% d'ee) en tots els casos assajats. La influència dels diferents fragments fosfit en els valors d'enantioselectivitat obtinguts ha estat també estudiada. En aquesta reacció, els lligands amb un grup fosfit de tipus biarílic mostraren ser més eficients que els anàlegs derivats de TADDOL. Particularment, el lligand derivat del fragment 3,3'-difenil-(S_a)-octahidro-[1,1'-binaftalè]-2,2'-diol (**3c**) va proporcionar els millors resultat en termes d'eficiència catalítica i enantioselectivitat dels productes hidrogenats.

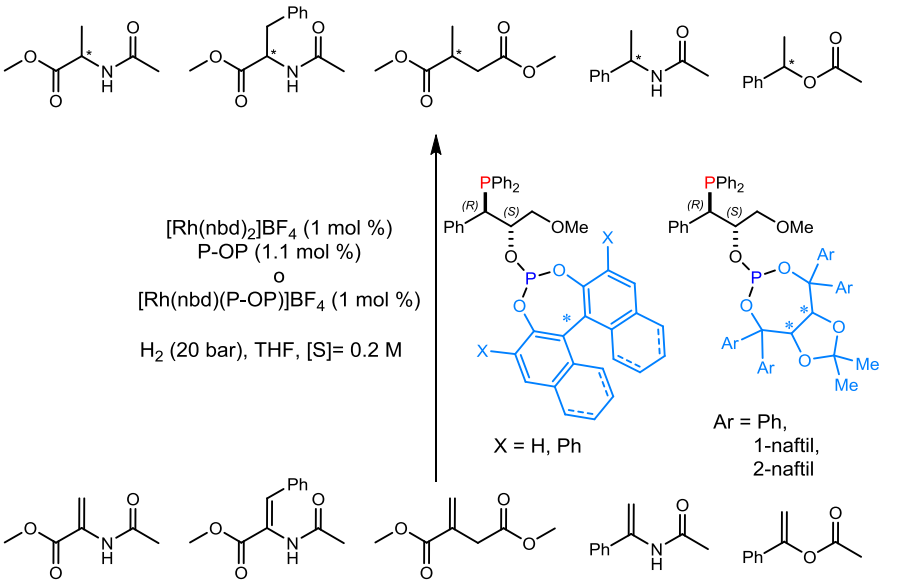

Esquema 5. Hidrogenació asimètrica d'alquens funcionalitzats catalitzada per rodi.

Summary in English:

The synthesis of enantiopure phosphine-phosphite (P–OP) ligands with new phosphite fragments and coordination studies with rhodium and iridium precursors for asymmetric hydrogenations have been performed. The resulting P–OP-rhodium and iridium complexes were efficiently employed in asymmetric hydrogenations of an array of structurally diverse substrates. The designed P–OP ligands were synthesized by a well-established synthetic route developed in the group, which comprised the ring-opening of an enantiopure Sharpless epoxy ether with a phosphorus nucleophile and the *O*-phosphorylation of the resulting phosphino alcohol with the corresponding phosphorus electrophiles (chlorophosphite derivatives). The synthetic route towards the highest performing precatalysts in rhodium-mediated hydrogenative transformations has been optimized by developing a chromatography-free synthesis involving the crystallization of the target [Rh(P–OP)] precatalysts as the purification method. Studies on [Ir(P–OP)]-mediated asymmetric hydrogenations of a variety of seven-membered heterocycles that contain C=N bonds have revealed that these iridium complexes are excellent catalysts (up to full conversion; up to 97% ee). The enantioselectivity has been rationalized by means of DFT calculations, which have identified the position of the Cl-ligand in catalytically relevant iridium structures and a number of non-covalent interactions (*i.e.* N–H···Cl, C–H···π and C–H···H–Ir interactions) as key features in the rationalization of the stereochemical outcome of the reactions. As regards the hydrogenation of functionalized alkenes, [Rh(P–OP)] precatalysts incorporating new phosphite fragments have been prepared. High catalytic activity (>99% conversion) and excellent enantioselectivity (up to >99%) were achieved in asymmetric hydrogenations of a variety of functionalized alkenes by P–OP ligands incorporating 3,3’-diphenyl-[1,1'-biaryl]-2,2'-diol-derived phosphite groups.

Resum en català:

S'ha dut a terme la síntesi de lligands enantiopurs fosfina-fosfit (P–OP) amb nous fragments fosfit i els corresponents estudis de coordinació amb precursors de rodi i iridi per hidrogenacions asimètriques. El complexes de tipus P–OP-rodi i iridi es van utilitzar eficientment a hidrogenacions asimètriques d'una sèrie diversa de substrats. Els lligands P–OP dissenyats es van sintetitzar mitjançant una ruta sintètica ben establerta pel grup d'investigació, que consisteix en l'apertura d'un epoxi-èter enantiopur de Sharpless amb un nucleòfil de fòsfor i la *O*-fosforilació del fosfino-alcohol resultant amb els electròfils de fòsfor corresponents (derivats de tipus clorofosfit). La ruta sintètica pels precatalitzadors més efectius a les transformacions hidrogenatives mediades per rodi es va optimitzar, desenvolupant una síntesi sense separacions cromatogràfiques basada en la cristal·lització dels precatalitzadors [Rh(P–OP)] desitjats com a mètode de purificació. Estudis sobre les hidrogenacions asimètriques utilitzant complexes [Ir(P–OP)] d'un conjunt de sistemes heterocíclics de set membres contenint la funció C=N va revelar que aquests complexes d'iridi són excel·lents catalitzadors (conversions completes i excessos enantiomèrics de fins el 97%). La enantioselectivitat d'aquest procés s'ha racionalitzat mitjançant càlculs teòrics DFT, que han identificat la posició del lligand-Cl a estructures catalíticament rellevants dels complexes d'iridi, així com també una sèrie d'interaccions no-covalents (per exemple interaccions N–H···Cl, C–H···π i C–H···H–Ir), que són els trets clau a l'hora de racionalitzar el resultat estereoquímic de les reaccions. Pel que fa a la hidrogenació d'alquens funcionalitzats, es van preparar precatalitzadors [Rh(P–OP)] que incorporen nous fragments fosfit. Es va assolir una alta activitat catalítica (conversió >99%) i enantioselectivitat excel·lent (fins a >97%) a les hidrogenacions asimètriques d'un conjunt d'alquens funcionalitzats amb lligands P–OP que incorporaven grups derivats del 3,3'-difenil-[1,1'-biaril]-2,2'-diol.

Resumen en castellano:

Se ha estudiado la síntesis de ligandos enantiopuros fosfina-fosfito (P–OP) con nuevos fragmentos fosfito, así como sus propiedades de coordinación con precursores de rodio e iridio para hidrogenación asimétrica. Dichos complejos de rodio e iridio se han utilizado satisfactoriamente en hidrogenaciones enantioselectivas de un conjunto de sustratos con estructuras diversas. Los ligandos P–OP diseñados se sintetizaron mediante una ruta sintética establecida por el grupo de investigación, que consiste en la apertura de un epoxi-éter enantiopuro de tipo Sharpless con un nucleófilo de fósforo, y posterior *O*-fosforilación del fosfino-alcohol resultante con los correspondientes electrófilos de fósforo (derivados de tipo clorofosfito). La ruta sintética de los precatalizadores de rodio más eficientes para transformaciones hidrogenativas se optimizó a través de una síntesis sin separaciones cromatográficas basada en la cristalización de los correspondientes precatalizadores como método de purificación. Estudios realizados en hidrogenación asimétrica sobre una variedad de heterociclos de siete miembros con enlaces C=N en su estructura revelaron que complejos de iridio derivados de ligandos P–OP son catalizadores excelentes, proporcionando conversiones completas y enantioselec-tividades elevadas (hasta 97% ee). La enantioselectividad de la reacción fue racionalizada mediante cálculos DFT, los cuales identificaron la posición del ligando cloro, así como una serie de interacciones no covalentes (por ejemplo N–H···Cl, C–H···π y C–H···H–Ir) en intermedios de iridio catalíticamente relevantes, como factores clave en la racionalización de los resultados. En lo que respecta a la hidrogenación de alquenos funcionalizados, precatalizadores de rodio incorporando nuevos fragmentos fosfito fueron evaluados, de los cuales aquellos derivados del grupo 3,3’-difenil-[1,1'-biaril]-2,2'-diol proporcionaron resultados excelentes tanto en términos de actividad catalítica (conversión >99%) como de enantioselectividad (>99% ee).